

Gasification Burning of Biomass

Aysha Irshad

Submitted in accordance with the requirements for the degree of
Doctor of Philosophy

The University of Leeds
School of Chemical and Process Engineering

September 2017

The candidate confirms that the work submitted is her own, except where work which has formed part of jointly-authored publications has been included. The contribution of the candidate and the other authors to this work has been explicitly indicated below. The candidate confirms that appropriate credit has been given within the thesis where reference has been made to the work of others.

This copy has been supplied on the understanding that it is copyright material and that no quotation from the thesis may be published without proper acknowledgement.

The right of Aysha Irshad to be identified as Author of this work has been asserted by her in accordance with the Copyright, Designs and Patents Act 1988.

List of publications

- **Aysha Irshad**, Abdulaziz Alarifi, Shaun Thompson, Cristopher.J. Melton, G.E. Andrews, B.M. Gibbs and H.N. Phylaktou, Use of cone calorimeter for investigating biomass gasification staged combustion. in conference proceedings : 22nd European Biomass conference and exhibition proceedings, 23rd -26th June 2014, Hamburg, Germany.

Candidate as the lead author of the paper conducted the experiments with Shaun Thompson, Cristopher J. Melton and Abdulaziz Alarifi. Candidate analysed the data of the experiments and written the paper under the supervision of Dr. Herodotos Phylaktou, Prof. Gordon Andrews, and Prof. Bernard Gibbs.

(Results are given in Chapter 4).

- Muhammad Azam Saeed, **Aysha Irshad**, Gordon E. Andrews, Herodotos N. Phylaktou & Bernard M. Gibbs. Agricultural waste biomass energy potential in Pakistan. Proceedings of the International Bioenergy (Shanghai) Exhibition and Asian Bioenergy Conference, European Biomass and Energy Conference (EUBCE), 2015. Shanghai, China, DOI: <http://dx.doi.org/10.5071/IBSCE2015-1CO.1.2>

The candidate as secondary author of this publication has reviewed the literature and performed the energy calculations for wood, oil seed residue and banana tree waste, while primary author Muhammad Azam Saeed performed the energy calculations for the crop residues. Both Muhammad Azam Saeed and candidate were involved in the writeup of the publication under supervisions of the Prof. Gordon Andrews, Dr. Herodotos Phylaktou and Prof. Bernard Gibbs. (calculations are included in Chapter 1)

Acknowledgements

I am very grateful to my supervisors, Dr. Herodotos Phylaktou, Prof. Gordon Andrews and Prof. Bernard Gibbs for their supervision, continual guidance and support. Their help with positive comments, discussion and suggestions throughout the experimental and thesis works have contributed to the completion of this research.

I am also thankful to Dr. Andrew Ross for his advice and help to work on his rig.

I also thank SCAPE labs technical staff, especially Edmund Woodhouse, Gurdev Bhogal (for the technical help regarding the cone calorimeter), Adrian Cunliffe and Karine Alves Throne for help in the analytical laboratory.

I am grateful to the University of Engineering & Technology, Lahore, Pakistan. For awarding me Faculty Development Programme (FDP) Scholarship to pursue my PhD in University of Leeds.

I would like to thank all my colleagues, Abdulaziz Alarifi, Jackie Chan, Hamed Sattar, Azam Saeed, Philip Bowa, James Hammerton, Bintu Grema Mustafa and Miss Mat Kiah for help and support.

Very special thanks to my Husband Muhammad Asif Saleem who struggled with me during my PhD and provided moral support. Special thanks to my Parents, for who I am today is because of them. I am also thankful to my siblings, and friends in Pakistan and UK for their moral support and prayers.

Abstract

Biomass combustion for heat applications uses two stage combustion with a gasification first stage followed by oxidation of the gases in a second stage combustion, where most of the heat release occurs. These type of combustion system are gasification or log boilers. However, there has been little study of the optimisation of the gasification stage for biomass applications and this was the objective of this research.

The cone calorimeter was used in its controlled atmosphere configuration. A 180°C gas sample line was used to sample the raw gases from the rich burning gasification zone and transfer them via a heated pump and filter to the heated Gasmeter FTIR, which was calibrated for 60 species. Hydrogen was computed from the CO measurements. The test facility was also operated on nitrogen in order to measure the composition of the gases evolved under heating with no combustion. were H₂O, CO₂, CO, formic acid, xylene, trimethylbenzene, acetic acid, formaldehyde, acrolein, acetone, furfural, methyl tertiary butyl ether (MTBE) and propanol were the major gases with other hydrocarbons. The energy in the devolatilised gases from the heated biomass in nitrogen was determined from the gas composition and flow rate and a very high conversion of energy from solid biomass into gaseous products was demonstration for a range of biomass.

The Chemical Equilibrium and Applications (CEA) software was used to predict the adiabatic equilibrium gas composition as a function of equivalence ratio for the range of biomass compositions. The predicted optimum equivalence ratios for the maximum yield of CO was in good agreement with the experimental measurements. The experimental optimum equivalence ratio for pine was 2.7. The total energy in the gases from the gasification zone showed a thermal efficiency of 80%. Major components were H₂O, CO₂, CO with hydrocarbons benzene, acetylene, ethylene and naphthalene.

Table of contents

List of publications	iii
Acknowledgements	iv
Abstract	v
List of figures	x
List of tables	xviii
Abbreviations & symbols	xix
Chapter 1 Introduction	- 1 -
1.1 Energy sources and greenhouse gas emissions	- 1 -
1.2 Biomass as energy	- 2 -
1.3 UK energy situation	- 3 -
1.4 Renewable heat incentive scheme UK	- 5 -
1.5 Biomass to energy conversion processes	- 6 -
1.5.1 Biological/biochemical processes.....	- 6 -
1.5.2 Thermochemical processes	- 6 -
1.6 Torrefaction	- 8 -
1.7 Energy crisis in Pakistan	- 8 -
1.8 Energy potential from biomass in Pakistan.....	- 10 -
1.9 Woody (forestry) resource of Pakistan	- 11 -
1.9.1 Sustainability and tree rotation period for forests in Pakistan....	- 12 -
1.9.2 Growing stock in the different forests	- 12 -
1.10 Estimation of energy from oil seed residues in Pakistan	- 14 -
1.11 Estimation of energy obtained from banana tree waste in Pakistan ...	- 15 -
Chapter 2 Literature review	- 17 -
2.1 Theory of gasification	- 17 -
2.1.1 Drying.....	- 17 -
2.1.2 Pyrolysis.....	- 17 -
2.1.3 Gasification	- 18 -
2.2 Stoichiometric air to fuel ratio	- 22 -
2.3 Equivalence ratio (\emptyset).....	- 23 -
2.4 Effect of equivalence ratio on the product gas composition in gasification	- 25 -
2.5 Effect of temperature on the product gas composition in the gasification of biomass	- 29 -
2.6 Effect of moisture/steam on the gasification of biomass.....	- 32 -

2.7	Effect of biomass particle size	- 33 -
2.8	Pyrolysis and chemistry of wood	- 35 -
2.9	Cellulose/Lignin ratio	- 38 -
2.10	Volatile products from pyrolysis of wood	- 42 -
2.11	Gasification for electricity and heat production	- 49 -
2.12	Commercial biomass log boilers.....	- 49 -
2.13	Research aims	- 62 -
2.14	Research objectives	- 62 -
Chapter 3 Experimental methodologies		- 64 -
3.1	Analytical laboratory tests.....	- 64 -
3.1.1	Elemental analysis	- 64 -
3.1.2	Thermo-gravimetric analysis (TGA)	- 65 -
3.1.3	Bomb calorimeter test	- 65 -
3.2	Equilibrium Calculation	- 66 -
3.3	Cone calorimeter	- 67 -
3.3.1	Insulation of cone calorimeter box.....	- 70 -
3.3.2	Raw sampling methods.....	- 70 -
3.4	Gas analysis equipment	- 74 -
3.4.1	Sampling system for the FTIR.....	- 74 -
3.4.2	FTIR analyser.....	- 75 -
3.4.3	Paramagnetic oxygen spectrometer.....	- 83 -
3.4.4	Non-dispersive Infra-red (NDIR) analyser	- 84 -
3.5	Heat release rate calculations	- 85 -
3.6	Emission index EI	- 86 -
3.7	Hot gas efficiency (HGE)	- 87 -
3.8	Test materials.....	- 87 -
3.9	Experimental procedure for the cone calorimeter test	- 87 -
3.10	Furnace reactor	- 90 -
Chapter 4 Development of the experimental methodology for the cone calorimeter tests.....		- 94 -
4.1	Ultimate and proximate analysis of the wood	- 94 -
4.2	Equilibrium calculations	- 104 -
4.3	Steps towards the development of gasification tests	- 108 -
4.3.1	Mass loss of samples.....	- 110 -
4.3.2	Metered equivalence ratio (ϕ_m).....	- 113 -
4.3.3	Heat release rate (HRR)	- 115 -

4.3.4	Carbon monoxide and hydrogen emissions	- 121 -
4.3.5	Carbon monoxide emission index (El _{CO})	- 124 -
4.3.6	Emission based equivalence ratio (ϕ_e).....	- 125 -
4.3.7	Temperature rise of the pine wood.....	- 126 -
4.4	Test with Insulation of the box of the cone calorimeter (configuration 2)	- 127 -
4.5	Influence of insulation below the test biomass for an insulated compartment (configuration 3).....	- 134 -
4.6	The problem of gas sampling from the chimney exit so that mean sample was achieved (configuration 4)	- 139 -
4.6.1	Initial single hole sample tube, as used in all the previous tests.	- 140 -
4.6.2	Traverse of the single hole sample tube (Figure 4.47 a)-	140 -
4.6.3	Traverse of the single hole sample tube with grid plate mixer at the entry to the chimney (Figure 4.47 b).....	- 143 -
4.6.4	Four-hole sample probe (Figure 4.48) and no inlet grid plate....	- 144 -
4.6.5	76mm diameter 20 hole 'X' probe at the bottom of the chimney	- 145 -
4.6.6	Repeatability of the test in the final test configuration	- 147 -
4.7	Final optimised rich burn gasification cone calorimeter test conditions	- 148 -
4.8	Technical issues regarding insulations and emissions	- 148 -
4.9	Conclusion:.....	- 152 -
Chapter 5 Results of gasification tests on cone calorimeter		- 154 -
5.1	Influence of equivalence ratio on the product gas composition-	154 -
5.1.1	Equivalence ratios at Steady operation.....	- 154 -
5.2	Effect of equivalence ratio on HGE.....	- 169 -
5.3	Effect of biomass moisture content.....	- 173 -
5.4	Influence of different biomass materials on gasification	- 178 -
5.5	Conclusions:.....	- 201 -
Chapter 6 Results for pyrolysis tests on cone calorimeter		- 202 -
6.1	Mass loss and temperature profiles of pyrolysis tests on the cone calorimeter.....	- 205 -
6.2	FTIR results.....	- 210 -
6.3	Effect of biomass types on pyrolysis.....	- 227 -
6.4	FTIR results for the pyrolysis of different biomass species.....	- 230 -
6.4.1	Product yields.....	- 233 -

6.5	Temperature distribution inside different woods	- 244 -
6.6	Mass balance	- 249 -
6.7	Energy contents of the products of pyrolysis	- 252 -
6.8	Conclusions	- 254 -
Chapter 7 Results for pyrolysis tests on furnace reactor		- 256 -
7.1	FTIR emissions	- 258 -
7.2	Yields of liquids gases and chars	- 261 -
7.3	Pyrolysis liquids	- 264 -
7.4	Conclusions	- 265 -
Chapter 8 Conclusions and future work		- 267 -
8.1	Applications of biomass two stage combustion	- 267 -
8.2	The principles of two stage combustion.....	- 268 -
8.3	Elemental and TGA results.....	- 269 -
8.4	Equilibrium calculations	- 269 -
8.5	Development of the experimental methodology	- 270 -
8.6	Gasification of biomass in the cone calorimeter	- 271 -
8.7	Energy conversion efficiency for gasification rich combustion. -	272 -
8.8	Pyrolysis tests on the cone calorimeter	- 273 -
8.9	Heated FTIR performance for gas composition analysis.	- 273 -
8.10	The cone calorimeter as a biomass characterisation method.. -	274 -
8.11	Future work	- 274 -
References.....		- 276 -
APPENDICES.....		Error! Bookmark not defined.

List of figures

Figure 1.1: H/C v. O/C plots for wood in comparison to different types of coal	3 -
Figure 1.2 Renewable energy sources of UK in 2015 [11].....	4 -
Figure 1.3 Fuel sources for electricity generation in UK in 2014 & 2015 [11].....	4 -
Figure 1.4 Fuel sources for electricity generation in Pakistan in 2012 [20]	9 -
Figure 2.1 Boudouard reaction equilibrium [63]	21 -
Figure 2.2 Effect of the Air factor (λ) on the composition of producer gas (equilibrium) for woodchip gasification [69].	26 -
Figure 2.3 predicted equilibrium concentration of CO and CO ₂ for different biomasses [69].....	27 -
Figure 2.4 Experimental concentrations and CV of product gas from gasification of wood chips in downdraft gasifier [70].....	28 -
Figure 2.5 Biomass components (a) cellulose (b) hemicellulose (c) lignin [84]	36 -
Figure 2.6 Steps and compounds for the decomposition of (a) Cellulose (b) hemicellulose (Xylan) (c) Lignin ; HAA: hydroxy acetaldehyde; HA: hydroxy acetone [83]	39 -
Figure 2.7 Percentage yield of volatiles vs temperature for biomass samples [99] (under nitrogen).....	42 -
Figure 2.8 HDG Navora log wood boiler design [122].....	56 -
Figure 2.9 Froling S3 Turbo log boiler design [124].....	57 -
Figure 2.10 HDG EURO log wood boiler design [122].....	59 -
Figure 2.11 Veissmann Vitoligno 250-S log boiler [125].....	60 -
Figure 2.12 HDG Bavaria log boiler design [122]	61 -
Figure 3.1 Cone calorimeter detailed schematic [129].....	68 -
Figure 3.2 Cone calorimeter setup	69 -
Figure 3.3 Insulated cone calorimeter box with cooling jacket	71 -
Figure 3.4 Schematic of the sampling method 1 from the chimney and relative positions of the sampling point and thermocouples	72 -
Figure 3.5 Schematic of the sampling method 2 from the chimney and relative positions of the sampling point and thermocouples	73 -
Figure 3.6 Types of probes used in the present research (a) 4 holes probes (b) x probe with 20 holes	73 -
Figure 3.7 (a) Superwool insulation (b) chimney	74 -
Figure 3.8 Cone calorimeter- FTIR schematic.....	75 -
Figure 3.9 Working principle of the FTIR analyser.....	76 -
Figure 3.10 Certified mixture bottles validation [134].....	80 -
Figure 3.11 Carbon monoxide measurements (FTIR & NDIR) from cone calorimeter test [134]	81 -

Figure 3.12 Certified mixture bottle comparison with FTIR (a) CO ₂ (b) CO (c) Propane	- 82 -
Figure 3.13 Certified mixture bottle comparison with FTIR (a) CO ₂ (b) CO (c) Propane (d) NO	- 83 -
Figure 3.14 Schematic diagram of Paramagnetic Oxygen Spectrometer [135]	- 84 -
Figure 3.15 NDIR analyser Principle [136]	- 85 -
Figure 3.16 biomass test samples	- 88 -
Figure 3.17 Thermocouples test (a) schematic (b) Pine wood thermocouple holes (c) Sample with thermocouples inside box	- 89 -
Figure 3.18 Schematic of furnace reactor	- 91 -
Figure 3.19 Furnace rig.....	- 92 -
Figure 3.20 (a) Pine 20x20x20mm cubes (b) feedstock basket.....	- 93 -
Figure 4.1 TGA normalised mass vs temperature for some biomass samples	- 95 -
Figure 4.2 volatiles mass loss rate vs temperature of biomass from TGA	- 95 -
Figure 4.3 atomic H/C vs. O/C of biomass samples	- 100 -
Figure 4.4 H/C v Stoichiometric A/F by mass of biomass samples.....	- 101 -
Figure 4.5 Stoichiometric (A/F) vs % hemicellulose for the biomass studied	- 101 -
Figure 4.6 Stoichiometric (A/F) vs % lignin for the biomass studied	- 102 -
Figure 4.7 Stoichiometric (A/F) vs % lignin for the biomass studied	- 102 -
Figure 4.8 % lignin vs. % cellulose for the biomass species studied	- 103 -
Figure 4.9 % VM vs H/C molar ratio for biomass samples	- 104 -
Figure 4.10 Equilibrium concentrations and adiabatic flame temperature of gaseous products as a function of equivalence ratio (\emptyset) for pine wood gasification using CEA software.....	- 105 -
Figure 4.11 Equilibrium concentrations and adiabatic flame temperature of gaseous products as a function of equivalence ratio (\emptyset) for dry ash wood gasification.	- 106 -
Figure 4.12 Equilibrium concentrations and adiabatic flame temperature of gaseous products as a function of equivalence ratio (\emptyset) for the gasification of white wood pellets	- 107 -
Figure 4.13 Equilibrium concentrations and adiabatic flame temperature of gaseous products as a function of equivalence ratio (\emptyset) for the gasification of China's biomass skin	- 108 -
Figure 4.14 (a) normalised mass vs time (b) Mass loss rate (MLR) vs time for 20mm thick wood load (5 wood sticks).....	- 110 -
Figure 4.15 steady state flame combustion at heat flux 70 kW/m ² , air flow 9 g/(m ² .s)(a) 5 ash sticks (b) 5 pine sticks	- 111 -
Figure 4.16 (a) mass vs time (b) Mass loss rate (MLR) vs time for 40 mm thick wood load (10 pine wood sticks) at air flow rate 12.8 g/(m ² .s).....	- 112 -

Figure 4.17 Steady state flame combustion for 40mm thick wood load (10 pine sticks) air flow 12.8 g/(m ² .s) (a) heat flux 50 kW/m ² (b) heat flux 70 kW/m ²	113 -
Figure 4.18 Equivalence ratio (ϕ_m) for tests with (a) 20mm thick wood load (5 sticks) (b) 40 mm thick wood load (10 sticks) at 12.8 g/(m ² .s)	114 -
Figure 4.19 Total HRR _(OC) as % of total HRR _(MLR) kW/m ² for tests with 200 thick wood load	116 -
Figure 4.20 % CO comparison from raw sampling (FTIR) and dilute sampling (NDIR)	117 -
Figure 4.21 Primary and secondary gasification HRR expressed as a % of total..	120 -
Figure 4.22 % CO from gasification stage for 20 mm thick wood load (a) 70 kW/m ² (b) 50 kW/m ²	121 -
Figure 4.23 % CO from gasification stage for (a) 40 mm thick wood load at air flow 6.3 L/min. (b) comparison between 40 mm and 20 mm thick wood load at 50 kW/m ² & 12.8 g/(m ² .s).....	122 -
Figure 4.24 % H ₂ from the gasification stage (a) 20 mm thick wood load (b) 40 mm thick wood load at airflow 12.8 g/(m ² .s)	123 -
Figure 4.25 CO emission index (EI _{CO}) for tests (a) 20 mm thick load (b) 40 mm thick wood load at airflow 12.8 g/(m ² .s).....	124 -
Figure 4.26 THC emissions during gasification of 5 wood sticks at heat flux 70 kW/m ² .- 124 -	
Figure 4.27 EB equivalence ratio ϕ_e for tests with 20 mm thick wood load.....	125 -
Figure 4.28 EB equivalence ratio ϕ_e for tests with 20 mm thick wood load at air flow 12.8 g/(m ² .s)	126 -
Figure 4.29 Temperature vs time for test with 40mm thick wood load (10 pine sticks) (a) at 50 kW/m ² (b) 70 kW/m ² at air flow 12.8 g/m ² .s.....	127 -
Figure 4.30 Water vapour released during rich combustion heating of 'dry' biomass.....- 127 -	
Figure 4.31 Heat flux 50 kW/m ² , air flow 12.8 g/(m ² .s) (a) MLR (g/s) (b) equivalence ratio ϕ_m	128 -
Figure 4.32 Heat flux 50 kW/m ² , air flow 12.8 g/(m ² .s) (a) CO % vol. vs time (b) THC % vol. vs time	129 -
Figure 4.33 Heat flux 50 kW/m ² , air flow 12.8 g/(m ² .s) (a) O ₂ % vol. vs time (b) ϕ_e vs time	130 -
Figure 4.34 Heat Flux at 50 kW/m ² , air flow 12.8 g/(m ² .s) (a)PHRR vs time (b) PHRR as % of Total HRR _{MLR} vs time	131 -
Figure 4.35 Heat flux 70 kW/m ² , air flow 9 g/(m ² .s) (a) MLR (g/s) (b) metered equivalence ratio ϕ_m	131 -
Figure 4.36 Raw % CO at heat flux 70 kW/m ² , air flow 9 g/(m ² .s).....	132 -
Figure 4.37 Heat flux 70 kW/m ² , air flow 9 g/(m ² .s) (a) % H ₂ O (b) % CO ₂	132 -

Figure 4.38 Tests with Insulation of gasification zone at heat flux 70 kW/m ² (a) MLR (g/s) (b) equivalence ratio \varnothing_m	- 133 -
Figure 4.39 % CO at heat flux 70 kW/m ² with insulation of the gasification zone..	- 133 -
Figure 4.40 Comparison of % CO with 20mm insulation underneath the pine wood with tests 40 mm thick pine (2 layers) at 12.8 g/(m ² .s).....	- 134 -
Figure 4.41 Thermocouples inserted 5mm from top surface in 40mm thick pine (2 layers of 5 sticks) with insulation and without insulation at 70 kW/m ² airflow 12.8 g/(m ² .s)	- 135 -
Figure 4.42 20 mm thick insulation under 5 wood sticks at heat flux 70 kW/m ² (a) MLR (g/s) (b) equivalence ratio \varnothing_m	- 136 -
Figure 4.43 Steady state flame combustion of 5 pine wood sticks insulated box, 20 mm insulation underneath, heat flux 70 kW/m ² , air flow 9 g/(m ² .s)	- 137 -
Figure 4.44 20 mm thick insulation under 5 wood sticks at heat flux 70 kW/m ² (a) % CO from gasification zone (b) % THC from gasification zone	- 137 -
Figure 4.45 20 mm thick insulation under 5 wood sticks at heat flux 70 kW/m ² (a) % H ₂ O from gasification zone (b) \varnothing_e	- 138 -
Figure 4.46 Flame from chimney exit for standard sampling probe at steady state flame combustion of pine at 70kW/m ² , 9 g/(m ² .s)	- 138 -
Figure 4.47 (a) Traverse with single hole probe (b) Single hole probe traverse, orifice under chimney	- 141 -
Figure 4.48 Configuration of 4 hole probe inside chimney.....	- 142 -
Figure 4.49 % CO and \varnothing_e with single holes probe travers with and without mixing orifice plate at 9 g/(m ² .s) 70 kW/m ²	- 142 -
Figure 4.50 EB Equivalence ratio \varnothing_e for tests with different sampling methods, heat flux 70 kW/m ² , air flow 9 g/(m ² .s).....	- 143 -
Figure 4.51 % CO emissions for tests with different sampling methods, heat flux 70 kW/m ² , air flow 9 g/(m ² .s).....	- 144 -
Figure 4.52 % CO ₂ and H ₂ O emissions for tests with different sampling methods, heat flux 70 kW/m ² , air flow 9 g/(m ² .s).....	- 145 -
Figure 4.53 % THC and O ₂ emissions for tests with different sampling methods, heat flux 70 kW/m ² , air flow 9 g/(m ² .s).....	- 145 -
Figure 4.54 % CO comparison of x-probe holes facing up and down	- 147 -
Figure 4.55 Repeatability of the tests on cone calorimeter (a) MLR (g/s) (b) FTIR CO % (c) Raw O ₂ % (d) FTIR CO ₂ %	- 147 -
Figure 4.56 Superwool paper after the test#	- 149 -
Figure 4.57 Kaowool 20mm insulation (a) Before test (b) After test	- 150 -
Figure 4.58 draft extruder door sealant after the test	- 150 -
Figure 4.59 Emissions from used kaowool board.....	- 151 -
Figure 4.60 Emissions from superwool paper	- 151 -

Figure 4.61 Emissions from heated box	- 152 -
Figure 5.1 Variation of mass loss rate with time, air flow 19.2 g/(m ² .s)	- 157 -
Figure 5.2 Variation of mass loss rate with time for test at different flow rates	- 158 -
Figure 5.3 Variation of \emptyset_m with the air flow rate	- 159 -
Figure 5.4 Variation of experimental and predicted (equilibrium) CO concentration with \emptyset	- 159 -
Figure 5.5 % CO variation with time in different tests listed with steady state \emptyset_m ..	- 160 -
Figure 5.6 Variation of experimental % THC concentration with \emptyset_m	- 161 -
Figure 5.7 Variation of experimental and predicted (equilibrium) CO ₂ concentration with \emptyset	- 162 -
Figure 5.8 % CO ₂ against time in different tests listed with steady state \emptyset_m	- 162 -
Figure 5.9 Variation of experimental and predicted (equilibrium) H ₂ O concentration with \emptyset	- 163 -
Figure 5.10 % H ₂ O variations with time in different tests listed with steady state \emptyset_m	- 164 -
Figure 5.11 Variation of calculated and predicted (equilibrium) H ₂ concentration with \emptyset	- 164 -
Figure 5.12 Variation of experimental and predicted (equilibrium) CH ₄ concentration with \emptyset	- 165 -
Figure 5.13 CH ₄ concentration variation with time in different tests listed with steady state \emptyset_m	- 165 -
Figure 5.14 Temperature of the pine wood at two locations at air flow 19.2 g/(m ² .s), heat flux 70 kW/m ²	- 166 -
Figure 5.15 % O ₂ (dry basis) from the gasification zone at different equivalence ratios for pine wood	- 167 -
Figure 5.16 variation in the yields of gaseous products and Hot gas efficiency as a function of \emptyset_m	- 167 -
Figure 5.17 Hydrocarbon species emitted at $\emptyset_m = 2.8$	- 168 -
Figure 5.18 HGE as a function of \emptyset_m	- 169 -
Figure 5.19 Heating value as function of time for air flow 19.2 g/(m ² .s), $\emptyset_m = 2.8$..	- 170 -
Figure 5.20 Heating value proportion of hydrocarbon gases	- 170 -
Figure 5.21 Heating value as function of time (a) air flow 25.6 g/(m ² .s), $\emptyset_m = 2$ (b) air flow 31.6 g/(m ² .s), $\emptyset_m = 1.6$	- 172 -
Figure 5.22 Comparison of metred equivalence ratio \emptyset_m with emission based equivalence ratio \emptyset_e for pine wood tests	- 173 -
Figure 5.23 CO ₂ concentration as a function of time for ash wood at different moisture content	- 174 -
Figure 5.24 CO concentration as a function of time for ash wood at different moisture content	- 175 -

Figure 5.25 H ₂ concentration (calculated) as a function of time for ash wood at different moisture content	- 176 -
Figure 5.26 H ₂ O concentration as a function of time for ash wood at different moisture content	- 177 -
Figure 5.27 Heating value as a function of time for dry ash.....	- 177 -
Figure 5.28 Heating value as a function of time wet ash	- 178 -
Figure 5.29 mass vs time for different biomass at air flow 19.2 g/(m ² .s), heat flux 70 kW/m ²	- 179 -
Figure 5.30 MLR (g/s) vs time for different biomass at 19.2 g/(m ² .s), heat flux 70 kW/m ²	- 181 -
Figure 5.31 Metered equivalence ratio (\varnothing_m).....	- 182 -
Figure 5.32 % CO for tests with different biomass at air flow 19.2 (g/m ² .s)	- 183 -
Figure 5.33 % CO for tests with different biomass (a) for 5 biomass wood sticks, corn cons and china's biomass (B) biomass pellets (c) wood blocks.....	- 184 -
Figure 5.34 % CO ₂ for tests with different biomass at air flow 19.2 (g/m ² .s)	- 185 -
Figure 5.35 % H ₂ O for tests with different biomass at air flow 19.2 (g/m ² .s)	- 186 -
Figure 5.36 % H ₂ for tests with different biomass at air flow 19.2 (g/m ² .s).....	- 187 -
Figure 5.37 % THC for tests with different biomass at air flow 19.2 (g/m ² .s)	- 188 -
Figure 5.38 % CH ₄ for tests with different biomass at air flow 19.2 (g/m ² .s)	- 188 -
Figure 5.39 % C ₂ H ₂ for tests with different biomass at air flow 19.2 (g/m ² .s)	- 189 -
Figure 5.40 % C ₂ H ₄ for tests with different biomass at air flow 19.2 (g/m ² .s)	- 190 -
Figure 5.41 % C ₆ H ₆ for tests with different biomass at air flow 19.2 (g/m ² .s)	- 191 -
Figure 5.42 Elco (g/kg of biomass) for different biomass materials at air flow rate 19.2 (g/m ² .s)	- 191 -
Figure 5.43 % O ₂ dry for gasification of different biomasses at air flow rate 19.2 g/(m ² .s)	- 193 -
Figure 5.44 \varnothing_e for different biomass at air flow 19.2 g/(m ² .s)	- 194 -
Figure 5.45 comparison of mass loss from load cell with mass obtained from FTIR for the gasification of different biomasses at air flow 19.2 g/(m ² .s)	- 196 -
Figure 5.46 Higher heating values of gaseous products (MJ/kg of gases) for gasification of selected biomasses with time at air flow 19.2 g/(m ² .s)	- 199 -
Figure 6.1 TGA % volatile yield vs temperature for biomass samples	- 203 -
Figure 6.2 Mass loss over temperature range for pine wood from TGA analysis..	- 204 -
Figure 6.3 Percentage mass loss w.r.t. time for pyrolysis of pine wood.....	- 205 -
Figure 6.4 Temperature of pine wood (a) 3mm from top surface (b) 3mm from bottom surface	- 206 -
Figure 6.5 MLR (g/s) and average wood temperature w.r.t time for pine wood pyrolysis	- 206 -
Figure 6.6 Heating rate of pine wood pyrolysis at different heat flux.....	- 208 -

Figure 6.7 MLR vs temperature for pyrolysis tests at different heat flux.....	- 209 -
Figure 6.8 FTIR product gases concentration as a function of temperature for the of pyrolysis of pine wood at different heat flux	- 211 -
Figure 6.9 concentration vs time for o-xylene, m- xylene p-xylene, 1,2,3- trimethylbenzene, 1,2,4- trimethyl benzene, 1,3,5- trimethyl benzene.	- 214 -
Figure 6.10 Cumulative yields (g/g biomass) for pyrolysis of pine at 10 kW/m ²	- 215 -
Figure 6.11 Cumulative yields (g/g biomass) for pyrolysis of pine at 15 kW/m ²	- 215 -
Figure 6.12 Cumulative yields (g/g biomass) for pyrolysis of pine at 20 kW/m ²	- 216 -
Figure 6.13 Cumulative yields (g/g biomass) for pyrolysis of pine at 25 kW/m ²	- 216 -
Figure 6.14 Comparison of mass obtained from FTIR with mass loss of wood from load cell for the pyrolysis of pine wood at different heat fluxes	- 217 -
Figure 6.15 HHV of product of pyrolysis from pine wood at different heat flux	- 222 -
Figure 6.16 % yield of CO ₂ and H ₂ O from pyrolysis of pine wood at different heat flux...	- 223 -
Figure 6.17 % yield of CO and some hydrocarbons from pyrolysis of pine wood at different heat flux.....	- 226 -
Figure 6.18 % yield for liquids (at room temperature) , gases and chars for the pyrolysis of pine wood at different temperatures.....	- 227 -
Figure 6.19 Mass vs time for pyrolysis of biomass at heat flux 20 kW/m ²	- 228 -
Figure 6.20 Mass loss rate (g/s) vs time for pyrolysis of biomass at heat flux 20 kW/m ²	- 229 -
Figure 6.21 Product gases concentration recorded from FTIR as a function of time for the of pyrolysis of different biomass at heat flux 20 kW/m ²	- 231 -
Figure 6.22 comparison of cumulative yields of products of pyrolysis from different biomass at heat flux 20kW/m ²	- 235 -
Figure 6.23 yield of acids with pyrolysis of different biomass.....	- 242 -
Figure 6.24 Yield of alcohols with pyrolysis of different biomass	- 242 -
Figure 6.25 Yield of aldehydes with pyrolysis of different biomass	- 243 -
Figure 6.26 Yield of phenols and cresols of different biomass.....	- 243 -
Figure 6.27 Temperature of woods (a) 3mm from top surface (b) 3mm from bottom surface	- 244 -
Figure 6.28 Cone test mlr and TGA mass loss rate vs time for different wood types.	- 245 -
Figure 6.29 variation of mass loss rate and average temperature as a function of time.- 246 -	
Figure 6.30 Concentration vs avg. wood temp. for some gaseous products from the pyrolysis of different wood types at heat flux 20 kW/m ²	- 247 -
Figure 6.31 Comparison of mass obtained from FTIR with mass loss of biomass from load cell for the pyrolysis of different biomass at heat flux 20 kW/m ²	- 251 -

Figure 6.32 HHV of the products of pyrolysis of different biomass at heat flux 20 kW/m ²	- 253 -
Figure 7.1 Heating rate of pine wood pyrolysis inside the furnace reactor.....	- 257 -
Figure 7.2 Temperature profiles for the pyrolysis at selected temperatures	- 258 -
Figure 7.3 Selected specie concentration as a function of time.....	- 259 -
Figure 7.4 Specie concentration vs time for the pyrolysis of pine wood at different temperatures in furnace reactor	- 260 -
Figure 7.5 % yields of liquid vapour and char on dry basis for the pyrolysis of pine wood cubes and comparison with literature.....	- 262 -
Figure 7.6 % yields of CO ₂ and CO on dry basis.....	- 264 -
Figure 7.7 % yields of gaseous products from the pyrolysis of pine wood.....	- 264 -

List of tables

Table 1.1 RHI Tariff for non-domestic biomass boilers	6 -
Table 1.2 Electricity cost by fuel type in Pakistan (Rs./Kwh).....	10 -
Table 1.3 Yearly energy potential from the forests and wood lands of Pakistan	13 -
Table 1.4 Yearly energy potential from the oilseed residues of Pakistan.....	14 -
Table 1.5 Yearly energy potential from banana tree residues in Pakistan	15 -
Table 2.1 Characteristics of some pyrolysis processes	18 -
Table 2.2 List of reactions occurring inside a typical gasifier	20 -
Table 2.3 Product gas composition and heating values from gasification of biomass from different researchers and comparison.	34 -
Table 2.4 cellulose/Lignin content of some biomass	40 -
Table 2.5 Comparison of gaseous products yield from the pyrolysis of biomass reported in the literature	50 -
Table 2.6 Comparison of condensable products yield from the pyrolysis of biomass reported in the literature	53 -
Table 3.1 Concentration ranges and number of data points for the FTIR calibration.	78 -
Table 4.1 Elemental analysis , proximate analysis, CV and stoichiometric air to fuel ratio for biomass studied.	96 -
Table 4.2 Particle size, density, hemicellulose, cellulose and lignin contents for different biomass studied.....	98 -
Table 4.3 Conditions for the tests performed.....	109 -
Table 4.4 Summary of test results for the main flaming rich combustion phase for the gasification zone and comparison with equilibrium	122 -
Table 5.1 Conditions of air flow for the tests.....	155 -
Table 5.2 Ultimate and proximate analysis of biomass gasification char samples	171 -
Table 6.1 Elemental, proximate analysis and CV of char/residue left after pyrolysis of pine wood at different heat flux.....	220 -
Table 6.2 Elemental balance for pine wood pyrolysis (as received basis)	221 -
Table 6.3 Energy balance for the pyrolysis of pine wood at different heat fluxes ..	224 -
Table 6.4 % Yields of selected components from the pyrolysis of pine wood at different heat flux. (dry basis)	225 -
Table 6.5 Yields (g/g dry biomass) of the some products of pyrolysis of different biomass at heat flux 20 kW/m ²	239 -
Table 6.6 Top and avg. temp. corresponding to the release of products of pyrolysis and comparison with literature.....	248 -
Table 6.7 Overall mass balance for the pyrolysis tests on cone calorimeter.....	250 -

Abbreviations & symbols

Abbreviations:

AEDB	=	Alternative Energy Development Board	
A/F	=	Air to fuel ratio	
CEA	=	Chemical equilibrium with applications	
CHP	=	Combined Heat and Power	
DECC	=	Department of Energy and Climate Change	
EI	=	Emission Index	
EBER	=	Emission based equivalence ratio	
FAO	=	Forest and Agricultural Organization	
FC	=	Fixed carbon	
GCV	=	Gross calorific value of fuel	MJ/kg
GHG	=	Green house gases	
FTIR	=	Fourier Transform Infar-red spectroscopy	
HETAS	=	Heating equipment testing and approval scheme	
HGE	=	Hot gas efficiency	
HHV	=	Higher heating value	MJ/m ³
HRR	=	Heat release rate	kW/m ²
IGCC	=	Integrated gasification combined cycle	
LHV	=	Lower heating value	MJ/m ³
MCS	=	Microgeneration certification scheme	
MFR	=	Mass flow rate	g/s
MLR	=	Mass loss rate	g/s
NDIR	=	Non-Dispersive Infra-red	
NEPRA	=	National electric power regulatory authority	
PHRR	=	Primary heat release rate	kW/m ²

RHI	=	Renewable heat incentive	
SHRR	=	Secondary heat release rate	kW/m ²
TCD	=	Thermal conductivity detector	
TGA	=	Thermo-gravimetric analysis	
VM	=	Volatile matter	

Symbols:

λ	=	Air factor	
\emptyset	=	Equivalence ratio	
\dot{q}	=	Heat release rate	KJ/s
p_{CO}	=	Carbon monoxide concentration	%
Δh_c	=	Net heat of combustion	kJ/g
r_o	=	Stoichiometric oxygen to fuel mass ratio	
\dot{m}_{O_2}	=	Mass flow rate of oxygen	g/s
\dot{m}_a	=	Mass flow rate of inlet (ambient) air	g/s
\dot{m}_e	=	Mass flow rate of exhaust	g/s
$Y_{O_2}^a$	=	Mass fraction of oxygen in ambient air	
$Y_{O_2}^e$	=	Mass fraction of oxygen in combustion products	

Chapter 1 Introduction

In this chapter the importance of biomass as an alternative energy source to fossil fuels is discussed. The contribution to UK energy needs, particularly through the use of biomass boilers, is discussed and thermochemical conversion routes of biomass are reviewed. As this project is sponsored by the Govt. of Pakistan, particular reference is made to Pakistani energy crisis and estimates are made on the potential of electricity generation via gasification route from different biomass sources in Pakistan (Including forest, banana tree waste, and oil seed residue).

1.1 Energy sources and greenhouse gas emissions

There are three major categories of energy sources: Fossil fuels, renewable sources and nuclear sources. Biomass was the first energy source known to mankind from thousands of years that got replaced by fossil fuels with the passage of time. Fossil fuels account for 81.5% of the primary energy consumed in the world in 2016 [1]. Global warming is due to greenhouse effect, where water vapour, CO₂, methane (CH₄) and nitrous oxide (N₂O), act to absorb infrared radiation leaving the earth and hence act as an insulation blanket that has warmed the earth. The globally average combined land and ocean surface temperature calculated by linear trend shows a rise of 0.85 °C from 1880 to 2012, mainly due to human activity [2]. Fossil fuels are the dominant source of greenhouse gases (GHG) today, particularly for CO₂ which is a dominant GHG. In 2011 CO₂ emissions sourced from fossil fuels combustion, cement industry, flaring, forestry and other land use were 31.5 Gt, which have been estimated to increase from 37.2 to 43.1 Gt in 2035 [3].

Based on these facts that global warming is existing and its major cause is human made CO₂ emissions, an international binding agreement under United Nations was made, known as Kyoto Protocol that commits state parties to reduce the emissions and set reduction targets. Kyoto Protocol has two commitment

periods, one from 2008 to 2012 in which it was decided to reduce GHG's emissions to at least an average value of 5% below 1990's level. In the second amendment, it was committed to reduce GHG's emissions by 18% below 1990's level in period from 2018 to 2020 [4]. The Paris Agreement is an agreement within the United Nations Framework Convention on Climate Change (UNFCCC) that brings all nations into a common cause to undertake ambitious efforts to combat climate change and adapt to its effects, with enhanced support to assist developing countries to do so. On November 2017, 195 UNFCCC members have signed the agreement, and 170 have become party to it. The agreement aims to respond to the global climate change threat by keeping a global temperature rise this century well below 2 degrees celsius above pre-industrial levels and to pursue efforts to limit the temperature increase even further to 1.5 degrees Celsius [5].

Other gases released by fossil fuels are SO_x and NO_x . They cause acid rain and NO_x also is a key chemical in ozone formation in the atmosphere, so NO_x have a key role in the formation of ground level ozone and photochemical smog.

At present energy consumption rates, world oil and gas reserves are estimated to last well beyond 2050, and coal is available to the end of this century [6]. An energy substitute for the fossil fuels is required with the depletion of these reserves and in this regard biofuels are becoming more important.

1.2 Biomass as energy

Bioenergy is the largest renewable energy resource today, 14% out of total 18% renewables in the world energy mix. Bioenergy supplies 10% of the global energy supply [7]. Biomass is said to be carbon neutral and it releases heat and carbon dioxide during combustion that was stored during its growth. Combustion is the reverse process of photosynthesis. It provides carbon from biosphere rather than long term storage as in the case of fossil fuels, so it is a renewable energy source [8].

The main components of biomass are cellulose, hemicelluloses and lignin. In biomass, cellulose is most abundant 40-60%, followed by hemicellulose 20-40% and then lignin 10-25% [9]. Due to different classes of biomass and different

types of growing conditions, the composition of these components differs in each biomass.

Major elements present in biomass are carbon, oxygen and hydrogen. Biomass has more oxygen as compared to fossil fuels, typically 30- 40% on dry basis and this is the reason for its lower calorific value. Carbon is the major constituent of biomass and is present in the range 30-60% on dry basis. Hydrogen ranges from 5 to 6%. Other elements are N, S and Cl which are usually present at less than 1% , in most biomasses, but this can exceed 1% on dry basis if the biomass is derived from agriculture where N based fertilisers are used or high S in waste wood from wood preservatives [10].

In comparison to coal, Biomass has high amount of oxygen and hydrogen as shown in the Van Krevelen diagram in Figure 1.1. Also biomass has high volatiles as compared to coal that make them very reactive [10].

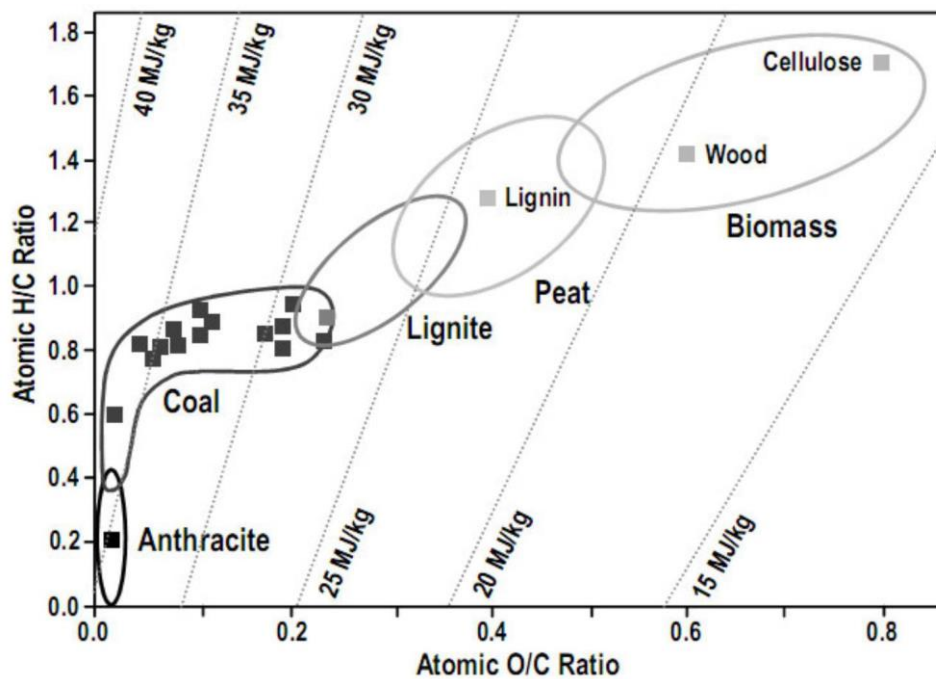


Figure 1.1: H/C v. O/C plots for wood in comparison to different types of coal

1.3 UK energy situation

In the UK, in 2015, bioenergy accounts 71% of the total renewable energy sources used for electricity, heat and transport sector. As shown in the Figure 1.2.

Figure 1.3 shows the share of different fuel types to the electricity supplied in UK in 2014 and 2015. It shows that electricity supplied from coal fell from 28% to 21% due to plant closures and conversions, including a conversion of a third unit at Drax from coal to high-range co-firing. 7.2 % of the total electricity of UK was generated from bioenergy that was 30% of the total electricity from renewable sources. Bioenergy for the production of electricity mostly came from plant biomass that is 25.3% of total bioenergy [11].

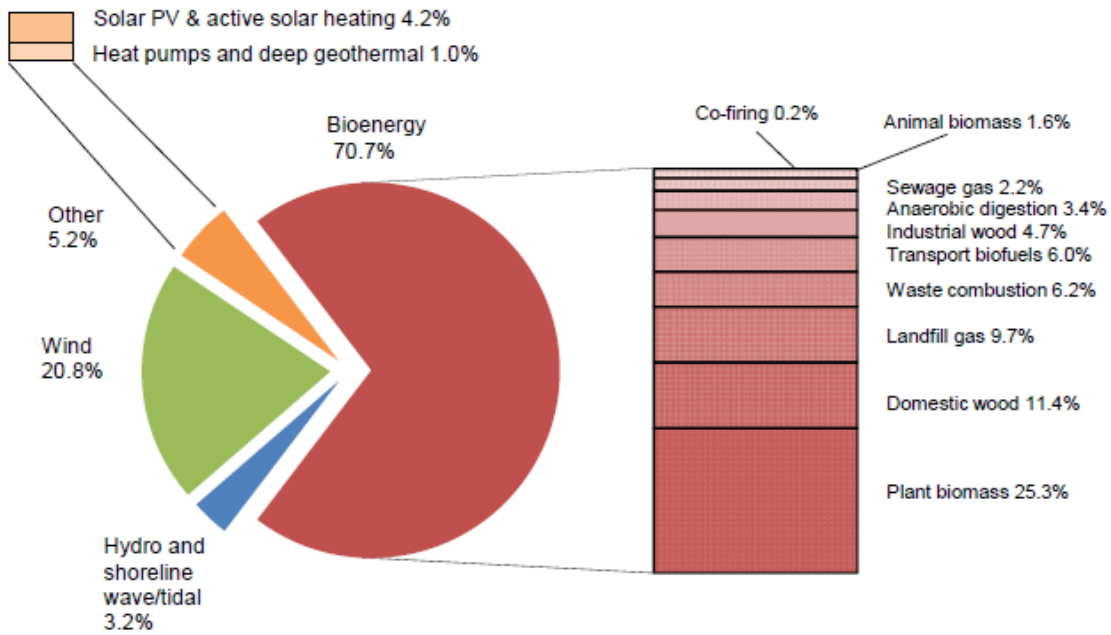


Figure 1.2 Renewable energy sources of UK in 2015 [12]

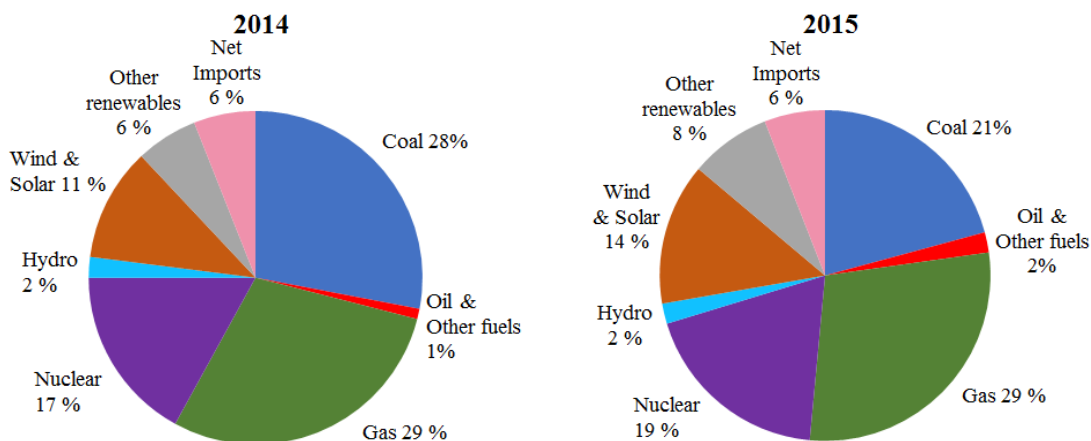


Figure 1.3 Fuel sources for electricity generation in UK in 2014 & 2015 [12]

In 2015, heat energy from renewables increased by 20% as compared to 2014 while 86% of this additional heat energy was generated from wood combustion of domestic and industrial wood. Domestic wood is 11.4% & industrial was 4.7% of total bioenergy. Of this additional 20%, Around 11 per cent of renewable heat was supported by The Renewable Heat Incentive (RHI) [11].

1.4 Renewable heat incentive scheme UK

The Renewable Heat Incentive (RHI) is a UK Government funded scheme for the encouragement of the renewable technologies. This was started by the introduction of the Climate Change Act of 2008 to reduce UK's greenhouse gas emissions upto 80% of 1990's levels by 2050 [13]. This scheme is supported by (office of gas and electricity markets) ofgem.

The scheme is guaranteed for 20 years for non-domestic applicants and 7 years for domestic applicants who wish to replace their heating system with a supported renewable heat technology. This scheme was launched in 2011/2012.

Renewable technologies for domestic application include, biomass boilers, solar water heating and certain heat pumps, while for non-domestic includes technology for biomass, heat pumps, deep geothermal, Solar thermal collectors, biomethane and biogas, Combined heat and power (CHP) system.

Air Quality standards for RHI non-domestic as well as domestic scheme requires that emission from biomass boilers do not exceed a 30 g/GJ for particulate matter and 150 g/GJ for oxides of nitrogen, NO_x (expressed as NO_2), if they are eligible for RHI payments. Renewable heat incentive for the domestic scheme requires that the installation and the appliance for small to medium sized plants (upto and including 45 kW) to be certified under Microgeneration Certification Scheme (MCS) or equivalent standards.

Table 1.1 RHI Tariff for non-domestic biomass boilers

Tariff Name	Eligible Technology	Eligible Sizes	Tier	Tariffs applicable from 1st April 2017 (p/kWh)
Small Commercial Biomass	Solid biomass including solid biomass contained in waste	Less than 200kW	Tier 1	2.85
Medium Commercial Biomass			Tier 2	0.75
Large Commercial Biomass		200 kW and above; less than 1M	Tier 1	5.24
			Tier 2	2.27
		1MW and above	N/A	2.05

Tariff from 1st April 2017 for the domestic biomass boilers and stoves is 4.28 p/KWh, and for non-domestic is provided in the Table 1.1.

1.5 Biomass to energy conversion processes

Energy from biomass can be obtained by different conversion processes depending on the type of feed stock, desired energy requirements means end use and the environmental impacts. Two major categories of conversion processes are biological and thermal.

1.5.1 Biological/biochemical processes

Biological processes include fermentation and anaerobic digestion. Fermentation is used mainly for the production of ethanol. While in the anaerobic digestion, using the bacteria in the absence of air, biogas composed of methane and carbon dioxide is produced. In these processes biomass with the high moisture content is preferred. However, in both processes the product only has part of the energy in the original biomass.

1.5.2 Thermochemical processes

Thermochemical processes comprise of Combustion, Gasification and pyrolysis [14].

1.5.2.1 Combustion

In combustion, biomass is burnt completely in the air and all its energy content is turned into hot gas for the downstream heating purposes. Thermal energy produced from the biomass can be used for heating or electricity production. Efficiency of combustion plants range from 90%+ for water heating and 20-40% for steam generation followed by steam turbine electric power generation [14]. Any type of biomass can be burnt but moisture content should be less than 50% otherwise energy is wasted for boiling water in the biomass and pre-drying of biomass using solar energy is preferable.

1.5.2.2 Gasification

Gasification is a well-known thermochemical process that converts a solid fuel (usually biomass or coal) into a combustible gaseous product (syngas) through partial oxidation, using a gasifying agent in sub stoichiometric conditions [15]. Product gas (syngas) has a low calorific value 4-6 (MJ/m³) if air is used in the gasifier, higher CV can be achieved in oxygen blown gasifiers but this is not the object of the present work. Some solid products like char and ash and some condensable products like tars are also obtained as a result of gasification. Syngas can be used as a fuel for the purpose of direct combustion or fuel for gas engines or gas turbines to produce electricity, or as feedstock to produce chemicals like methanol. Overall efficiency of 30-60 MW plant for producing electricity using gases in turbines is 40- 50% [14]. However, it must be recognised that all small scale (<~50MW) biomass thermal plants operate with staged combustion using gasification in the primary stage and secondary air added for the second stage combustion. The vast majority of work on gasification has not been carried out to optimise this thermal heating process, but as part of gas turbine or gas engine use of the gas from the gasifier.

1.5.2.3 Pyrolysis

Pyrolysis is heating of biomass in the absence of air. Pyrolysis yields liquid, solid (charcoal) and gaseous products. Liquid product is bio oil and it can be attained with maximum efficiency of 80% with flash pyrolysis. Bio oil can run engines and turbine. Bio-oil and tars is undesirable in gasification burners as they can lead to

carbonaceous deposits on combustion heat transfer surfaces. They can occur through inefficiencies in the gasification process.

1.6 Torrefaction

Biomass has some inferior properties compared to the coal: low energy density, high moisture contents, hygroscopic nature, fibrous nature that makes size reduction to the homogenous particles difficult and high O/C ratio [16]. Torrefaction is a mild pyrolysis in the absence of oxygen in the temperature range of 200- 300 °C. Between these temperatures, the wood hemicellulose fraction is decomposed and torrefied wood and volatiles are formed [17]. Torrefaction yields a solid uniform product with reduced volatiles and moisture. Torrefied biomass retains 40 -80% of original mass and 80-90% of energy of biomass causing an increase in energy density. The equilibrium moisture content of torrefied biomass is reduced to typically 3%, but this depends on the conditions of torrefaction. Torrefaction causes a reduction in the O/C ratio and is better suited for gasification [18].

1.7 Energy crisis in Pakistan

Pakistan is facing a serious problem of energy shortage over many years. Pakistan is a developing Asian country with total population about 182 million and over 30% of population (more than 55 million people) have no access to electricity [3]. Of those who have access to electricity, the problem of load shedding (deliberate periodic shutdowns) is causing serious frustration. The supply and demand gap has exceeded 6 GW in peak loads in 2015. This gap caused a load shedding of 6-12 hrs in urban and 12-18 hrs in the rural areas [19].

According to the official statistics, the total production potential of energy in Pakistan was 94.65 billion KWh in 2014 whereas energy consumption was 70.1 billion KWh [20]. However, this electricity consumption is that paid for and not the real used electricity. At times of peak demand, there is insufficient supply of electricity, also losses of 30-40% are observed due to poor transmission and distribution system as well as electricity theft [19].

Pakistan generates more than 60% of its electricity from oil and gas (fossil fuels), as shown in Figure 1.4 [21]. Pakistan has limited crude fuel oil resources and a large amount of fuel oil is being imported. During July 2016, 4.98 million metric tons of crude oil was imported compared to 4.81 million tons of the corresponding period last year showing a growth of 3.5 percent, 42% of this crude oil was utilized for power generation [22].

Table 1.2 shows the electricity unit cost by fuel type and it clearly shows that most expensive electricity is generated from High Speed diesel (HSD) and residual fuel oil (RFO), making the unit price of electricity very high. Although the reduction in the international prices of crude oil reduced the price of electricity in year 2014-2015 but still it the most expensive option.

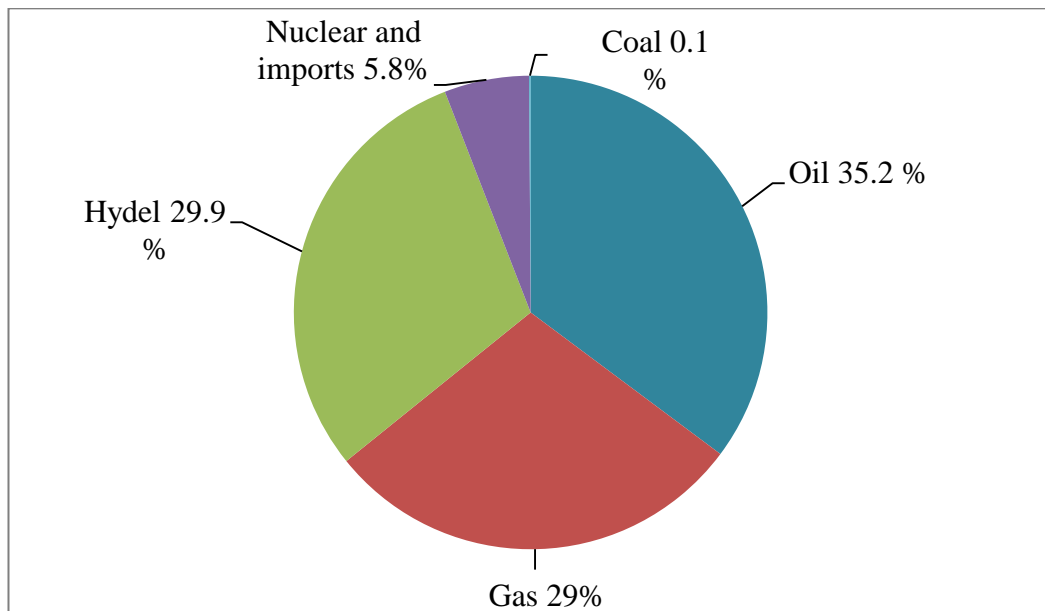


Figure 1.4 Fuel sources for electricity generation in Pakistan in 2012 [21]

The electricity supply shortfall is worst in winter when hydro plants start losing capacity due to the freezing temperature of hydro reservoirs. This leads to a demand for more electricity from gas plants to balance the gap between supply and demand. In summer the high consumption of electricity due to the use of air conditioners in the hot humid climate, compels the government to import large amounts of furnace oil for the diesel electric power generation.

Table 1.2 Electricity cost by fuel type in Pakistan (Rs./Kwh) [19]

Period	Hydel	HSD	RFO	Gas	Nuclear	Imports	Average Unit Price
2013-2014	-	21.85	15.97	4.81	1.32	9.35	10.59
2014-2015	-	17.14	12.54	4.81	1.19	10.03	9.84

This cost is not affordable for the Government and the import cost of the furnace oil destabilizes the economy. Industrial investors are not willing to invest in factories in Pakistan as the electric power supply cannot be guaranteed. About 40% of the local textile industry has shifted to Bangladesh [23, 24].

Furthermore, depletion of the total proved reserves of the gas in Pakistan is expected in 12 years and coal reserves are for more than 500 years at the end of 2015 with current rate of use and production. But coal in Pakistan is not anthracite and bituminous, it is low quality sub bituminous and lignite. [6]

1.8 Energy potential from biomass in Pakistan

Biomass has an important potential contribution in the primary energy mix of Pakistan. The country produces a significant amount of biomass in the form of crop residues and animal waste for example bagasse, rice husk, and dung etc. Much of the residue and dung is collected and used as unprocessed fuel by households of rural areas for heating and cooking by direct combustion. These biomass fuels, along with wood contribute to about 36% of the total primary energy mix [25]. The Alternative Energy Development Board (AEDB) was formed by the Ministry of Water and Power of Pakistan and this is developing strategies, policies and plans for the utilization of biomass resources to achieve targets approved by Government.

AEDB [26] has estimated the energy potential from the residues of five major crops (i.e. wheat, cotton, rice, sugarcane and maize), based on the existing uses of the residues, the technical potential of crop harvesting residues was estimated at about 25.1 million tonnes/year (96,890 GWh/year of thermal energy). In case

of farmers' willingness to sell their biomass residues, the technical potential of crop harvesting residues decreases to about 20.5 million tonnes/year (79,250 GWh/year of thermal energy). The total installed power capacity of the cogeneration plants using bagasse generated from the 86 existing sugar mills in Pakistan is estimated at about 1,840 MWe [26].

1.9 Woody (forestry) resource of Pakistan

Pakistan has poor forest resources, it is not possible to meet the growing demands for timber, fuel wood and wood based products with the existing forest cover. The current forest area is roughly 5 % of total land area including farmland trees. Only 10% of fuelwood requirements are met from state forests and plantations. 90% of the remaining requirement is met from farm trees [27]. Introduction of fast growing trees on short rotation basis in the farmland and irrigated plantations can enhance wood production. Trees are planted on farmlands as boundary markers of farms, many trees can be accommodated in between, as currently the system is unplanned.

The private farmland plantations are currently contributing four times as much of the timber and nine times as much of the fuel wood that are being produced by state forests [28]. It is further estimated that farmers can increase 8 to 10% trees cover by planting along farm boundaries without affecting the annual crop yield [29]. Farmlands also have the highest potential for enhancing the production of wood through various agroforestry practices. The cultivated area in Pakistan constitutes more than 20% of the land area. Agroforestry is a traditional method of combining trees with agricultural crops. If 20 trees on a short rotation of 5-10 years per hectare (0.01 km²) are added through a suitable agroforestry system an additional of 26 million m³ of fuelwood per year has been estimated [30].

The forest area of Pakistan has been estimated by the Food and Agricultural Organization of United Nations (FAO) in 2010 as 16,870 km² which is 2.19 % of the total land area (770,880 km²) of Pakistan. Other wooded land estimated by FAO was 14,550 km², which is 1.88 % of the total land area of Pakistan [31]. The forest area of Pakistan includes coniferous and non-coniferous forests while scrub forests fall in the category of other wooded land. Linear plantations, farmland trees and miscellaneous plantations are categorized as other land

which contributes further 1% to the total land area of Pakistan. The contribution of total tree area towards the total land area of Pakistan is 5.1 %. Categories of forests and the total tree area of Pakistan are provided in Table 1.3.

1.9.1 Sustainability and tree rotation period for forests in Pakistan

The rotation period of an even age stand of tree is the period between the plantation and a time when that stand becomes ready to be cut. This period, usually called the "optimum" rotation period, becomes important when a forester tries to determine the most beneficial harvest conditions. The rotation period is usually reached when a stand is economically mature or growing beyond natural maturity.

The Pakistan Forest Institute in Peshawar has undertaken a study [32] on the rotation and economic management of the coniferous forests of Pakistan. It was found that the financially best rotation period ranged between 50-70 years. Studies suggests that if a longer rotation period is employed, the process becomes uneconomic and valuable resources are underutilised. The study suggested a period of 50 years over which all over mature trees are cut down and a new system of management introduced [32]. Using a rotation period of 50 years the forest may be sustainably used if 2% of the forest is cut down annually, along with the plantation of 2% new forest trees.

The most common trees in the irrigated plantations and other land include *Eucalyptus camaldulensis*, *Dalbergia sissoo*, *Bombax ceiba*, *Populus deltoids* and *Acacia nilotica* [31]. The optimum rotation period for these trees have been found to be 10 years for *Eucalyptus camaldulensis* [32], 22 years for *Dalbergia sissoo* [33], 15 years for *Bombax ceiba* [29], 10 years for *Populus deltoids* and 9-14 years for *Acacia nilotica* [34].

An average rotation period for trees in irrigated plantations as well as for trees in the other land is about 15 years, which allows 6.5% of the forest to be harvested annually provided the equivalent number of trees are planted annually.

1.9.2 Growing stock in the different forests

Food and Agricultural Organization of United Nations FAO [31] defines growing

stock as the “Volume over bark of all living trees more than 4 cm in diameter at breast height (or above buttress if these are higher). This includes the stem from ground level or stump height up to a top diameter of 1 cm, and may also include branches to a minimum diameter of 5 cm” [31]. Growing stock for coniferous forests as well as non-coniferous forest as reported by FAO is given in the Table 6. Total growing stock for the other land has been estimated to be 97 million m³ [27].

Table 1.3 Yearly energy potential from the forests and wood lands of Pakistan [27, 31]

Category	Area km ²	Growing stock m ³ /km ²	Growing stock (x10 ⁶) m ³	Growing stock (x10 ⁹) kg	Annual cutting rate %	Annual cutting rate of total growing stock (x10 ⁹) kg/y	
Coniferous Forests	11,110	12380	137.5	96.3	2	1.93	
Non-Coniferous forest	Riverain forest, Mangrove forest	2,360	3900	9.2	6.4	2	0.13
	Irrigated plantations	3,400	3900	13.3	9.3	6.5	0.60
Other wood land (Scrub forest)	14,550	3900	56.7	39.7	2	0.79	
Other land (Linear plantations, farmlands, misc. plantations)	7,980	-	97.0	67.9	6.5	4.4	
Total	39,400		314	220		7.87	
Heating value of green wood with moisture contents 50% 'MJ/kg'						9.5	
Total energy contents from wood per year 'GJ/y'						74.74 x10 ⁶	
Total energy obtained 'GWh/y'						2.08 x10 ⁴	
With 32% efficiency 'GWh/y'						6650	
Total average requirement in Pakistan in 2014 'GWh/y'						7.0x10 ⁴	
Contribution of wood towards annual consumption of electricity						9.5 %	

Wood density used for the calculations is taken to be 700 kg/m³ as is used by FAO. The conversion efficiency of a gasification plant is taken to be 32% [35, 36]. The calculations in Table 1.3 show that the total energy potentially obtainable from wood is 6650 GWh/y, which would contribute 9.5% towards the annular electricity demand of Pakistan.

1.10 Estimation of energy from oil seed residues in Pakistan

The major oilseed crops grown in the Pakistan include Sunflower, Canola, Cottonseed and Rapeseed/ Mustard. Although the cotton crop is grown for its lint, cottonseed contributes 50 to 60 % of local edible oil production [37].

In Pakistan oil seed extraction is done by oil expellers (traditional kohlus), low and high pressure expellers and solvent extraction plants. Oil expellers (kohlus) are used for the extraction of oil from rapeseed and mustard and these are located in the villages [38]. Extraction of cotton seed oil and sunflower seed oil is done by low and high pressure expellers. The residue from this process is then exposed to a solvent for further oil extraction [39].

The quantities of oil seed crop residues in Pakistan and the energy contents of these residues are summarised in Table 1.4.[37, 40-44]

Table 1.4 Yearly energy potential from the oilseed residues of Pakistan

Crops	Seeds production (x10 ⁶) kg	Oil production (x10 ⁶) kg	Seed waste (x10 ⁶) kg	Residue type	Residue production (x10 ⁶) kg	Calorific value 'MJ/Kg'	Heat (x10 ⁶) MJ
Cotton seed	3592	431	3161	Cake	1006	20.8	20920.64
				Hull	2155	17.5	37716.00
Rapeseed / Mustard	218	68	150	Cake	150	20	3000.00
Sunflower	265	101	164	Cake	131	15.8	2072.96
				Hull	33	17.6	577.28
Canola	16	6	10		10	23.6	236.00
Total heat contents of the four major biomass residues 'GJ/y'							64.5 x10 ⁶
Total energy obtained 'GWh/y'							17.92 x10 ³
With 32% Efficiency 'GWh/y'							5734
Contribution of oil seeds residue towards annual consumption of electricity							8.2 %

Cotton seed and sunflower seed residues consist of hulls and cakes, while mustard, rapeseed and canola seeds residues consist of compressed cake. Cotton seeds hull is 37-60% of the total weight of the seed depending upon the type of the seeds [45], while sunflower hull makes 18-20 % by weight of the

processed seed [46]. Table 1.4 shows that oilseed crop residue have the potential to generate 8.2% of the annual electricity demand in Pakistan.

1.11 Estimation of energy obtained from banana tree waste in Pakistan

In Pakistan banana cultivation started after independence. The major banana producing area is Sindh province and 90% of bananas in Pakistan comes from this province [47]. The banana plant has a large residue after that banana crop has been picked with 100% of the waste burnt in the field. Banana plants are cut every four months and thrown into the field side or along the road side. When they are dry they are burnt with no use of the energy released [48]. Table 1.5 summarises the energy potential of banana tree waste in Pakistan.

Table 1.5 Yearly energy potential from banana tree residues in Pakistan

Area Km ²	No of banana tree per Km ²	Frequency of cutting per year	Weight of air dried banana tree Kg	Total banana tree waste (x10 ⁶) Kg/y	Calorific value 'MJ/kg'	Energy content from banana tree waste (x10 ⁶) MJ/y
296 [49]	173000	3	7 [48]	1075	17.8 [50]	1908
Total heat contents from banana tree residue 'GWh/y'						5300
With 32% efficiency 'GWh/y'						1696
Contribution of banana tree residue towards annual consumption of electricity						2.4 %

So it its seen that 20% of the annual electricity demand can be fulfilled using forest, oil seed residues and banana tree wastes.

We have shown [24] that residue from the 4 major crops (rice, wheat, sugarcane and maize/corn) have the potential to generate 56% of annual electricity demand in Pakistan using 35% collection efficiency of those waste resources and 30% electrical generator efficiency.

In a similar way it is possible for the small biomass based plants to provide heating and hot water for domestic, neighbourhood, communal apartment blocks, and small industrial units. As will be shown in Chapter 2 the technology

for such units is already advanced but there is still room for significant improvement by optimising the primary (gasification) stage of these appliances- this is one of the main objectives of this study. This is directly relevant to both developing countries such a Pakistan but also for more developed nations, such as the UK.

Chapter 2 Literature review

2.1 Theory of gasification

The following physiochemical processes occur in a typical gasifier, within the temperature ranges indicated in brackets.

1. Drying ($> 150\text{ }^{\circ}\text{C}$)
2. Pyrolysis (Thermal decomposition) ($150\text{-}700\text{ }^{\circ}\text{C}$)
3. Reduction (Gasification) ($800\text{-}1100\text{ }^{\circ}\text{C}$)
4. Combustion ($700\text{-}1500\text{ }^{\circ}\text{C}$)

Processes 1, 2 and 3 are endothermic while process 4 is exothermic which provides heat for rest three processes [51].

2.1.1 Drying

Different biomasses have different moisture contents, for example freshly cut wood contains 30 to 60% moisture content while in most of the gasifiers biomass usually with 10-20% moisture is used. For the vaporization of every kg of moisture 2260 kJ of energy is utilized. For this purpose biomass is dried before gasification usually relying on natural processes. Final drying occurs by receiving heat from the hot zone when feed is introduced into the gasifier. Loosely bound water in biomass is removed above $100\text{ }^{\circ}\text{C}$. [52].

2.1.2 Pyrolysis

Heating of feed in the absence of air or oxygen is called Pyrolysis. Pyrolysis cause the thermal breakdown of the larger hydrocarbon molecules into the smaller molecules. A series of complex physical and chemical process occur during devolatilisation or pyrolysis process. The rate of heating of the biomass effects the yield and composition of the products. Rapid heating to a moderate temperature ($400\text{-}600\text{ }^{\circ}\text{C}$) yields higher volatiles and more liquids, slower heating to the same temperature produces more char [53]. The residence time of product

gases in the reactor also affects the composition. Characteristics of some pyrolysis process is given in the Table 2.1. Pyrolysis process starts from 130 °C – 150 °C. Pyrolysis of hemicellulose occurs from 150-350 °C, cellulose pyrolysis occurs from 275- 350 °C and lignin pyrolysis occurs from 250 -500 °C [9, 51, 52, 54].

Products of pyrolysis are classified as

1. Solid (char or carbon)
2. Liquids (Tars and heavier hydrocarbons)
3. Gases (CO, H₂, CO₂, H₂O, CH₄, C₂H₂, C₂H₄ etc.)

Table 2.1 Characteristics of some pyrolysis processes [52, 55]

Pyrolysis process	Residence time	Heating rate	Final temperature (°C)	Aim products
Carbonization	Days	Very low	400	Charcoal
Conventional	5-30 min	Low	600	Char, Bio-oil, Gas
Fast	< 2 s	Very High	~ 500	Bio oil
Flash	<1 s	High	< 650	Bio-oil, Gas

It is clear that the conditions under which pyrolysis occurs strongly determine the product type and yield and hence this is a critical area which controls the efficiency of the biomass combustion systems depending on the specific application. This work focuses on the pyrolysis and gasification conditions and processes with the aim optimising these for the use of biomass in small heating plant.

2.1.3 Gasification

Gasification involves a series of endothermic reactions supported by the heat produced from the combustion step. The gasification stage is called reduction stage where reactions occur between product gases and char produced from the

pyrolysis. Char produced through pyrolysis of biomass is not pure carbon. It contains certain amount of hydrocarbons. Biomass char is generally more porous (40 – 50%) and more reactive than coal char (2-18%) [56]. Typical reactions of this stage are listed in the Table 2.2.

The rate of gasification of char depends on its reactivity and the gasifying medium.

2.1.3.1 Gasifying agents

Common gasifying agents are air and steam, pure O₂ and CO₂ or mixtures of all can be used as gasifying agents. Although air is cheapest and most commonly used yet it contains 79% by volume of N₂ that reduces the heating value of product gases. When pure O₂ is used as gasifying agent, heating value of product gases improves but O₂ production demands high operating costs [57]. Hydrogen content and heating value of product gases improves to a large extent if steam is used as a gasifying medium, heating value of gases in this case has been reported to be about 10-15 MJ/m³ [58, 59]. Without steam heating value is reported to be 3-6 MJ/m³ [60].

The use of CO₂ as gasifying medium is promising because of its presence in the product gases. It can convert char, tars, and hydrocarbon gases into H₂ and CO especially if some catalyst is present like Ni/Al. CO₂ gasification in the presence of a catalyst transformed tars and also causes a decrease of the amounts of CH₄ and C₂-fraction (C₂H₂, C₂H₄, C₂H₆) as well as an increase in H₂ and CO yields. Examples are given by reaction R7 and R8.

The catalyst also improves the reaction rate of steam with the char and also can participate in secondary reactions, thus leading to decrease in tar content of the gas. The high H₂ production during steam gasification can be attributed by the reactions R2, R3 and R5.

Rate of Char-Oxygen reaction R10 is the fastest among the four reactions R1, R2, R4 and R11. The rate of char- steam reaction or steam gasification of carbon R2 is three to five orders of magnitude slower than that of char-oxygen reaction R10.

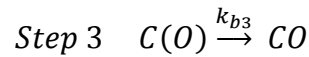
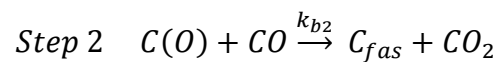
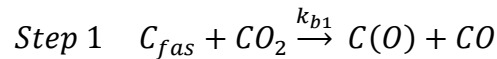
Table 2.2 List of reactions occurring inside a typical gasifier

No.	Reaction	Energy (+ is endothermic)	Reaction name
R1	$C + CO_2 \leftrightarrow 2CO$	$\Delta H_r = +172 \frac{kJ}{mol}$	Boudouard Reaction
R2	$C + H_2O \leftrightarrow H_2 + CO$	$\Delta H_r = +131 \frac{kJ}{mol}$	Steam gasification of carbon
R3	$CO + H_2O \leftrightarrow CO_2 + H_2$	$\Delta H_r = -41.2 \frac{kJ}{mol}$	Water-Gas Shift Conversion
R4	$C + 2H_2 \leftrightarrow CH_4$	$\Delta H_r = -75 \frac{kJ}{mol}$	Carbon Hydrogenation / Methanation/ Hydrogasification
R5	$CH_4 + H_2O \leftrightarrow CO + 3H_2$	$\Delta H_r = +206 \frac{kJ}{mol}$	Steam Reforming/ Inverse methanation reaction
R6	$2CO + 2H_2 \leftrightarrow CH_4 + CO_2$	$\Delta H_r = -247 \frac{kJ}{mol}$	Methanation Reaction
R7	$CO_2 + 4H_2 \leftrightarrow CH_4 + 2H_2O$	$\Delta H_r = -165 \frac{kJ}{mol}$	Methanation Reaction
R8	$CH_4 + CO_2 \leftrightarrow 2H_2 + 2CO$	$\Delta H_r = +246.98 \frac{kJ}{mol}$	CO ₂ reforming with methane
R9	$C_2H_4 + 2CO_2 \leftrightarrow 2H_2 + 4CO$	$\Delta H_r = +292.41 \frac{kJ}{mol}$	
Oxidation Reactions			
R10	$C + O_2 \rightarrow CO_2$	$\Delta H_r = -394 \frac{kJ}{mol}$	Char-oxygen reaction
R11	$C + \frac{1}{2}O_2 \rightarrow CO$	$\Delta H_r = -111 \frac{kJ}{mol}$	
R12	$CO + \frac{1}{2}O_2 \rightarrow CO_2$	$\Delta H_r = -284 \frac{kJ}{mol}$	
R13	$H_2 + \frac{1}{2}O_2 \rightarrow H_2O$	$\Delta H_r = -242 \frac{kJ}{mol}$	

The Boudouard reaction or char –carbon dioxide reaction is six to seven orders of magnitude slower than R10 [61]. The rate of R2 (steam gasification of carbon) is two to five times faster than Boudouard reaction R1 [62].

2.1.3.2 Boudouard reaction model

Boudouard reaction R1 [52] is described by the following steps. In the first step, CO₂ dissociates at a carbon free active site (C_{fas}), releasing carbon monoxide and forming a carbon-oxygen surface complex, C(O). This reaction can move in the opposite direction as well. Third step produces a molecule of CO from carbon-oxygen complex [62, 63].



The rate of char gasification reaction is insignificant below 750 °C as shown in the figure 2.1. below 650 °C, production of CO₂ is more as compared to CO.

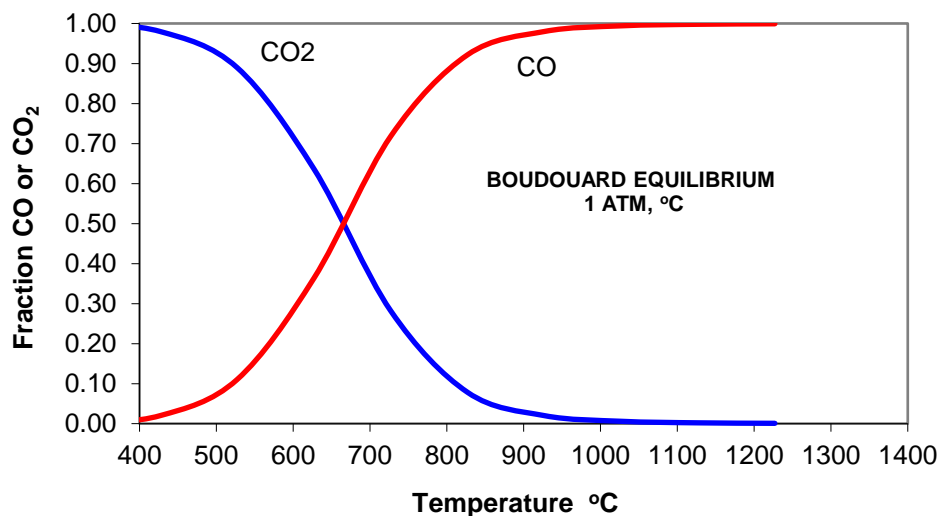
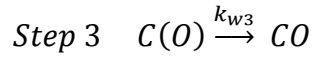
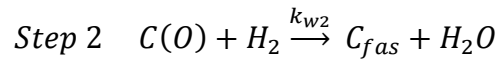
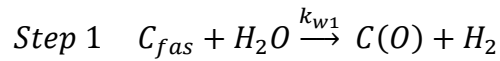


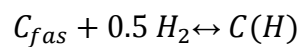
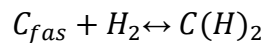
Figure 2.1 Boudouard reaction equilibrium [64]

2.1.3.3 Steam gasification of char model

The steps for the steam gasification of char R2 are summarized below. The first step involves the dissociation of H₂O on a free active site of carbon (C_{fas}), that release hydrogen and form a surface oxide complex of carbon C(O). This reaction can also move in the opposite direction. In the third step surface oxide complex produces a molecule of CO and active site [62, 63].



Some models also include the possibility of hydrogen inhibition by C(H) or C(H)₂ complexes as follows [62]:



The presence of hydrogen inhibits strongly the char gasification rate in H₂O. For example, 30% H₂ in the gasification atmosphere can reduce the gasification rate by a factor as high as 15 [65]. So continuous removal of H₂ is the effective means to accelerate the reaction.

Equilibrium constant for this reaction also become greater than 1 at 700 °C.

2.1.3.4 Water-gas shift reaction model

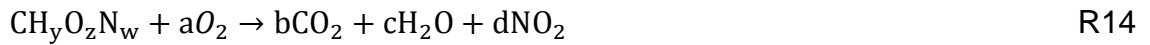
Water gas shift reaction R3 is an important gas-phase reaction, that can increase the hydrogen content of the gas on the expense of carbon monoxide.

This reaction is slightly exothermic, and equilibrium constant is high at low temperature that shows that more H₂ is produced at low temperature . But at low temperatures rate of reaction is slow. Optimum yield is obtained at about 225 °C [52]. At high temperatures, rate of reaction increases but yield decreases. To overcome this issue, catalysts are used at low temperatures to enhance the rate of reaction.

2.2 Stoichiometric air to fuel ratio

Biomass is classified as an oxygenated hydrocarbon with a general elemental HCO composition. Nitrogen (N) content is very low and sometimes negligible. In combustion applications, with N included, the elemental formula can be expressed as CH_yO_zN_w where y, z and w represent H/C, O/C and N/C ratios

respectively. Air is composed Nitrogen 76.8%, Oxygen 23.16% and inert components 0.04% on dry basis by mass. For complete combustion, stoichiometric air-fuel (dry ash free) is given by equation 1.



$$\text{Stoichiometric } \left(\frac{A}{F}\right) = \frac{\left[\left(1+\left(\frac{y}{4}\right)\right)\frac{z}{2}+w\right].137.94}{(12+y+16z+14w)} \quad (1)$$

The stoichiometric actual A/F can be calculated from equation 1 is on dry ash free basis and the stoichiometric A/F wet basis can be calculated by taking into account the moisture and ash content of the biomass (equation 2).

$$\text{Stoichiometric (A/F)}_{\text{wet}} = \text{Stoichiometric (A/F)}_{\text{daf}} \times [1 - (x_w + x_a)] \quad (2)$$

Where x_w and x_a are the mass fractions of the moisture and ash contents in the sample respectively.

2.3 Equivalence ratio (\emptyset)

The equivalence ratio is defined as the ratio of the stoichiometric A/F ratio (calculated from elemental analysis) to the measured A/F ratio as given below:

$$\emptyset = \frac{(\frac{A}{F})_{\text{Stoichiometric}}}{(\frac{A}{F})_{\text{Measured}}} \quad (3)$$

Also

$\emptyset = 1$ implies sufficient air is there to burn all the fuel

$\emptyset > 1$ implies a rich fuel mixture. Air is insufficient to burn all the fuel

$\emptyset < 1$ implies lean mixture (excess air than stoichiometric)

Sometimes the mixture strength is represented by a term 'Air factor' or 'Excess air ratio' denoted by lambda – λ , which is an inverse of equivalence ratio \emptyset .

Thus $\lambda = 1/\emptyset$, if $\lambda < 1$ then mixture is rich and if $\lambda > 1$ then mixture is a lean.

However there are many researchers who used the term of equivalence ratio (ER) for the excess air ratio (λ), and the literature reviewed below has most of the papers defining excess air ratio (λ) as equivalence ratio (ER), however they have not used the symbol \emptyset for defining equivalence ratio, and it can be concluded that different research group used different terms to define air factors or equivalence ratios. The term ER was used in their work to discuss what is air factor λ in present work. Basu [52] have also defined equivalence ratio as an inverse of what is used in the present work.

In the present experimental work, two types of equivalence ratio have been used, one is the metered equivalence ratio \emptyset_m , that is actually the compartment equivalence ratio CER defined by Gottuk and Lattimer's [66] "the ratio of the mass of any fuel entering or burning in the compartment to the mass of air entering the compartment normalized by the stoichiometric fuel-to-air ratio".

$$\emptyset_m = \frac{(m_a/m_f)_{stoichiometric}}{\dot{m}_a/\dot{m}_f} \quad (4)$$

\dot{m}_a is the rate mass of air supplied in to the enclosure

\dot{m}_f is the rate mass of fuel consumed, obtained from mass loss rate of biomass from load cell.

\emptyset_m takes into account all air supplied to the whole compartment, even if it was not actually taking part in the combustion.

Second is the emission based equivalence ratio EBER (\emptyset_e) this is a complicated method to back calculate the equivalence ratio based on the products sampled. EBER (\emptyset_e) is defined as 'The ratio of the mass of fuel involved in the reaction that produced the sampled mixture to the mass of air involved in producing the sampled mixture normalised by the stoichiometric fuel-to-air ratio'. This equivalence ratio is based on the carbon balance, and the method of calculation is developed by Abdulazaiz Alarifi [67]. This method is similar to the work of Chan [68] but EBER takes into account a large number of hydrocarbon species measured by the FTIR and validation of EBER (\emptyset_e) was done by Chan's air to fuel ratio model.

Literature below shows how product gas composition varies with different parameters.

2.4 Effect of equivalence ratio on the product gas composition in gasification

Equivalence ratio strongly influences the gasification and the end products. It should be above 1 to ensure that the fuel is gasified rather than combusted so that required gases CO and H₂ are obtained instead of more CO₂ and H₂O. However very high values ($\phi > 5$) results in many problems including incomplete gasification, excessive soot/char formation and low heating value of the product gases. In practical gasifiers the equivalence ratio varies from 2.5 to 5 [52].

Theoretical knowledge of the composition of the syngas provides valuable information about the optimal parameters of the gasification process, in order to obtain the maximum possible energy content in the gaseous fuel. As a first assumption of the syngas composition, a thermodynamic analysis is commonly used, which is based on the equilibrium in the gasification zone.

Equilibrium models show that there is an optimum value of equivalence ratio where the composition of gases have maximum % of combustible gases i.e. CO and H₂.

Puig-Arnavat [69] presented a mathematical model for the biomass gasification processes developed in the equation solver program Engineering Equation Solver (EES). It was based on thermodynamic equilibrium calculations and included some modifications to be adapted to a real process. The model could be used to predict the producer gas composition, yield, and heating value for a certain biomass with a specific ultimate composition and moisture content. The model was validated with published experimental data from different authors for downdraft, fluidized-bed gasifiers and different biomasses, and showed good agreement between reported data and modelled values.

This model was used to evaluate the influence of different operating parameters like ϕ on the producer gas. This study defined Equivalence ratio (ER) as the inverse of what is used in the present work.

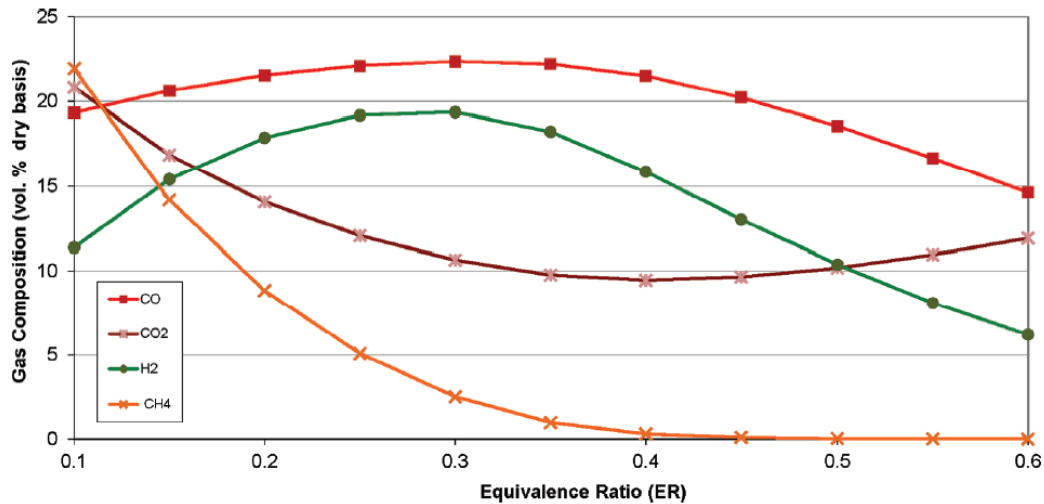


Figure 2.2 Effect of the Air factor (λ) on the composition of producer gas (equilibrium) for woodchip gasification [70].

Figure 2.2 shows the modelling result for woodchip gasification with 11.7 % moisture contents assuming 3% heat losses and 2% carbon losses and it can be seen that % of CO and H₂ was maximum near $\lambda = 0.3$ ($\phi = 3.33$).

Plis and Wilk [70] predicted the equilibrium compositions of the biomass using a computer code by means of energy equation solver. Parameters taken into consideration were biomass composition, moisture contents of the biomass, the excess air ratio λ , gasification temperature and heat losses from the reactor. Figure 2.3 shows the resulted equilibrium concentrations of CO and CO₂ for different biomasses and peak values of CO are observed between $\lambda = 0.32$ - 0.37 ($\phi = 2.7 - 3.1$).

Afterwards the influence of excess air ratio λ on the experimental composition of product gas for the gasification of two biomass species (Wood pellets and oat husk pellets) in a fixed bed. The internal diameter of the gasifier was 0.25 m and total height was 0.6m with the maximum capacity of 20 kg wood pellets. A syngas sample was cleaned by a system of filters and supplied to CO and H₂ analysers. Measurement of these two gases was online while other gases were investigated by chromatographic analysis offline.

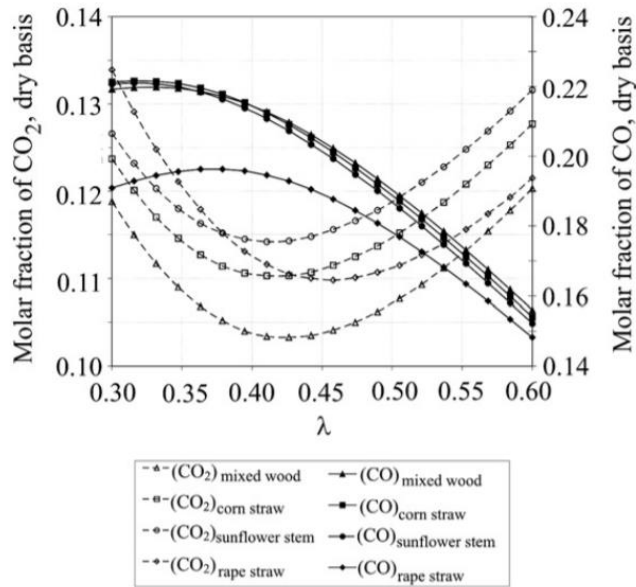


Figure 2.3 predicted equilibrium concentration of CO and CO₂ for different biomasses [70]

Tests were performed at $\lambda = 0.2$ ($\emptyset = 5$) and $\lambda = 0.29$ ($\emptyset = 3.5$) and average value of the concentration of CO at the steady state vol. % in at $\lambda = 0.2$ ($\emptyset = 5$) was 23-24% and at $\lambda = 0.29$ ($\emptyset = 3.5$), was 27-28%. For H₂, there was not much difference in the average values but the average value at steady state at $\emptyset = 3.5$ was slightly higher than at $\emptyset = 5$.

Zainal et al. [71] investigated the influence of equivalence ratio on the gasification of wood chips in a downdraft biomass gasifier. In this study term the air factor λ was varied from 0.26 to 0.46 ($\emptyset = 2.2$ to 3.8) and effect was studied on the gas composition, cold gas efficiency, calorific value of the gas. Concentration of CO increased from 23 to 25% as λ decreased from 0.46 to 0.38 (\emptyset increased from 2.2 to 2.6) and concentration of methane increased from 1.5 to 2.1% as λ decreased from 0.46 to 0.37 (\emptyset 2.2 to 2.7) Figure 2.4, further reduction in the λ from 0.36 to 0.26 (\emptyset 2.7 to 3.8) caused concentration of CO and methane decrease again. H₂ concentration increased overall as λ increased from 0.26 to 0.45 (\emptyset decreased from 3.8 to 2.2). trend of CO₂ concentration was inverse of CO, with minimum concentration of 12% at $\lambda = 0.37$ ($\emptyset = 2.7$), maximum concentration of CO₂ was 16% at $\emptyset = 2.2$, calorific value of the product gases was maximum at $\lambda = 0.38$ ($\emptyset = 2.6$) [71]

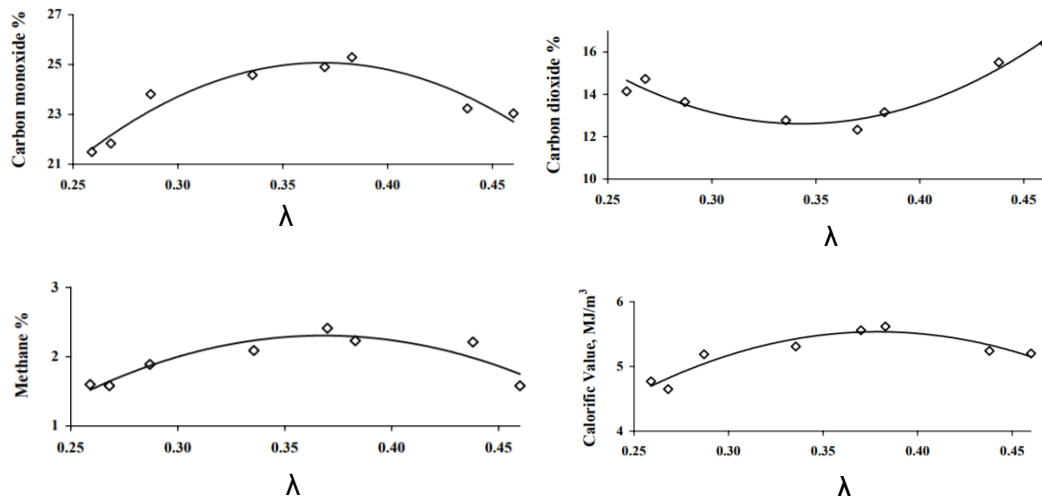


Figure 2.4 Experimental concentrations and CV of product gas from gasification of wood chips in downdraft gasifier [71]

Qin et al. [72]. studied the gasification of wood (beech saw dust) and straw (pulverized wheat straw pellets) in a laboratory scale entrained flow reactor at atmospheric pressure. excess air factor λ of 0.25 ($\emptyset = 4$), 0.35 ($\emptyset = 2.45$) and 0.5 ($\emptyset = 2$) at fixed temperature of 1350 °C. gases from the gasifier were cooled to get water condensed and flue gas was analysed by a NDIR gas analyser and by GC. Their work claim to have all the fuel converted with no char left, only some soot was left as the residue. Gas yields were reported in Nm³/kg fuel. Yields of H₂, CO and hydrocarbons C_xH_y was highest at $\emptyset = 4$ and lowest at $\emptyset = 2$. While yield of CO₂ was lowest at $\emptyset = 4$ and highest at $\emptyset = 2$. They showed a 30 % decrease in the yield of H₂ as equivalence ratio was decreased from 4 to 2. Yield of CO was almost same at $\emptyset = 4$ and $\emptyset = 2.85$, while there was a decrease of 13% as \emptyset changed from 2.85 to 2. Soot yield was highest 40 g/kg fuel at $\emptyset = 4$ and lowest 10 g/kg fuel at $\emptyset = 2$ [72].

Narváez et al. [73] investigated the effect of \emptyset on gas yield, gas composition, LHV, tar contents, for the gasification of pine sawdust in a bubbling fluidized bed reactor at 800 °C. they varied λ from 0.26 to 0.44 (\emptyset from 2.3 to 3.8). They reported that gas yield decreased from 2.6 Nm³/kg fuel to 1.9 Nm³/kg fuel and tar contents increased from 7 g/ Nm³ to 27 g/ Nm³ as \emptyset increased from 2.3 to 3.8.

As \emptyset increased from 2.3 to 3.5, CO₂ composition increased from 15% vol. to 16% vol., Methane composition increased from 3% vol. to 4.2% vol. and Ethyne

increased from 1.7 % to 2%. These compositions decreased to the original values from $\emptyset = 3.5$ to 3.8. CO volume % decreased from 14% to 13 % as \emptyset increased from 2.3 to 3.8 while volume % of H_2 showed a very small increase from 9.5 to 9.8%. CO concentration remained fairly constant at \emptyset 2.3 and 2.9, but there was no data point in between to check any variation. However CO concentration decreased slightly as \emptyset increased from 2.9 to 4.

LHV of the raw gas at the gasifier exit was reported to have increased from 3.8 MJ/Nm³ to 6.2 MJ/Nm³ as \emptyset increased from 2.3 to 3.8. This might be due to the fact that hydrocarbons also show an increase as \emptyset increase. Other reason is that this value includes tars as this value is for raw gases. Tars decrease as \emptyset decrease as hence LHV also decrease [73].

Lv et al. [74] studied the gasification of pine sawdust with air in a fluidized bed reactor in the presence of steam. They examined the effect of \emptyset on the gasification process in terms of gas yields and LHV at 800 °C and steam rate of 0.8 kg/hr. Equivalence ratio \emptyset was varied from 3.7 to 5.3 (λ from 0.19 to 0.27). Maximum concentration of CO was 40% at $\emptyset = 4.3$ ($\lambda = 0.23$), CO₂ was minimum with 16% at this equivalence ratio. H_2 concentration remained fairly constant at 32% while there was a slight increase in the % volume for methane and ethylene as \emptyset was increased from 3.7 to 5.3.

Gas yield (Nm³/kg biomass) also increased from 1.88 to 2.37 \emptyset increased from 3.7 to 4.3 [74].

From the literature reviewed in this section, it was concluded that there exists an optimum value of \emptyset that gives high % CO and H_2 , and high calorific value gases, this optimum \emptyset value may vary depending upon the type of biomass and type of gasifier, usually its in the range of 2.5 to 4.

2.5 Effect of temperature on the product gas composition in the gasification of biomass

Narváez et al. [73] studied the effect of bed temperature on various factors in the gasification of pine sawdust in an atmospheric bubbling fluidized bed. Bed temperature was raised from 700 to 850 °C with increments of 50 °C at $\lambda=0.3$ (\emptyset

= 3.33). It was reported that % by vol. of H₂ and CO increased from 5 to 10% and 12 to 18% respectively. The reason for this increase was the improvement in the gasification reactions with temperature. Other hydrocarbon contents were almost constant or there was a very slight decrease. However CO₂ reduced to 13% from 15.7%. LHV of producer gas improved from 4 MJ/Nm³ to 5 MJ/ Nm³ due to the increase of H₂ and CO. Tars present in producer gas reduced to a very large extent, from 19 g/m³ to 2.5 g/m³ [73].

Qin et al. [72] studied the effects of temperature on the products (solid, liquid and gas) distribution by the gasification of wood (beech saw dust) and straw (pulverized wheat straw pellets).

There was an increase of 72% in the yield of producer gas (Sum of H₂, CO, CO₂ and C_xH_y up to C₃ species) when temperature of wood gasification at $\lambda = 0.25$ ($\emptyset = 4$) was increased from 1000 °C to 1350 °C at (steam to carbon ratio) S/C = 0.5. This increase is attributed to the steam cracking and reforming of tars and higher hydrocarbon also gasification of soot increases at high temperature. Without steam i.e. S/C = 0 , yield of gaseous products increased by 23% when gasification temperature was raised from 1200°C to 1350 °C. Molar ratio of H₂/CO which is very important from point of view of gasification was increased from 0.6 to 1 as temperature was increased from 1000°C to 1200°C but remained fairly constant after 1200°C to 1350°C at S/C = 0.5 [73].

The effect of temperature on soot yield showed that by increasing temperature from 1000 °C to 1200°C at steam to carbon ratio (S/C) = 0.5 soot yield increased sharply from 8.5 g/kg to 58.7 g/kg fuel. Then it declined to 35.3 g/kg fuel as the reaction temperature further increased to 1350 °C. Possible reason is that at high temperature soot starts to gasify. Same behaviour was observed for experiments without steam from 1200°C to 1350°C [73].

The effect of gasification thermal reforming temperature on the product gas composition was also studied by Aljbour and Kawamoto [75] for the bench scale gasification of cedar wood. At $\lambda = 0.2$ ($\emptyset = 5$) without steam, temperature was increased from 650 °C from 950 °C (923K to 1223 K) with the intervals of 100°C and significant increase in volume % of hydrogen from 17% to 38% was observed. CO concentration increased from 42% to 50%, whereas this remained

less effected at low temperatures. However, there was a decrease in CO₂ concentration from 27 to 6%. HHV of the product gases increased from 9.3 MJ/Nm³ to 12.1 MJ/Nm³ for this temperature rise [75].

Lv et al. [74] studied the effect of temperature on the gasification of pine sawdust in a fluidized bed reactor. Temperature was varied from 700-900 °C in 50 °C increments at biomass feed rate of 0.445 Kg/h air flow rate 0.5 Nm³/h and steam rate of 1.2 kg/h. They showed that H₂ concentration increased from 22 % (vol.) to 40 % and CH₄ concentration decreased from 9 % to 6 %. The reason for this trend was explained that at high temperature endothermic reactions causing steam reforming of CH₄ to produce H₂, CO₂ and CO increased.

CO concentration was decreased from 43 % to 34 % as temperature was raised. He reason for this decrease was that CO was mainly produced by the exothermic reaction of carbon/char with oxygen R9 and at higher temperature this reaction was not favourable. C₂H₄ and C₂H₆ also showed a downward trend with rise of temperature, which was attributed due to the thermal cracking and steam reforming. They also reported increase in the carbon conversion efficiency and steam decomposition (SD) with temperature due to the endothermic nature of reaction R2 steam gasification of carbon [74].

Wu et al. [76] studied the effect of gasification temperature on the hydrogen production from biomass component lignin in the presence of Ni–Ca–Al catalyst in a two staged fixed bed reactor. Biomass samples were pyrolysed in the first stage and the derived products were gasified at the second stage with water injection rate of 0.02 g min⁻¹. Increase in temperature form 700 to 900 °C showed significant effect on gas yield and hydrogen production. The gas yield was increased from 42.8 to 55.1 wt. % and the hydrogen production was increased from 10.5 to 17.8 (mmol/g biomass). Reason suggested for increased gas yield and hydrogen production was secondary reactions in which higher hydrocarbons cracked to non-condensable gases and steam reforming of hydrocarbons at high temperatures [76].

From the literature reviewed in this section, it was concluded that increasing the temperature of gasification increased the gas production, yield of CO and H₂ and

possible reason is high rate of boudouard reaction and more secondary reactions that involve cracking of hydrocarbons.

2.6 Effect of moisture/steam on the gasification of biomass.

Aljbour and Kawamoto [75] studied the effect of steam to carbon S/C ratio on the product gas composition from the gasification of wood at the gasification thermal reforming temperature of 850 °C. Steam to carbon ratio was increased from 0 to 2 at the increment of 0.5 at $\emptyset = 5$. It was shown that the production of H₂ and CO₂ increased, while that of CO decreased. H₂/CO ratio increased by 0.7 to 2.6 and CO₂/CO ratio increased from 0.4 to 1.5. They reported this change due to the water gas shift reaction. They also found that increase in H₂ production was more significant as S/C was raised from 0 to 1, from 1 to 2 there was insignificant increase in the hydrogen concentration [75].

Lv et al. [74] varied steam to biomass ratio S/B from 0-4 at 800 °C and showed that the introduction of steam (S/B from 0 to 1.35) initially improved the gas yield, LHV and carbon conversion efficiency but over the S/B range from 1.35 to 4.04, gas yield, carbon conversion efficiency and LHV exhibited decreasing trend which was explained by that excessive quantity of low temperature steam (154 °C) lowered reaction temperature and degraded gas quality [74].

Narváez et al. [73] studied the effect of H/C ratio to the gasifier by modifying the moisture content of the biomass fed. H/C was varied from 1.6 to 2.3, at gasifier temperature of 800 °C and $\emptyset = 3.2$. Their work showed that increasing moisture content of the biomass to 25% i.e. H/C to 2.3, the H₂ content in the raw product gas increased from 6% to 9% by volume. CO also increased from 14 % to 16 % by volume while CO₂ decreased from 15.5 % to 12.5 % by volume. LHV of the gases increased from 4 to 6 MJ/Nm³. Tar contents of the raw gas decreased from 18 to 2 g//Nm³. The decrease in tars and increase in CO and H₂ was attributed due to the steam reforming of hydrocarbons [73].

From the literature reviewed in this section it was concluded that production of H₂ increases in some cases by increasing steam to biomass ratio but increasing the ratio too much decreases the quality of the gas in terms of heating value.

2.7 Effect of biomass particle size

It is generally accepted that the gas yield and composition are related to the heating rate of the biomass particles. High heating rates produce more gases and less condensate. As smaller particles have large surface area and are heated fast. It can be expected that the size of biomass particle influence the product gas composition.

Lv et al. [74] studies the effect for four particle sizes (avg. size 0.25mm, 0.38mm, 0.54mm, and 0.75mm) on the gas yield and composition for the gasification of biomass at 800 °C and showed that the smaller particles produced more CO, CH₄, C₂H₄ and less CO₂ than the larger particles. This was the reason of improved gas yield, LHV, carbon conversion efficiency and steam decomposition with small particle size of biomass. Possible explanation provided was the resistance to mass transfer in the large particles and the product gas inside the particle is more difficult to diffuse out and process is mainly controlled by the gas diffusion [74].

Hernández el al. [77] also studied the effect of particle size (0.5mm,1mm, 2mm, 4mm and 8mm) on the product gas composition and gasification of biomass in an entrained flow gasifier at 1050 °C and showed that the concentration of all the combustible species (CO, H₂ and CH₄) increased as the fuel particle size reduced, whereas CO₂ concentration decreased. LHV of the gases and cold gas efficiency of gases was higher with the small particle size while the gas yield was very slightly increased [77].

Similar trends were shown by Lou et al. [78] who studied the catalytic steam gasification of biomass in a fixed bed. Range of particle size studied was from 0.075mm to 1.2mm, they also showed that more char and tars were produced with larger particle sizes, temperature was increased from 600 °C to 900 °C and the difference in the % of char and tars between different particle size feed was higher at low temperatures and less at high temperatures. For the smaller particle size (below 0.075 mm), there was negligible production of char and tar (0.4%) at lower temperature (700 °C), However, for the largest particle size (0.6–1.2 mm), residual solids remain above 10% even at the maximum temperature (900 °C) of operation [78]

Table 2.3 Product gas composition and heating values from gasification of biomass from different researchers and comparison.

	Plis & Wilk [70]		Di Blasi et al. [79]	Lucas et al. [80]	Gordillo & Annamalai [81]	Wang et al. [82]	Narvaez et al. [73]	Czernik et al. [83]	Present work
Fuel	Wood pellets		Beech wood	Wood pellets	Dairy biomass	Cedar wood chips	Pine sawdust	Wood shavings, sawdust	Pine wood
Particle size	D= 6mm, L = 10-30mm		3 (2.5%)-5(95%) mm	D=12mm		150-300mm	-4.0 to +8.0 mm	< 20x5x5 mm	20x20x100 mm
Setup- Gas analysis	Fixed bed gasifier, updraft – CO, H ₂ analyser, GC		Fixed bed gasifier, updraft-GC with TCD	Fixed bed gasifier, updraft. Preheated air at 350 °C- Micro GC with TCD	Fixed bed gasifier, updraft, Steam/Fuel = 0.35 -MS	Fixed bed gasifier, updraft, Steam ratio = 0.5 - Micro GC	Bubbling fluidised bed,- Total organic carbon analyser for tars, On line gas analysis gas analyser, Offline gas analysis GC with TCD	Fluidised bed reactor, GC-MS	Cone calorimeter, FTIR
Bed temperature	300-950 °C		300-1200 °C	1000 °C	200-1150 °C	250 °C-1100 °C	530-800 °C	743-857 °C	200-700 °C
Moisture contents wt. %	7.0	7.0	5.0-6.0	8.2	25	9.9	19-25%	12-17%	5.2 %
Air/fuel ratio kg/kg	1.73	1.14	1.05-1.27						
Excess Air ratio/Air factor	0.30	0.20	0.20-0.25			0.16-0.26	0.26-0.44	0.273-0.333	0.13-0.62
Ø	3.33	5	4-5		1.59 -6.36	3.8-6.25	2.3-3.8	3-3.6	1.6-7.8
Syngas composition vol %									
CO	27.47	25.53	28.6-30.0	30.0	12.5-9.5	12-14	13-14	12.9-16.7 %	8-15 %
CO ₂	6.22	7.06	7.0- 5.5	6.0	10-17	16-17	15-17	15.9 – 16.4 %	11.8-12.7 %
H ₂	7.13	7.96	7.0	10.60	17-20	8-14	8-10	7.9-9.8 %	4.2-8.6 %
CH ₄	1.88	1.44	1.80	3.2		2-1.8	3.8-4	3.4 – 4.2 %	0.2 – 0.8 %
C ₂ +	0.14	0.12	-	0.5			1.8-2 as C ₂ H ₂	1.3 – 1.6 % as C ₂ H ₄	6-7 %
O ₂	1.44	3.49	-	-		0.55		0.8 – 1%	0.8-0.4 %
N ₂	54.68	56.67	55.60-55.70	41				49.4 – 54 %	
LHV MJ/Nm ³	4.99	4.67	5.10-5.25	6.9	HHV: 3.8-3.9	HHV: 4-4.6	3.7-6.3	5.2 – 6.2	HHV: 4-5

It was concluded that small size particles release more CO due to high surface area exposed and less resistance to heat and mass transfer.

Table 2.3 compares the product gas composition and heating value of previous work done on the gasification of biomass in fixed bed and fluidized bed gasifiers by some researchers, In the last column, results of the present work discussed in the Chapter 5 are also listed.

2.8 Pyrolysis and chemistry of wood

In order to understand the pyrolysis mechanism, knowledge of wood structure and its chemistry is necessary. Lignocellulosic biomass is the non-grain portion of the biomass (e.g. stalks, cobs), it is non starch fibrous part of the plant material, and unlike carbohydrate or starch, it is not easily digestible by the humans and is often called residues of agricultural stover.

The major constituents of lignocellulosic biomass consist of cellulose (a polymer glucosan), hemicelluloses (which are also called polyose), lignin, organic extractives, and inorganic minerals. The weight percent of cellulose, hemicellulose, and lignin varies in different biomass species of wood and biomass.

Cellulose makes up the cell walls, and provides the tensile strength of the wood matrix. Its amount varies from cotton 90% to 33% for most other biomass plants. It is represented by the general formula $(C_6 H_{10}O_5)_n$ [52]. Cellulose is a linear homopolysaccharide of cellobiose monomers, composed of two β -glucopyranose units as presented in Figure 2.5 (a). All the covalent linkages between the β -glucopyranose motifs of the framework are β -1,4-glycosidic bonds. The degree of polymerization of the native cellulose depends on the source and can reach more than 5000 [84].

Hemicellulose is similar to cellulose, and grows around the cellulose fibres. It makes the cell walls of the plant having random amorphous structure with little strength. It consist of group of carbohydrates with a branched chain structure

with a low degree of polymerization and is represented by generic formula $(C_5H_8O_4)_n$. typical hemicellulose xylan is shown in the Figure 2.5 (b).

The third major component of wood is lignin. It is the integral part of the secondary cell walls of the plant and the main binder for the agglomeration of fibrous cellulosic components while also providing a shield against the rapid microbial or fungal destruction of the cellulosic fibers. It acts as a cementing agent for cellulosic fibres and holds them together.

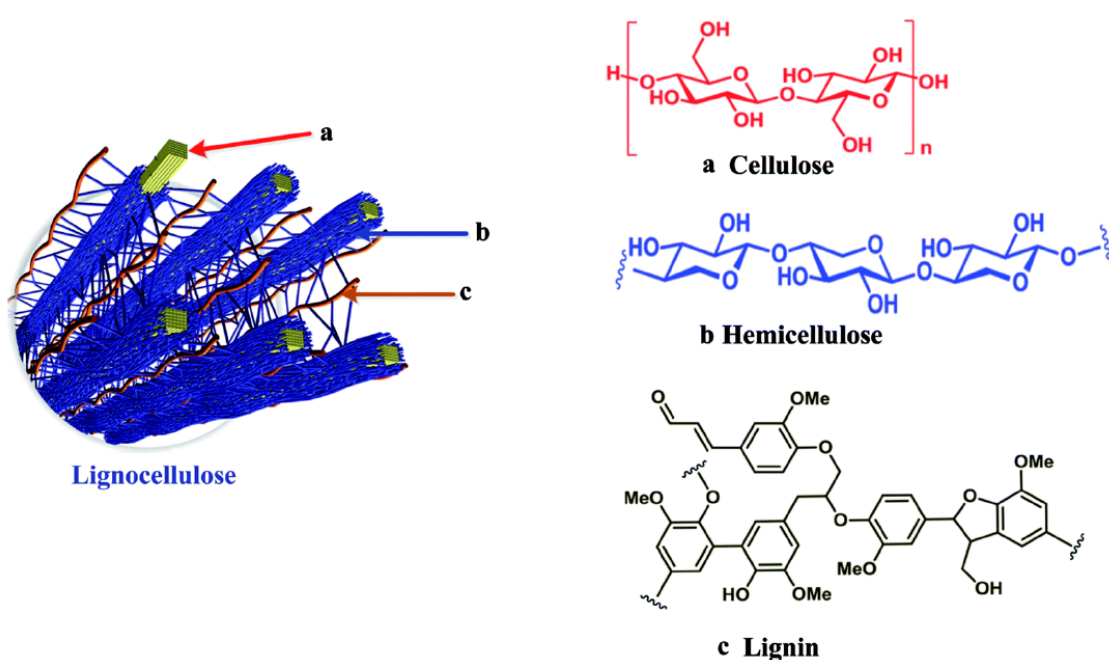


Figure 2.5 Biomass components (a) cellulose (b) hemicelulose (c) lignin [85]

Lignin gives rigidity to the wood, allowing trees to grow upright. “Lignin is a three dimensional, highly branched, polyphenolic substance that consists of an irregular array of variously bonded “hydroxy-” and “methoxy-”substituted phenylpropane units” shown in the Figure 2.5 (c) [52, 55]

Different chemical bonds within the polymers are broken during the heating process of the biomass, which results in the release of volatile compounds and in rearrangement within the structure of the residue. These reactions are considered as primary mechanisms. Then some volatile compounds released as a result of primary mechanisms are unstable and can undergo additional

conversions named secondary reactions such as cracking or recombination. Cracking reactions consist of breaking of the chemical bonds within the volatile compounds, that result in the formation of low molecular weight molecules. As the breaking of the same chemical bonds can undergo either from the polymer (hemicellulose, cellulose or lignin) or within the volatile compounds, there are similarities in the products obtained from the fragmentations and the cracking reactions. Recombination is also called re-condensation and it involves the combination of volatile compounds to give a higher molecular weight compound that might not be volatile under the conditions of the temperature of the reactor. [84].

Primary pyrolysis products components formed from cellulose and hemicellulose are anhydrosugars, low molecular weight carbonyls, carboxylic acids and furans [86], while lignin forms mono aromatic such as phenols, guaiacols and its derivatives [87]. Secondary reactions of these primary tars produce catechols, cresols, xylenols, phenol, and PAHs [87, 88]

Heavy hydrocarbons are called tars and in a combined meeting of the IEA Bioenergy Gasification Task, the Directorate General for Energy of the European Commission (DG XVII) and US DoE in Brussels (March 1998), It was decided to define tars as the hydrocarbons with molecular weight higher than benzene [89].

According to Mohan et al. (2006) [55], the general changes that might occur during pyrolysis of biomass are listed below

1. Heat transfer within the biomass from a heat source, to increase the Temperature of the biomass
2. Initiation of primary pyrolysis reactions at this higher temperature to releases volatiles and formation of char;
3. Flow of hot volatiles toward the cooler solids results in heat transfer between hot volatiles and cooler un-pyrolysed biomass
4. Condensation of some of the volatiles in the cooler parts of the biomass, followed by the secondary reactions to produce tars
5. Autocatalytic secondary pyrolysis reactions proceeding while primary pyrolytic reactions (step 2, above) simultaneously occurring in competition

6. Further thermal decomposition, reforming, water gas shift reactions, radicals recombination, and dehydrations might also occur, which are function of the pyrolysis residence time, temperature and pressure.

Demirbas (2000) states that the thermal degradation of cellulose proceeds through two types of reaction: a gradual degradation, decomposition and charring on heating at lower temperatures, and a rapid volatilization accompanied by the formation of levoglucosan on pyrolysis at higher temperatures. In the pyrolysis reactions, methanol is produced from the breakdown of the methyl esters and/or ethers from the decomposition of pectin like plant materials. Methanol also arises from the methoxy groups attached to different structures like uronic acid and e 4-O-methyl- α -D-glucuronic acid [90, 91]. Acetic acid is formed in the thermal decomposition of all three main components of wood biomass [92].

Collard 2014 has summarized the main steps of conversion of cellulose, hemicellulose (xylan) and lignin regarding the release of volatile compounds during each step and is illustrated in the Figure 2.6 (a ,b and c) [84] .

Acetic acid comes from the elimination of acetyl groups originally linked to the xylose units. Furfural is formed by the dehydration of the xylose unit.. Degradation of xylan yields water, methanol, formic acid, acetic acid, propionic acid and hydroxy acetone [92].

2.9 Cellulose/Lignin ratio

The high content of volatiles in biomass as compared to coal is one of the reasons why biomass has a high rate of decomposition at lower temperatures ranging from 160 °C to 300 °C. The ease of release of these volatiles influence the combustion properties i.e. high rate of burning and ease of ignition for high volatile matter biomass [93]. Cellulose, lignin and hemicellulose are responsible for the variation in the rates of devolatilisation [94]. This according to Sheng and Azevedo [95], can be attributed to the varying air to fuel ratio of these polymers which depend on their chemical formulae; cellulose $C_6H_{10}O_5$, hemicellulose $C_5H_{10}O_5$, lignin as a mixture of $C_{15}H_{14}O_4$, $C_{22}H_{28}O_9$, $C_{20}H_{22}O_{10}$ with air to fuel

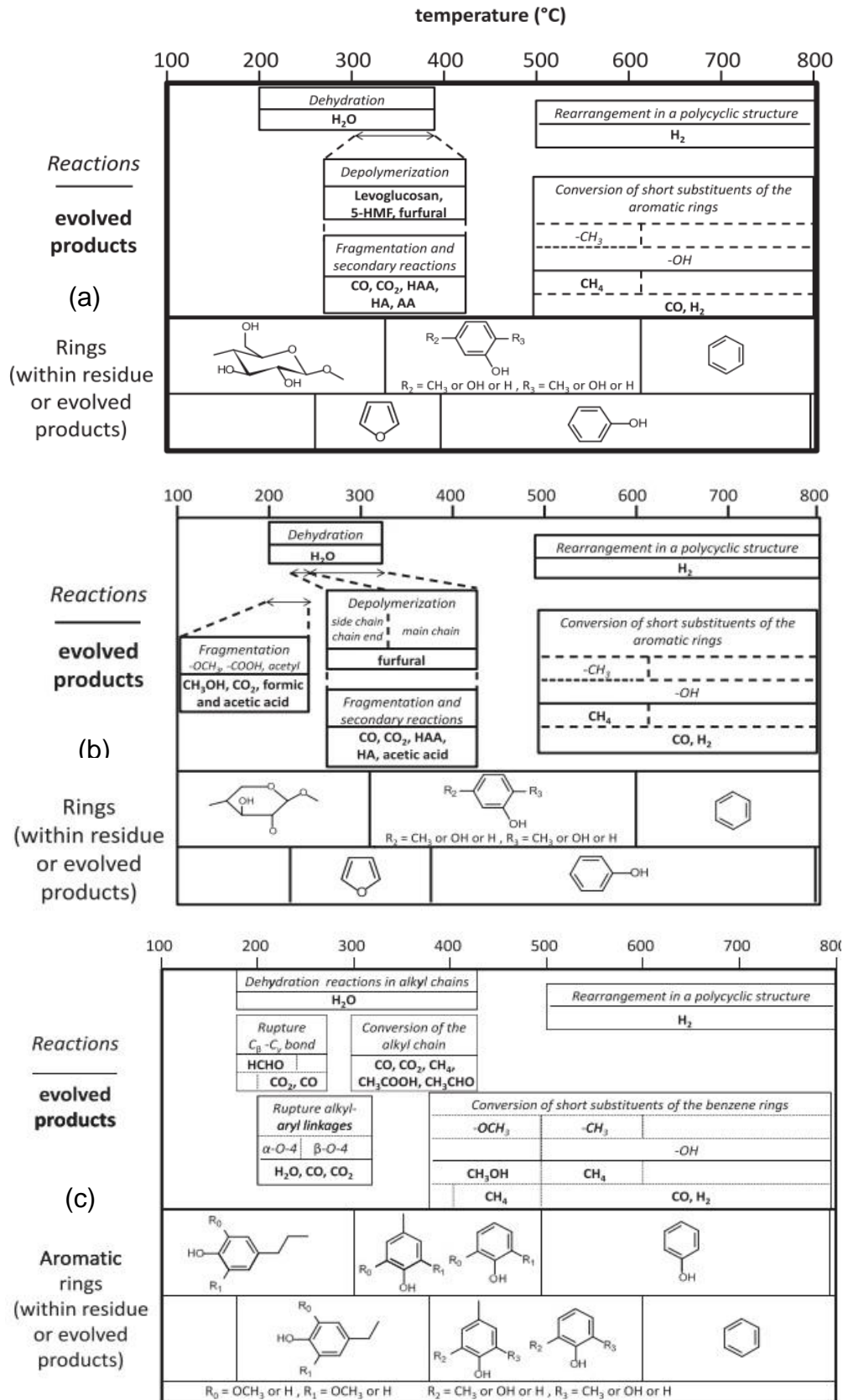


Figure 2.6 Steps and compounds for the decomposition of (a) Cellulose (b) hemicellulose (Xylan) (c) Lignin ; HAA: hydroxy acetaldehyde; HA: hydroxy acetone [84]

ratios of 5.10, 4.5 for cellulose and hemicellulose and a range of 6.7-8.9 for lignin [95, 96]

McKendry reported the proportions of cellulose, lignin and hemicellulose for hard wood, softwood and wheat straw as shown in the Table 2.4.

Table 2.4 Cellulose/lignin content of some biomass [97]

Biomass	Lignin %	Cellulose %	Hemi-cellulose %
Softwood	27-30	35-40	25-30
Hardwood	20-25	45-50	20-25
Wheat straw	15-20	30-50	10-40

In order to determine the influence of cellulose and lignin on gasification of biomass, Lv et al. [98] found out that the pure cellulose material had the highest peak temperature with longer gasification period for the mass loss rate. They also showed that tar and gas yield increased with increasing cellulose content but char yield decreased during pyrolysis of biomass. They proved the two stages of decomposition, the first showing rapid mass loss due to the volatilization of cellulose, while mass loss in the second stage was slow due to the decomposition of lignin. They concluded that higher the cellulose content, higher will be the rate of pyrolysis with more volatiles and less char. Therefore, depending on the heating rate and residence time, the stages of reaction and subsequent product gas yield of gasification is very dependent on the ratio of lignin and cellulose. It can be concluded that the higher the cellulose content, the faster the rate of pyrolysis associated with the products reduced by char produced in the second stage as the lignin is decomposed.

Yang et al. [9] studied the characteristics of hemicellulose, cellulose and lignin pyrolysis using a TGA coupled with FTIR and a packed bed coupled with micro-GC. They showed a quick pyrolysis of hemicellulose and cellulose with release of gas products using TGA. They reported main weight loss of hemicellulose

between 220- 315 °C and of cellulose 315- 400 °C, and discovered that decomposition of lignin was difficult and weight loss happened over wide range (160 – 900 °C). They discovered using FTIR that pyrolysis of the three components resulted in the same components including CO₂, CO, CH₄ and some organics having aldehydes, carboxylic, ketone and ethers group with C-O-C and C=O bonds. For H₂ yield and total gas yield measurement, micro GC was used with packed bed. They discovered that highest yield of CO₂ was obtained with hemicellulose, while higher yield of CO was obtained from cellulose. Higher H₂ and CH₄ yields were obtained with lignin. They also reported that at lower temperature release of CO₂ was higher as compared with CO. First CO₂ peak from hemicellulose was from 200 to 400 °C and made argument that releasing of CO₂ was mainly caused by the cracking and reforming of functional group of carboxyl C=O and COOH. They made argument that highest peak of CO₂ from hemicellulose can be attributed to the cracking and abscission of C-C and C-O bonds connected with the main branch of hemicellulose and causing high pyrolysis reactivity of hemicellulose.

Lignin caused two peaks of CO₂ release one low peak from 200 – 400°C, other higher peak from 600 °C – 800 °C. While cellulose released only one small peak from 350 to 400°C.

They reported that high peaks of CO was obtained with hemicellulose and lignin from temperature above 600 °C, below this temperature very low peaks of CO were observed from all three biomass components. CO was also reported to be released by the cracking of C=O and COOH group.

Highest peak of CH₄ was obtained from lignin at temperature 400 – 600 °C.

The releasing of the organic compounds with groups C=O and C-O-C occurred at low temperatures 200 – 450 °C for all three components. Hemicellulose released all organic compounds from 200 – 350 °C. Lignin and cellulose released these organic compounds from 350- 450 °C while lignin showed negligible peaks at 300-450 °C. Evolution of H₂ was zero before 400 °C, after 400 °C it raised for lignin and hemicellulose [99].

Hemicellulose react more readily than cellulose and furan derivates might readily be found among the decomposition products. Lignin gives higher yields of

charcoal and tars from wood. Decomposition of lignin may produce guaiacols and phenols [90].

2.10 Volatile products from pyrolysis of wood

Thermogravimetric analyses (TGA) of many biomass samples showed that the temperature range at which 85-90% of these volatiles are driven off is from 275 to 450° C as shown in the Figure 2.7 , reproduced from [100].

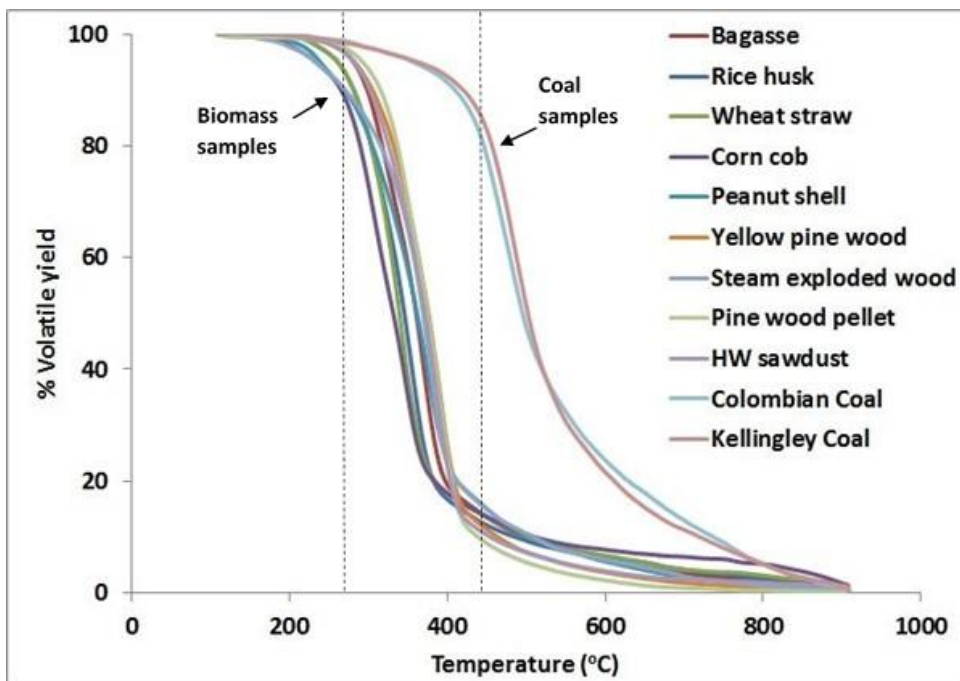


Figure 2.7 Percentage yield of volatiles vs temperature for biomass samples [100] (under nitrogen)

Basilakis et al. [101] investigated the volatile release of three types of tobacco, Three model compounds (xylan, chlorogenic acid and D- glucose) and wheat straw by coupling FTIR by TGA and quantified 20-23 components. 5-30 mg of the sample was heated in helium at a rate of 30 °C/min., gases from the reactor flowed to the gas cell at 155 °C where volatiles were analysed by FTIR. For wheat straw yield of quantified components were H₂O 19%, tars 30%, CO₂ 10%, CO 6%, CH₄ 1%, ethylene 0.2%, HCN 0.2%, methanol 1%, formaldehyde 0.8%, acetaldehyde 7%, formic acid 1.4%, acetic acid 4.5%, phenol 0.5%, acetone 2%, levoglucosan 1%.

Meng et al. [102] investigated the pyrolysis of 3 biomass materials (corn cobs, tree roots and bagasse) using TGA-FTIR with four components (CO, CO₂, NH₃, and CH₄) quantified while H₂O, HCN and CH₃COOH rest being identified. DTG curves of the three biomass shows different peaks and it was concluded that initial peak in the corn cobs was due to the release of water and the second peak was attributed to the pyrolysis of hemicellulose. While first mass loss peak of the bagasse was due to the pyrolysis of the hemicellulose.

Shen et al. [91] studied the mechanism of hemicellulose (extracted from the beech wood) pyrolysis using TG-FTIR and discovered the main gaseous and bio-oil components qualitatively. Heating rate for TG-FTIR was changed from 3-80 k/min and nitrogen was used as carrier gas. CO and methanol were found to be released around the first peak of the sharp mass loss rate, while the second peak of mass loss rate was due to evolution of CO₂, aldehyde and products, CO₂ and acetic acid were also obtained during whole sharp mass loss stage due to the cleavage of acetyl groups from the xylan chain. They also employed a fluidised bed reactor to investigate the product of hemicellulose pyrolysis at different temperatures (400 °C – 690 °C). It was found that gas yield increased while char yield decreased with increasing temperature, while tars yield first increased upto 475 °C and then started decreasing. Main compounds from bio-oil were found to be methanol, acetic acid, acetone and furfural. For the gaseous compounds, It was found that formation of CO was enhanced with elevated temperatures CO yield increased from 6.02 % (wt.) to 13.33% as temperature increased from 570 °C to 690 °C. CO₂ yield did not changed to greater extent however it started decreasing after 570 °C from 25.78% (yield wt.%) to 22.87% at 690 °C. Yield of H₂ and hydrocarbon gases increased with increasing temperature.

Pielsticker et al. [103] studied the gas yield from the flash pyrolysis of bituminous coal and torrefied biomass from poplar wood in the temperature range between 873-1273 K (600 – 1000 °C) for 22 gas species . A small scale fluidised bed reactor coupled with FTIR was utilised. FTIR used in their work was Gasmeter DX-2000 FTIR spectrometer with thermo-electrically cooled MCT detector. Hot gas sampling was done at 180 °C. They performed online measurements with scan time of 1 s. offline measurements were also performed to study the peak gas

composition. For that case FTIR gas cell was enclosed by switching the two valves as soon as the peak concentration of the product gas was reached and remaining gas flow from the reactor was by passed but offline analysis was not used for measurements of yields. They have reported the yields of, H₂O, CO, CO₂, NO, NO₂, N₂O, NH₃, SO₂, COS, CS₂, methane, ethylene, acetylene, propene and benzene. Their work showed that gas yield increased while char yield decreased with increase in temperature. In this temperature range, H₂O, CO₂, CO and CH₄ were the main pyrolysis gases, less significant species were ethylene, propene and benzene.

Scott and Piskorz [104] studied the flash pyrolysis of biomass (poplar aspen wood) in a fluidised bed reactor in a temperature range of 450 – 650 °C. They analysed gas sample by dual column GC, although the liquid fraction was condensed but hot sample of product gases was also taken from the space directly above the fluidised bed and analysed chromatographically at 150 °C for compounds boiling at 100 °C or less. They calculated the yields of CO, CO₂, methane, ethane, ethylene, propene, H₂, acetaldehyde, ethanol, methanol, acetic acid, water, tars and char. There was an increase in the yield of gas and uniform decrease in the yield of char with increase in temperature. Yields of tars and organic liquids increased from 450 to 500 °C and then decreased with increasing temperature. Yield of CH₄ and CO increased to a very large extent as temperature was increased from 550 °C.

Commandre et al. [105] have studied the fast pyrolysis of wood at high temperature range (650 °C – 950 °C) and high heating rate (10³ K/s) in an entrained flow reactor. sample was collected from different heights of the reactor and after condensation of water it was send via heated line to FTIR, NDIR, TCD for H₂ and methane and total hydrocarbon analyser using 2 FID detectors. Yields of CO, CO₂, H₂, methane, ethylene and acetylene were reported as a function of temperature., Yields of all gases increased with temperature except for CO₂ that started decreasing after 750 °C and C₂H₄ that started decreasing after 800 °C. Yield of H₂ was almost 0 % at 650 °C and it increased to 1% at 950 °C.

Liu et al. [106] studied the pyrolysis of wood's lignin and TGA -FTIR was used and phenol was found to be the main volatile product in addition to alcohols,

aldehydes and acids, Methanol was detected to be the most important alcohol . Main gaseous products were CO, CO₂ and CH₄.

Devolatilisation of biomass and its components (xylan, cellulose, lignin, pine wood, wood pellets, olive stones, hazelnut shells) was studied qualitatively by Biagini et al. [54] in TGA-FTIR, a paper sludge and a coal sample was also study for comparison. Detected components were CO₂, CO, H₂O, methane, methanol and formic acid. More complex organic compounds were hardly distinguished as narrow temperature range release several organic species simultaneously. Biomass released gases earlier than coal. Cellulose decomposition started near 300 °C, xylan decomposition started near 250 °C and lignin decomposition started near 200 °C, decomposition of biomass started near 250 °C, for biomass CO₂ started coming off near 200 °C, CO at 250-270 °C methane at 300-350 °C. For coal sample, CO, CO₂ and CH₄ started coming off at 400 °C.

Experimental work studied so far is for biomass with small particle size. Yields of the major gaseous components from above pyrolysis literature are at selected temperatures are listed in the Table 2.5.

Some work has previously been done by Blasi et al. [62, 107] on the pyrolysis of biomass with large particle size comparable with the present work. They pyrolysed 4 cm diameter, 4 cm long wood samples using a furnace having diameter of 65 mm that employed radiant heaters for heating, exposing the target samples to heat fluxes ranging from 28 to 80 kW/m². A condenser was used to collect the water and condensable species. The non-condensable gases were analysed using a GC by withdrawing samples from the gas stream at specified time intervals. Their “integrated” gaseous yields are included in Table 2.5. Temperatures of the wood were attained in the same range at current work at relatively higher heat flux and the possible reason was that the sample was exposed to the flow of nitrogen from all directions that caused cooling. They showed that gas yield increased while char yield decreased with increasing heat flux, while liquid yields started decreasing slightly for some woods after a heat flux of 45 kW/m².

Another work of Blasi et al. [108] on the pyrolysis of agricultural residues (wheat straw, olive husks, grape residues and rice husk) and wood chips have been

investigated on bench scale in the same furnace that employed radiant heaters, exposing the target samples to the desired heat fluxes in a temperature range of 650- 1000 K (377- 727 °C). Biomass particle size was 1-3 mm in this study and particles were packed in a stainless steel mesh of cylindrical shape holder of diameter 4mm, yields of the resulting gas species at selected temperature are reported in the Table 2.5.

In the Table 2.5, yields of some gases of the pyrolysis of pine wood are also listed from the present work discussed in the Chapter 6.

For the yields of the organic liquids and tars, most of the research has studied pyrolysis on the rigs where liquid fractions are separated and analysed in GC-MS and reported separately in different publications and yields are based on the total mass of the liquid fraction instead of total mass of the biomass fed. However there is some work done with Py-GC-MS where vapours are directly analysed by the GC-MS.

Torri et al. [109] has performed on line gas chromatography combined with mass spectroscopy (Py-GC-MS) and atomic emission detection (Py-GC-AED) to study the pyrolytic behaviour of different biomass (poplar, sweet sorghum, corn stover and switchgrass). Helium (100ml/min) was used a carrier gas and to quantify the principle lignin phenols and hemicellulose/cellulose degradation products, an internal standard (o-isoeugenol) was used in the Py-GC-MS. Temperature of pyrolysis was 500 °C. Acetic acid and hydroxy acetone were found to be the main pyrolysis products.

Yields of some of the condensable components from the pyrolysis of this work along with others is listed in the Table 2.6. Also yields of the some products of pyrolysis work from the present work is also listed in the last row of the table.

Li et al. [110] conducted the comparative study of the pyrolysis of lignocellulosic biomass (corn stalk) and alga biomass on Py-GC-MS. Biomass sample was heated to 600 °C at a heating rate of 20 °C/ms. Helium was employed as a carrier gas at a rate of 1ml/min. main compounds found for corn stalk in order of decreasing peak area were, 4-vinylphenol, 2-methoxy-4-methylphenol, acetic acid, furfural, 1,2-cyclopentanedione, guaiacol, levoglucosan, furfuryl alcohol and formic acid.

Branca et al. [111] analysed the pyrolysis liquids from beech wood pyrolysis on GC-MS. Pyrolysis experiments were performed in a furnace 63 mm internal diameter and 450 mm length, nitrogen was fed through a jacket at reactor top and heated by electric furnace and distributed by perforated steel plate. Beech wood particles were cut in parallelepipeds 5-20mm thick and pre-dried. Reactor temperature was varied between 600 – 900 K (327-627 °C). Nitrogen was used as carrier gas and liquids were collected after condensation of the product gases and stored at a temperature of 4 °C, with no light exposure. Before analysis sample was filtered with 0.45 micron filter. A sample volume of 1ml was in acetone (4.5% pyrolysis liquid in acetone) was injected inside GC-MS. They quantified forty compounds using fluoranthene as internal standard. Yields of the liquids were reported as % of the initial dry wood mass. Some major compounds in order of decreasing yields at 527 °C, were acetic acid, hydroxy acetaldehyde, hydroxy propanone, syringol, formic acid and levoglucosan.

Nunes et al. [112] studied the pyrolysis and gasification of eucalyptus wood, plastic waste and industrial sludge (particle size 106-150 µm, weight 1gm) in a two stage downdraft fixed bed hot rod reactor with a throat section for additional gasification stage. In the first stage of the reactor, effect of pyrolysis temperature on the yields of tars, chars and gases was studied, nitrogen was used as a carrier gas, heating rate to the peak temperature (500 °C) was 10 °C/min. Tars were collected from the throat and the reactor and components washed with solvent, afterwards solvent was evaporated in a very severe condition that caused the low boiling tars and oils removed from the final collected tars (only high boiling tars that cause deposition and corrosion problems were left). The effect of temperature in the range of 200-450 °C on the char and tars for eucalypts wood showed that char yield decreased rapidly from 200-300 °C and reached a limiting value of 15% at 450 °C. Tar yield increased significantly with temperature upto 350 °C, from 400 to 450 °C this value did not change and became maximum with 30% at these temperatures.

Demirbas [92] studied the effect of temperature (625-875K, 350-600 °C) on the yield of compounds in the bio oils obtained from the pyrolysis of biomass. Heating rate was 10 K/s and solid residence time 45-55 s in a tubular reactor (height 95mm, ID 17mm, OD 19mm) inserted vertically into electrically heated tubular

furnace. Collected sample was a mixture of oil and water soluble fraction, mixture was placed in 500 ml separating funnel and dichloromethane DCM was used for separating bio oil from aqueous phase. Bio oil was analysed using GC- MS. Major compounds found were acetic acid, hydroxy acetone, methanol, furfural, dimethoxy phenol, 2- cyclopentene-1-one, and levoglucosan. Yields of some components at selected temperatures are listed in the Table 2.6. The overall trend for the liquid yields was found that yields of liquids increased upto a temperature of 520 °C and the started decreasing by increasing temperature.

Conclusion of literature reviewed this sections are that at low temperature, concentration of CO₂ is higher than CO. CH₄ is also not a major component of pyrolysis at low temperature. Yields of CO and CH₄ become higher at temperature above 550 – 600 °C. By increasing temperature char and gas yield increased, liquid yield increase upto a certain temperature e.g. 450 – 500 °C, after this temperature by increasing temperature yields of liquid tars and condensate decreases. Major liquid components reported by most researchers are acetic acid, hydroxy acetone, methanol, furfural, acetaldehyde and levoglucosan. It can also be seen from Table 2.5 and Table 2.6 that the particle size of the biomass effects the product yields to a large extent.

Some of the researchers [101, 102] have used TGA in combination with an FTIR analyser. The limitation of this method is that TGA takes a tiny fraction of biomass at uniform temperature with respect to time and the flow rate is too low for many FTIR analysers including the one used in the present work. So larger biomass samples will behave differently and need to be pyrolysed in larger reactors and combined with FTIR analysis for meaningful data that would be applicable to biomass boilers. Perhaps the most directly comparable work, that sought to address some of the main issues identified above was by Blasi and coworkers [107]. In their work condenser was used to collect the water and condensable species. The non-condensable gases were analysed using a GC by withdrawing samples from the gas stream at specified time intervals. Their “integrated” gaseous yields are included in Table 2.5 while liquid yields from another set of tests in another pyrolysis work [111] with small particle size feed are included in Table 2.6.

It should be noted that the separation of condensable elements from the gases is only necessary because of the sample collection methods and the analytical equipment used and should also be noted that it is possible that some of the components may alter as they condense out [111].

Separation of species is not representative of the processes actually involved in log boilers and other small scale fixed bed biomass plants where these products are not separated and certainly they should not be allowed to condense out but are instead transported into the secondary combustion zone where they are burnt.

2.11 Gasification for electricity and heat production

Gasification offers greater flexibility both in terms of possible biomass feedstock and end use of energy. For example, in addition to drive a gas turbine, gas from gasifier can be used to generate steam in the gas boilers, sometimes in combination with natural gas. Larger steam turbine systems in power plants having capacity 200 MW or larger are relatively efficient at energy conversion. Smaller biomass steam turbine systems (20-100MW) require further research to improve their cost comparativeness with fossil fuels [113].

Other research is continuing to small modular biomass conversion system (100kW to 5MW) to provide electricity cost effectively to communities and industries [113].

Also gasification is becoming important for small scale heating applications for domestic and communal scale by using boilers (20kW- 1MW).

2.12 Commercial biomass log boilers

Biomass log boilers that use a gasification zone filled with biomass are common for small-scale space and water heating applications. This type of boiler can be fed with chips or pellets instead of logs, but logs are most commonly used as they are the lowest cost option. For the case of log boilers, most of these systems operate on batch combustion where the fuel is loaded either daily or periodically depending on the operation parameters and demand.

Table 2.5 Comparison of gaseous products yield from the pyrolysis of biomass reported in the literature

Biomass / Pyrolysis type	Pyrolysis temp. range studied / Heating rate	Method used / (yield basis)	Temp. for reported yield / (yield basis)	Particle size	Yields (kg/kg biomass) % by mass								
					H ₂ O	CO ₂	CO	CH ₄	C ₂ H ₄	C ₂ H ₆	H ₂	Char	Ref.
Wheat straw (Slow)	(ambient-900 °C)/ 30 °Cmin ⁻¹	TG-FTIR (Quantitative)	(ambient-900 °C) / (daf)		19	10.05	6.05	1	0.2	-	-		[101]
Xylan (Slow)	(ambient-900 °C) 30 °Cmin ⁻¹	TG-FTIR (Quantitative)	(ambient-900 °C) / daf		32	15	9	1	0.4	-	-		
Torrefied biomass (Slow)	600 °C- 1000 °C	Small scale fluidized bed reactor- FTIR (Quantitative)	600 °C / (dry)	120-150 µm	2	6.5	20	1.8	0.4	-	-	27	[103]
Pine-wood (Fast)	650 °C- 950 °C / >10 ³ °Cs ⁻¹	Entrained Flow reactor- FTIR (Quantitative)	650 °C / (dry)	80 -200 µm	-	4	20	2	1.1	-	0	-	[105]
Aspen-poplar (Flash)	450 °C- 650 °C / ~ 10 ⁵ °Cs ⁻¹	Fluidized bed reactor- GC (Quantitative)	600 °C / (wet)	105 -250 µm	12.5	7	11	1	0.4	0.2	0.19		[104]
Aspen-poplar (Flash)			500 °C / (wet)	105 -250 µm	15.2	5.4	3.4	0.25	0.1	0	0		
Beech wood (Fast)	1000 °C	Drop tube furnace – Micro chromatograph (Quantitative)	1000 °C / (dry)	0.35 mm	15	13	45	6	1.5	1	2.5		[114]
Pine-wood (Slow)	330 °C- 680 °C / ~ 6-18 °Cmin ⁻¹	Quartz furnace heated by radiant source / GC (Quantitative)	450°C / (dry)	4cm dia. 4cm length	-	8.3	4	1.2	-	-	-	33	[107]
Beech wood (Slow)			450°C / (dry)	4cm dia. 4cm length	-	9	4	1.3	-	-	-	27	

Biomass / Pyrolysis type	Pyrolysis temp. range studied / Heating rate	Method used / (yield basis)	Temp. for reported yield / (yield basis)	Particle size	Yields (kg/kg biomass) % by mass								Ref.
					H ₂ O	CO ₂	CO	CH ₄	C ₂ H ₄	C ₂ H ₆	H ₂	Char	
Redwood (Slow)			500 °C / (dry)	4cm dia. 4cm length	-	6	3	1.3	-	-	-	40	[107]
Fir wood chips (Slow)	380 °C -750 °C / 25 °Cmin ⁻¹	Quartz furnace heated by radiant source / GC (Quantitative)	525°C / (dry)	1-3 mm	-	13	5.8	0.6	-	-	0.01	28	[108]
Wheat straw (Slow)			500°C / (dry)	0.5-1 mm	-	13.8	5.8	0.5	-	-	0.02	30	
Olive Husks (Slow)			525°C / (dry)	0.5-3 mm	-	14	4.5	1	-	-	0.01	32	
Grape residues (Slow)			525°C / (dry)	1-3 mm	-	14	2.5	0.5	-	-	0.02	38	
Rice husks (Slow)			500 °C / (dry)	0.2-1 mm	-	10	5	0.5	-	-	0.01	43	
Corn cobs Tree roots Bagasse (slow)			Ambient- 850 °C / 20 °Cmin ⁻¹	TG-FTIR (Quantitative for 4 species)	Mass yields not reported	<150 µm	✓	✓	✓	✓			
Palm Oil Waste (slow)	250, 280, 300, 325, 355, 400, and 450 °C, / 30 °Cmin ⁻¹	TG-FTIR (Qualitative)	Yields not reported	<1 mm	✓	✓	✓	✓					[115]

Biomass / Pyrolysis type	Pyrolysis temp. range studied / Heating rate	Method used / (yield basis)	Temp. for reported yield / (yield basis)	Particle size	Yields (kg/kg biomass) % by mass								
					H ₂ O	CO ₂	CO	CH ₄	C ₂ H ₄	C ₂ H ₆	H ₂	Char	Ref.
Rice husk (slow)	400, 450, 500, 550 and 600° C,	Fluidized catalyst bed reactor- Packed column GC (Quantitative)	Yields not reported	0.25–1.0 mm		✓	✓	✓	✓	✓	✓	29 at 500 °C	[116]
Pine-wood	300 °C, 420 °C, 600 °C, 720 °C / 5, 20, 40 and 80 °Cmin ⁻¹	Pyrolysis static batch reactor-Packed column GC (Quantitative)	Mass yields not reported			✓	✓	✓		✓	✓	29.7 at 420°C, 5°C/min.	[117]
Pine-wood, Cellulose, Xylan (slow)	Ambient-700 °C / 10 °Cmin ⁻¹	Tubular stainless steel fixed bed reactor- GC (Quantitative)	Yields not reported	0.15–0.45 mm		✓	✓	✓			✓	28 (pine at 500 °C)	[118]
Hemicellulose, Cellulose, Lignin	Ambient-900 °C / 10 °Cmin ⁻¹	TG-FTIR (Qualitative)	Yields not reported	50 – 100 µm	✓	✓	✓	✓					[9]
		Packed Bed- Micro GC (Quantitative)				✓	✓	✓	✓	✓	✓		
Present work (slow)	Ambient – 500 °C	FTIR / dry	Ambient – 500 °C	2 x 10 x 10 cm	24.58	14.73	5.00	0.45	0.11	0.64		29	

Table 2.6 Comparison of condensable products yield from the pyrolysis of biomass reported in the literature

Biomass / Pyrolysis Type	Pyrolysis Temp.	Analysis method / (Yield basis)	Particle size	Yields (kg/kg biomass) % by mass (dry)											
				Acetaldehyde	Formic acid	Acetic acid	Methanol	Ethanol	Hydroxy acetone	Furfural	Furfural Alcohol	Phenol	Guaiacol	Ref.	
Spruce wood	500 °C	GC/MS/ dry	< 1.2 mm		0.40	5.36	2.8			5.0	0.77		0.28	0.36	[92]
Beech wood	500 °C	GC/MS/ dry	< 1.2 mm		0.30	5.3	2.24			3.2	0.77		0.18	0.36	
Olive husk	500 °C	GC/MS/ dry	< 1.2 mm		0.42	4.9	3.4			6.1	0.43		0.70	0.38	
Hazelnut shell	500 °C	GC/MS/ dry	< 1.2 mm		0.46	5.35	3.0			5.7	0.45		0.7	0.38	
Wheat straw (Slow)	(ambient-900 °C)	FTIR / (daf)		7.8	1.5	4.5	1.1								[101]
Xylan (Slow)	(ambient-900 °C)	FTIR / (daf)		4.5	1	2.5	1.7								
Poplar (Slow)	500 °C	Py-GC-MS / dry	< 1mm			3.1	0.13			2.0	0.08	0.05	0.33	0.14	[109]
Corn (Slow)	500 °C	Py-GC-MS / dry	< 1mm			2.6	0.10			1.7	0.07	0.03	0.06	0.13	
Sorghum (Slow)	500 °C	Py-GC-MS / dry	< 1mm			2.7	0.01			2.3	0.15	0.06	0.06	0.09	
Switchgrasses (Slow)	500 °C	Py-GC-MS / dry	< 1mm			2.4	0.11			2.1	0.13	0.03	0.03	0.09	
Beech wood (Slow)	527 °C	GC-MS / dry	5-20mm		0.667	5.3						0.064	0.05	0.2	[111]

Aspen-poplar (Flash)	500 °C	Dual column CC / wet	105 -250 µm	0.87		1.08	0.7								[104]
Aspen-poplar (Flash)	600 °C	Dual column CC / wet	105 -250 µm	3.28		1.16		0.33							
Almond Shells (Flash)	460 °C	CC / dry	0.297-0.50 mm	0.01		9.0			1.5						[119]
Present Work (Slow)	Ambient - 500 °C	FTIR	2 x 10 x 10 cm	0.4	5.9	1.5	0.43	0.33		1.37	0.74	0.43	0.7		

Log boilers, also called gasification boilers control heat release by controlling air flow into the boiler. In gasification boilers, the fuel first burns in a rich combustion zone, (gasification zone) such that the airflow splits with part going to the log zone. Here gasification reactions results in the formation of CO and H₂ rich gases. After gasification is completed in an insulated compartment (to maintain high temperature), secondary air is added in secondary combustion chamber to burn completely the CO and H₂ released from the gasification zone before heat extraction. H₂ and CO yields in the gasification rich zone decrease as the zone cools. Therefore preheating of inlet air results an increase in the thermal efficiency [120]. Continuously feed biomass chip or pellet boilers work in a similar way with the biomass first gasified and then the gases are burnt in a secondary zone.

In gasifiers (log boilers included), the overall performance is characterized by the heating value or heat release rate which is dependent on two elements; the product gas composition and efficiency [121]. These two elements according to Basu [51] are affected by the specific composition of the biomass, the gasification medium, biomass moisture content, temperature, pressure, design etc. This explains why it is a challenge to predict to a great accuracy the composition of product gas.

Even though design and control of secondary air has improved greatly with the inclusion of oxygen sensor in the flue gas, there is still a huge gap in the primary air control which is one of the main parameters affecting gasification products and yield [73]. One of the challenges for batch fed systems including log boilers is the control of heat output to match the demand cycle, ease of biomass loading, auto ignition or start up option and ash removal. Very strict emission limits have made it necessary to introduce downdraft boilers [122].

In most commercially available biomass boilers designs, the primary and secondary air split is fixed by the ratio of two flow divider orifice areas. An oxygen sensor in the flue gas controls the overall excess air, but there is usually no separate control of the primary/secondary air split. The variation in the biomass HCO composition results in the stoichiometric air to fuel ratio (A/F) varying between 4 and 8. In order to achieve the optimum gasification for a given biomass, control of the airflow split is required.

HDG biomass log boilers are provided by Euroheat Natural Energy Company (a registered manufacturer with HETAS) to many distributors in UK . HETAS is the independent UK body recognized by Department for Environment, Food and Rural Affairs (DEFRA) for the official testing and approval of domestic solid fuels, solid fuel and wood burning appliances and associated equipment and services. All HDG boilers discussed below are MCS approved and qualify for RHI [123]. Some boilers from Viessmann and Froling are also discussed and compared below. Log boilers units can provide heat output from 12 to 250 kW, while wood chip boilers can provide heat output upto 1 MW [124].

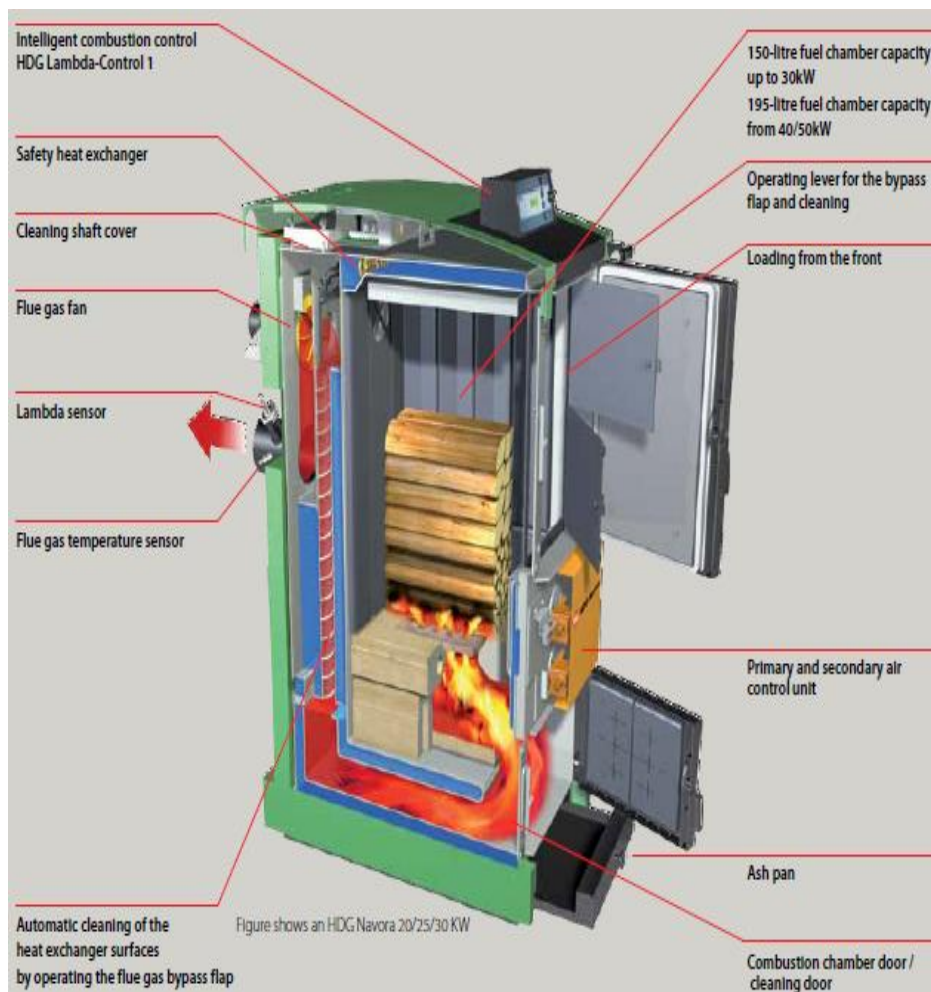


Figure 2.8 HDG Navora log wood boiler design [123]

The design of HDG Navora (20, 25, 30 KW) is shown in the Figure 2.8 . It is a front loaded, bottom burning, combustion controlled log wood boiler. It can burn wood upto half meter long (19”), large wood chips and pressed briquettes. Primary air flows through the logs and gathers heat prior to the gasification. Secondary air is introduced in the secondary combustion chamber and burn out

the product gases from the gasification zone. An air control unit splits the primary and secondary air, while the induce draft fan at the end controls the flow rate of the total air. The ignition of wood is not automatic and cardboard, paper pieces or twigs are placed on the top of wood and burnt manually to start and generally difficult task to accomplish (information not provided on the brochure) .

The exhaust has a temperature and lambda (oxygen) sensor for combustion control. Through oxygen and flue gas temperature sensors, combustion values are evaluated to regulate the primary thermal output of the boiler. Very longer loading cycles are achieved due to the large fuel chamber, 150 litres. It can be seen that the gasification zone of the boiler is water cooled and we know that for the efficiency of the boiler to be maximum, gases of gasification zone should be at as high temp as possible. However, the efficiency of HDG Navora is rated to be 91%.

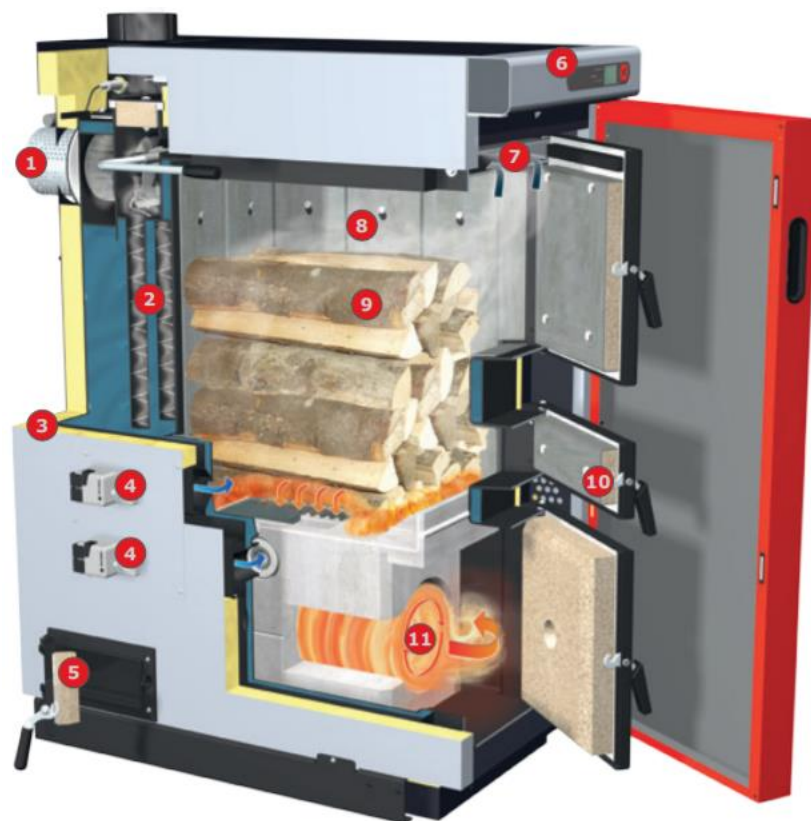


Figure 2.9 Froling S3 Turbo log boiler design [125]

<ol style="list-style-type: none">1. Draft fan2. Heat exchanger3. Thermal insulation4. Primary and secondary air controls5. Opening for ash removal6. Lambda controller	<ol style="list-style-type: none">7. Carbonization gas extraction system8. Inner wall cladding9. Primary combustion zone (gasification zone)10. Pre-heating chamber door11. Secondary combustion zone
--	---

The Froling boilers [125] shown in the Figure 2.9 and design is similar to HDG navora except the shape of the combustion chamber that is cylindrical producing swirling motion and increasing residence time for complete combustion. Also it has a pre-heating combustion door to start ignition manually by twigs, cardboards etc initially if there is no burning load in the boiler already.

The HDG EURO log wood boiler (Figure 2.10) (30, 40, 50kW) is top loaded and can burn log up to half meter in length, can also burn pressed briquettes, wood chips and shavings. It has a strong cast iron grate which supports the logs. The fuel chamber is made up of 10mm thick stainless steel to ensure long life. Primary air flows through the logs and cause gasification. Secondary air is heated by the burning bed before it burns out the product gases of the gasification zone in a special vortex combustion chamber.

Overall excess air is controlled via lambda sensor. Size of fuelling chamber is 220 litres so high loading cycles are achieved. Also in this boiler gasification zone is water cooled although to achieve maximum efficiency, gases exiting the gasification zone should have maximum temperature. Efficiency of HDG EURO is rated as 90 %.

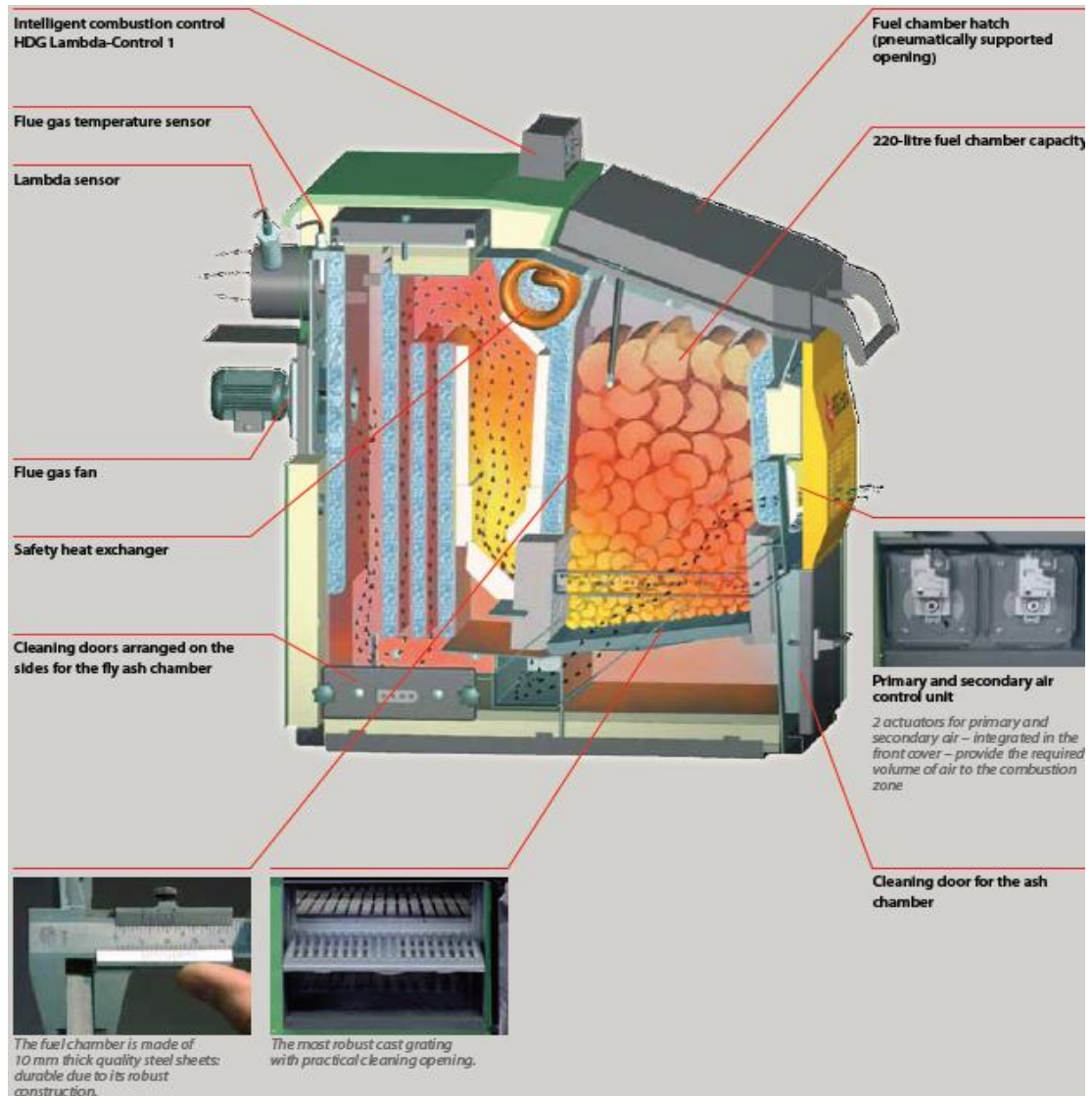


Figure 2.10 HDG EURO log wood boiler design [123]

The zone above the grate is referred to as a wood gasification zone with the gases burning downstream in a ceramic tunnel and cylindrical nature of the combustion chamber induces a swirling motion thereby increasing the residence time necessary for achieving complete combustion. A preferable approach in this design would be for the air to flow down through the log bed so that it is preheated prior to the burning or gasification zone. No mention is made of the problem of lighting the logs.

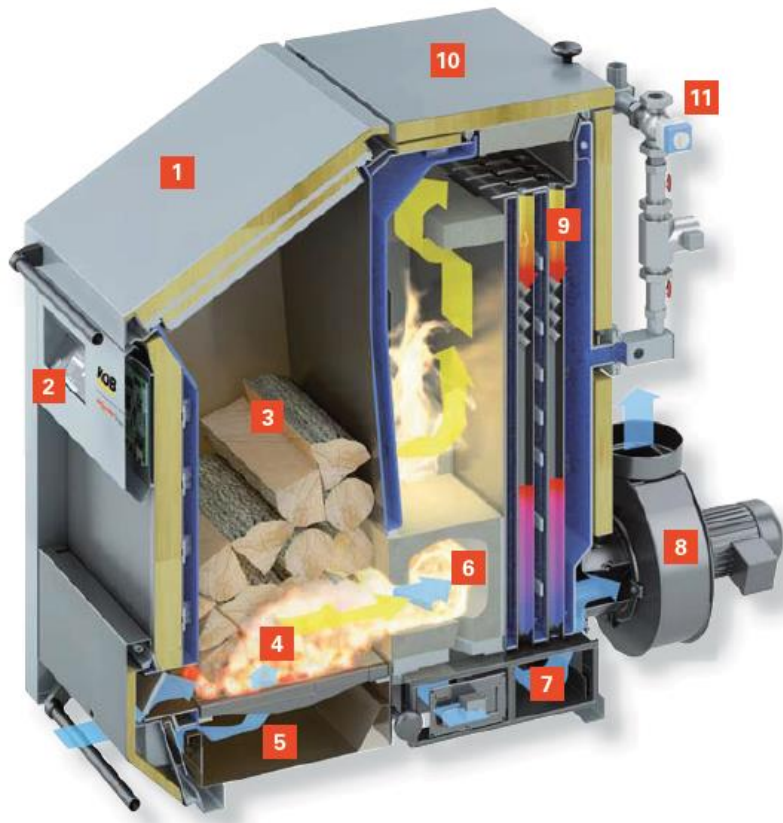


Figure 2.11 Veissmann Vitoligno 250- S log boiler [126]

<ol style="list-style-type: none">1. Hopper door2. Weather compensated control3. Tapering hopper4. Gasification zone5. Ash grate6. Combustion chamber	<ol style="list-style-type: none">7. Fly ash tray8. Induced fan9. Heat exchanger10. Cleaning hatch11. Lambda control
--	--

The Vitoligno 250-S [126] log burners (Figure 2.11) by Veissmann have an exhaust fan that controls the air inflow and hence the thermal output for a batch loaded boiler. Log boilers with a rated heating output range of 40 to 75 kW can be charged with logs of 50 cm in length. In the 85 to 170 kW range the hopper width increases to 1080 mm, allowing convenient charging even with logs of 1 m in length.

In this design the air is entrained below the log bed with the air flowing through a cast iron grating and fireclay board. Air is also indicated to flow above the bed. How the logs are supported above the grate is not clear and possibly simply sit on the grate.

HDG Bavaria (Figure 2.12) (22-49 kW, 65-125 kW, 175-250 kW) is a natural ventilation boiler with bottom lateral burning and patented highly fireproof vortex combustion chamber that allows burning of logs (length depends on the model), wood chips and briquettes. This boiler is top loaded. Manual primary and secondary air regulation ensures the uniform burning performance of different fuels. In this design primary air splits and part of it air flows down the bed and hot gases are shown to flow back towards the bottom of the grate. Efficiency of this boiler is not reported.

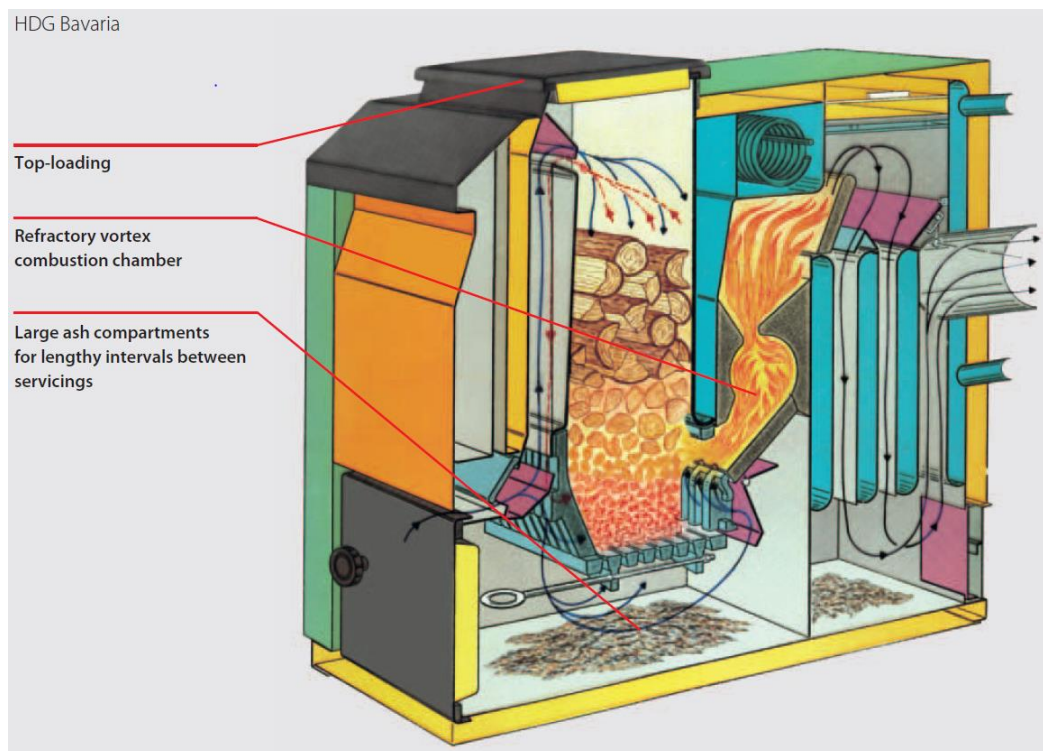


Figure 2.12 HDG Bavaria log boiler design [123]

All commercially available wood log boilers reviewed have disadvantage of water cooling of gasification zone, although to get high efficiency, gasification process should take place adiabatically to increase flame temperature of products of combustion. Also there is no separate air inlet into primary and secondary gasification zones; rather a split is made between two regions and the overall excess air is controlled by the lambda sensor and control system. Primary air is always a fixed ratio of the overall excess air. There is no temperature or CO sensor at the end of primary gasification zone to optimize the flow of air required in the primary gasification zone to increase the efficiency. Lack of information

about the gas composition from the gasification zone cause low thermal or conversion efficiency.

One of the challenges is the ignition of the log boiler. In the Froling case for example, they recommend kindling with log and twigs which can be a testing and generally difficult task to accomplish. This challenge can be alleviated by using a natural gas or oil burner is coupled to the system which can also complement the demand of heat during peak duration. With the infrastructure already in place, inclusion of natural gas burner in the log boiler design will not only alleviate the issues associated with start-up, but also supplement the energy demand and improve reliability of the biomass log boilers.

2.13 Research aims

1. To provide data that can be used to optimise the first stage of two stage biomass combustion
2. To determine the composition of the low temperature pyrolysis gases for application to biomass combustion modelling

2.14 Research objectives

In this work we employed a modified cone calorimeter, described in the next chapter (usually used for the characterisation of burning samples for fire applications), in combination with online heated FTIR analyser using a heated sampling line. In the light of the pyrolysis and gasification literature and the current design and performance of log boilers reviewed, the research objectives of this work are listed below.

1. To determine for pine wood the optimum gasification zone equivalence ratio for maximum energy yield, using variable air flows and heating rates.
2. To investigate the efficiency of biomass to gaseous products in rich combustion for different biomasses at the optimum air flow determined above.

3. To quantify the gaseous yields and energy yield from solid to gas from the pyrolysis in nitrogen of relatively large (20mmx20mmx100mm) samples of pine wood over the 250 – 500°C temperature range.
4. Study the effect of biomass type on the product distribution and yields of the product of pyrolysis in nitrogen

Chapter 3 Experimental methodologies

This chapter focuses on the experimental methodologies used by the author in conducting the experiments and the analysis in the presented work. At first the analytical testing (proximate and ultimate analysis) for determining the fuel characters are discussed and then the details of the experimental setup presented in this work are specified for cone calorimeter and Furnace rig. Finally, the details and the specifications of the gas sampling and analysis equipment is provided and then the examples of typical calculations methods are presented.

3.1 Analytical laboratory tests

In this work analytical laboratory tests and techniques were used mainly to identify the characteristics of raw materials used as fuel and the chars left after burning in the experiments.

3.1.1 Elemental analysis

The elemental analysis of wood samples was done using a Thermo Flash EA2000 manufactured by Thermo Scientific, it has a single reactor for the detection of carbon, hydrogen, nitrogen and sulphur (CHNS) while oxygen (O) was found by simply subtraction method using the following equation.

$$\% O = 100 - (\%C + \%H + \%N + \%S + \%Moisture + \%Ash) \quad (5)$$

The Flash 2000 elemental analyser requires finely grinded sample in order to improve its reactivity for a complete combustion in the test chamber. The sample is dropped, encapsulated in an airtight tin, by the auto-sampler into the furnace through a quartz reactor where the sample would combust reaching 1800 °C. The CHNS in the material sample is flash combusted into CO₂, H₂O, NO_x and SO₃ possibly. Nitrogen oxides and sulphur trioxide, possibly formed, are reduced to elemental nitrogen (N₂) and sulphur dioxide, and the oxygen excess is retained. Then helium is switched on to convey combustion products to the chromatographic column (CC). Then N₂, CO₂, H₂O & SO₂ are separated in the

chromatographic column. Where the products pass to the thermal conductivity detector (TCD) to determine the percentages of carbon, hydrogen, nitrogen and sulphur in proportion of the electrical signal produced by the different oxides present in the mixture.

3.1.2 Thermo-gravimetric analysis (TGA)

TGA-50 Shimadzu TGA with a TA60WS processor was used for the proximate analysis for the determination of volatile matter (VM), moisture content (MC), and fixed carbon (FC) contents of the wood samples, ash contents were calculated by subtracting percentages of volatile matter, water, and fixed carbon from 100. In this analyzer, sample is subjected to ascending high temperatures in an inert atmosphere to heat and remove moisture and volatiles from the sample, after that atmosphere is changed to oxygen rich to allow combustion and conversion of fixed carbon, ash left as the final weight.

A temperature programme was set for the TGA analysis as follows:

1. Heating up the sample, under nitrogen atmosphere, from ambient temperature to 110°C at the rate of 10°C /min and holding it at this temperature for 10 minutes to remove completely moisture content from the sample and hence providing the mass of moisture in the sample by weight loss.
2. Increasing the temperature from 110°C to 910 °C at the rate of 25°C /min and holding it at this temperature for 10 min to get the weight of the volatile loss
3. Heating from 910 °C to 920 °C at the rate of 10°C /min and introduction of O₂ during this step that reacts with fixed carbon in the char. Holding the sample at 920 °C for 10 minutes. Therefore the mass loss here provides the fixed carbon content of the material. Ash is left behind and found by difference

3.1.3 Bomb calorimeter test

Parr 6200 oxygen bomb calorimeter was utilized for determination of the gross calorific value of the samples. Calorific values are measured by comparing the heat obtained from the sample to the heat obtained from a standardising material, whose calorific value is known. A representative sample (nearly 1g) was first pelletised using hydraulic manual press. This pellet was then placed in

a small crucible that was held in the bomb head. A loop of the fused wire was placed just above the sample without touching the sample and the crucible. Bomb head was secured with bomb cylinder and screwed tightly to prevent air leakage. Bomb was then filled with oxygen to a pressure of 25 bar and placed in the bucket containing 2 kg deionized water with a thermistor and stirrer in the water. The lid of the bomb calorimeter was then closed and ignition was activated through the fused wire. Sample was burnt in a high-pressure oxygen atmosphere (25 bar) within a metal pressure vessel or bomb. The energy released by the combustion is absorbed within the calorimeter and the resulting temperature change was recorded and used to measure the heating value of sample. The bomb calorimeter is routinely calibrated using ten measurements of standard benzoic acid pellets of known calorific value.

The higher heating value (HHV) of any biomass material can be calculated with good accuracy from the following [127]:

$$\text{HHV (kJ/kmol)} = 0.2326(146.58C + 56.878 H - 51.53O - 6.58A + 29.45) \quad (6)$$

Where C, H, O and A are the mass fraction of carbon, hydrogen, oxygen and ash respectively in the dry biomass.

HHV of the chars left after gasification and pyrolysis was calculated using a unified correlation for solid liquid and gaseous fuels by Channiwala and Parikh [128] as follows:

$$\text{HHV} = 0.3491C + 1.1783H + 1.005S - 0.1034O - 0.0151N - 0.0211A \quad (7)$$

Where C, H, S, O, N and A are the mass fraction of carbon, hydrogen, sulphur, oxygen, nitrogen and ash respectively in the dry biomass.

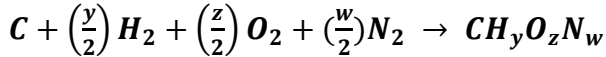
3.2 Equilibrium Calculation

Equilibrium models can be used to estimate the maximum achievable equilibrium yields of CO, H₂ and other gases during gasification based on fuel composition, equilibrium temperature and gross calorific value of fuel. The CEA (Chemical Equilibrium and Applications) software by NASA was used to perform the thermodynamic equilibrium calculations of the gasification of biomass to predict the composition of gases as a function of equivalence ratio ϕ . The programme calculates equilibrium compositions using a Gibbs Free Energy minimization

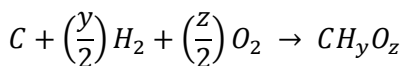
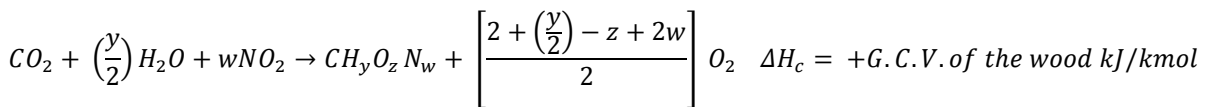
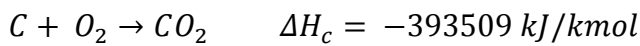
method. Gibbs Free Energy of a mixture system is at its minimum when the system reaches equilibrium at constant temperature and pressure. The software is able to calculate the product compositions of each gas in the system at equilibrium state based on the Gibbs Free Energy theory. The software use input information; temperature, pressure, enthalpy, entropy, internal energy, specific heat capacity and mole fractions of the reactants for calculation of the output data at equilibrium for every mole of mixture.

The problem type chosen for this project was ‘ combustion’ and it is constant enthalpy and pressure HP to reflect the adiabatic process. Input data was the value of pressure, an estimated temperature to start the calculations, reactant fuel oxidant mixture was specified with equivalence ratio ϕ from 0.5 to 8, Elemental composition of the components C, H and O in the biomass and standard heat of formation of the wood calculated by the method from literature [127] that used following set of equations.

The formation of 1 mol of solid biomass wood ($CH_yO_zN_w$) from solid carbon, hydrogen and oxygen can be written as and in reality the reaction cannot occur.



The formation of $CH_yO_zN_w$ is based on the following reactions



$$\Delta H_f = -393509 - \frac{y}{2}(241818) + w(33180) + G.C.V.of the wood \text{ KJ/kg} \quad (8)$$

3.3 Cone calorimeter

The cone calorimeter (Figure 3.1) was developed for fire testing and research by Babrauskas in the early 1980’s. It derived its name from the geometric

arrangement of electric radiant heater that can emit irradiance of 0-100 kW/m². This equipment measures successfully the heat release rate (HRR) of different materials by measuring oxygen depletion which is also called oxygen consumption calorimetry [129]. It has since been recognised as one of the most significant instruments for bench scale fire testing, and its procedure is described in ASTM E 1354 and ISO 5660 [130]. Other characteristics can also be measured using the apparatus such as effective heat of combustion, mass loss rate, ignitability and smoke generation for small samples of materials used in furniture and building materials.

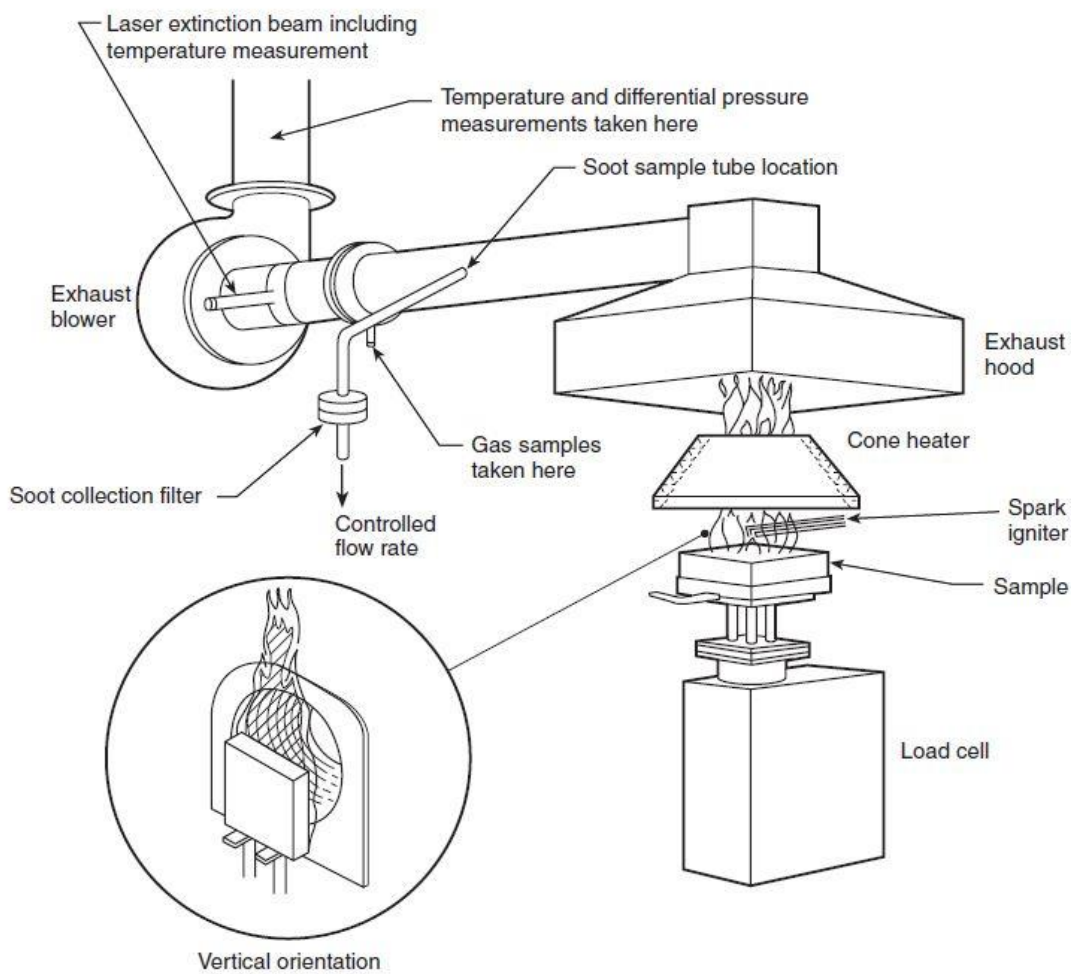


Figure 3.1 Cone calorimeter detailed schematic [130]

The Leeds cone calorimeter is (Figure 3.2) the standardised version, purchased from FTT (Fire Testing Technology Ltd.). In this work the modification used is a manufacturer supplied enclosure with the conical heater fitted to the top side with 80 mm diameter for the top opening and 177 mm for the bottom one with 65 mm

depth for the conical heater. The enclosure box is 38 cm long, 30 cm wide, 33 cm high.

On the top of cone calorimeter heater, a chimney was placed. This chimney was made of stainless steel with an internal diameter of 8 cm and height of 21 cm.

Load cell is placed inside the box. Introducing the chimney or extended exhaust has been adopted by other researchers and standards for different purposes.

The standard setup of the cone calorimeter test method according to BS ISO 5660:2015 tests samples with a 100 mm by 100 mm and a depth from 5 to 50 mm mounted on a load cell measuring the loss of weight as it burns during the test. The sample is mounted 25 mm below the conical heater, this distance is vital for ensuring that the designated heat flux is applied to the sample surface uniformly.



1. Combustion box enclosure	4. Control panel
2. Hood	5. Heated FTIR pump and filter assembly
3. Heated FTIR line	6. Flow meter

Figure 3.2 Cone calorimeter setup

The burning gases mixture released by the sample travels through the conical heater (chimney is not present in the standard method) and is mixed with more

fresh air after exiting the cone. The gases are then collected by the metal hood aided by the fan motor pulling the smoke through the exhaust duct. The flow recommended by the standard is 24 l/s which is measured by the thermocouple and pressure ports fitted across the orifice plate at the exhaust stack. A sampling ring is positioned further down the exhaust duct by 685 mm where 12 holes facing downstream collect a representative homogeneous gas sample which then goes through soot filters and sample treatments to remove water (cold trap and drying agent) before it reaches gas analysers. A laser system is applied on the smoke, just after the ring sampler, monitoring the obscuration and smoke production.

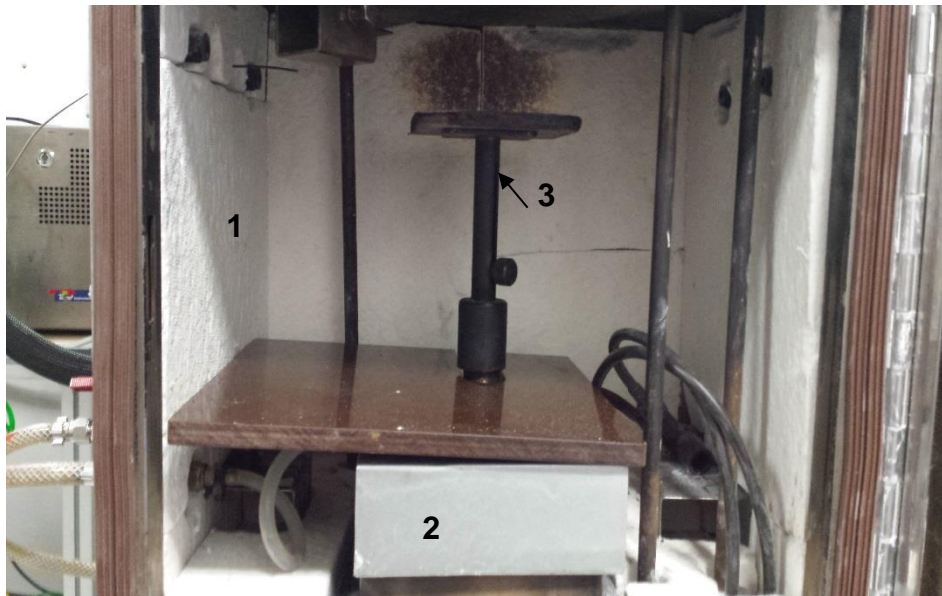
Burning inside box takes place with a controlled air flow which creates a primary gasification zone. The exit mass flow rate of the products from the box can be calculated with inlet air flow rate and measured mass loss rate of the sample. Gases leaving from the box are the raw gases that are leaving the primary gasification zone and enter the secondary combustion zone where excess air is introduced for the burning of the gases from the primary zone. The gases from the gasification stage were recorded using heated FTIR and the sampling was done from the chimney above the heater.

3.3.1 Insulation of cone calorimeter box

In order to avoid heat losses from the box, 2.5 mm thick kaowool insulation board was used to insulate the box. The top surface and the door was insulated from outside, while the rest of the box was insulated from the inside. After insulation, the internal dimensions of the box became 33 cm long, 27.5 cm wide, 30.5 cm high.

3.3.2 Raw sampling methods

In order to achieve gasification conditions inside the box a series of experiments were performed with different configuration of the sampling points and sampling probes in order to reach the desired results.



- 1. kaowool insulation
- 2. cooling jacket on load cell
- 3. Load cell

Figure 3.3 Insulated cone calorimeter box with cooling jacket

In the very first tests performed, the configuration was same as was used for the previous fire research. There was a raw sampling point 6cm high from the bottom of the chimney to sample the gases leaving the primary combustion zone. This sampling point is attached to the FTIR to record the composition of the gases leaving the primary gasification stage. Thermocouple was inserted in the chimney 9 cm above this gas sampling point to record the temperature of the gases leaving the primary combustion zone. Another thermocouple was inserted in the space above the centre of the chimney (hood) and has adjustable location in respect to the top of the chimney (Figure 3.4).

In this configuration sampling was done by a single hole gas sampler that was sampling from the centre of the chimney. This method takes assumption that gases are fully mixed inside the chimney but it was proved that this is not actually happening.

Another probe was used in the process of the development of the testing method to get the representative mixture of the gases from the chimney. The probe had 4 equidistance holes of 1.88 mm diameter 1.6 cm apart. This probe was inserted at the same position as shown in the Figure 3.6 (a)but it was inserted fully (8 cm) inside the chimney.

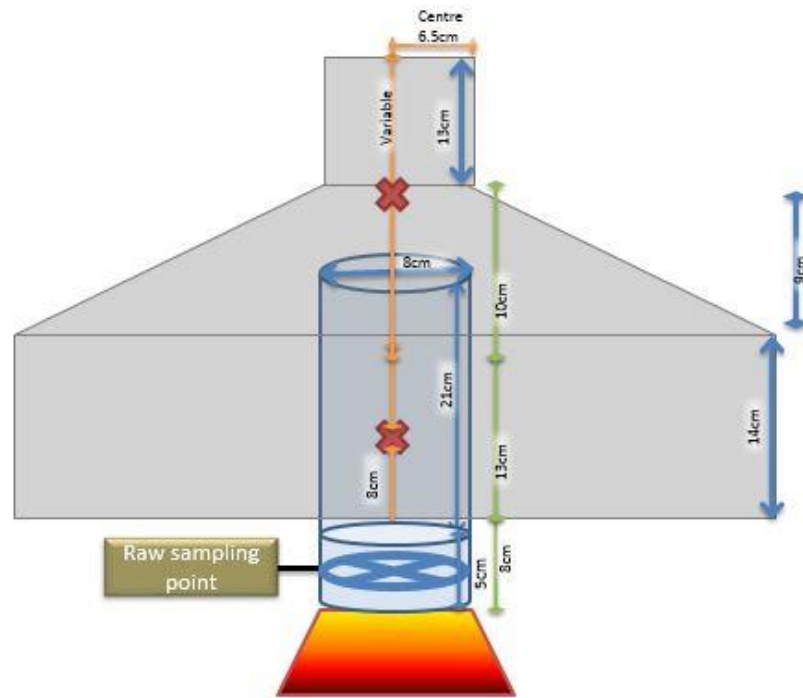


Figure 3.5 Schematic of the sampling method 2 from the chimney and relative positions of the sampling point and thermocouples

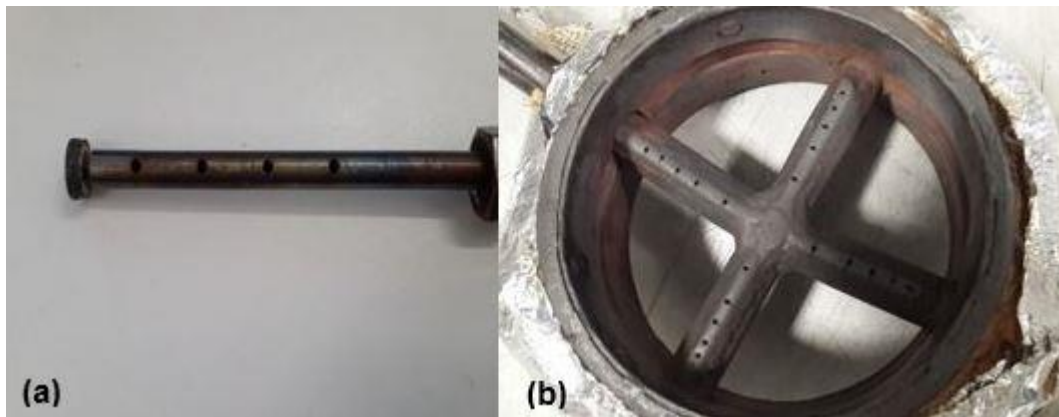


Figure 3.6 Types of probes used in the present research (a) 4 holes probes (b) x probe with 20 holes

3.3.2.1 Insulation seals

A superwool paper insulation (Figure 3.7 (a)) was used to fill the gaps between the chimney (Figure 3.7 (b)) and the top section of the cone, chimney was not bolted to the top section of the cone, it was resting on the top section of the cone on its own, later when an additional x – probe section was used, superwool paper was used to fill the air gaps and it was make sure that there were no air leaks.

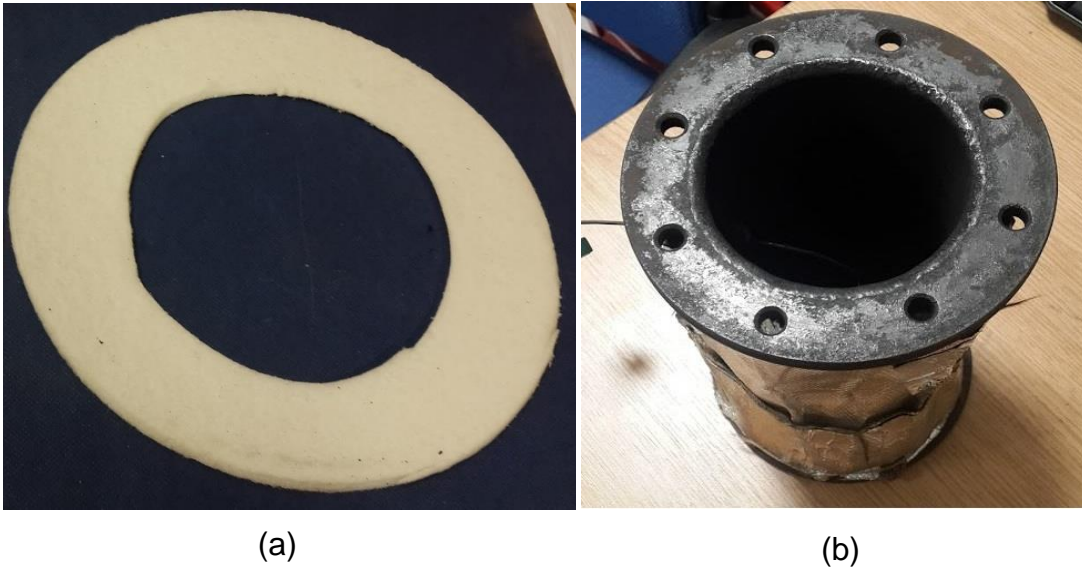


Figure 3.7 (a) Superwool insulation (b) chimney

3.4 Gas analysis equipment

The product gas analysis was done at two points, first point is from chimney, before the secondary combustion zone and sampling from this point is called “Raw sampling”. Here FTIR spectrometer analyses the composition of about 50 species. FTIR spectrometer analyses wet gas sample, downstream of the FTIR analysis, is a condenser with cooling water and silica gel tube for the removal of water vapours from the gases before they pass a paramagnetic oxygen analyser for O₂ level measurements after primary combustion zone.

Second sampling point is after secondary combustion stage when gases has become diluted with air, a paramagnetic oxygen analyser, and a NDIR gas analyser for CO and CO₂ measurements.

3.4.1 Sampling system for the FTIR

Sampling lines used in this work are made of PTFE (Polytetrafluoroethylene) with an outer diameter of 6 mm and an inner diameter of 4.5 mm. When used as heated sampling lines it was aimed to be heated to 180 °C during tests. PTFE sampling lines are capable of handling temperatures up to 200 °C.

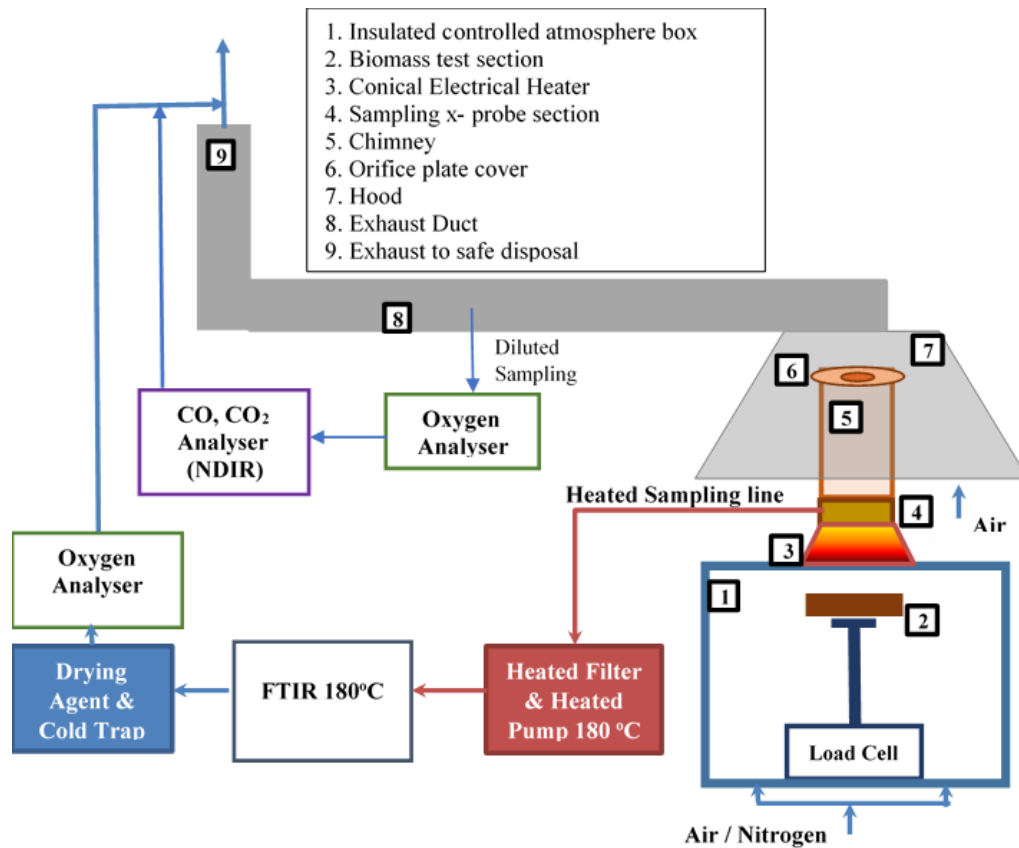


Figure 3.8 Cone calorimeter- FTIR schematic

Gas was sampled with the help of a heated diaphragm pump placed inside a portable sampling unit. For the operation of the pump and the correct analysis of the gases, sample should be free of soot, for this purpose a heated (180 °C) cylindrical particulate filter was used upstream of the pump inside the portable sampling unit. Sample from this unit was pumped to the FTIR analyser using a heated FTIR line. A heated pump located before the gas cell has the advantage of preventing pressure drop at the gas cell. The sample cell of the FTIR is also heated at 180°C so that all gases are analysed and calibrated in the presence of water vapour.

3.4.2 FTIR analyser

A heated Tetmet Gaset CR-series FTIR spectrometer was used for the present research. This FTIR is purpose built portable unit that has UK Environmental Agency MCERT approval for legislated flue gas composition measurements. It was calibrated by the manufacturer for 60 gaseous species also the annual maintenance and water calibrations are done annually. This analyser uses a

liquid nitrogen cooled MCT (mercury-cadmium telluride) spectrometer detector enables the resolution of 8 or 4 cm^{-1} , with a minimum scan frequency of 10 Hz and covers wave number range from 600 to 4200 cm^{-1} and gives 0.3 – 2 ppm minimum detection limits, depending on the gas. As it is fully heated it measures the total water vapour present in the sample. H_2 is not absorbed by the infrared and cannot be detected by FTIR. Gas spectra was recorded after every 5 s.

3.4.2.1 Principle of FTIR measurement

Fourier transform infrared (FTIR) is an infrared spectroscopy technique for chemical analysis compounds. The technique is based on two basic principles; firstly, molecular vibrations take place in the infrared region, secondly, each compound has a characteristic absorption frequency and the intensity of absorption is correlated to the concentration of that compound. Most targeted gases have their peak vibrations in the wavelength range from 2.5 – 16 μm equivalent to the wave number range 4000 – 625 cm^{-1} .

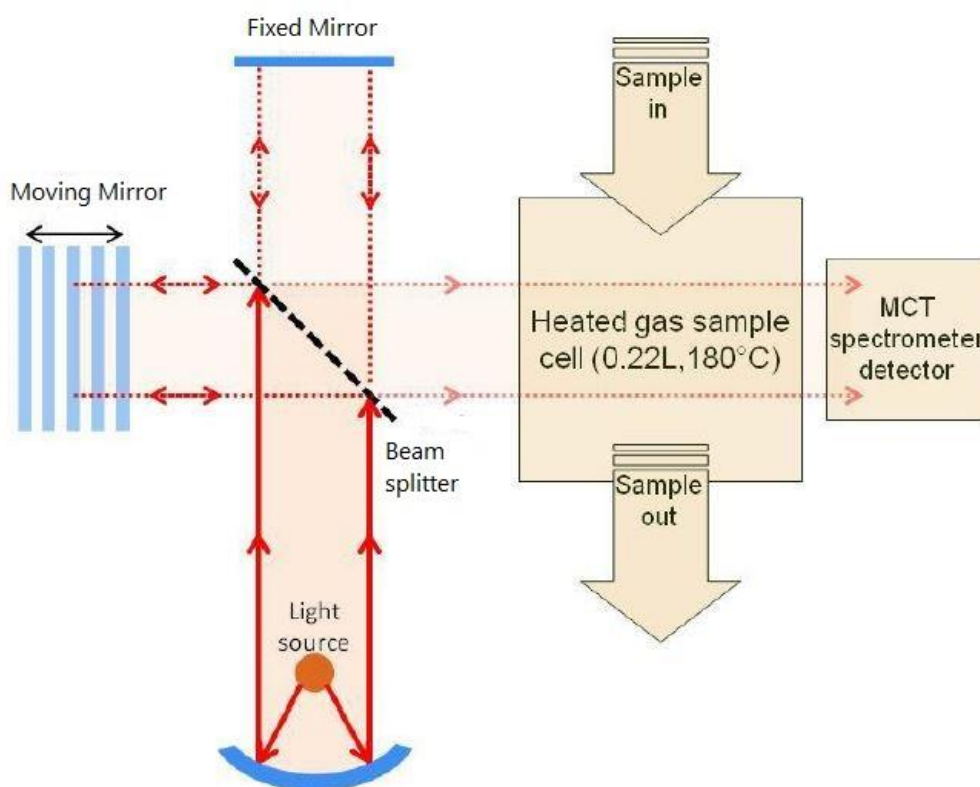


Figure 3.9 Working principle of the FTIR analyser

The Gasmet FTIR CR-2000 has a heated sample cell (up to 180 °C), which has a multi-pass fixed 2 m path length and a sample cell volume of 0.22 litres. The detection cell is gold coated aluminium to achieve high corrosion resistance.

In a FTIR, Infra-Red radiations generated by the source materials are first passed through a interferometer that consist of a beam splitter, a fixed mirror, and a mirror that can move back and forth, very precisely. Radiation from the source strikes the beam splitter and separates into two beams. One beam is transmitted to the fixed mirror and second beam is reflected to the moving mirror. The fixed and moving mirrors reflect the radiation back to the beam splitter. The leaving signal comprise of the two beams interfering each other known as an interferogram. This interferogram is passed through the sample where some of the radiations are absorbed depending upon the types of species present. The resulting spectrum represents the molecular absorption and transmission. Like a fingerprint, two unique molecular structures cannot produce the same infrared spectrum. The measured interferogram signal is “decoded” via well-known mathematical technique called the Fourier transformation done by computer programme which presents the user with the spectral information for analysis.

3.4.2.2 Analysing FTIR spectra

The recorded FTIR sample spectra were analysed (qualitatively and quantitatively) using Calcmet software [131]. Calcmet can analyse the sample for more than 50 components. However, it is not recommended to analyse more than 50 components at one time for the best accuracy of analysis. Calcmet provides many useful features, such as simultaneous analysis, identification of gas components using a library search routine and ensuring quality of analysis by monitoring residual absorbance. The maximum acceptable value for overall residual is 0.2, when it is exceeded the spectrum is re-analysed with less interfering species to improve the quality of the readings by reducing the residual value, if that cannot be achieved then the analysis are ruled out as inconclusive and discarded [131].

The Gasmeter FTIR used in the present work had the calibration points and ranges of main components frequently used in fire research FTIR gas analysis is shown in the Table 3.1.

Table 3.1 Concentration ranges and number of data points for the FTIR calibration.

Sr. #	Gas name	Formula	No. of calibration points	Calibration range [ppm]
1	Water Vapour	H ₂ O	22	5000-380000
2	Carbon dioxide	CO ₂	7	3000-301000
3	Carbon monoxide	CO	10	103-9960
4	Nitrous oxide	N ₂ O	3	100-500
5	Nitrogen monoxide	NO	9	50-2008
6	Nitrogen dioxide	NO ₂	3	50-4885
7	Ammonia	NH ₃	5	50-503
8	Hydrogen cyanide	HCN	3	100-500
9	Methane	CH ₄	5	100-995
10	Ethane	C ₂ H ₆	2	99-506
11	Propane	C ₃ H ₈	2	101-500
12	Butane	C ₄ H ₁₀	2	100-500
13	Pentane	C ₅ H ₁₂	3	50-500
14	Iso-pentane	C ₅ H ₁₂	1	100
15	Hexane	C ₆ H ₁₄	3	50-500
16	Heptane	C ₇ H ₁₆	3	50-500
17	Acetylene	C ₂ H ₂	2	98.8-500
18	Ethylene	C ₂ H ₄	2	93-493
19	Propene	C ₃ H ₆	2	100-500
20	1,3-Butadiene	C ₄ H ₆	1	100
21	Benzene	C ₆ H ₆	3	50-500
22	Toluene	C ₇ H ₈	3	50-500
23	m- xylene	C ₈ H ₁₀	3	50-500
24	o-xylene	C ₈ H ₁₀	3	50-500
25	p-xylene	C ₈ H ₁₀	3	50-500

26	1,2,3-Trimethylbenzene	C ₉ H ₁₂	3	50-500
27	1,2,4-Trimethylbenzene	C ₉ H ₁₂	3	50-500
28	1,3,5-Trimethylbenzene	C ₉ H ₁₂	3	50-500
29	Ethylbenzene	C ₈ H ₁₀	2	100-500
30	Methanol	CH ₃ OH	3	50-500
31	Ethanol	C ₂ H ₅ OH	3	50-500
32	Propanol	C ₃ H ₇ OH	3	50-500
33	MTBE	C ₅ H ₁₂ O	3	50-500
34	Formaldehyde	CH ₂ O	1	96
35	Acetaldehyde	C ₂ H ₄ O	2	50-200
36	Formic acid	CH ₂ O ₂	3	50-500
37	Acetic acid	C ₂ H ₄ O ₂	3	50-500
38	Acrolein	C ₃ H ₄ O	3	50-500
39	1-Ethyl-naphthalene	C ₁₂ H ₁₂	3	50-500
40	Dimethyl ether	C ₂ H ₆ O	3	50-500
41	Acetone	C ₃ H ₆ O	3	50-500
41	Furfural	C ₅ H ₄ O ₂	3	20-100
43	Furfuryl alcohol	C ₅ H ₆ O ₂	1	100
44	Guaiacol	C ₇ H ₈ O ₂	5	10-200
45	p-Cresol	C ₇ H ₈ O	1	50
46	Phenol	C ₆ H ₆ O	2	20-100
47	i-Butane	C ₄ H ₁₀	2	70-102
48	1-Butene	C ₄ H ₈	2	98-501
49	i-Butene	C ₄ H ₈	1	74
50	Pentene	C ₅ H ₁₀	2	100-250
51	Hexene	C ₆ H ₁₂	4	100-500
52	Heptene	C ₇ H ₁₄	3	100-500
53	Octene	C ₈ H ₁₆	3	100-500
54	Nonene	C ₉ H ₁₈	3	100-500

3.4.2.3 FTIR validation

The Gasmeter FTIR used in the present work has also been used by Andrews, for exhaust emissions measurement in on-road vehicles and there was an extensive calibration exercise undertaken for this application [132, 133]. This included comparison over a legislated transient test for vehicle emissions on a legislated test facility. This demonstrated good agreement with the legislated measurement techniques for CO, CO₂ and NO_x. The Gasmeter FTIR had reference gases calibrated by the manufacturer for 63 different gases. Also the annual maintenance and water calibration is carried out by the manufacturer. Calibration was also validated many times for different projects [134]. Alarifi [135] also checked the calibration of FTIR by a certified bottle (16.23% CO₂, 1063 ppm Hexane and the rest Nitrogen) and found very good agreement as shown in the Figure 3.10.

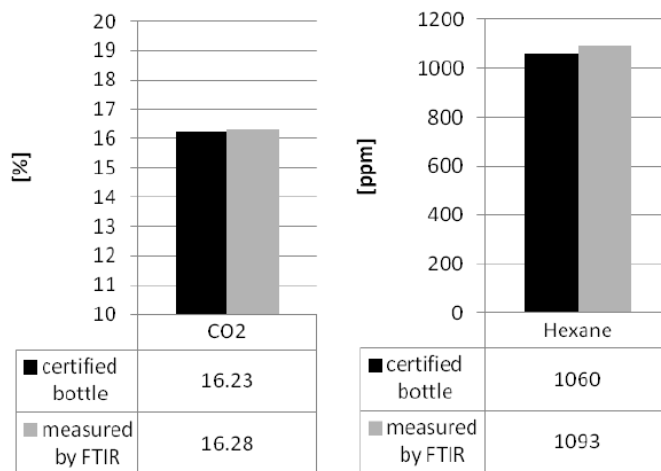


Figure 3.10 Certified mixture bottles validation [135]

Alarifi also checked emissions during fire using a NDIR analyser connected to the outlet of the FTIR. The outlet gas sample was dried using an ice bath and drying agent before it enters the NDIR to be analysed for CO and CO₂. A very good agreement was found by the two independent gas analysers for CO under fire conditions in laboratory test (cone calorimeter) as shown in the Figure 3.11.

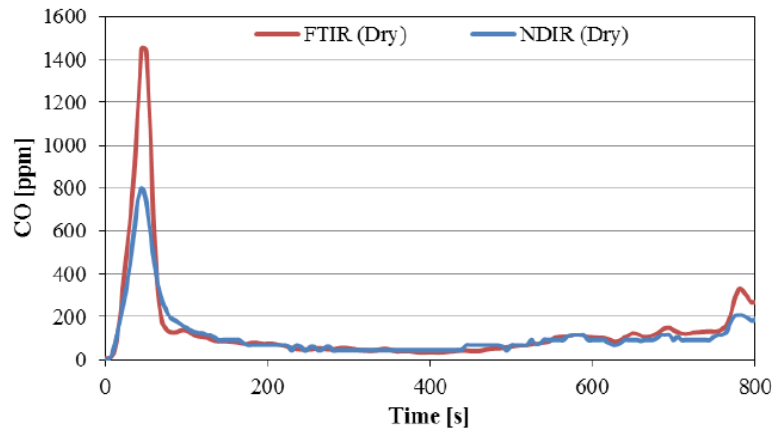


Figure 3.11 Carbon monoxide measurements (FTIR & NDIR) from cone calorimeter test [135]

For the present work validation of the results was done again using certified bottle, having mixture of CO 7%, CO₂ 10%, Propane 300 ppm and balance nitrogen, results for the reading of FTIR are shown in the Figure 3.12. It can be seen that FTIR reading was in very good agreement with the actual concentration of the gases. FTIR was calibrated with CO upto 1% , it can be seen in the Figure 3.12 (b) that it can read the high concentration of 7% CO with very low error.

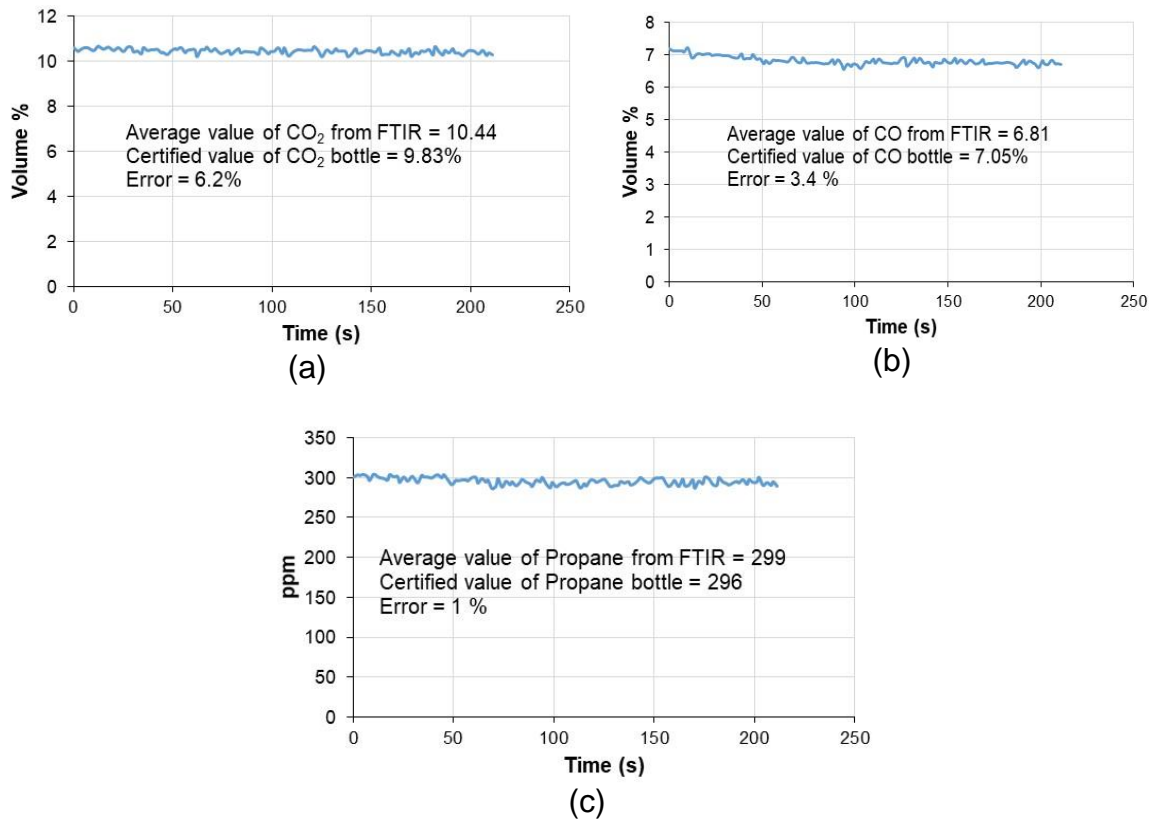


Figure 3.12 Certified mixture bottle comparison with FTIR (a) CO₂ (b) CO (c) Propane

Another bottle having a mixture of CO 4500 ppm, CO₂ 14 %, NO 800 ppm, Propane 5000 ppm and the balance nitrogen was checked using FTIR and the results are shown in the Figure 3.13. It can be seen that FRIT was reading very close.

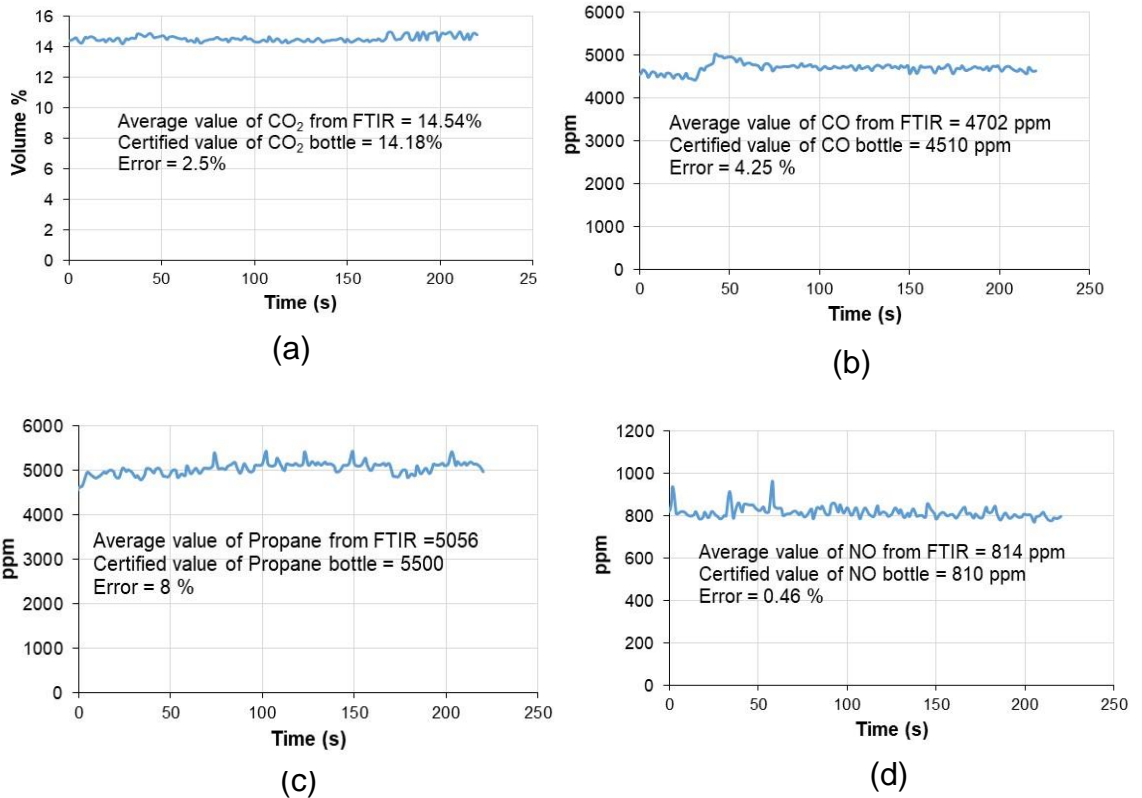


Figure 3.13 Certified mixture bottle comparison with FTIR (a) CO₂ (b) CO (c) Propane (d) NO

3.4.3 Paramagnetic oxygen spectrometer

Two paramagnetic oxygen analysers were used in this research work. One analyser was placed downstream of the FTIR for 'Raw' gas O₂ measurements and the second oxygen analyser was for the dilute sampling of the gases of combustion after dilution with the air.

Unlike most other gases O₂ is attracted by a strong magnetic field (is paramagnetic) and therefore its detection is possible by a paramagnetic analyser. The level of O₂ in the exhaust (raw and dilute) was measured by two different Servomex 1400 Series with detection range of 0-100%. A focused magnetic field is created. Any oxygen that is present will be attracted into the strongest part of the magnetic field.

In paramagnetic analyser dry gas is introduced into a chamber containing nitrogen filled "dumbbells" placed within a magnetic field. The dumbbells can rotate about a vertical shaft against a torque produced by a hairspring. O₂ is attracted by the strongest part of the magnetic field, and produces a torque that causes dumbbell to rotate against the hairspring. A mirror attached to the shaft

reflects light from a source to the scale that detects the deflection by photo detector and passes current signal to coil wound around dumbbells and produces a torque opposite to original torque (produced by O₂) to bring dumbbells to its original position. This current produced is proportional to concentration of O₂ in gases.

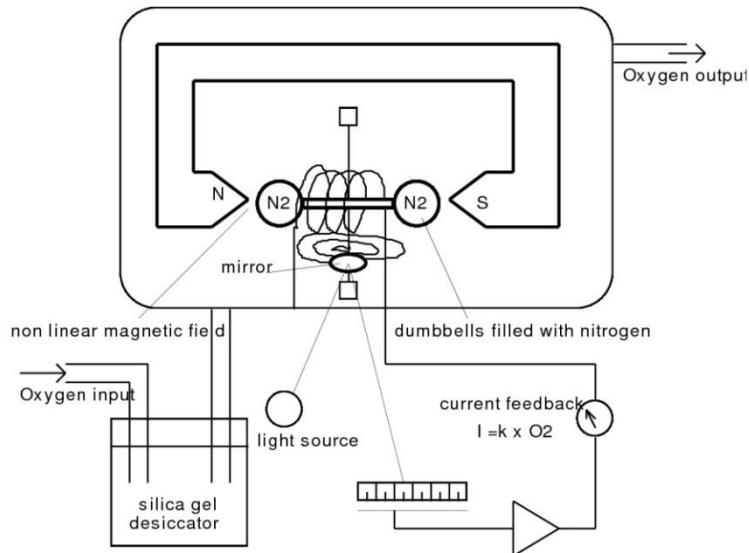


Figure 3.14 Schematic diagram of paramagnetic oxygen spectrometer [136]

3.4.4 Non-dispersive Infra-red (NDIR) analyser

The levels of CO₂ and CO in the dilute gas mixture were analysed by a Hartmann and Braun Uras 10E model NDIR. Typical NDIR analyser consists of two infrared sources, a reference cell filled with a non-absorbing gas usually nitrogen, a sample cell having a sample of exhaust gases which are needed to be measured, and a detector. Energy from infrared source is passed through the reference and sample cells to the detector. When the sample cell contains no gas or filled with an inert gas, the radiations reaching the detector from this cell the same as the reference cells radiations. But, when sample cell contains sample gases, radiations are absorbed that reduce the radiations that reach the detector. The difference between signal received from the two beams is measured by the detector and is proportional to the amount of absorbing gas in the sample cell.

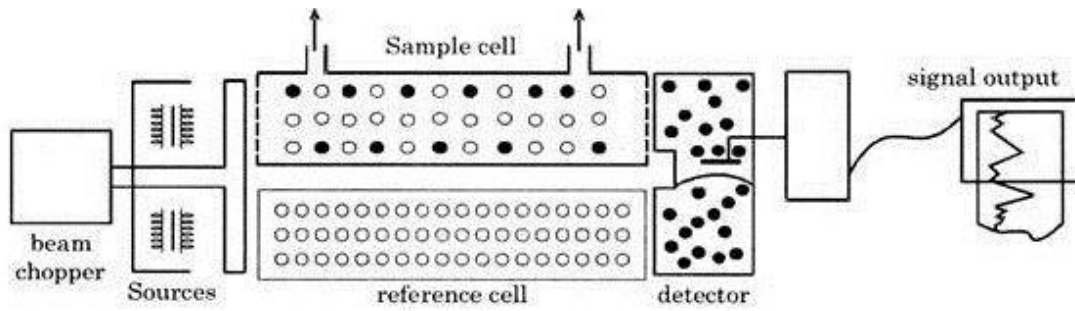


Figure 3.15 NDIR analyser principle [137]

3.5 Heat release rate calculations

The HRR was calculated by two methods, one based on the biomass mass loss rate (MLR) and the other based on the principle of oxygen consumption calorimetry which requires the air mass flow rate and the oxygen concentration downstream of the combustion zone. The relationship between HRR and MLR is given by equation.

$$HRR = \Delta h_c \times MLR \quad (9)$$

where

$$\Delta h_c = \text{Net heat of combustion (kJ/g)}$$

Oxygen consumption calorimetry is based on the fact that a constant amount of heat is released per kg of oxygen consumed, for complete combustion of liquid or solid fuels. Hugget [138] found the value of this constant to be 13.1 kJ/g of oxygen with an accuracy of $\pm 5\%$ or better. The generalized HRR is given in equations below [130]

$$\dot{q} = E \cdot (\dot{m}_a Y_{O_2}^a - \dot{m}_e Y_{O_2}^e) \quad (10)$$

Where

\dot{q} heat release rate kW

E Net heat released per unit mass of oxygen consumed 13.1 kJ/g of oxygen

\dot{m}_a Mass flow rate of inlet (ambient) air

\dot{m}_e Mass flow rate of exhaust

$Y_{O_2}^a$ Mass fraction of oxygen in ambient air (0.232 g/g air)

$Y_{O_2}^e$ Mass fraction of oxygen in combustion products

This concept is same as it was found that for many organic fuels about 3 MJ of energy is released per kg of air burned by complete combustion. In other words 1 kg/s air can sustain a 3MW fire [99].

For example for ethanol stoichiometric air to fuel ratio is 9 and CV is 27 MJ/kg, that gives heat release per kg of air = $27/9 = 3$ MJ/kg

Similarly air to fuel ratio of wood is ~ 6 and its CV is ~ 18 and it gives heat release per kg air = $18/6 = 3$ MJ/kg

As discussed above, there were two oxygen sampling points, one after primary gasification zone (enclosed box) and other in the exhaust duct to measure corresponding heat release rates by oxygen consumption calorimetry.

3.6 Emission index EI

The emission index (EI) is defined as [133]

$$EI = \frac{\text{Mass of the emissions}}{\text{Mass of the fuel}} \quad (11)$$

The EI is related to the volumetric species concentration C and the exhaust A/F by mass

Or

$$EI = K \times C \times \left[1 + \left(\frac{A}{F} \right) \right] \times 1000 \text{ g/kg fuel} \quad (12)$$

where

K = Ratio of molecular weight of the gas component to that of the exhaust sample.

For many combustion situations the molecular weight of the exhaust gases is approximately equal to that of air to less than 2% error. For CO the K value is 0.968 if the concentration C is a fraction, with appropriate conversion used if the actual measurement is % or ppm. The combustion efficiency due to CO, hydrogen and hydrocarbons can be determined from equation 12 by multiplying by the CV kJ/g for each component with EI and dividing by the CV of the biomass. This is then an energy ratio which is the % of the original biomass energy that remains in the CO, H_2 and hydrocarbons that flow from the gasification zone into the secondary combustion zone.

3.7 Hot gas efficiency (HGE)

Sometimes gases are burnt and used in a furnace or boiler without cooling and it gives greater utilization of energy. Log boilers are also one of these systems in which sensible heat of the gases is utilized for heat transfer in the secondary stage. For these types of system hot gas efficiency is used as a measure of gasifier efficiency [52]. Hot gas efficiency is defined as

$$HGE = \frac{(HHV \text{ of the product gases} + \text{Sensible heat of the gases}) \left(\frac{MJ}{kg \text{ biomass}} \right)}{HHV \text{ of the Fuel}} \quad (13)$$

HHV of product gases was calculated using the HHV (MJ/kg of specie) of the components gaseous species from the literature [139] and multiplying this value by the emission index kg of specie/kg of biomass.

3.8 Test materials

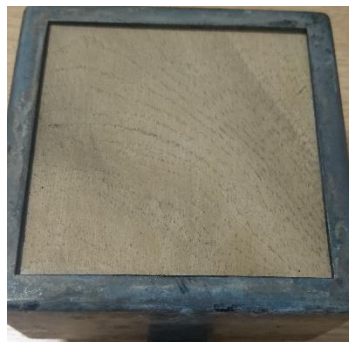
Woody biomass as well as biomass from crop residues were used in the present research. Different biomass of different sizes were used. Pine, ash and sycamore wood were used in stick form. Pine wood was purchased from the local timber shop in UK. Ash and sycamore wood sticks were collected from the UK. Eucalyptus and acacia wood was used in the form of blocks and were brought from Pakistan. Crop residues corn cobs, wheat straw, and rice husk were brought from Pakistan as well. Wood pellets, sunflower shell pellets, torrefied wood pellets, soft wood sawdust raw and torrefied, grade B wood and torrefied sawdust were obtained from local power plants. Some big size pellets made up of corn straw having skin colour, and sawdust mixed with clay having dark colour made by piston hydraulic machine were also tested. These pellets were brought from China. Some of the biomass arranged in the in the test section are shown in the Figure 3.16.

3.9 Experimental procedure for the cone calorimeter test

1. Wood and biomass samples were placed in the sample holder 100mm x 100mm x 20mm and the details of the particle size are provided in the Table 4.2.



Pine wood



Acacia wood



Eucalyptus wood



Dry ash wood



Wet ash wood



Mountain ash pellets



Grade B torrefied wood



White wood pellets



Sunflower shell pellets



China's biomass black



China's biomass skin



Corn cobs

Figure 3.16 biomass test samples

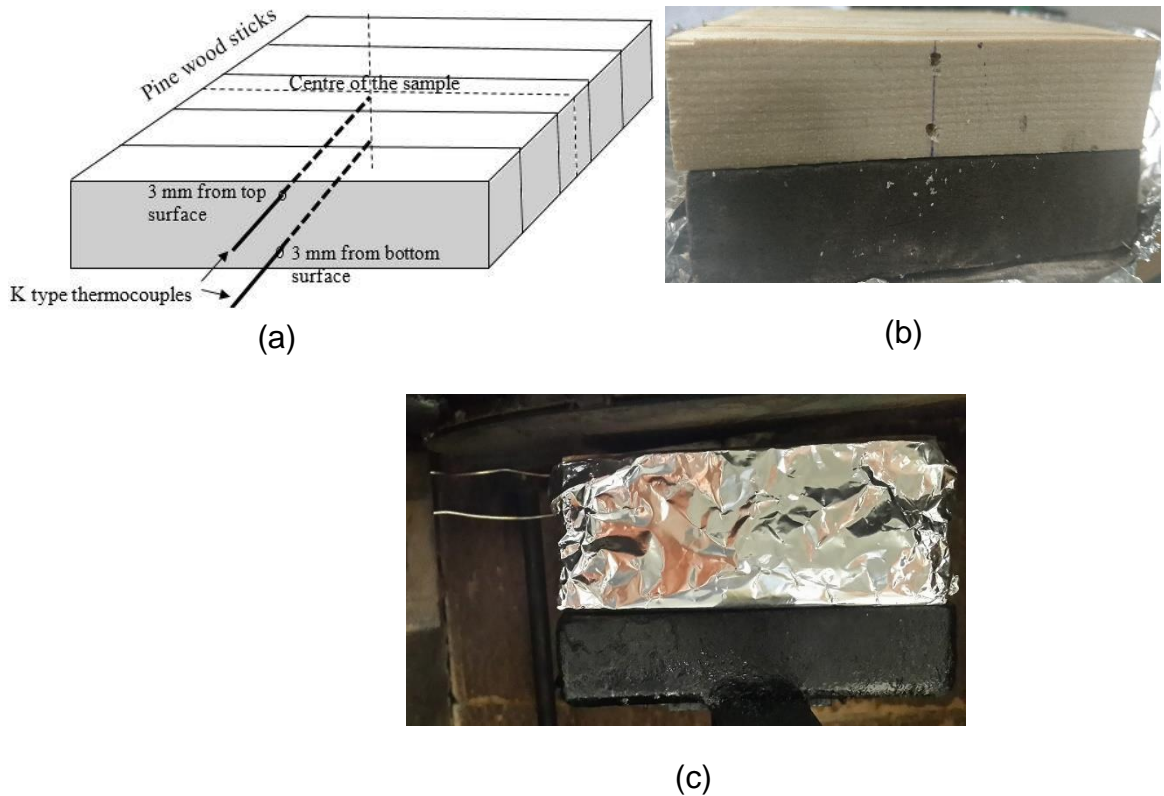


Figure 3.17 Thermocouples test (a) schematic (b) Pine wood thermocouple holes (c) Sample with thermocouples inside box

2. Thermocouples were inserted in some of the tests with pine wood and hard woods. To record the sample temperature during tests two 1.5mm thick type K thermocouples were inserted from the side wall with the recording tip reaching the centre-line of the central wood stick at 5mm from the top and 5 mm from bottom surface of the wood with 40mm thickness tests done initially. When experiments were performed with 20mm wood thickness in the final setup, thermocouple were inserted 3mm from top and bottom surface of the wood.
3. After the calibration of the analysers and FTIR, heater of the cone calorimeter was switched on with the temperature set point corresponding to the desired heat flux that is already determined by a heat flux meter while shutters of the heaters are still on.
4. When the desired heat flux was achieved, Primary airflow into the enclosure (gasification zone) was regulated by a gauge and measured by a flow-meter.

5. The sample holder with biomass was mounted on the pedestal of the mass balance, a 25mm gap was allowed between the surface of the sample and the cone heater.
6. Door of the enclosure was closed and shutters off to start heating of the biomass
7. The mass balance measured the changes in the mass of the sample throughout the test period.
8. After the test debris was collected and analysed.

3.10 Furnace reactor

Pyrolysis tests were also performed in a furnace reactor for the validation of the tests done on the cone calorimeter. Reactor consists of a single vertical tube furnace (Elite Thermal Systems Ltd., Model TSV12/100/750) with furnace bore: 90 mm O/D x 80 mm I/D x 1100 mm long; heated length: 750 mm and maximum furnace temperature of 1200 °C. Schematic of the reactor is shown in the Figure 3.18. The biomass used in the present work was pine wood cubes of 20x20x20 mm and were placed inside a metal basket such that basket was filled more than half, basket was inserted into the reactor with a K-type thermocouple inserted into the middle of biomass load to monitor the temperature. Nitrogen was fed through an inlet at the top of the reactor to remove oxygen and gaseous products made during the experiment. Flow rate of nitrogen in the present work was 2.5 litres/minute and it was chosen because the FTIR require minimum flow rate of 2 litres/minute. The reactor was purged for 5 minutes with the nitrogen before heating the reactor. Furnace temperature was set to the desired test temperature. Under the furnace attached was a condenser and a catch pot for the removal of the condensates from the products of the pyrolysis. Condenser was maintained at 5°C using a water chiller. Gases from condenser and catch pot flowed to the set of impinges for further removal of the particulates and condensable. Gases from the impinges were transported to the FTIR via heated sampling line. Test time was 15000 s (allowing maximum release of volatiles), heater was switched off and after further 5000 s nitrogen was switched off along with FTIR, furnace was left to cool to room temperature before retrieving the charred products. Condensate was collected from the catch pot and impinges, as sample gases were cooling down before heated FTIR, a heated line of 5 meter

was used so allow gases to become hot, but still tars were collecting inside the line and the filter of the FTIR. After every test, PTFE pipe from the inside of the heated line was weighed and replace. Filter of FTIR was also weighed and replaced.

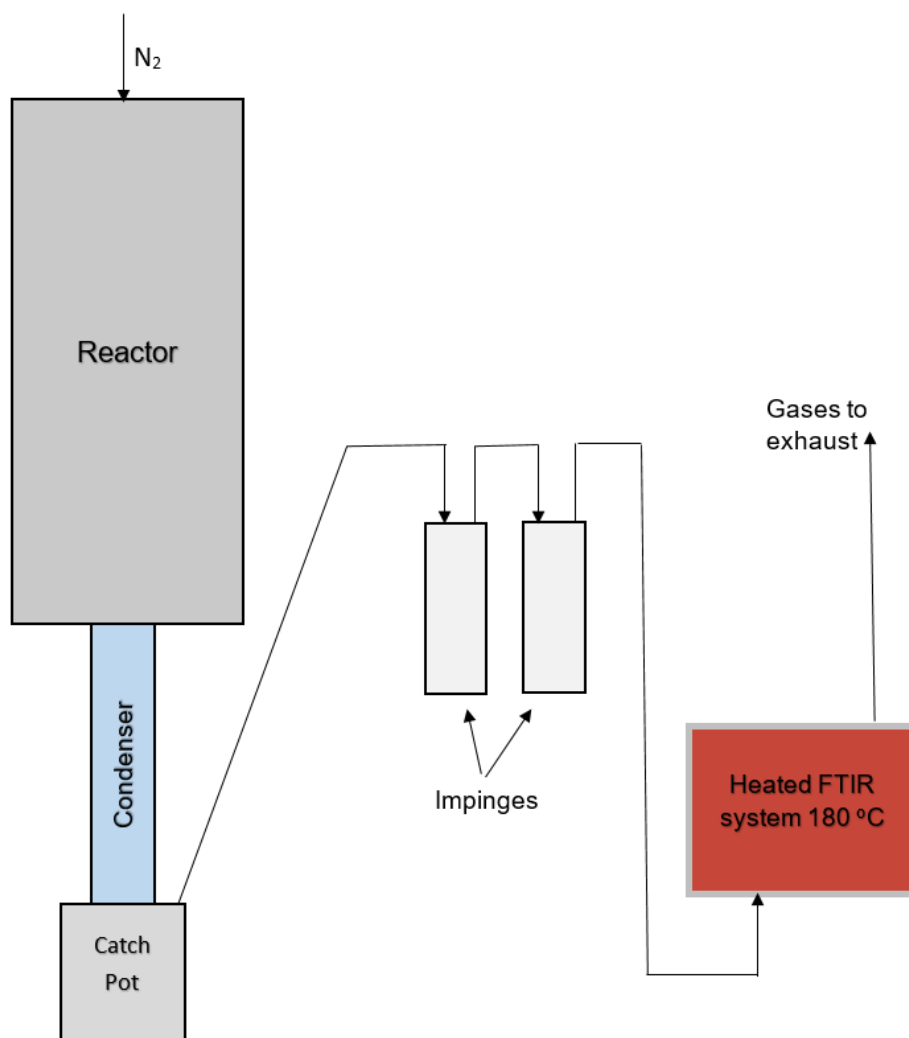


Figure 3.18 Schematic of furnace reactor



1. Reactor	5. Temperature controller
2. Condenser	6. Impinges
3. Catch pot	7. Heated sampling FTIR line
4. Chiller	8. Flow meter

Figure 3.19 Furnace rig



(a)



(b)

Figure 3.20 (a) Pine 20x20x20mm cubes (b) feedstock basket

Chapter 4 Development of the experimental methodology for the cone calorimeter tests

4.1 Ultimate and proximate analysis of the wood

Elemental composition, proximate analysis (by TGA) and calorific value of the biomass is shown in the Table 4.1. Biomass from crop residues have less volatiles as compared to the woody biomass. Agricultural crop residues had higher ash compared to woody biomass. The high ash content is associated with higher alkaline metal content which is a leading cause of fouling and deposition in boilers, thereby lowering the efficiency and also increasing the cost of operation/maintenance. The material of construction and design of the boiler or heat exchanger for this fuel type must be able to bear high ash content and prevent fouling. The process temperature must also be monitored to prevent slagging of ash. Heating values of the crop residues were less due to high ash contents.

The TGA analysis normalised to the initial dry weight is shown in Figure 4.1 as a function of temperature. There was considerable variation in the temperature at which the biomass lost weight. Mass loss rate of volatiles with respect to temperature (Figure 4.2) highlights the release of volatiles with temperature more effectively. This variation was due to the different proportions of hemi-cellulose, cellulose and lignin in the biomass composition. Figure 4.1 has the temperature range for hemi-cellulose, cellulose and lignin decomposition marked. Biomass with a high temperature for the final mass loss are high in lignin and biomass with a low temperature at which weight loss occurs are usually high in hemi-cellulose. The range for cellulose is the linear dependence of weight loss on temperature, between the initial slow start of weight loss as a function of temperature and the final slow loss of weight as a function of temperature due to lignin decomposition. However, there is no agreed methodology to derive the

proportion of hemi-cellulose, cellulose and lignin in biomass, apart from the above qualitative considerations.

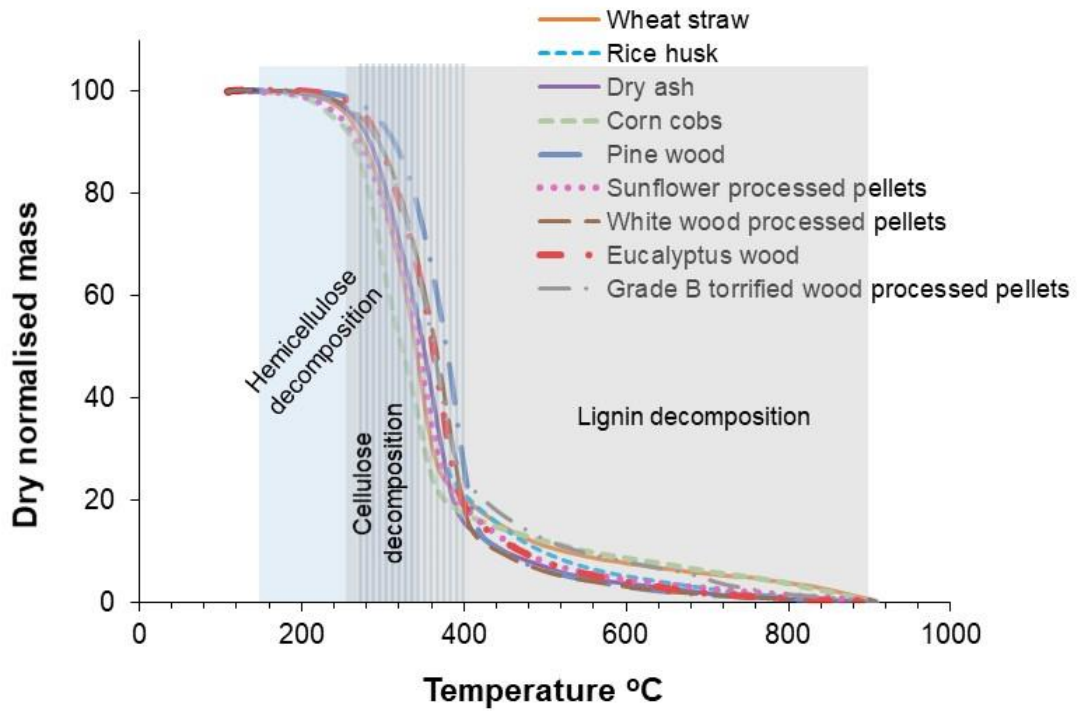


Figure 4.1 TGA normalised mass vs temperature for some biomass samples

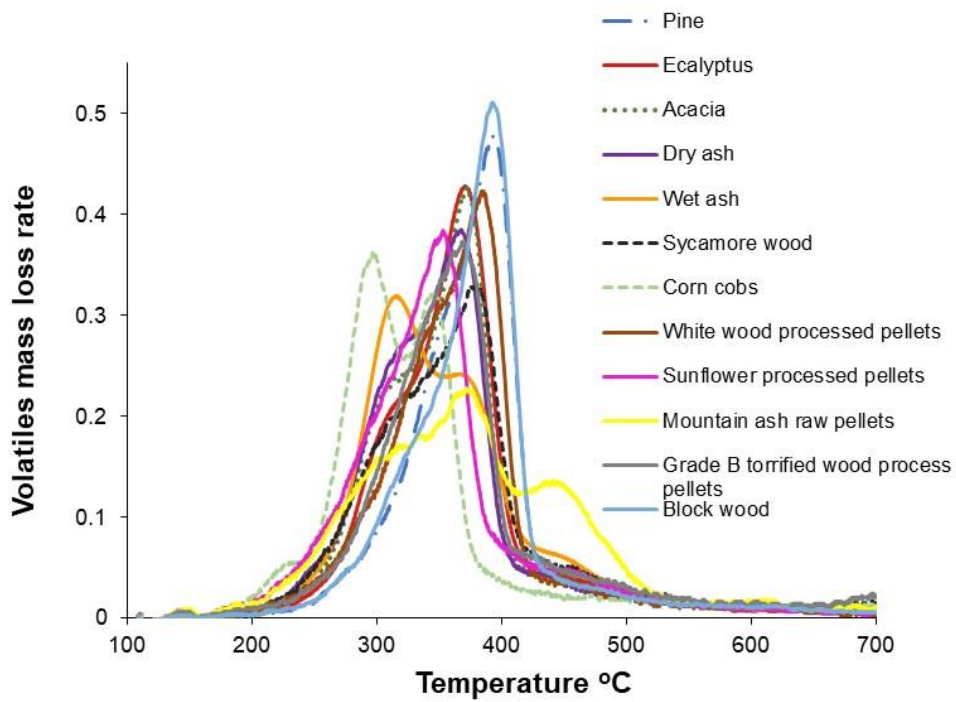


Figure 4.2 volatiles mass loss rate vs temperature of biomass from TGA

Table 4.1 Elemental analysis , proximate analysis, CV and stoichiometric air to fuel ratio for biomass studied.

Biomass	C % daf	H % daf	N % daf	S % daf	O % daf	VM % daf	VM % ar	FC % daf	H ₂ O % Ar	Ash % ar	GCV MJ/kg		Stoich. (A/F)(g/g)	
											Actual	Daf	actual	Daf
Pine wood	48.4	6.1	0.2	0.0	45.4	87.3	81.4	12.7	5.2	1.6	18.9	20.2	5.3	5.7
Ash wood (dry)	48.7	6.5	0.7	0.0	44.1	82.2	74.6	17.8	5.1	4.2	18.3	20.2	5.4	6.0
Ash wood (Wet)	50.6	6.6	0.5	0.0	42.3	84.9	73.6	15.1	9.6	3.6	19.0	21.8	5.5	6.3
Eucalyptus Wood	52.2	6.0	0.7	0.0	41.1	82.0	71.4	18.0	6.4	6.5	19.2	22.0	5.5	6.3
Acacia Wood	49.1	6.0	0.3	0.0	44.6	79.9	73.6	20.1	5.8	2.0	19.0	20.6	5.3	5.8
Block wood	51.1	6.6	1.0	0.0	41.3	83.9	76.9	16.1	6.2	2.2	19.4	21.2	5.9	6.4
Sycamore Wood	54	6.8	0.8	0.0	38.4	83.0	72.5	17.0	8.0	4.6	19.9	22.8	6.1	6.9
White Wood processed pellets	48.8	6.0	1.4	0.0	43.8	86.7	79.6	13.3	4.3	3.9	19.3	21.0	5.4	5.9
Grade B torrefied wood processed pellets	49.0	6.0	2.8	0.0	42.2	80.5	64.2	19.5	6.7	13.5	17.2	21.6	4.8	6.1
Sunflower Shell processed pellets	49.8	5.8	2.1	0.0	42.3	82.3	74.2	17.7	6.2	3.7	19.4	21.5	5.4	6.0

Mountain ash raw pellets	53.8	6.5	1.0	0.0	38.7	87.0	75.2	13.0	9.7	3.9	19.3	22.3	5.9	6.8
China's biomass skin	42.1	5.6	2.0	0.0	50.3	84.1	58.5	15.9	6.9	23.5	11.6	16.7	3.3	4.7
China's biomass black	51.9	6.4	1.9	0.0	39.8	74.1	43.1	25.9	7.5	34.3	12.8	22.0	3.8	6.6
SPF (Spruce, pine, Fir) raw	53.4	6.6	1.0	0.0	39.0	84.4	75.3	15.6	6.0	4.8	18.6	20.9	6.1	6.8
SPF torrefied	56.0	7.2	1.1	0.0	35.6	79.4	72.8	20.6	5.4	3.0	20.1	22.0	6.8	7.5
Grade B wood	53.4	6.6	2.5	0.0	37.4	85.6	69.6	14.4	7.8	10.8	17.1	21.1	5.7	7.0
Grade B torrified wood	54.5	6.3	2.7	0.1	36.5	81.3	65.2	18.7	5.8	14	17.6	21.9	5.7	7.0
Corn cobs	45.9	6.0	1.2	0.0	46.8	82.5	69.4	17.6	7.1	8.8	14.8	17.6	4.9	6.9
Wheat straw	49.0	6.8	1.1	0.2	42.9	84.1	57.3	15.9	5.5	26.3	14.1	20.7	4.2	6.2
Rice husk	48.4	6.4	1.4	0.0	43.7	80.0	53.7	13.5	6.7	26.2	13.7	20.4	4.0	6.0

Table 4.2 Particle size, density, hemicellulose, cellulose and lignin contents for different biomass studied

Biomass	Hemi-cellulose %	Cellulose %	Lignin %	Particle size mm	Initial mass in the cone test section (g)	Density kg/m ³	
						Particle	Bed
Pine wood	34.9	40.5	24.6	100 x 20 x 20	107	540	
Ash wood (dry)	37.2	43.5	19.4	D = 20, L = 100	83	620	
Ash wood (Wet)	38.1	39.9	22.0	D = 20, L = 100	101	750	
Eucalyptus Wood	38.9	36.9	24.2	100 x 100 x 20	160	910	
Acacia Wood	32.0	42.0	26.0	100 x 100 x 20	162	960	
Block wood	38.2	38.9	22.9	100 x 100 x 20	135	760	
Sycamore Wood	44.2	33.3	22.5	D = 20, L = 100	53	260	
White Wood pellets	34.8	39.8	25.4	D= 5, L = 7-25	135		675
Grade B torrefied wood pellets	33.4	40.8	25.8	D= 5, L= 10-35	160		780
Sunflower Shell pellets	35.9	39.9	24.2	D = 7, L = 5-20	135		670
Mountain ash pellets	44.7	30.3	25.0	D= 5, L = 10-25	84		420
China's biomass skin	48.3	42.6	9.1	30 x 30 x 100	245		900
China's biomass black	34.8	27.7	37.4	30 x 30 x 100	350		1290
SPF raw	42.8	34.0	23.3	0.1 – 5	44		215
SPF torrefied	26.6	22.0	51.4	0.1 – 5	36		180
Grade B wood	31.0	23.2	45.8	0.1 -10	36		180
Grade B torrefied wood	48.7	28.9	22.4	5-20	44		215
Corn cobs	63.2	35.9	1.0	D= 2.5, L= 10	73		300
Wheat straw	41.9	42.2	15.9	5-30	29		95
Rice husk	35.2	42.6	22.1	D= 1, L-10	33		105

Note: Red coloured percentage are outside the range of validity of the correlations

The proportions of cellulose, hemicellulose and lignin in the biomass samples were calculated using the correlation proposed by Sheng and Azevedo [95] given in equations 14 and 15. These correlate from many biomass over the range of H/C from 1.26 to 1.69, O/C from 0.56 to 0.83 and VM from 73 to 86%. The correlation coefficient was 90% for cellulose and 81% for lignin.

$$\text{Cellulose} = -1019.07 + 293.810 (O/C) - 187.639 (O/C)^2 - 65.1426(H/C) - 19.3025(H/C)^2 - 21.7448(VM) - 0.132123(VM)^2 \quad (14)$$

$$\text{Lignin} = -612.099 - 195.366 (O/C) - 156.535 (O/C)^2 - 511.357 (H/C) - 177.025 (H/C)^2 - 24.3224(VM) - 0.145306 (VM)^2 \quad (15)$$

Hemi-cellulose was assumed to be the remaining mass of the dry ash free biomass. The proportion of hemi-cellulose, cellulose and lignin from these correlations are calculated for the present biomass and are shown in the Table 4.2 . Some of the present biomass samples had O/C outside the range of validity of the correlations. Some biomass samples had O/C more than 0.56 e.g. China's biomass skin, while some biomass have O/C less than 0.56 e.g. SPF raw, SPF torrefied, grade B wood, Grade B torrefied wood. Corn cobs have volatile matter daf (dry ash free) was slightly higher than 86% and the calculated hemicellulose, cellulose and lignin do not seems correct.

Figure 4.3 shows the H/C as a function of the O/C for the biomass in Table 4.1. The variability of H/C and O/C is due to different proportions of hemicellulose, cellulose and lignin present in the biomass samples. Figure 4.1 also shows the compositions of cellulose, hemicellulose and lignin based on the chemical formulas discussed in Section 2.9. [96].

The variation of H/C and O/C lead to variations in the stoichiometric air to fuel ratio of the biomass. The biomass in Table 4.1 had a stoichiometric A/F range, on a dry ash free (daf) basis, from 4.7 to 7.5. The stoichiometric A/F ratio were converted from a daf to actual fuel mass stoichiometric ratio as shown in Table 4.1. The significance of this large variation in the stoichiometric A/F ratio is that a biomass log or gasification boiler or a pellet boiler would have to have controls that altered the feed rate in proportion to the biomass composition. This can be done for the overall equivalence ratio of the boiler using oxygen feedback. However, for two stage gasification/oxidation combustion the air split between

the two zones should be altered to achieve an optimum rich gasification zone equivalence ratio for optimum gasification. The main objective of this work was to investigate the optimum A/F for the highest energy in the evolved gases for each biomass. To keep the gasification zone at the optimum A/F whilst controlling the overall excess air level requires control of the air split between the primary and secondary zones and most two stage boilers do not have this air split control, as shown in Chapter 2.

The stoichiometric A/F_{daf} are shown as a function of the H/C in Figure 4.4 for all the biomass in Table 4.1. The stoichiometric A/F of hemicellulose (3.15), cellulose (5.10) and Lignin (9.56) are shown for comparison. The variation of the biomass stoichiometric A/F is related to the variation of hemi-cellulose, cellulose and lignin in the biomass.

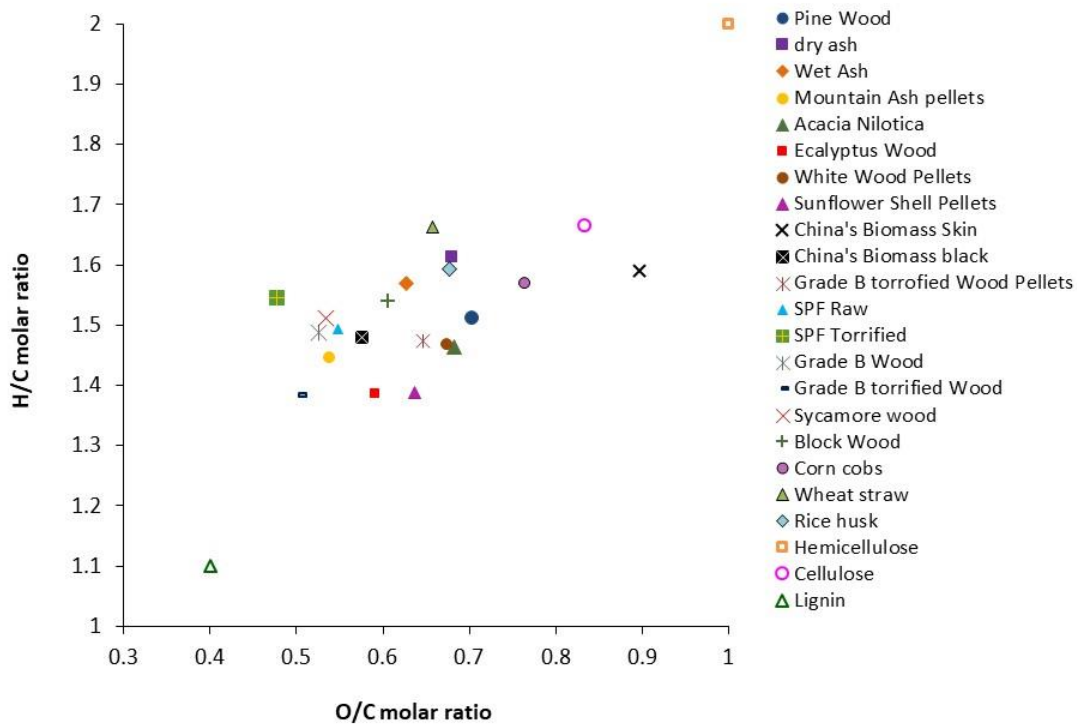


Figure 4.3 atomic H/C vs. O/C of biomass samples

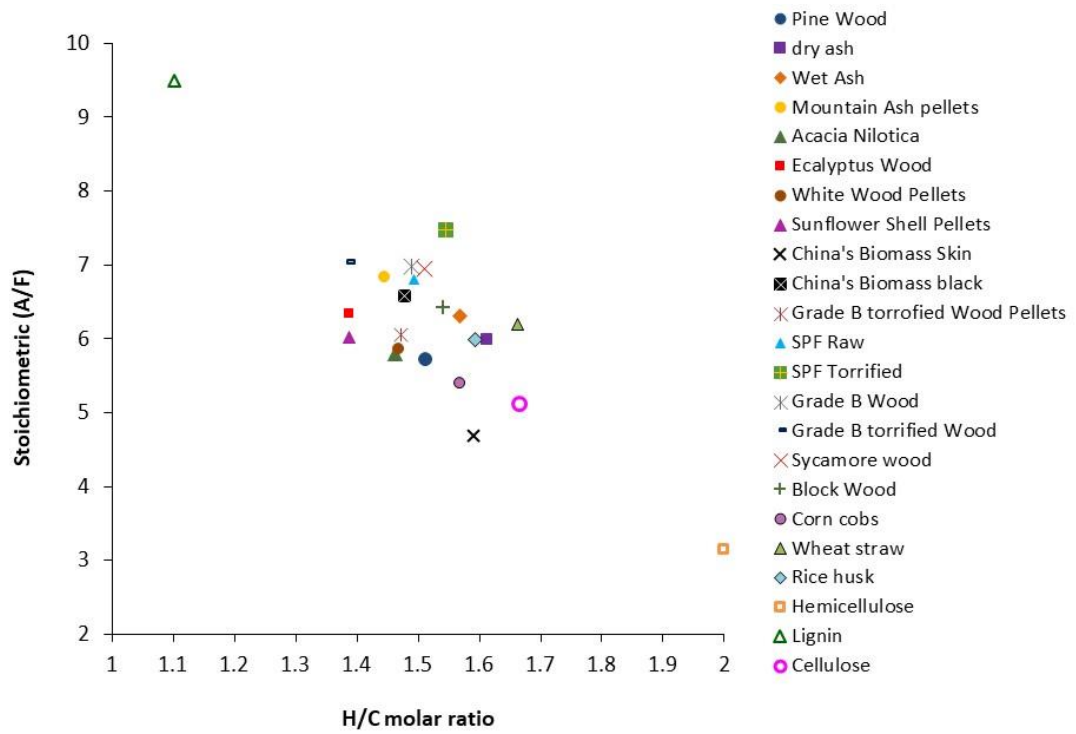


Figure 4.4 H/C v Stoichiometric A/F by mass of biomass samples

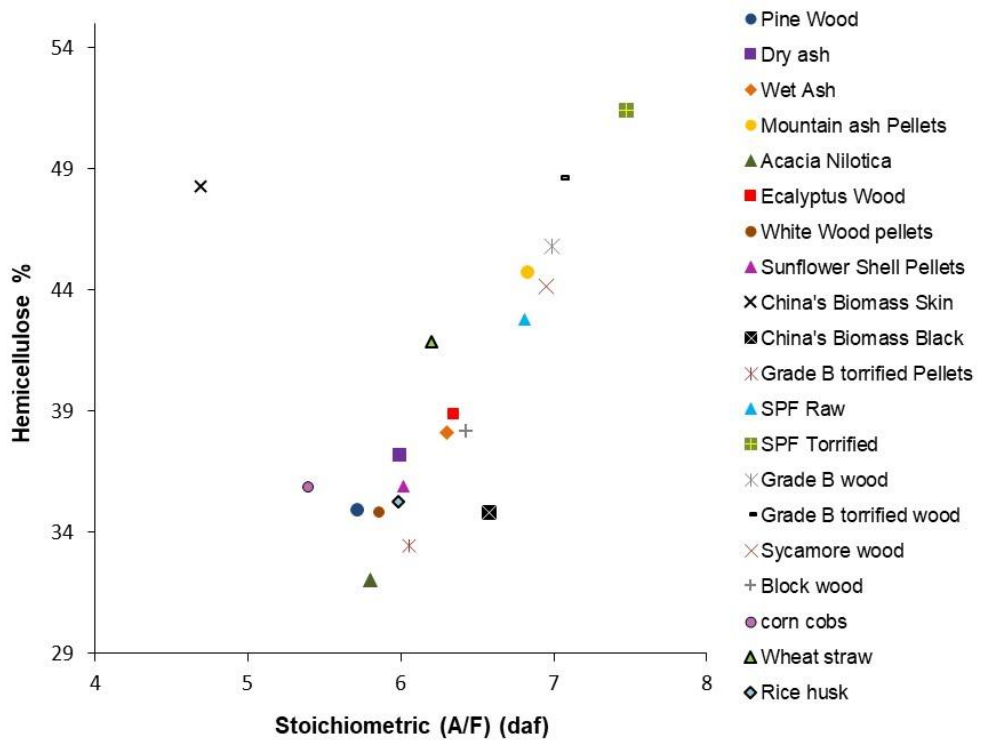


Figure 4.5 Stoichiometric (A/F) vs % hemicellulose for the biomass studied

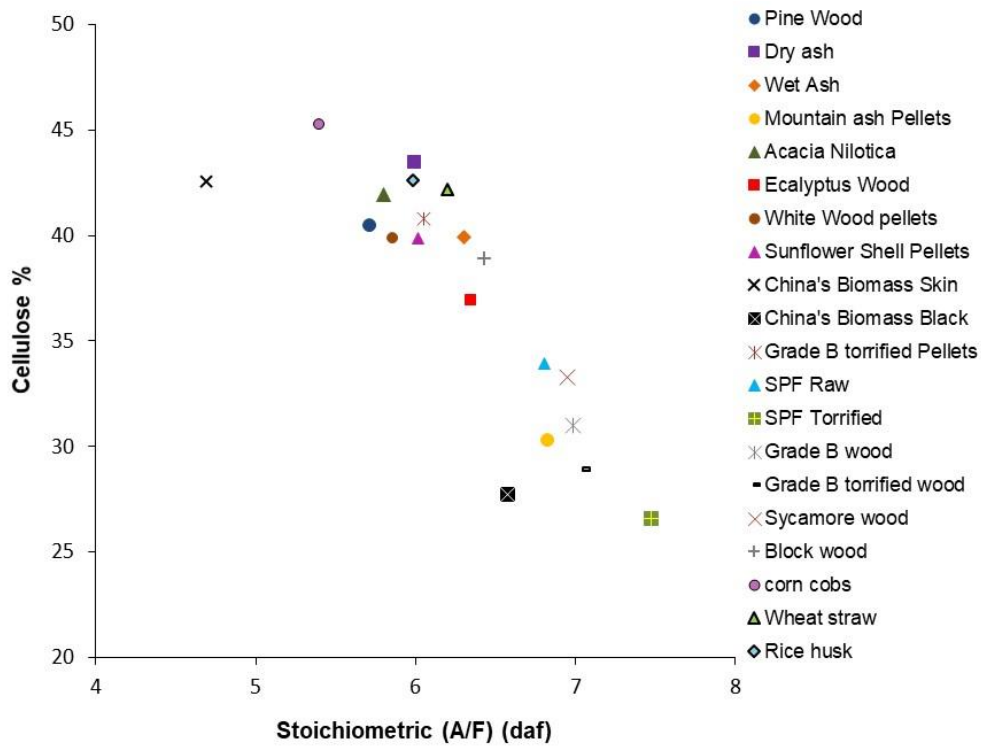


Figure 4.6 Stoichiometric (A/F) vs % lignin for the biomass studied

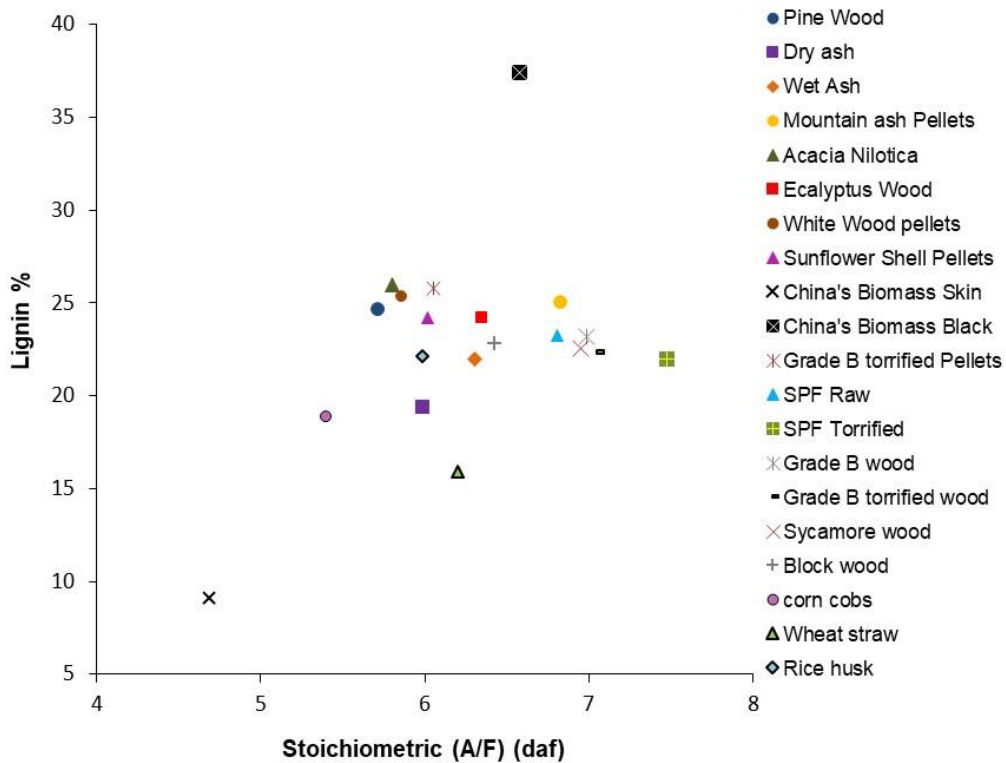


Figure 4.7 Stoichiometric (A/F) vs % lignin for the biomass studied

Stoichiometric (A/F) is plotted vs. hemicellulose, cellulose and lignin in the Figure 4.5, Figure 4.6 and Figure 4.7. There is a direct relationship of hemicellulose with stoichiometric (A/F) but the trend is quite opposite than expected. Hemicellulose has least air to fuel ratio among the three biomass basic constituents and it concludes that if % of hemicellulose in biomass increases, stoichiometric air to fuel ratio should decrease. Similarly stoichiometric (A/F) vs cellulose is having unexpected trend and lignin has no trend with stoichiometric (A/F). These results raise a question on the credibility of the above correlations used for calculations of hemicellulose, cellulose and lignin.

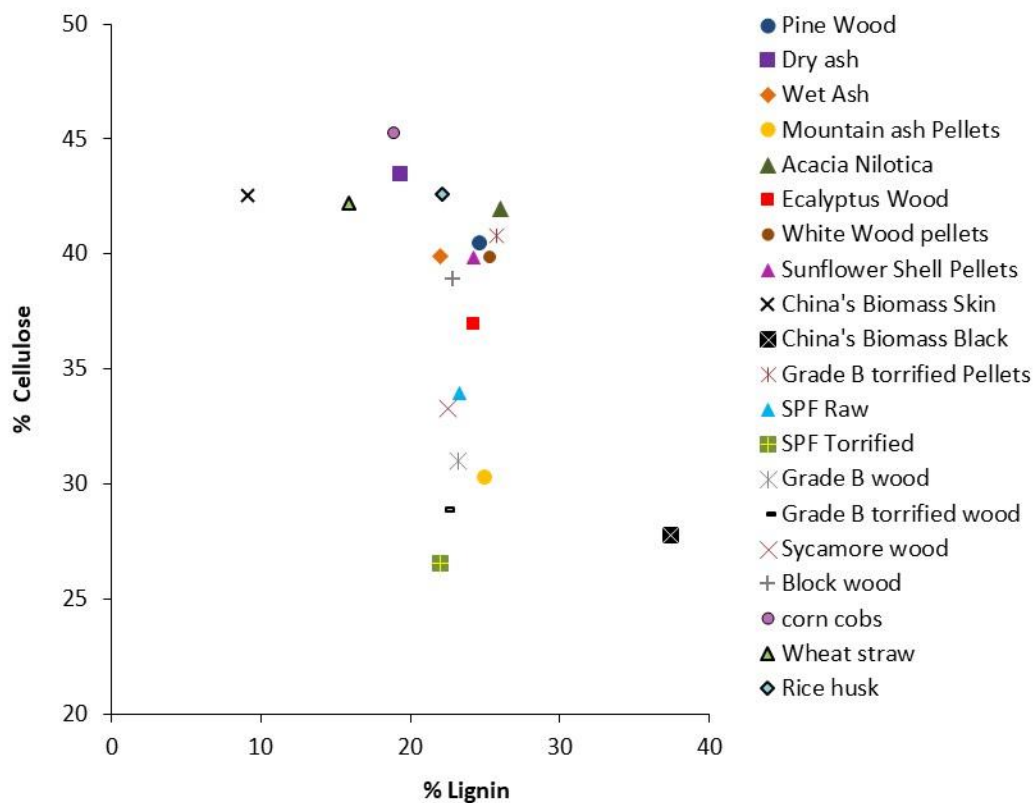


Figure 4.8 % lignin vs. % cellulose for the biomass species studied

As discussed in the section 2.9, a higher cellulose content in the biomass results in a high rate of pyrolysis with high volatile yields, peak gasification temperature and prolonged gasification time. Figure 4.8 shows the % cellulose vs. % lignin (calculated from the correlations given above) for the biomass in Table 4.2. Figure 4.8 shows a poor correlation with cellulose varying from 22 to 43% at a constant lignin level of about 22%. The data with 43% cellulose are mainly crop residues at 22% lignin. Torrifed biomass have less cellulose for the same H/C

due to the thermal treatment. China's biomass black pellets (made up of sawdust and clay) showed the highest lignin contents with very low cellulose contents.

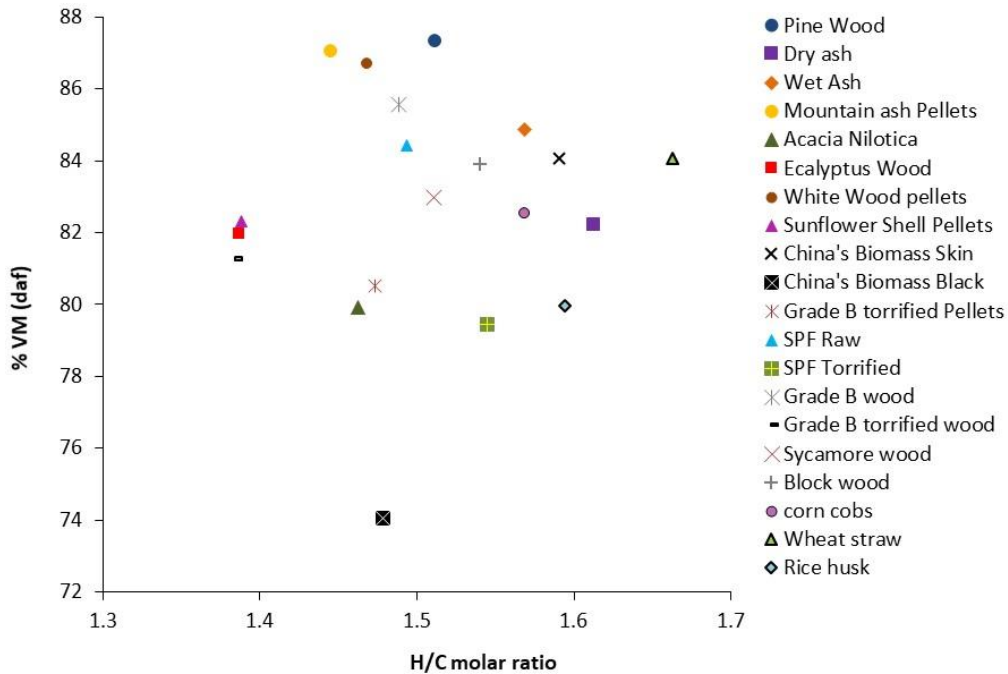


Figure 4.9 % VM vs H/C molar ratio for biomass samples

For the biomass samples in Table 4.1 the VM from the TGA is shown as a function of the H/C in Figure 4.9. This shows that highest %VM was obtained from pine wood, white wood pellets, ash wood and sawdust samples rather than expected from the crop residues as predicted by the cellulose to lignin ratio. However, torrefied biomass showed less volatiles. The China's black biomass had the highest lignin and lowest volatile fraction. The action of the thermal treatment is to reduce the VM whilst having little effect on the lignin as this is not decomposed until higher heating rates than are used in torrefaction processes.

4.2 Equilibrium calculations

Predictions of the adiabatic equilibrium compositions as a function of equivalence ratio were done using the CEA software, as discussed in section 3.2. Initially for this purpose an internal programme, FLAME, was used that calculates the adiabatic compositions of the products of combustion at equilibrium. As there was no further support available for the FLAME software the CEA software was used. The equilibrium calculations using Flame software

are shown in the Appendix A Figure A.1 for the comparison with the done with CEA. The equilibrium compositions as a function of ϕ for the pine wood using CEA software are shown in the

Figure 4.10 for pine wood.

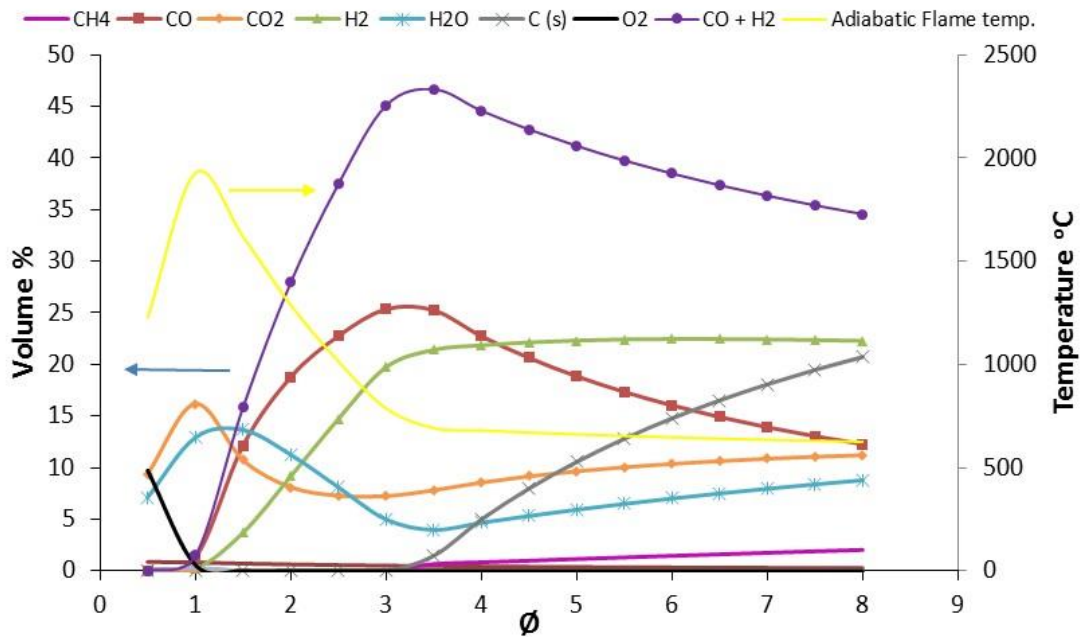


Figure 4.10 Equilibrium concentrations and adiabatic flame temperature of gaseous products as a function of equivalence ratio (ϕ) for pine wood gasification using CEA software.

Figure 4.10 shows that CO is 25% or more between ϕ 3 to 3.25. Also the combined volume concentration CO and H₂ was 46.7% at ϕ 3.5 and was more than 45% between ϕ 3 to 4. Fig. 4.5 also shows that no significant hydrocarbons were predicted at equilibrium until $\phi > 3.5$. Thus, the presence of hydrocarbons in experimental rich combustion of biomass is an indication of a poor gasification efficiency. It will be shown that this occurs due to heat losses from the rich burning zone, which does not burn at the equilibrium temperature. Fig. 4.5 also shows that the rich burning zone temperature decreased to 700°C (973K) at $\phi = 3.5$ and decreased very slowly for richer mixtures.

Equilibrium calculations were also performed for some other biomass materials to check that the predicted peak CO and hydrogen occur at the same

equivalence ratio or different for different biomass. Equilibrium calculations for dry ash, white wood pellets and China's biomass skin is shown in the

Figure 4.11 -Figure 4.13. It was seen that the equivalence ratios for the peak concentrations of CO and H₂ were different. Equivalence ratios corresponding to the peak combined CO and H₂ were 3.5, 4 and 4.5 for dry ash, white wood pellets and China's biomass skin respectively and this difference is attributed to the different O/C, H/C ratios and calorific value of the individual biomass species.

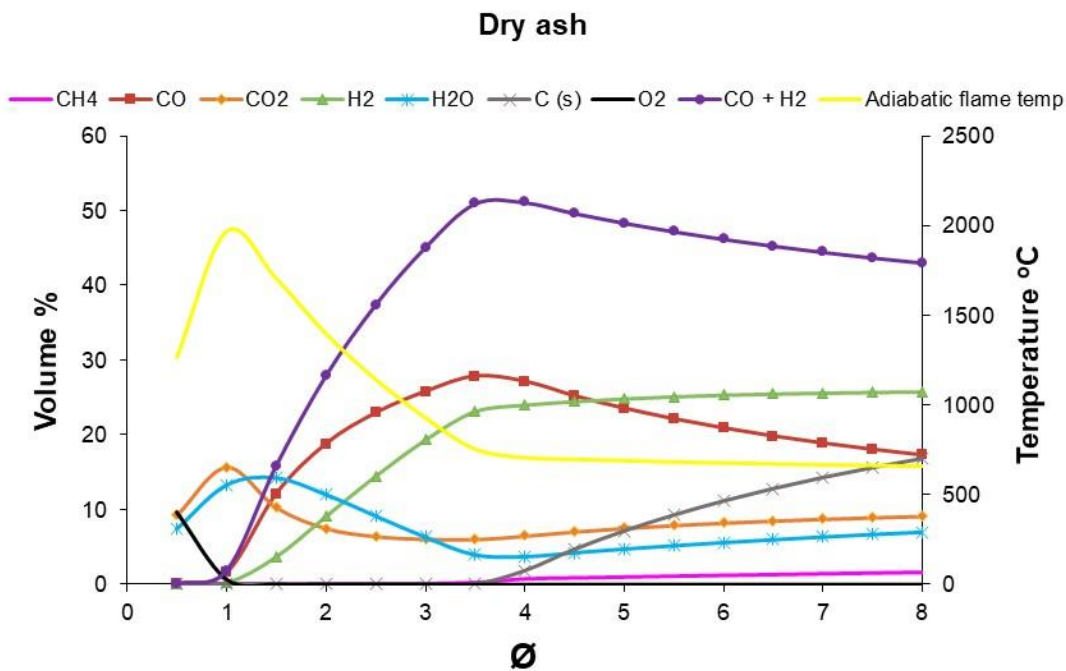


Figure 4.11 Equilibrium concentrations and adiabatic flame temperature of gaseous products as a function of equivalence ratio (\emptyset) for dry ash wood gasification.

For the cone calorimeter experimental conditions to come close to the equilibrium predictions the rich combustion or gasification zone should be as close to adiabatic as possible (minimum heat losses) and as close to the rich mixture adiabatic temperature as possible. In the development of the present use of the cone calorimeter with restricted air supply to the fire compartment, the addition of insulation to the chamber and to the sample support system, all led to more efficient rich burning and CO concentrations closer to the equilibrium in Figure 4.10, as is shown in this Chapter. Some commercial gasification burners water cool the gasification zone and this is detrimental to its efficient operation.

It is also likely that the gasification reactions will be closer to equilibrium if the rich zone is heated by co-firing with natural gas. This was demonstrated by Aljumaiah et al. [140] for a pine wood crib in a 1 m³ furnace heated by a natural gas burner. The same effect could be achieved by preheating the air to the gasification burners, using exhaust gas heat recovery. In the present work the external heating energy was provided by the cone calorimeter radiant electrical heater.

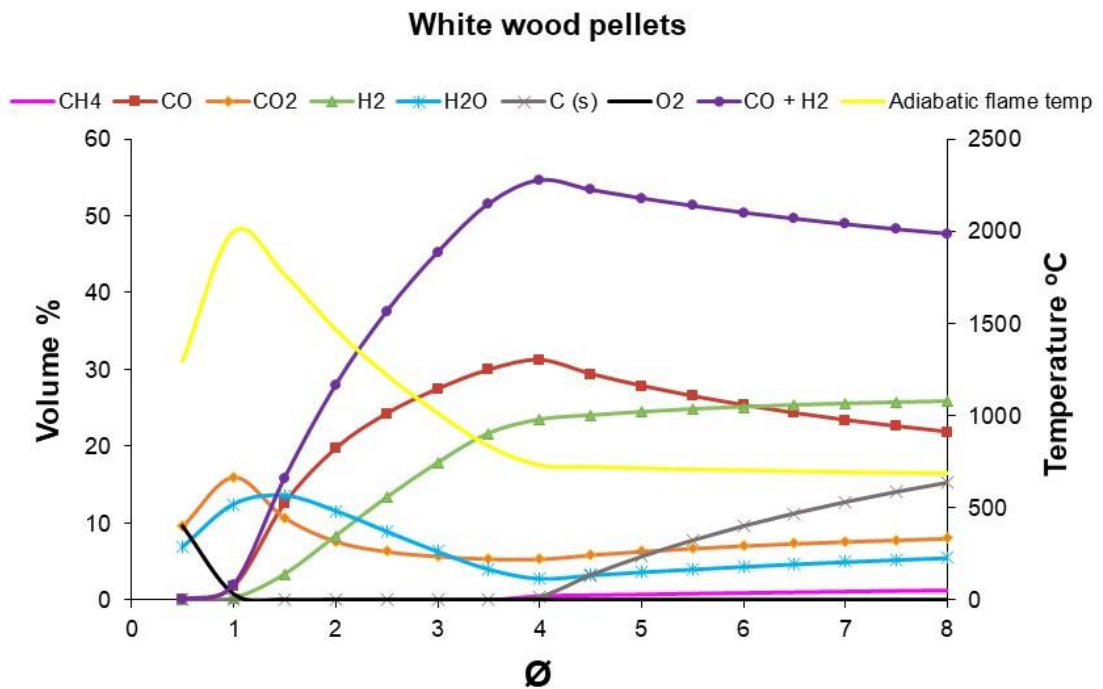


Figure 4.12 Equilibrium concentrations and adiabatic flame temperature of gaseous products as a function of equivalence ratio (ϕ) for the gasification of white wood pellets

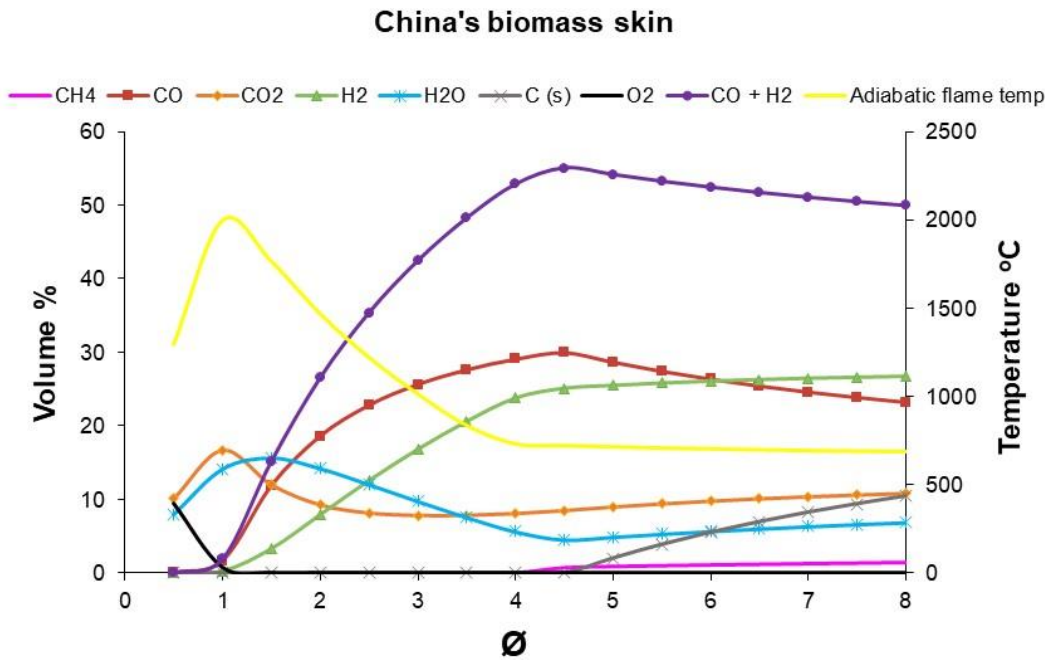


Figure 4.13 Equilibrium concentrations and adiabatic flame temperature of gaseous products as a function of equivalence ratio (\emptyset) for the gasification of China's biomass skin

4.3 Steps towards the development of gasification tests

Cone calorimeter is not designed to control the rich combustion (gasification) as discussed in the section 3.3. The modification in the standard version of cone calorimeter was used of an enclosure box to study the flashover fires. Flashover fires result due to the restricted ventilation. When this setup was used for gasification tests a number of problems were experienced starting with heat losses from the box as in the gasification burning of biomass the conditions inside the enclosure should be as adiabatic as possible. Modifications were then applied step by step by identifying the possible reasons causing the problems. Tests were performed in the following development order.

Configuration 1: Testing was performed with enclosure box as it is with chimney on the top of the box for the raw sampling by single hole probe to obtain initial set of results.

Configuration 2: Insulation of the enclosure box was done to minimise the heat losses from the box. Chimney and sampling method was same as before.

Configuration 3: Use of 20mm insulation underneath the sample to reduce the heat losses from the sample and to achieve better results in terms of CO%.

Configuration 4: Used various gas sampling techniques to achieve better mixed sample

At the start of this research experiments were carried out with the cone calorimeter in the standard format of the controlled atmosphere cone calorimeter with bare metal walls. The results showed that the gas composition for rich combustion was well below equilibrium, due to the conditions inside the box being far from adiabatic.

Table 4.3 lists the conditions of the initial tests. The HRR based on the air flow was the air flow in $g/(m^2.s)$ times the heat release per mass of air, which is 3.05 MJ/kg_{air}. This shows that some tests were performed with 10 pine sticks (2 layers of 5 wood sticks, i.e. 40 mm thick wood load) at two different heat flux to compare with single layer test and to study the effect of heat flux. In tests with 40mm thick wood load, thermocouples were inserted, one at 5mm from top surface and other at 5mm from the bottom surface. These tests were performed separately from the tests recording mass loss rate, as the insertion of thermocouples caused the weight of the fuel load to change due to the thermocouples lifting the wood slightly.

Table 4.3 Conditions for the tests performed

Test no.	Biomass	No. of sticks	Depth of wood load mm	Inlet air flow rate			HRR from air flow kW/m ²	Electrical radiant heat flux kW/m ²
				(Litres/min)	g/(m ² .s)	ACH		
1	Ash	5	20	4.4	9.0	7	27.5	70
2	Pine	5	20	4.4	9.0	7	27.7	70
3	Pine	5	20	5	10.2	8	31.1	70
4	Pine	5	20	6.3	12.8	10	39.0	50
5	Pine	5	20	9.4	19.2	15	58.6	50
6	Pine	5	20	12.5	25.6	20	78.7	50
7	Pine	10	40	6.3	12.8	10	39.0	50
8	Pine	10	40	6.3	12.8	10	39.0	70

4.3.1 Mass loss of samples

The biomass normalised mass loss and rate of mass consumption as a function of time during gasification are shown in Figure 4.14 (a) and (b), for five of the test conditions in Table 4.3 (20 mm thick wood load) in the 100mm square test section. Figure 4.14 shows that there were two stages to the gasification: an initial relatively high mass loss rate followed by a slower mass loss rate at the end of the wood burn out. The transition between these two stages was observed to coincide with the transition between flaming combustion and char combustion. This is most clearly seen for the ash/brush wood sample with 70 kW/m² heating. Pine wood at the same conditions clearly gasified at a slower rate. This could be due to the outer bark on the ash sample and the effectively greater surface area from the five round brush branches. Figure 4.14 (a) shows that the char burning stage for ash and pine was about 11-17% of the initial mass for 70 kW/m². For the lower heating rate of 50 kW/m² the flaming combustion mass loss rate for pine was lower and for three air flow rates was between 0.05 and 0.06 g/s compared with 0.07-0.08 g/s for pine at 70 kW/m².

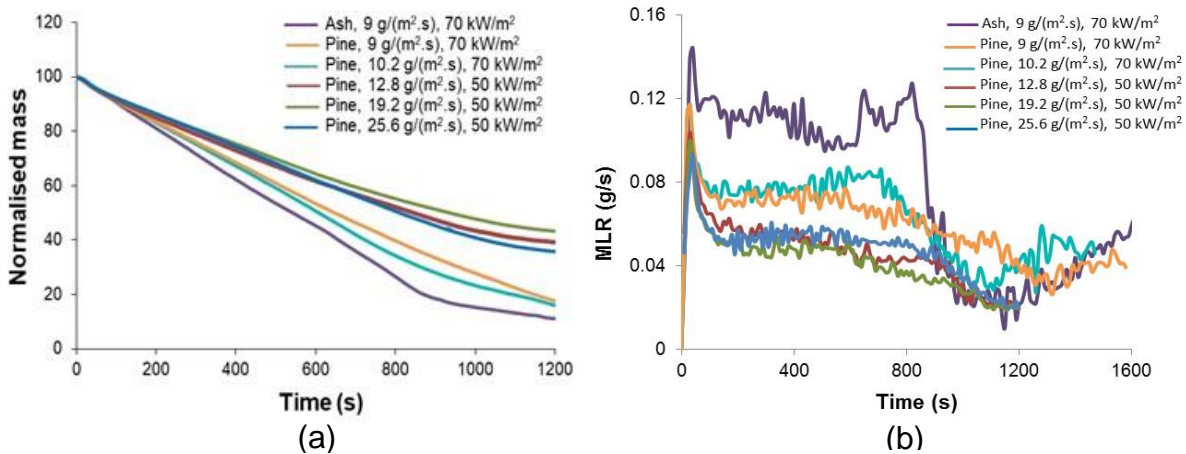


Figure 4.14 (a) normalised mass vs time (b) Mass loss rate (MLR) vs time for 20mm thick wood load (5 wood sticks)

The char burn out stage represents inefficient gasification. It is shown below that there is little production of CO. The reason is that the air flow to the gasification zone is constant and so as the mass burning rate slows in the char phase, the equivalence ratio of the zone moves towards stoichiometric. The result is that most of the char burns to CO₂ which is undesirable. In a practical gasification

burner this would not be an operational condition, as more biomass would be added to the gasification zone. Thus, in the present work this second stage char burn-out will be ignored as gasifiers are not normally operated to allow total burn-out.

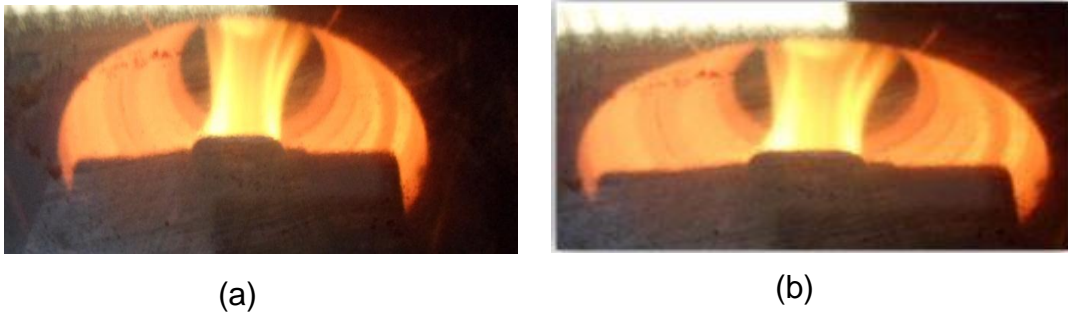


Figure 4.15 steady state flame combustion at heat flux 70 kW/m^2 , air flow $9 \text{ g/(m}^2\cdot\text{s)}$ (a) 5 ash sticks (b) 5 pine sticks

In the tests 1, 2 & 3 with a heat flux of 70 kW/m^2 , ignition for pine wood started after 6 s and for ash wood it started after 13 s. In the tests (4, 5 & 6) of 20 mm thick wood load with heat flux 50 kW/m^2 , ignition started in 8, 11 and 16 s for air flow rates of 12.8, 19.2 and $25.6 \text{ g/(m}^2\cdot\text{s)}$, respectively. This first stage, in which vigorous drying and devolatilisation of sample takes place, lasts for 40-70 seconds, as can be seen from the first initial peak of mass loss rate in

Figure 4.14 (b).

The flames produced inside the box during steady state flame combustion for test 1 and 2 are shown in the Figure 4.15. This shows some interesting features of the fires. The flames are in the centre of the chimney with a non-combusting zone around the flame. Thus, the mixture in the chimney is not uniform and a single hole gas sample probe will not measure the mean composition. This was found in the development of the methodology and a multi-hole gas sample probe was used. Also the gap between the flame and the wall of the chimney allowed air to back flow down the chimney and this was found to occur from the oxygen analysis after the FTIR. The solution to this problem was to put a restrictor at the chimney outlet, as is discussed later.

For tests 7 & 8 with 10 pine wood sticks (in two layers, 40 mm thick wood load) and air flow of $12.8 \text{ g/(m}^2\cdot\text{s)}$ at 70 kW/m^2 and 50 kW/m^2 a similar mass loss trend

was found to that with the thinner pine wood load, as shown in Figure 4.16 (a) & (b) However, there was a significant difference in that the rate of burning decreased with time, rather than the constant rate in the flaming combustion stage for the single layer test. The initial flaming combustion mass loss rate decreased from 0.11 to 0.05 g/s over the 2000 s flaming combustion phase, compared with 0.06 g/s for the load cell for the test at 70 kW/m² changed. This was found to be an experimental problem of overheating of the uncooled load cell at electrical heating rates above 70 kW/m². This load cell problem was solved by fitting a water cooled wall at the base of the compartment, where the load cell was mounted. Also operation at 70 kW/m² was not used in the rest of the work. In addition the test was not carried on to completion and once the steady state mass loss condition had been reached the test was ended at 600s to prevent any damage to the load cell. For this reason the calculations based on mass loss rate were only correct up to this point only and Figure 4.16 (b) shows the mass loss rate up to 800s was valid. To avoid operation near this critical temperature condition future tests were stopped at 600s. This gave sufficient time to determine the composition of the gases for the constant mass loss period.

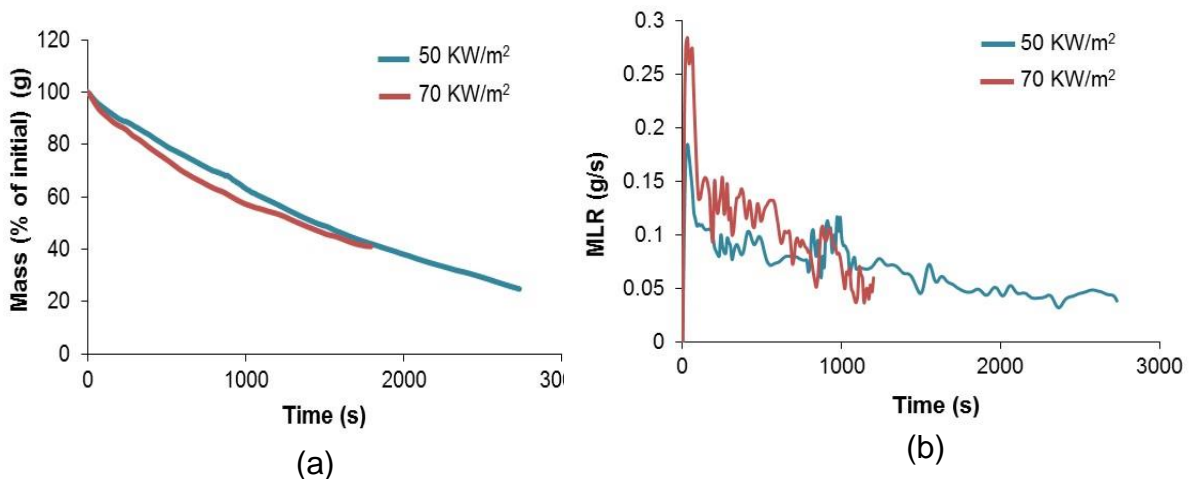


Figure 4.16 (a) mass vs time (b) Mass loss rate (MLR) vs time for 40 mm thick wood load (10 pine wood sticks) at air flow rate 12.8 g/(m².s).

The faster initial burn rate for the thicker sample in Figure 4.17 was a result of the thicker pine wood acting as a self-insulation so that the surface temperature exposed to the radiation was hotter. Also the release of volatiles from the flaming zone propagating through the thickness would result in the initial char layer

burning in the products of gas release from deeper within the wood. The results for the thicker specimen were not continued to completion of the char burn out, as this phase was not of major interest. Essentially in this work once the thicker wood had burned down to the same mass as the thinner layer started with, the mass burn rates were similar. As for the thinner layer, an increase in radiation from 50 to 70 kW/m² led to an increase in the mass burn rate. As a result of this it was decided that the test specimens should be insulated from the metal support to reduce the heat losses to the support and via this to the load cell housing. A 20 mm thick kaowool 100mm square insulating material was used below the test specimen in future work, as this made the tests closer to adiabatic.

Photographs of the flames for tests 7 (50 kW/m²) and 8 (70 kW/m²) with 40mm thick pine are shown in the Figure 4.17. Comparison with Fig. 4.7 for 20mm thick pine wood shows that the flames are larger and spread across the whole of the 100mm square test area. The flame is clearly weaker at the 50 kW/m² condition.



Figure 4.17 Steady state flame combustion for 40mm thick wood load (10 pine sticks) air flow 12.8 g/(m².s) (a) heat flux 50 kW/m²(b) heat flux 70 kW/m²

4.3.2 Metered equivalence ratio (ϕ_m)

The metered A/F for the thin and thick wood samples were determined from the measured constant air flow and the measured rate of mass consumption of the biomass. This was then converted to a metered equivalence ratio, ϕ_m , using the stoichiometric A/F for each biomass in Table 1. This metered equivalence ratio, ϕ_m , is shown as a function of time in Figure 4.18 (a & b). The higher mass loss rates leads to richer mixtures as the air flow is constant. Figure 4.18 shows that the aim of this work, to create rich burning gasification conditions, was achieved.

The equivalence ratio could be varied by changing the air flow, or the heating rate or the biomass.

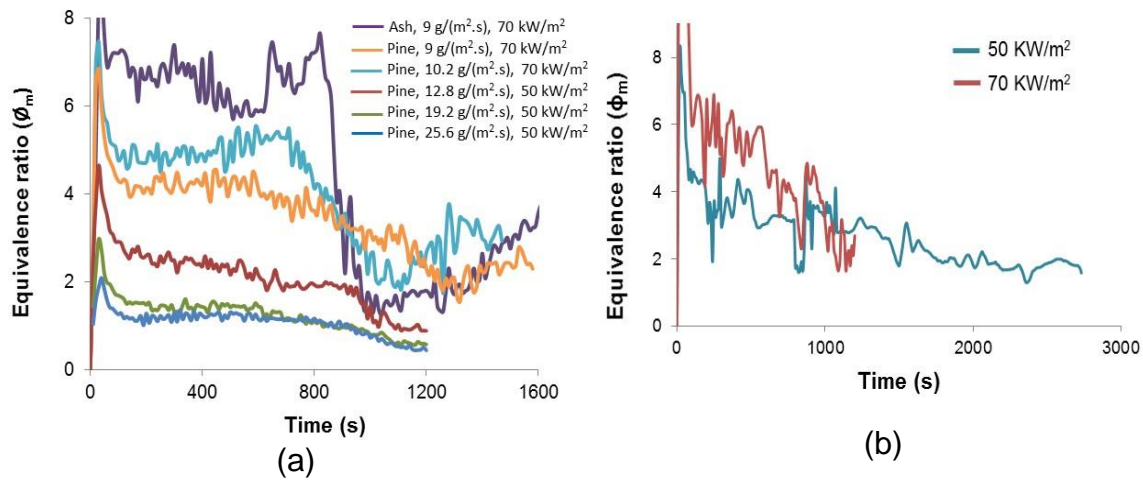


Figure 4.18 Equivalence ratio (ϕ_m) for tests with (a) 20mm thick wood load (5 sticks) (b) 40 mm thick wood load (10 sticks) at 12.8 g/(m².s)

Figure 4.18 (a) shows for the same air flow (9 g/m²s) and radiant heat flux (70 kW/m²) that the change from pine to ash gave a different ϕ_m due to the difference in the stoichiometric A/F in Table 4.1. This was about 9 for ash and 4 for pine.

These optimum equivalence ratios are richer than the optimum from the adiabatic equilibrium composition discussed above. Figure 4.18 (a) also shows that changing the air flow for pine at 50 kW/m² radiant heat flux decreased the ϕ_m from about 2.5 at the lowest air flow to 1.3 at the highest air flow. However, at the higher radiant heat flux of 70 kW/m² an increase in air flow from 9 to 10.2 g/m²s slightly increased the ϕ_m from 4.3 to 5. These effects complicate the influence of the radiant heating, as Figure 4.18(a) compared pine at 50 and 70 kW/m² but at slightly different air flow of 12.8 and 10.2 g/m²s. Fig. 4.10b shows that for the 40mm thick pine the influence of the radiant heating (50 to 70 kW/m²) was significant at constant air flow, with ϕ_m average of the first 700s reducing from about 5.5 to 3.5 as the heat flux was reduced. This is indicative of the higher heating resulting in a great evolution of volatiles and hence a richer mixture. In practical terms this is an influence of the biomass bed temperature on the rich zone equivalence ratio.

For optimum gasification, the equilibrium model predicted the values of ϕ_m should be 3-4. Figure 4.18 shows that test 2, 4 and 7 were close to this equivalence ratio. However, it shows that gasification two stage combustion needs to be able to control the equivalence ratio of the rich burning stage for the same overall equivalence ratio. Part of the complication of the above results is that the heat losses will vary with each test condition, with greater heat losses at the higher radiant energy and lowest air flow. A more consistent performance should occur if the rich burning zone was closer to adiabatic conditions and at a higher fixed bed temperature.

4.3.3 Heat release rate (HRR)

The total heat release rate (HRR) for all the tests was calculated based on the MLR as well as based on oxygen consumption calorimetry (OCC). Oxygen is measured after the dilution of the gases from the gasification stage and total HRR is measured which is HRR by oxygen consumption. Ideally if the burning of biomass fuel is complete, HRR_{MLR} should be equal to $HRR_{(OC)}$. As in the gasification burning, there are two stage of combustion, partial combustion occurs inside the primary zone and combustible gases are burnt inside secondary zone. Figure 4.19 shows the total $HRR_{(OC)}$ as a % of HRR_{MLR} , it can be seen that Total $HRR_{(OC)}$ is only 80-40 % of the total HRR_{MLR} , in the steady state flame combustion zone showing combustion inefficiency.

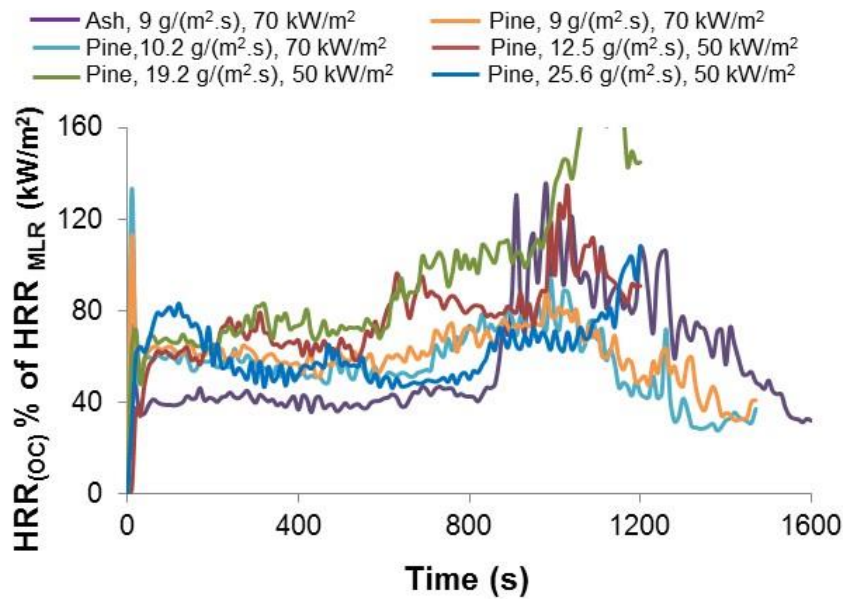


Figure 4.19 Total HRR_(OC) as % of total HRR_(MLR) kW/m² for tests with 200 thick wood load

Above calculations for HRR may have an error of $\pm 10\%$ as a correlation is used having $\pm 5\%$ error in it.

It was concluded that very little or no combustion was taking place in the secondary combustion zone after dilution of primary zone gases from chimney with air and it can be checked by the % CO measured from the dilute sampling. Figure 4.20 shows the comparison of % CO from raw sampling (measured using FTIR) and from dilute sampling after secondary combustion zone (measured by NDIR analyser), and it can be seen that % CO in the dilute sample is very similar to the one obtained from the raw sampling showing that very little or no combustion is taking place in the secondary combustion zone and it the inefficiency of the overall system. But the present work focuses on the primary gasification zone only and the secondary combustion is not the aim of the present work.

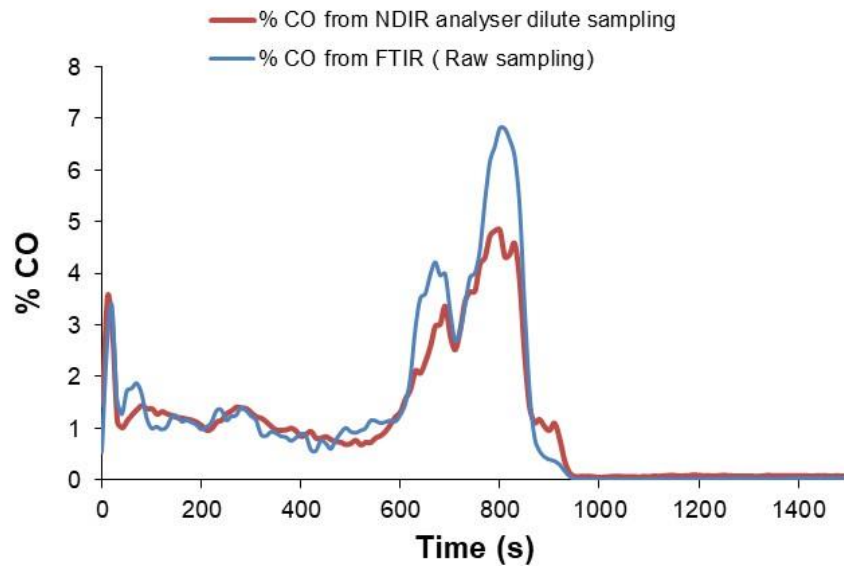


Figure 4.20 % CO comparison from raw sampling (FTIR) and dilute sampling (NDIR)

Reason for not burning the gases from the primary gasification zone could be the large dilution of exhaust gases from primary combustion zone that also causes cooling of the gases downstream. Dilution ratio for these tests was from 150 to 250.

Dilution ratio is defined as

$$\text{Dilution Ratio} = \frac{\text{Total MFR in exhaust duct after Secondary combustion}}{\text{Total MFR from exhaust chimney of Primary combustion}}$$

Flow rate of air in the secondary stage of combustion is 24 litres/sec and is equal to 29.4 g/s of air. Total MFR in secondary combustion zone is sum of air flow plus flow coming from primary zone.

The primary zone heat release rate (PHRR) based on oxygen consumption calorimetry was also calculated by measuring oxygen level from the chimney sampling. The contribution of secondary combustion to the total heat release was determined as the difference between the total heat release (based on oxygen consumption calorimetry for the cone calorimeter diluted flow) and the primary heat release from the primary rich zone oxygen consumption calorimetry (PHRR) however this SHRR is of the inefficient system.

$$\text{SHRR} = \text{Total HRR}_{\text{OCC}} - \text{PHRR}_{\text{OCC}}$$

If the system is considered to be 100% efficient and assuming that secondary combustion is burning most of the products from the primary gasification stage as in the log boilers, we can find out the contribution of PHRR towards the total HRR_{MLR}. As the aim of optimising the gasification stage should be to minimise the heat release in the primary gasification zone and maximise the release of heat in the secondary combustion zone. Then SHRR can be calculated as the difference between the total heat release (based on Mass loss rate) and the primary heat release as below:

$$\text{SHRR} = \text{Total HRR}_{(\text{MLR})} - \text{PHRR}$$

Primary and secondary HRR were evaluated as percentages (%) of the total HRR_(MLR) as shown in Figure 4.21.

In the tests (7 & 8) with the 40 mm thick pine wood the primary HRR in the steady state flame combustion zone was 10% of the total HRR at 70 kW/m² and 20% at 50 kW/m² as shown in the Figure 4.21(g & h), This shows that later in the combustion time the primary HRR increases and this is the transition from flaming combustion to char combustion with a lower mass burning rate but the same air flow and this results in a leaner mixture, as shown later, and more primary HRR. This phase of the combustion is not the aim of the present study, as in log or gasification burners more fuel is added to keep the combustion in the rich burning low primary HRR gasification zone.

For the thinner 20mm thick wood load there were conditions where ideal gasification HRR conditions were achieved with the proportion of HRR in the gasification zone being low. These are summarized in Table 4.4, which shows that the 70 kW/m² radiation flux, which would control the biomass gasification temperature, was necessary to get rich flaming combustion at < 20% of the overall HRR in the gasification zone, as shown in Figure 4.21 (a & b)) of the heat release for the ash and pine biomass. Both woods had very rich gasification zone ϕ_m of 5 – 6.8. Also this heating rate needed to be combined with a low air flow of 9 g/(m².s). to achieve the desired rich mixtures. These conditions are richer than the adiabatic equilibrium predictions gave for pine wood. This is due to inefficient gasification, as shown by the presence of HCs which have not been

converted to CO and H₂. Thus the movement of the peak Gasification efficiency to richer mixture is a feature of non-adiabatic gasification. For the 50 kW/m² heating the 20mm thick pine wood increased the proportion of the HRR in the gasification stage as the air flow was increased. This increase in air flow reduced ϕ_m and the proportion of HRR in the gasification zone increased until there was mainly combustion not gasification at 25.6 g/(m².s) (shown in Figure 4.21 (d, e & f)). The thicker 40mm thick pine wood both test conditions gave < 25% of the HRR in the gasification zone and had $\phi_m \sim 3$. For the thinner specimen at 50 kW/m² the gasification was poor and hence the sample thickness or sample insulation, is important. Normally in gasification heaters the bed thickness would be much greater than 40mm. The 70 kW/m² heating for the thicker sample gave good gasification at an air flow of 12.8 g/(m².s).

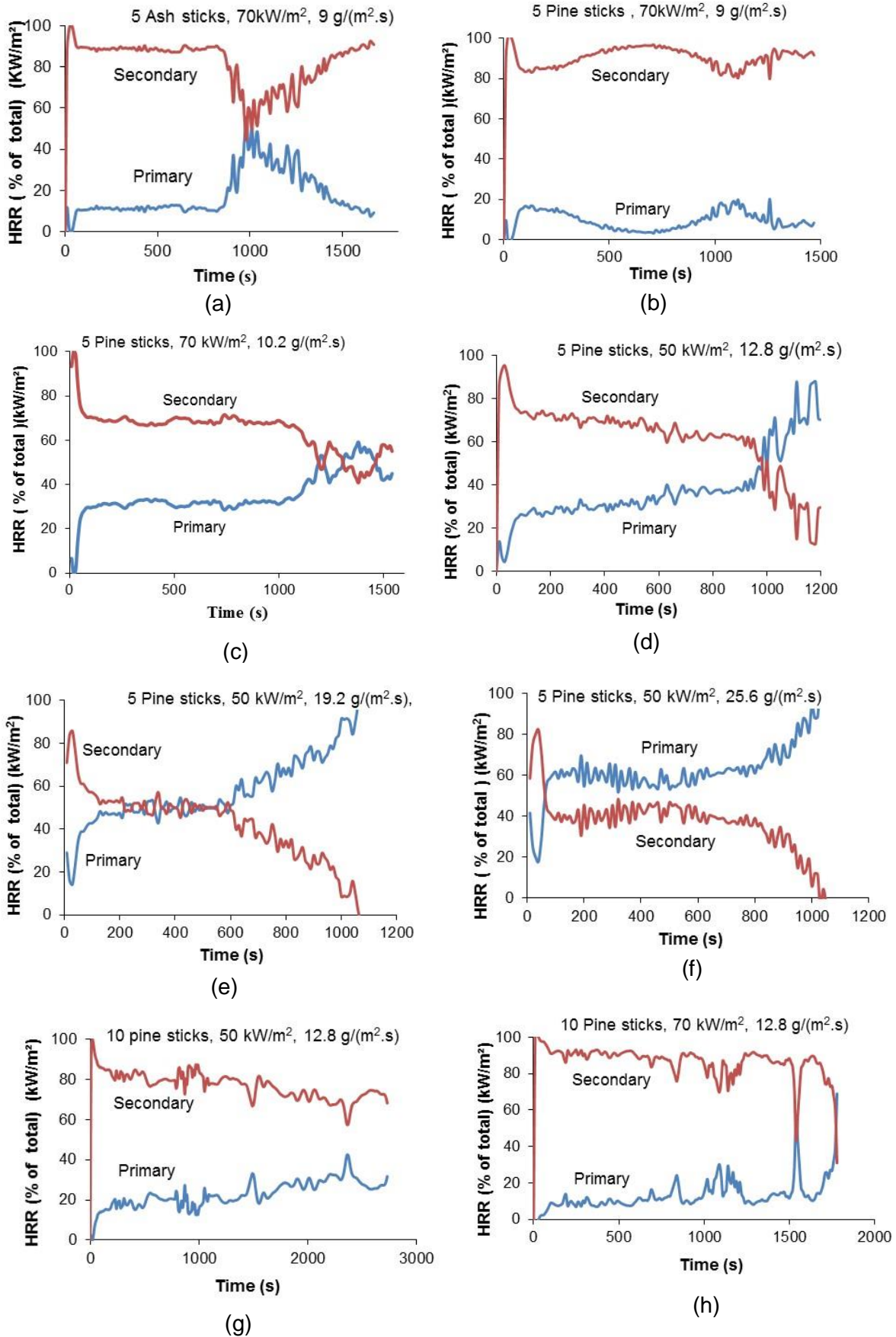


Figure 4.21 Primary and secondary gasification HRR expressed as a % of total

4.3.4 Carbon monoxide and hydrogen emissions

The percentage of CO from the raw sample from the outlet from the gasification zone is shown in Figure 4.22. There was no analyser for the measurement of H₂, so its equilibrium concentration was predicted from the measured CO using the water gas shift reaction (R3 in section 2.1.3).

Equilibrium constant for this reaction is given as

$$K = \frac{[CO][H_2O]}{[CO_2][H_2]}$$

where K is a function of equilibrium temperature, here a value of 3.5 is used, which corresponds to T_{eq} 1738 K [68].

It can be seen in Figure 4.22 (a) that in all tests with heat flux of 70 kW/m², the peak values for CO emissions were obtained during the first stage of drying, devolatilisation and flaming combustion. These values then dropped in the steady state flame combustion zone. The CO was recorded to be 13%, 10% and 3% in first stage for tests 2, 3 & 1 respectively. In the steady state flame combustion CO dropped to a very low value in all three tests, But in test 1 & 2 at 4.4 L/min, CO raised again to an average value of 5% and 3.5% respectively after

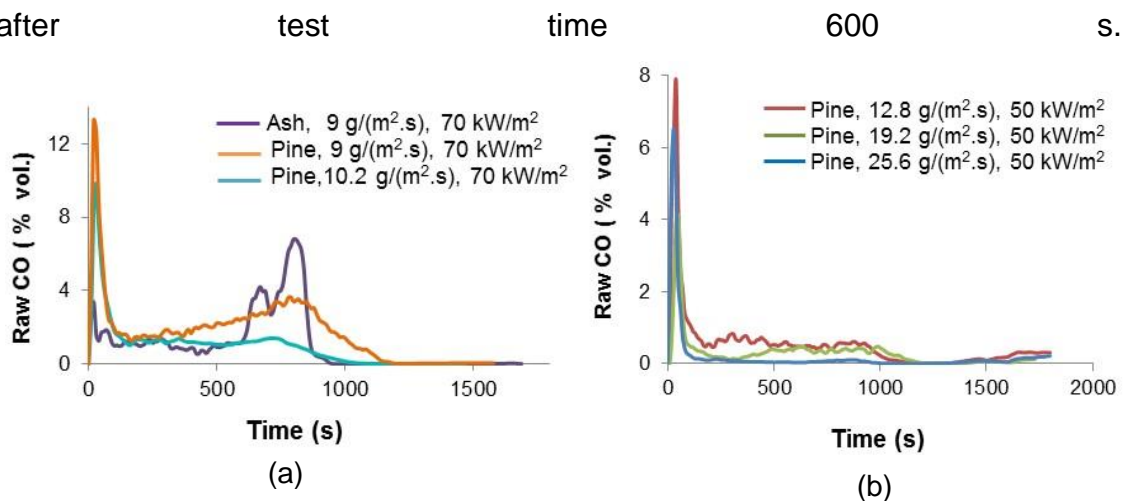


Figure 4.22 % CO from gasification stage for 20 mm thick wood load (a) 70 kW/m² (b) 50 kW/m²

A possible reason for the very low %CO was the low bed temperatures of the pine wood, as the Boudouard reaction R1 produces more CO at higher

temperatures. However, most of the trends in CO emissions are due to variations in \emptyset , as discussed below.

In tests 4, 5 & 6 at heat flux 50 kW/m² (Figure 4.22 b), the CO was 8, 4, and 6.5% respectively in the first drying stage. The CO then reduced to less than 1% in the steady state flame combustion zone with almost 0% with airflow 25.6 g/(m².s) bed temperature in the tests at 50 kW/m² is even less as compared with the tests with heat flux 70 kW/m².

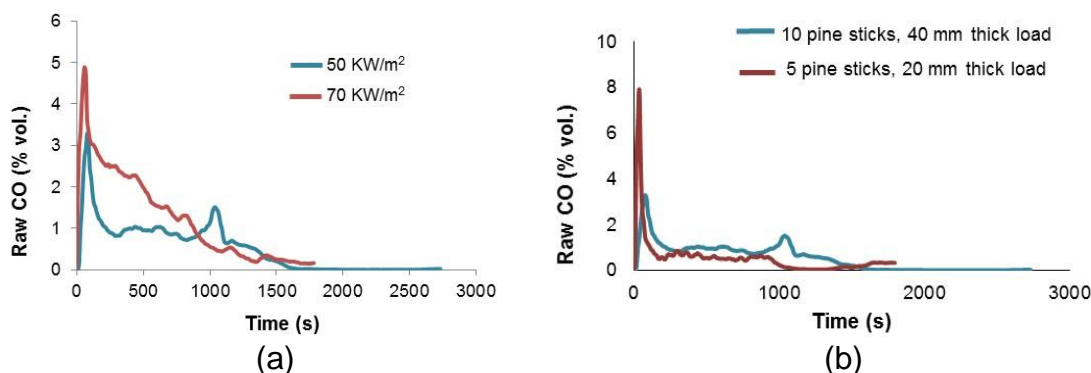


Figure 4.23 % CO from gasification stage for (a) 40 mm thick wood load at air flow 6.3 L/min. (b) comparison between 40 mm and 20 mm thick wood load at 50 kW/m² & 12.8 g/(m².s)

Table 4.4 Summary of test results for the main flaming rich combustion phase for the gasification zone and comparison with equilibrium

Test no.	Radiation kW/m ² -wood	Depth of wood load mm	Air flow L/min	% HRR Primary	Avg. \emptyset_m	Measured CO %	CO EI g/kg	Predicted	
								Eq. CO %	Eq. H ₂ %
1	70 -ash	20	4.4	10	6.8	1-4	20-60	14	22.4
2	70 -pine	20	4.4	5 -20	4.2	1-3	30-60	22	22
3	70 -pine	20	5	30	5	1	20	19	22
4	50 -pine	20	6.3	30	2.2	>1	20	20	10
5	50 -pine	20	9.4	50	1.6	>1	20	12	3.6
6	50 -pine	20	12.5	60	1.2	>1	5	5	2
7	50 -pine	40	6.3	10-20	2-3	1	20-50	22	14
8	70 -pine	40	6.3	20-25	3-5	1-3	20-25	22	22

For 40 mm thick wood load values of % CO was higher in the test with heat flux 70 kW/m² (Figure 4.23 (a)) showing the effect of temperature on the emissions. Also test 4 and test 7 are at same air flow and heat flux only variable being the thickness of the wood bed, and it can be seen from Figure 4.23(b) that the % CO is slightly higher in the 40 mm thick wood load.

Corresponding equilibrium % of H₂ calculated from water gas shift reaction are shown in

Figure 4.24.

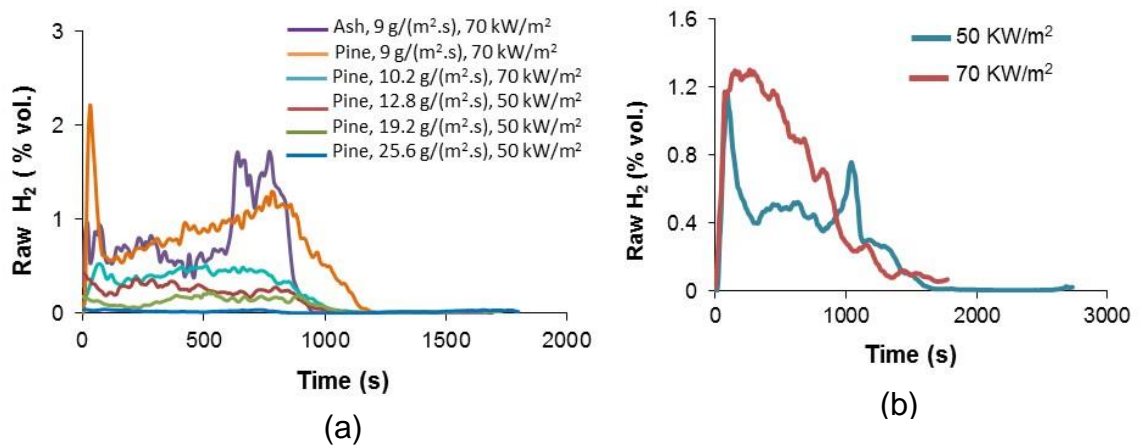


Figure 4.24 % H₂ from the gasification stage (a) 20 mm thick wood load (b) 40 mm thick wood load at airflow 12.8 g/(m².s)

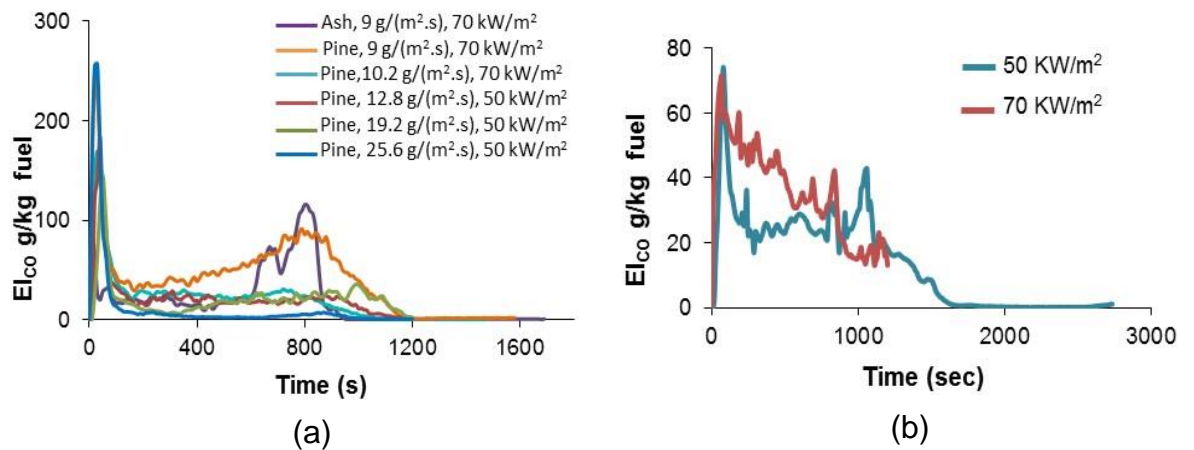


Figure 4.25 CO emission index (El_{CO}) for tests (a) 20 mm thick load (b) 40 mm thick wood load at airflow $12.8 \text{ g}/(\text{m}^2.\text{s})$

The measured values of CO were very low compared to those predicted for equilibrium as shown in Table 4.4. This indicates that reactions did not reach equilibrium during the test and this is demonstrated by the very high hydrocarbon emissions, which should be zero at equilibrium.

4.3.5 Carbon monoxide emission index (El_{CO})

The EI for CO are shown in the

Figure 4.25 for tests with 20 and 40 mm thick wood load. Table 4.4 compares the CO emissions during the near steady state flaming gasification stage of burning. This shows that the CO was only high ($>1\%$) for the thick pine wood samples. This indicates that a thick bed depth is needed for gasification burning to be effective in gasification. However, the conditions of these tests are clearly well removed from equilibrium and this indicates that the heat losses in this equipment badly affect its use to study the primary stage of two stage biomass combustion.

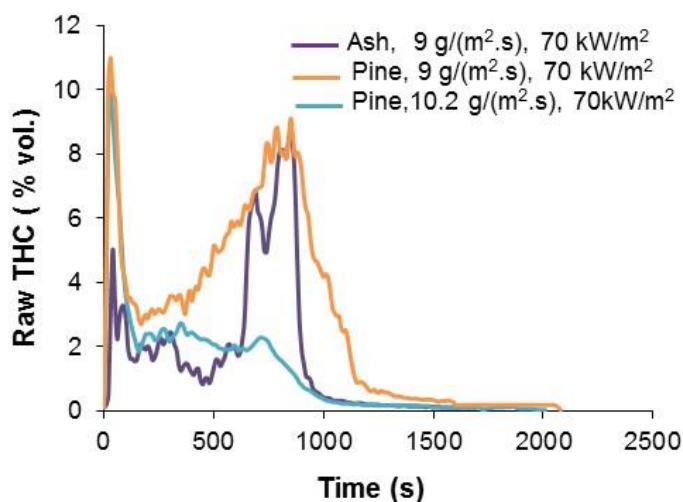


Figure 4.26 THC emissions during gasification of 5 wood sticks at heat flux $70 \text{ kW}/\text{m}^2$

A feature of inefficient gasification due to low zone temperatures is that there will be hydrocarbons at a significant level not gasified into CO and H_2 . This is shown

as an example for the present results in Figure 4.26. This shows that even at the highest radiant heating in the present work, which will give the highest temperature in the specimen, the total hydrocarbons (THC) equivalent of methane were very high. This does not matter from an energy point of view as these hydrocarbons in a staged system would burn in the second stage. However, they are undesirable as they are the source of soot emissions from biomass combustion.

4.3.6 Emission based equivalence ratio (ϕ_e)

Figure 4.27 shows the emission based equivalence ratio for the tests with 20mm thick wood load. This shows that all the tests were lean in the steady state flame combustion phase, except for pine wood and ash wood (after 600 s) at 70kW/m².

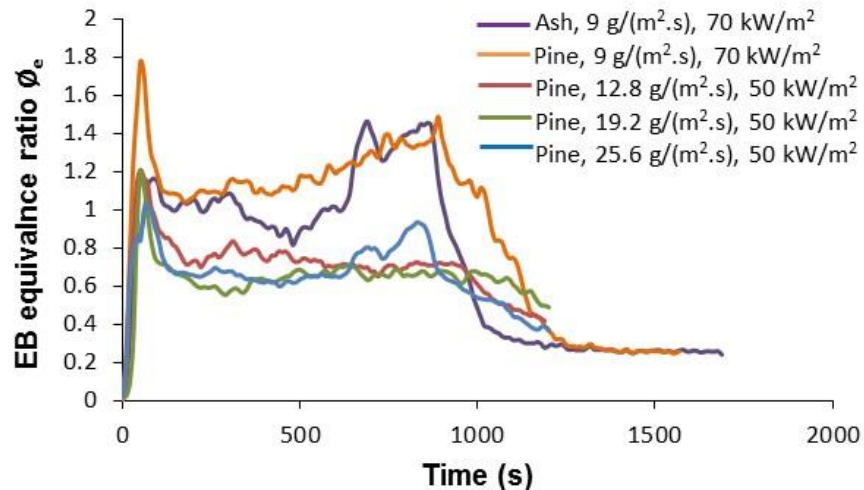


Figure 4.27 EB equivalence ratio ϕ_e for tests with 20 mm thick wood load

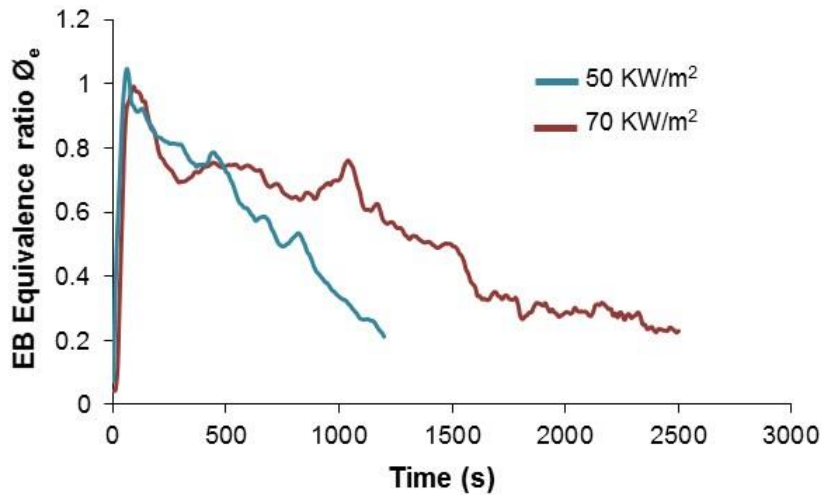


Figure 4.28 EB equivalence ratio ϕ_e for tests with 20 mm thick wood load at air flow 12.8 g/(m².s)

Similarly tests with 40mm thick wood load are shown in Figure 4.28, where a lean equivalence ratio occurred. This shows that there is a huge difference in metered equivalence ratios and emission based equivalence ratio. So it was concluded that in spite of the fact that box was provided with the limited air flow that should have provided rich combustion, but the conditions actually were lean inside the box.

4.3.7 Temperature rise of the pine wood

Temperature rise for the tests with 40mm depth (10 wood sticks) are shown in Figure 4.29 for 50 kW/m² and 70 kW/m². This shows the thermal wave that travels through the wood samples and that the adiabatic temperature was not achieved. Figure 4.29 shows that at 1000 s, the top thermocouple was at 700 °C for 70 kW/m² radiant heat, as compared to 600°C for 50 kW/m².

The results presented in this section using configuration 1 show that 70 kW/m² radiant flux was required for the better gasification because the zone was hotter. Also low air flow rates of about 9 g/(m².s) gave the better results. The other significant factor was that thicker wood depths of at least 40mm gave the better results in terms of %CO.

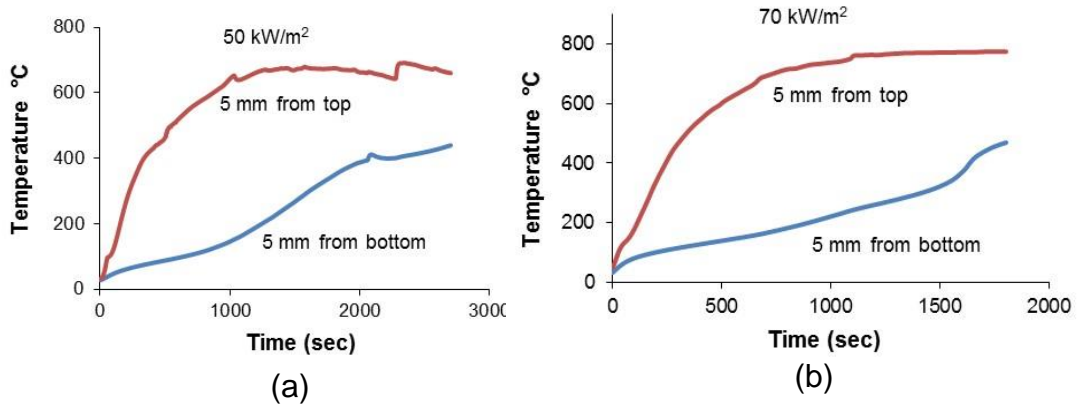


Figure 4.29 Temperature vs time for test with 40mm thick wood load (10 pine sticks) (a) at 50 kW/m² (b) 70 kW/m² at air flow 12.8 g/m².s

A feature of the slow thermal heating of the wood is that there was a continual release of water vapour during the gasification stage and the water is not flashed off, as it is in pulverised biomass combustion. This is illustrated in Figure 4.30. Water vapour was released for up to 1000s in the experiments and Figure 4.29 show that this is about the time it takes for the thermal wave to propagate through the thickness of the specimen.

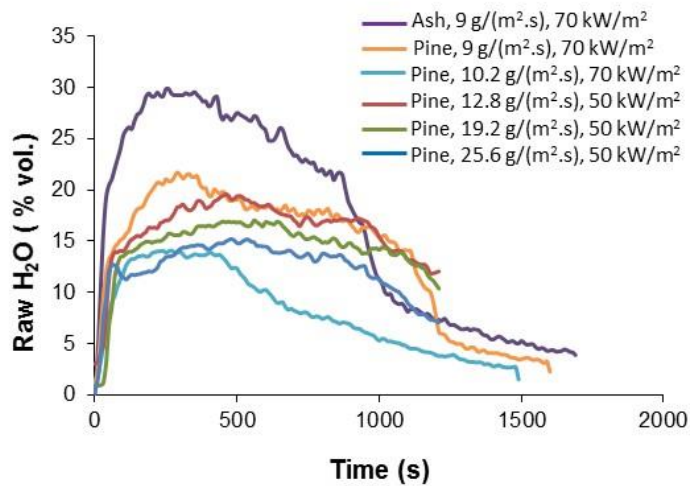


Figure 4.30 Water vapour released during rich combustion heating of 'dry' biomass.

4.4 Test with Insulation of the box of the cone calorimeter (configuration 2)

Insulation of the cone calorimeter box was done as discussed in the section 3.3.1. A cooling jacket on the bottom of the enclosure was used to cool the load cell.

Pine wood was investigated with 50 kW/m^2 radiant heat and an air flow of $12.8 \text{ g/(m}^2\cdot\text{s)}$ with and without the insulation of the enclosure. Figure 4.31 shows the comparison with insulation of insulated and uninsulated configurations for the mass loss rate (a) and metered equivalence ratio (b). The addition of insulation to the compartment walls resulted in an increase of about 30% in the mass loss rate of the wood and as a consequence an increase in the ϕ_m (that depends on the mass loss rate as the air flow is constant).

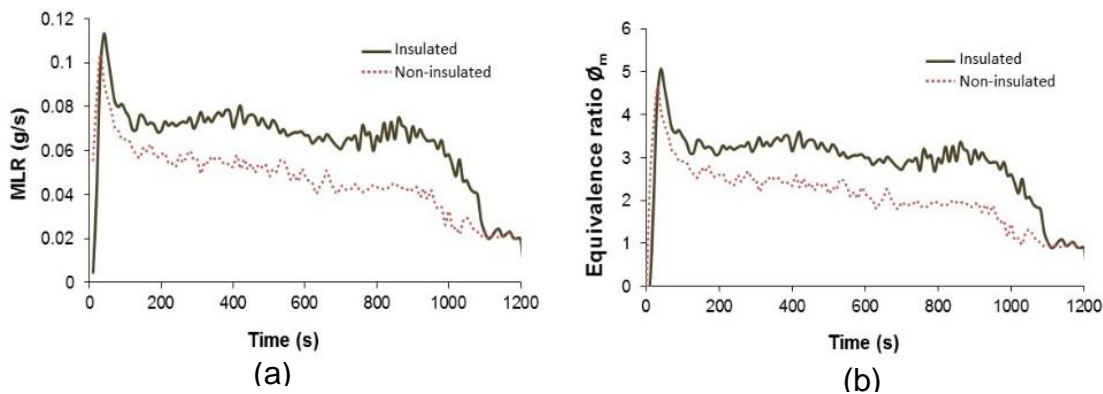


Figure 4.31 Heat flux 50 kW/m^2 , air flow $12.8 \text{ g/(m}^2\cdot\text{s)}$ (a) MLR (g/s) (b) equivalence ratio ϕ_m

The reason for this is that the combustion zone operates hotter with lower heat losses and this is then closer to equilibrium rich burning conditions. The richer mixtures and higher rich burn gasification conditions, the higher the CO emissions are, as shown in Figure 4.32 (a). However, Figure 4.32 (b) shows higher THC and this was not expected. This increase in THC is likely to be due to the richer mixtures, shown in Figure 4.32 (b). However, the presence of high levels of THC shows that the rich burn conditions are still well away from adiabatic equilibrium. The increase in CO after 700 s can be attributed to the rise of the temperature of the bed to a point where Boudouard reaction becomes dominant. Also the richer mixture at this time, shown in Figure 4.31 (b) will also produce higher CO. The change from rich to lean mixtures at the end of the test is the end of flaming combustion and the start of char smouldering combustion.

Figure 4.33 (a) shows the % O₂ in the gasification zone for the test in the insulated & non-insulated gasification zone. The hotter combustion with the insulated compartment results in more efficient combustion and lower oxygen levels.

Figure 4.33 (a) shows the % O₂ in the gasification zone for the test in the insulated & non-insulated gasification zone. Because of more consumption of O₂ in the gasification zone as CO and hydrocarbon yields increased, % O₂ from the gasification zone was lower as compared to the test without insulation of the box.

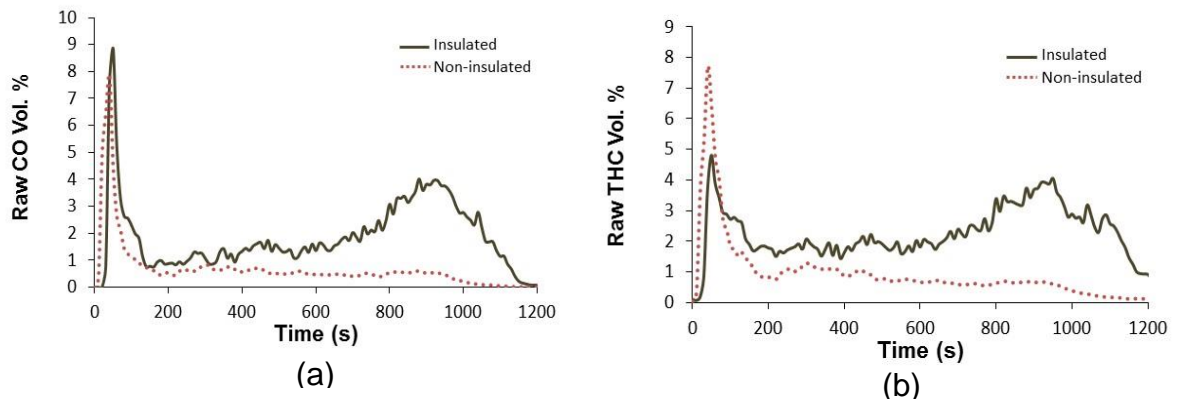


Figure 4.32 Heat flux 50 kW/m², air flow 12.8 g/(m².s) (a) CO % vol. vs time (b) THC % vol. vs time

There is also the problem that a true mean gas sample is not achieved. It is shown in Figure 4.33 (b) that the equivalence ratio calculated by carbon balance is much leaner than that based on the metered air and fuel consumption rates in Figure 4.31 (b). This indicates that the flame is centre rich and lean in the outer part of the chimney.

While Figure 4.33 (b) shows the gas analysis emissions based equivalence ratio ϕ_e for the insulated & non-insulated rich gasification combustion. The conditions in the compartment by gas analysis has moved from lean combustion to the stoichiometric combustion up to 600 s and to slightly rich combustion after 700s. The sudden reduction in ϕ_e after 1000 s was due to the end of flaming combustion.

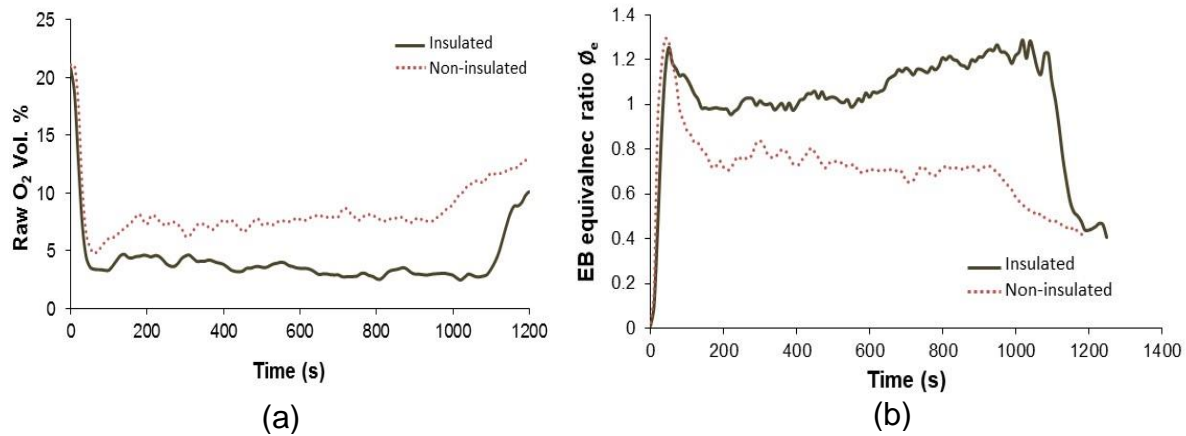


Figure 4.33 Heat flux 50 kW/m², air flow 12.8 g/(m².s) (a) O₂ % vol. vs time (b) ϕ_e vs time

Figure 4.34 shows the comparison of PHRR_{OC} and PHRR as % of total HRR_{MLR}. Figure 4.34 (a) shows that the PHRR in the rich burning combustion was higher for the Insulated test, due to the higher temperature of the burning zone which gave more efficient combustion. The PHRR_{OC} was only 30% of the total HRR_{MLR} so that the second stage combustion would dominate the total HRR in a practical two stage combustor. The lower proportion of PHRR_{OC} for the insulated case indicates that the total HRR_{MLR} was increased more than the PHRR_{OC} as shown by the higher MLR in Figure 4.34 (a). The very high proportion of the HRR_{OC} at the end of the burn out after 900s was due to the lower MLR of char combustion, which for the same air flow gave leaner mixtures and no gasification conditions. Normally a gasification burner would never be operated to complete burn out as fresh logs would be added before this occurred. Thus this late stage of the gasification combustion is not relevant and has been omitted in the tests in Chapter 5 onwards, as only the first 600s of burning was studied in the main body of this research. This was sufficient time to establish the steady state combustion after the initial flaming combustion, as shown Figure 4.31 - Figure 4.34.

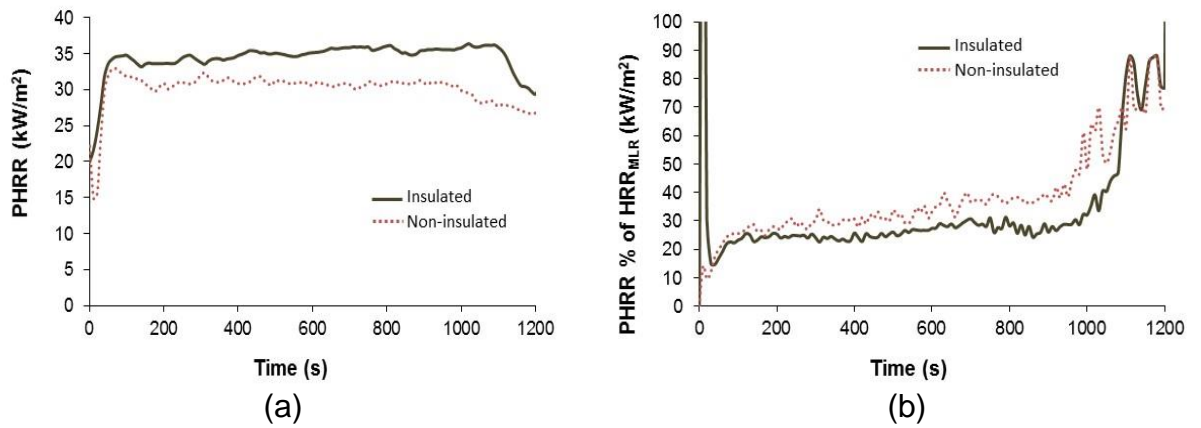


Figure 4.34 Heat Flux at 50 kW/m², air flow 12.8 g/(m².s) (a)PHRR vs time (b) PHRR as % of Total HRR_{MLR} VS time

Test were also performed for pine wood at 70 kW/m² with an insulated compartment for a higher heat flux at 70 kW/m² and air flow 9 g/(m².s) . Test time was restricted to 600 s for the reasons given above.

The limited test time also prevented the overheating of the load cell, which occurred later in the tests if the tests were carried out for longer than 600s. Figure 4.35 shows the effect of insulation for the 70 kW/m² test for the MLR and ϕ_m . There was a 25% increase in the MLR and 40% increase in the ϕ_m in the first 400 s, due to the higher temperatures with the insulated rich burning compartment.

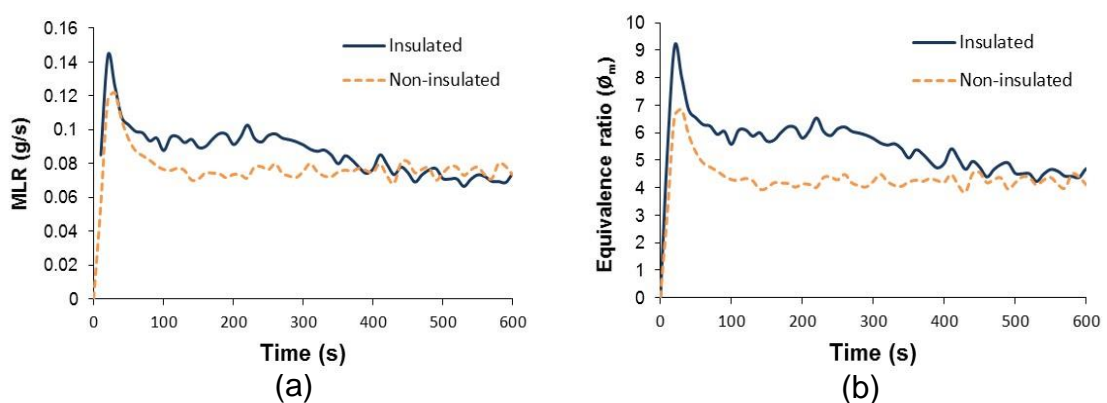


Figure 4.35 Heat flux 70 kW/m², air flow 9 g/(m².s) (a) MLR (g/s) (b) metered equivalence ratio ϕ_m

As the addition of the compartment insulation made the gasification zone richer, as shown in Figure 4.35 (b), the CO is expected to decrease as predicted from equilibrium chemistry in

Figure 4.10 The emissions from the tests showed this trend of decreased CO with addition of insulation.

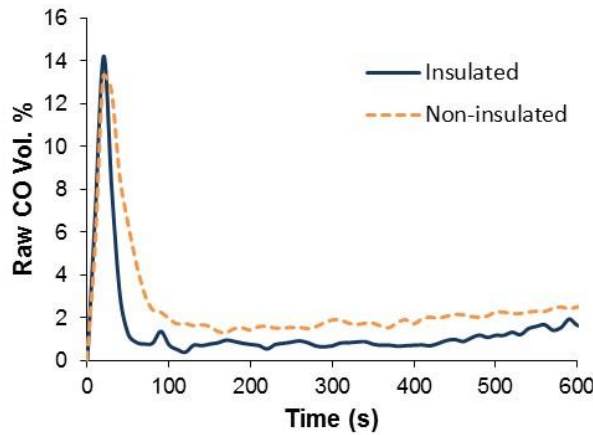


Figure 4.36 Raw % CO at heat flux 70 kW/m², air flow 9 g/(m².s)

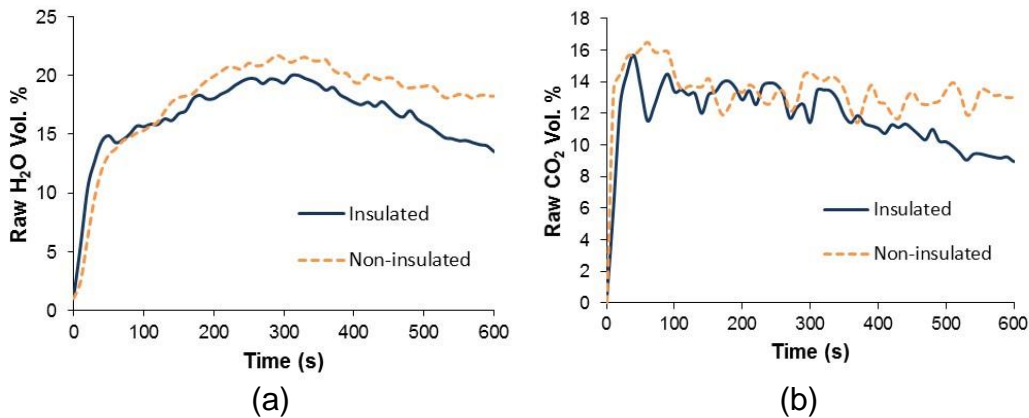


Figure 4.37 Heat flux 70 kW/m², air flow 9 g/(m².s) (a) % H₂O (b) % CO₂

However, the equilibrium chemistry also predicts in

Figure 4.10 an increase in the % H₂O and % CO₂, but Figure 4.36 shows that there was a slight decrease in these species. This may be due to improvements in the combustion efficiency of the rich primary zone, which would reduce CO and THC.

A test was performed at 12.8 g/(m².s) and 70 kW/m² to verify this assumption, that richer combustion at 9 g/(m².s) and a heat flux 70kW/m² produced less CO. Figure 4.38 shows that there was not much difference in the mass loss rates in both tests but ϕ_m changed because of the changing flow rate of air to the box. Figure 4.38 (b) shows that the gasification zone ϕ_m decreased from an average value of 6 to 4.

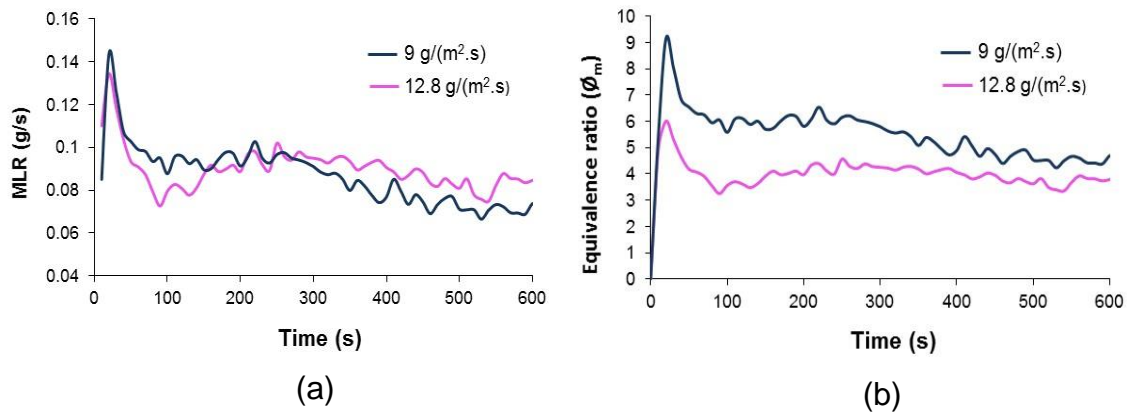


Figure 4.38 Tests with Insulation of gasification zone at heat flux 70 kW/m² (a) MLR (g/s) (b) equivalence ratio ϕ_m

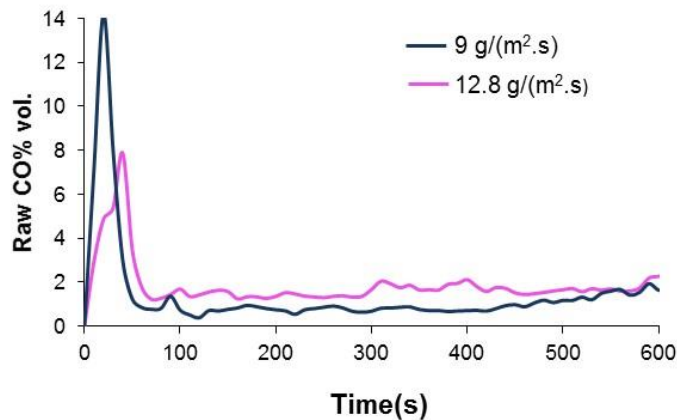


Figure 4.39 % CO at heat flux 70 kW/m² with insulation of the gasification zone

Figure 4.39 shows that CO increased with increase in air flow, due to leaner conditions inside the gasification zone as shown in Figure 4.38 (b). The equivalence ratio at the higher air flow was still rich, but was closer to the equivalence ratio of 3 for maximum CO emissions according to the equilibrium predictions in

Figure 4.10.

4.5 Influence of insulation below the test biomass for an insulated compartment (configuration 3)

Tests with insulation of the compartment for 40 mm thick pine wood in which 10 pine wood sticks were used in two layers of 5 sticks were shown above to have higher CO than for one 20mm layer of the same pine 20 x 20mm sticks (Figure 4.16- Figure 4.18). However, part of the gain in performance with 40mm thick wood (2 layers of 20mm) could be that the second layer provided 20mm of insulation to the first layer and thus there were lower heat losses from the heated surface. To investigate this 20mm thick ceramic wood insulating board was used below 20mm of wood and compared with the 40mm wood and 20mm wood with no insulation below in both cases. The tests was performed at a heat flux of 70 kW/m² and air flow 12.8 g/(m².s) to compare the CO % emissions with the previous tests.

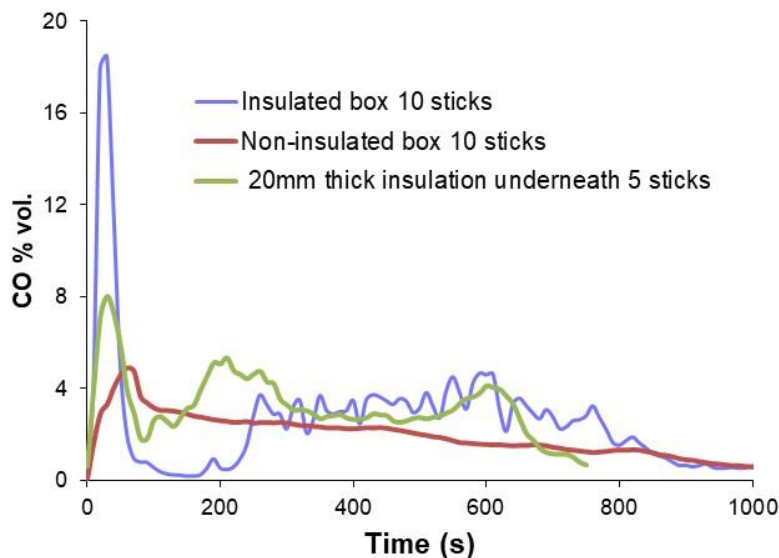


Figure 4.40 Comparison of % CO with 20mm insulation underneath the pine wood with tests 40 mm thick pine (2 layers) at 12.8 g/(m².s)

Comparison of the tests with the insulation of the gasification zone with the test without insulation in Figure 4.40 shows higher CO in the tests with insulation of the box. Comparison was also done for the test of thermocouples inserted to check the temperature of the wood and there was an increase in the temperature

of the wood at 5 mm from the top surface. The top temperature is limited by the temperature of the cone heater which was 870 °C for tests with 70 kW/m².

The tests were stopped after 600s as this was sufficient to establish the steady state burning condition, and ignores the char burn out phase as shown in Figure 4.14 - Figure 4.30. At 600s only the top wood layer was partly burned and the bottom layer was not touched by the fire. The increase in the CO % with the 40mm thick pine was possibly due to the bottom layer of the wood acting as insulation, so that the top layer operated richer. In order to check this explanation another experiment was performed at same conditions of heat flux and air flow (70 kW/m², 12.8 g/ (m².s)) with 5 pine wood sticks with an insulation of kaowool 20mm thick under the wood so that the total bed thickness remained at 40mm. The CO emission are shown in Figure 4.40 and were close to the test with the test of 10 pine sticks, but the initial high CO peak with flaming combustion was lower.

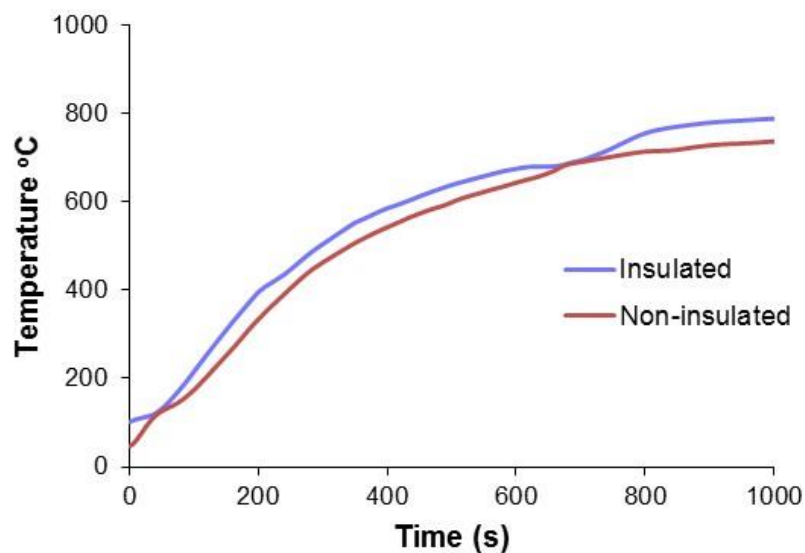


Figure 4.41 Thermocouples inserted 5mm from top surface in 40mm thick pine (2 layers of 5 sticks) with and without insulation at 70 kW/m² airflow 12.8 g/(m².s)

However the concentrations of CO were still far away from the equilibrium. The same configuration was operated with air flow to $9 \text{ g/m}^2\cdot\text{s}$ at the same 70 kW/m^2 heat flux and with insulation underneath to compare the two flow rates. Figure 4.42 shows the comparison of mass loss rate and metered equivalence ratio ϕ_m for the two tests and it shows that mass loss rate was almost same for the two tests and this was slightly higher than the tests without insulation underneath the wood. The flame produced in tests with 20mm insulation under wood is shown in the Figure 4.43 and comparison with the flames of 2 layers of wood (Figure 4.17) shows that flames look spreaded and it became clear that in the tests of two layers of pine wood only the layer was burning while bottom layer was acting as an insulation and was not contributing to the burning.

Comparison of the CO and THC in Figure 4.44 (a) for the gasification zone shows that although the test with $\phi_m = 6$ (air flow, $9 \text{ g/(m}^2\cdot\text{s)}$) was rich the CO was higher in comparison to $\phi_m = 4$ (air flow, $12.8 \text{ g/(m}^2\cdot\text{s)}$). This trend was against the equilibrium predictions. A similar trend was shown for the THC in Figure 4.44 (b).

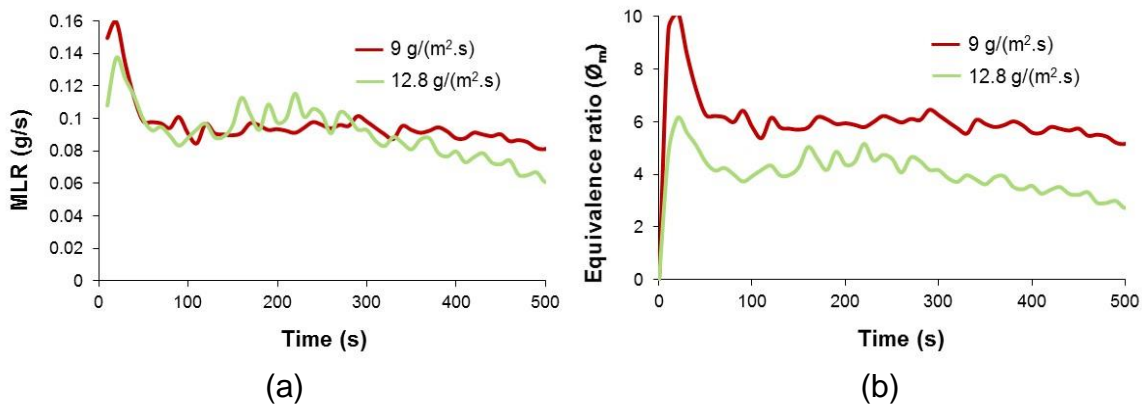


Figure 4.42 20 mm thick insulation under 5 wood sticks at heat flux 70 kW/m^2
(a) MLR (g/s) (b) equivalence ratio ϕ_m



Figure 4.43 Steady state flame combustion of 5 pine wood sticks insulated box, 20 mm insulation underneath, heat flux 70 kW/m², air flow 9 g/(m².s)

% H₂O was also slightly higher in rich test (Figure 4.45 a). Emission based equivalence ratio \varnothing_e showed a big difference when compared with \varnothing_m , showing that there is more air burning than entering the box, or the temperature of the wood is very far from equilibrium.

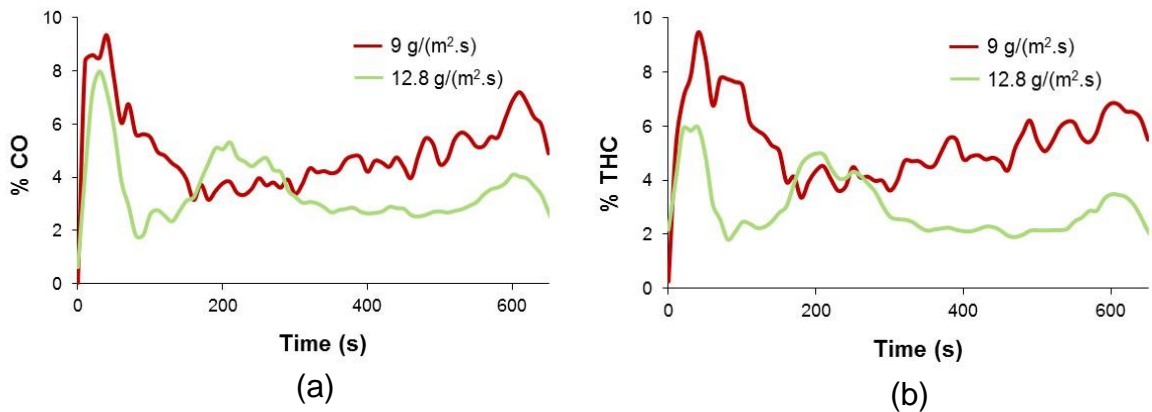


Figure 4.44 20 mm thick insulation under 5 wood sticks at heat flux 70 kW/m²
(a) % CO from gasification zone (b) % THC from gasification zone

\varnothing_e was shifted to the rich burning as compared to the tests without insulation of the box but still there was a problem inside the experimental technique. Next task was to identify the problem with testing conditions of 9 g/(m².s), heat flux 70 kW/m² and 20mm insulation under 5 wood sticks.

In the tests with 20mm insulation under the wood, the flame was coming out of the chimney top as shown in the Figure 4.46 and these flames were not seen in case of tests without insulation of the box. This is a clear illustration of the importance of minimising heat losses from the rich burn gasification zone.

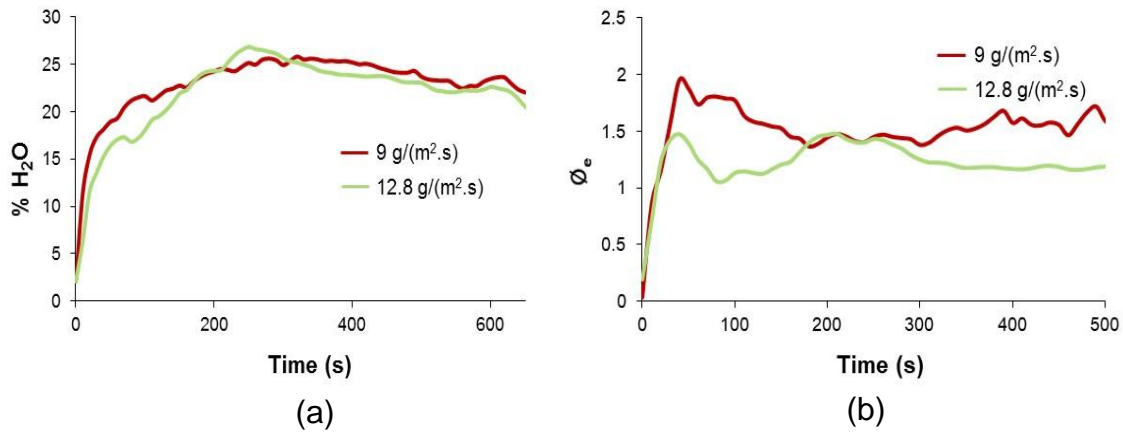


Figure 4.45 20 mm thick insulation under 5 wood sticks at heat flux 70 kW/m²
(a) % H₂O from gasification zone (b) Ø_e



Figure 4.46 Flame from chimney exit for standard sampling probe at steady state flame combustion of pine at 70kW/m², 9 g/(m².s)

4.6 The problem of gas sampling from the chimney exit so that mean sample was achieved (configuration 4)

The gas sampling for all the above tests used a single hole uncooled probe inserted into the top of the chimney, as shown in the Figure 3.4. The sample probe was located in the centre of the chimney. The chimney internal diameter was 80 mm and the gas sample tube was inserted 4mm from the wall about 150mm below the chimney exit. A problem area in the above results was that for rich mixtures there was quite a high oxygen level in the sample, as shown in Figure 4.33 (a). Also the CO levels were well below equilibrium. One possible explanation for this could be that the gases were not fully mixed inside the chimney and the gas sampling might not be representative of the actual concentration. Also the FTIR gas sample flow rate was 4 L/min and this is close to the lowest air flow used in the compartment box, which was 6 L/min. It is thus possible that air was entrained by the sample from outside the chimney and this contributed to the O₂ and low CO relative to equilibrium. Thus improvements to the gas sampling probe design and location were investigated.

The following tests were carried out to try to improve the mean gas sample and to remove the oxygen entrainment from the exit. All the initial tests were to improve the gas sample as a measure of the mean composition and the problem of the oxygen dilution by reverse suction by the gas sample probe was investigated last. In retrospect it would have been better to investigate the entrainment of air from the chimney exit first as this was the dominant problem. The following tests were carried out.

1. Initial single hole sample tube, as used in all the above tests.
2. Traverse of the single hole sample tube (Figure 4.47 (a))
3. Traverse of the single hole sample tube with grid plate mixer at the entry to the chimney (Figure 4.47 (b)), grid plate is shown in Appendix A Figure A.2
4. Four hole sample probe (Figure 4.48)
5. 76mm diameter 20 hole 'X' probe at the bottom of the chimney (Figure 3.6 (b))

6. Chimney exit backpressure orifice with 20 hole 'X' probe at the bottom of the chimney shown in Appendix A Figure A.5.

All the results that follow show the same pine wood test condition repeated for the above 6 gas sample probes and locations. All the tests was performed with the insulated compartment and 20mm insulation below the test fuel. The comparison was made for 20mm thick pine wood at 70 kW/m² with 9 kg/sm² air flow (27 kW/m² primary HRR).

4.6.1 Initial single hole sample tube, as used in all the previous tests.

All the different methods of sampling the raw exhaust gas from the chimney are compared in Figure 4.50 - Figure 4.53 equivalence ratio plots as a function of time are shown in Figure 4.50. This shows that the standard single hole central sample probe had the richest mixture initially and this was because it was located in the central rich region. This also had high CO and THC with low oxygen, all as expected for a locally rich mixture.

The % CO and the emission based equivalence ratio ϕ_e by carbon balance is shown as a function of radial distance for single hole probe with and without mixing plate under chimney in Figure 4.49 a and b. This shows that the chimney was not well mixed and was rich in the centre and lean at the chimney wall. This can also be seen in the flame photos in Figure 4.43 and Figure 4.46 with the luminous flame in the centre.

4.6.2 Traverse of the single hole sample tube (Figure 4.47 a)

For the same single hole probe was traversed across the chimney starting from 7cm from the wall of the chimney the sample probe was moved radially inwards by 1 cm so that the gas sample positions were 7, 6, 5, 4, 3, 2, 1 cm inside the chimney, as shown in the Figure 4.47 (a).

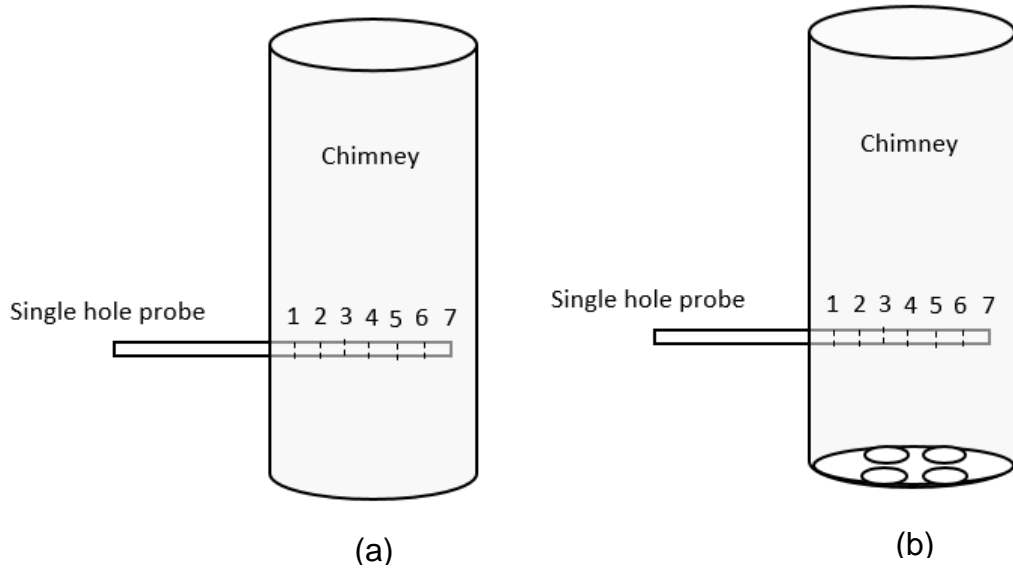


Figure 4.47 (a) Traverse with single hole probe (b) Single hole probe traverse, orifice under chimney

The first 100 s of the test time was not included due to the variable flaming combustion at the start of the test. The traverse of the sample probe was carried out in the same test during the steady state combustion period with 45- 50s at each location, which was sufficient time for the gas sample line to flush out and the FTIR to take sufficient readings to get a good average.

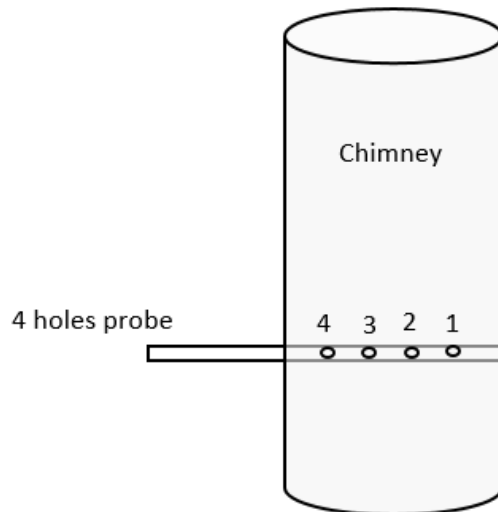


Figure 4.48 Configuration of 4 hole probe inside chimney

The mean of the radial traverse probe shows in Figure 4.50 a much leaner mixture than for the central location. This has lower CO and THC and higher oxygen, as expected for a leaner mixture.

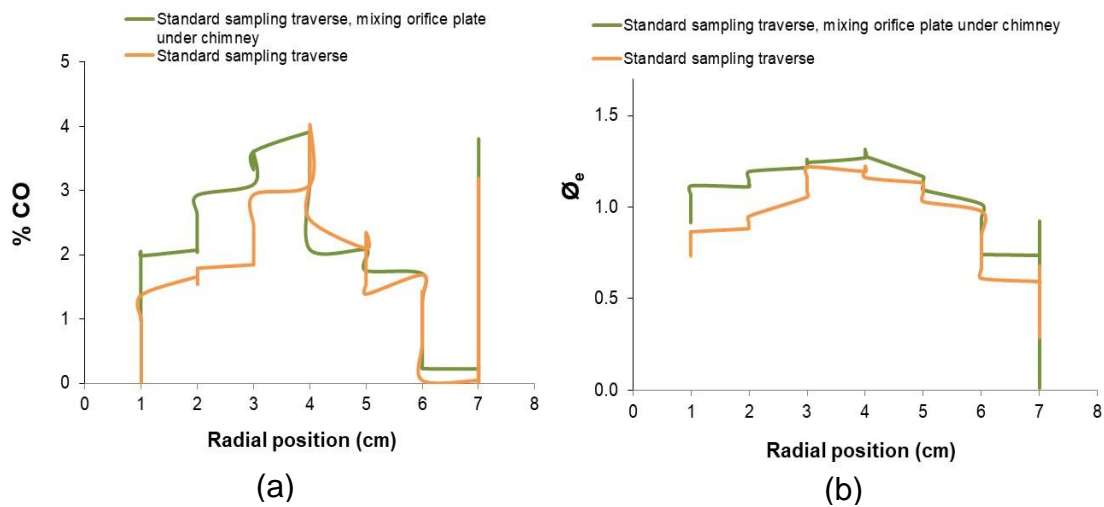


Figure 4.49 % CO and O_e with single holes probe traverses with and without mixing orifice plate at $9 \text{ g}/(\text{m}^2 \cdot \text{s})$ $70 \text{ kW}/\text{m}^2$

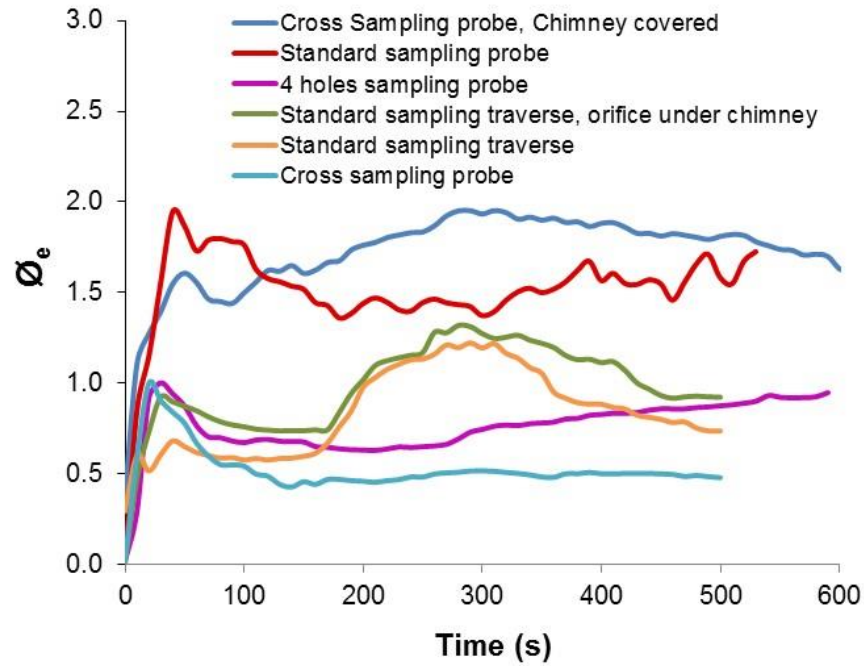


Figure 4.50 EB Equivalence ratio ϕ_e for tests with different sampling methods, heat flux 70 kW/m², air flow 9 g/(m².s)

4.6.3 Traverse of the single hole sample tube with grid plate mixer at the entry to the chimney (Figure 4.47 b)

An attempt to improve the mixing in the chimney was made by placed a four hole grid plate at the base of the chimney, to generate flow turbulence and mixing. The results in Figure 4.50 show a much leaner mixture than single central gas sampler and this is close to the mean of the radial traverse at the outlet plane without the grid plate at the chimney exit. Thus the impact of the grid plate at the chimney inlet is small. This was not expected, but is probably due to the very low flow rates used that result in little turbulence generation at the grid plate.

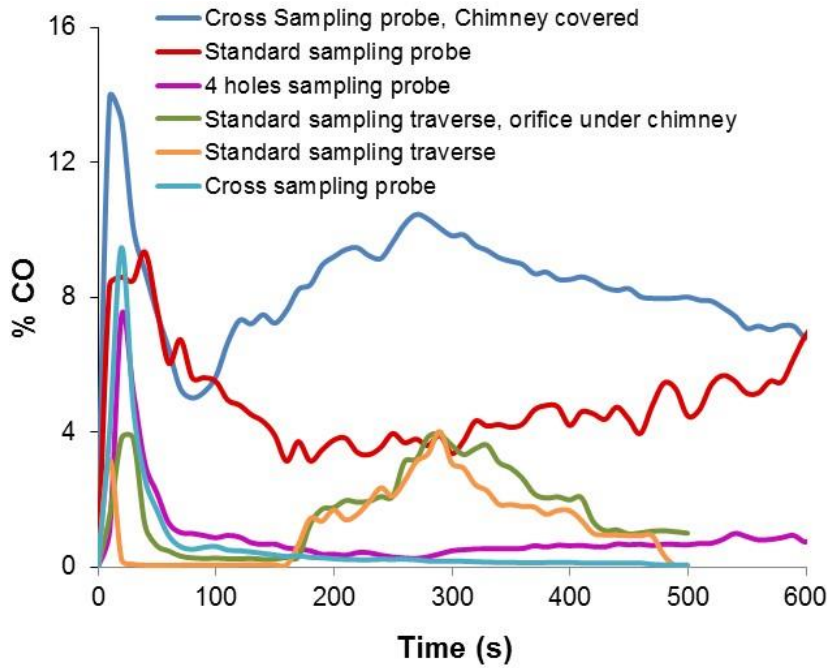


Figure 4.51 % CO emissions for tests with different sampling methods, heat flux 70 kW/m², air flow 9 g/(m².s)

4.6.4 Four-hole sample probe (Figure 4.48) and no inlet grid plate

The four-hole gas sampler gave the mean mixture much leaner than the single central probe, at about half the equivalence ratio of the single central sample point as shown in Figure 4.50. This leaner mixture produced much lower CO emissions, as shown in Figure 4.51. The CO₂ and H₂O concentrations were also much lower for the 4 hole sample probe, as expected for leaner mixtures, as shown in Figure 4.52. There was also lower THC emissions, as expected from the leaner gas sample, as shown in Figure 4.53. Also the oxygen level was higher for the four hole gas sampler due to the leaner mixture compared with the single hole locally rich mixture with near zero oxygen, as shown in Figure 4.53. However, the sample equivalence ratio was leaner than for the traverse results and this indicated that more gas sample holes were required to give a better approximation to the true mean composition of the exhaust.

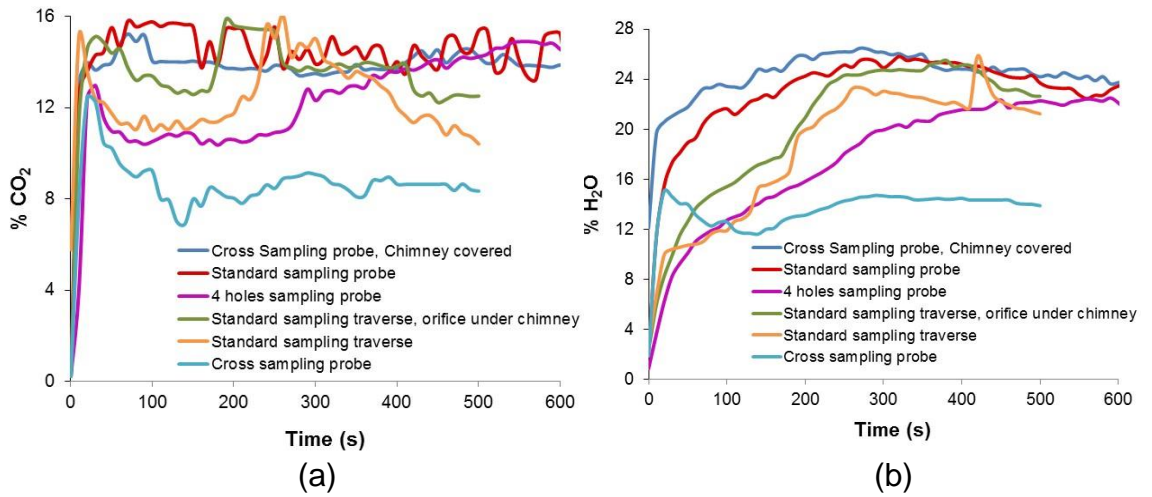


Figure 4.52 % CO₂ and H₂O emissions for tests with different sampling methods, heat flux 70 kW/m², air flow 9 g/(m².s)

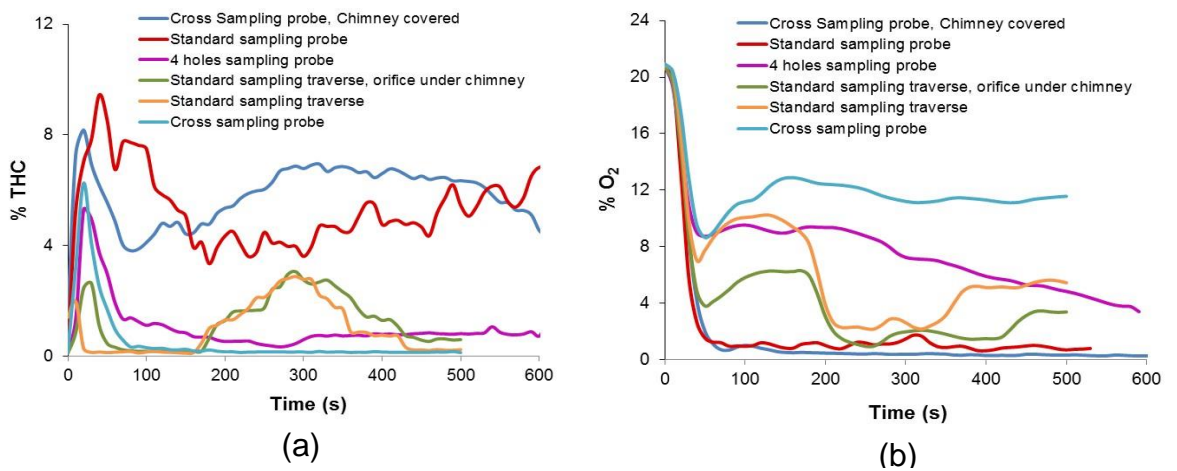


Figure 4.53 % THC and O₂ emissions for tests with different sampling methods, heat flux 70 kW/m², air flow 9 g/(m².s)

4.6.5 76mm diameter 20 hole 'X' probe at the bottom of the chimney

An existing 20 hole mean gas sampler in a 76mm diameter housing (Figure 3.6 b) was used with its own mounting flanges. This was placed at the base of the chimney in an attempt to stop the gas sampler entraining air from the chimney exit. The results in Figure 4.50 show a very lean equivalence ratio. This results in very low CO and THC emissions and higher oxygen. It was considered that these lean mixtures were not realistic when the metered equivalence ratio was

very rich. It was concluded that the problem was the entrainment of oxygen from the chimney exhaust plane, mainly due to the relatively high sample flow rate for the FTIR compared with the compartment air flow rate. The air flow compartment was checked for air leaks and none was found.

To prove that air entrainment from the exhaust chimney was the problem tests were carried out with N₂ at the same flow rate as the air. The standard single hole gas sample probe was used. It was found that even at high flow rates of nitrogen, the O₂ analyser downstream of FTIR was reading 10% O₂. Showing that air was entering the sampling system from the exit of the chimney. To prevent this a pressure loss was created at the chimney exit by placing an orifice plate there. This restricted the back flow of air into the chimney and the grid plate blockage was increased until O₂ analyser read zero while purging the box with nitrogen.

4.6.6. Chimney exit backpressure grid plate blockage with 20 hole 'X' probe at the bottom of the chimney.

Figure 4.50 shows that the impact of the chimney exit grid plate (with 90% restriction of the total chimney exit area) was to make the mean mixture much richer. By co-incidence the mean mixture was close to that for the central single hole sampling probe without an exit plane orifice. The CO and THC were high and the oxygen near zero after 100s, all as expected for rich mixtures.

The above test was carried out with the 'X' probe holes facing in the downward direction. However, after the experiment it was found that most of the sample holes were blocked by the soot as shown in Appendix A Figure A.3. Tests were performed with the X-probe holes facing upward towards the chimney exit and it was found that the blockage was very low as compared with the reverse sampling position shown in Appendix A Figure A.4. The CO emissions of the two tests are compared in Figure 4.54 which shows that with the X-probe facing downward the CO was lower than compared with the X-probe facing upward.

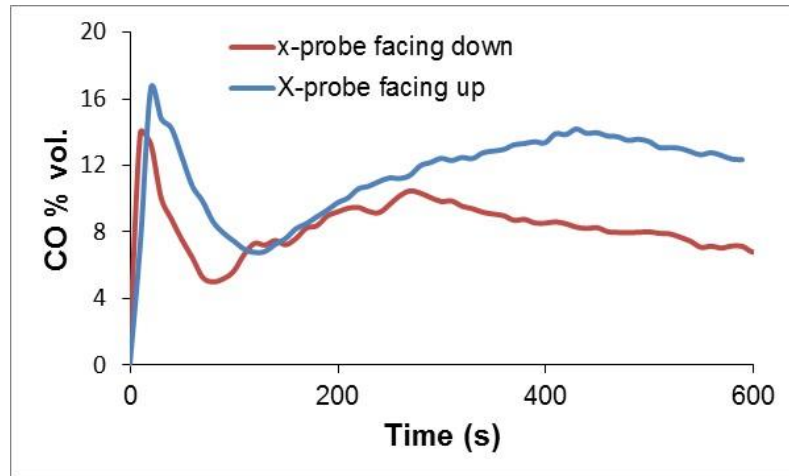


Figure 4.54 % CO comparison of x-probe holes facing up and down

4.6.6 Repeatability of the test in the final test configuration

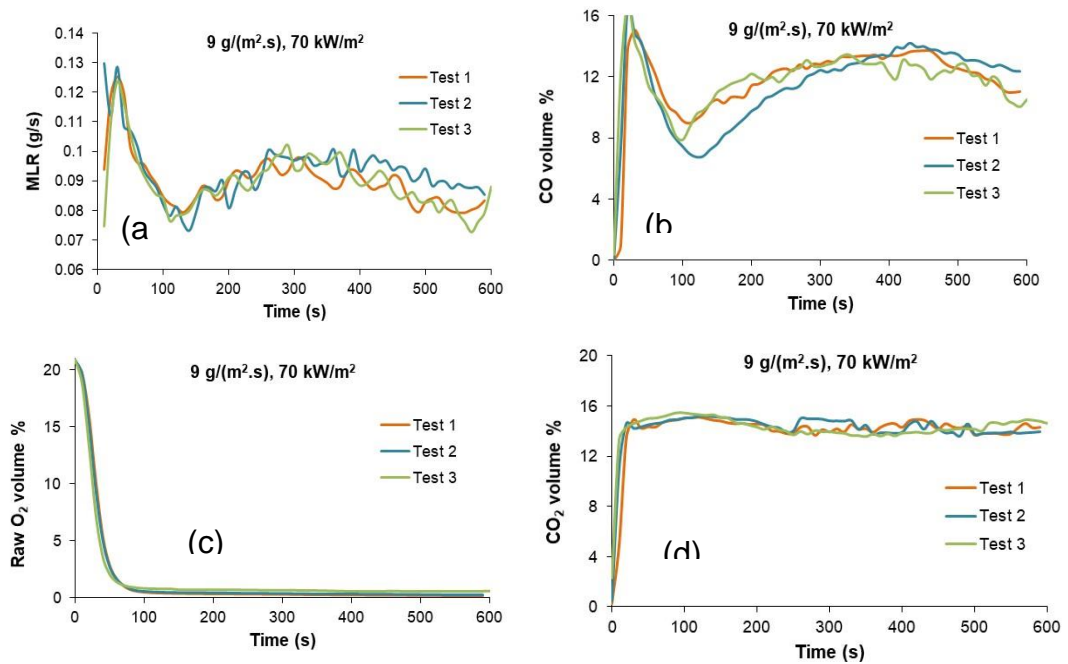


Figure 4.55 Repeatability of the tests on cone calorimeter (a) MLR (g/s) (b) FTIR CO % (c) Raw O₂ % (d) FTIR CO₂ %

Tests were performed to check the repeatability and this final configuration of the compartment test arrangement and chimney mean gas sampling. Figure 4.55 shows the repeatability of the tests at 9 g/(m².s) and 70 kW/m². The test was repeated three times at this condition and Figure 4.55 shows very good

agreement. Repeat tests were also performed at different flow rates and these showed good repeatability.

4.7 Final optimised rich burn gasification cone calorimeter test conditions

The detailed development of the experimental methodology used in the present work resulted in the following operating conditions.

The controlled atmosphere chamber around the cone calorimeter test section was insulated inside the chamber. The door was additionally insulated outside and the observation window was normally blocked with insulation, apart from when photographs were being taken.

The test sample was insulated with 20mm of kaowool board between the bottom of the sample and the metal holder.

The mean chimney gas sample was obtained from a 20 hole 'X' probe, with the sample holes on centres of equal area. This was mounted at the bottom of the chimney. There was a grid plate at the chimney exit which prevented the back flow of air into the chimney.

4.8 Technical issues regarding insulations and emissions

These technical issues were observed after all the tests with the desired setup discussed in the next chapter (Chapter 5) were completed, tests could not be repeated again by making further changes due to the time constraints, however some adjustments were applied in the emissions of CO₂ and H₂O recorded by some technical issues discussed in this section.

In the final experimental setup, box of the cone calorimeter was insulated and 20mm thick insulation of the same material kaowool board was used underneath the biomass sample to create the same effect as in the loaded log boilers. In the above discussion and results it was observed that the % CO₂ and % H₂O emissions were very high. It was suspected it could be due to either some leaks or some foreign bodies burning inside the test section.

Box was checked for leaks using soap water. However it becomes clear by looking at the superwool paper, kaowool insulation board and the door sealing after the test that some burning was taking place.

Kaowool insulation was heat treated before the test was started so that the binders inside are fully burnt and do not affect the test, however these boards were re-used for the tests initially and it was assumed that no emissions were resulted from it.

Superwool paper were converted to ashes and were burnt after each test and new paper was used in each test to seal the gaps of the chimney. Gasification tests were also causing the burning of the door sealant and it was changed after two tests.



Figure 4.56 Superwool paper after the test#

In order to check that if these materials caused emissions, Blank tests were performed with the heater on at 70 kW/m^2 and air flow of $9 \text{ g}/(\text{m}^2.\text{s})$ and $19.2 \text{ g}/(\text{m}^2.\text{s})$.

In the first test kaowool insulation board that was heat treated and used before in a gasification test was heated again under said conditions to check the emissions resulted.

Figure 4.59 illustrated the FTIR emissions from a heating a used kaowool insulation board and it was seen that more than 2% CO_2 and about 2% water was obtained from this test, but it was still unknown that how much emissions

were resulting from the superwool paper, A test was done with shutters closed and placing fresh superwool paper underneath chimney and the emissions resulted are shown in the Figure 4.60. It can be seen that H₂O was about 2% and CO₂ was about 1% while CO was negligible.

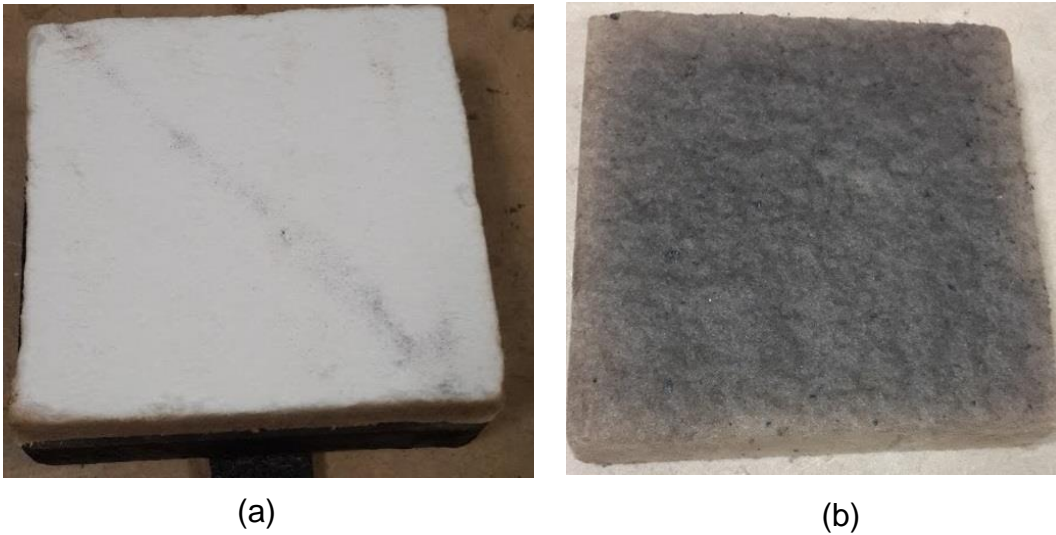


Figure 4.57 Kaowool 20mm insulation (a) Before test (b) After test



Figure 4.58 draft extruder door sealant after the test

Box was insulated from the kaowool insulation as well and the distance of the walls was big enough to make emissions out from there, kaowool was heat treated before the insulation of the box as well, but another test was done in

which air was passed through box heated by 70 kW/m^2 , superwool paper used underneath chimney was already burnt in a test and results of the emissions are shown in the Figure 4.61. It can be seen that H_2O emissions reached 2-2.5%, while CO_2 was less than 0.5%. It can be concluded that Kaowool insulation might absorb water in its pores and when box heats it liberates that water.

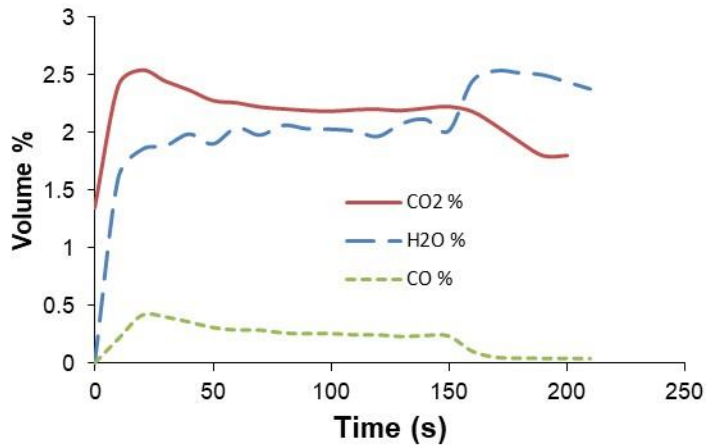


Figure 4.59 Emissions from used kaowool board

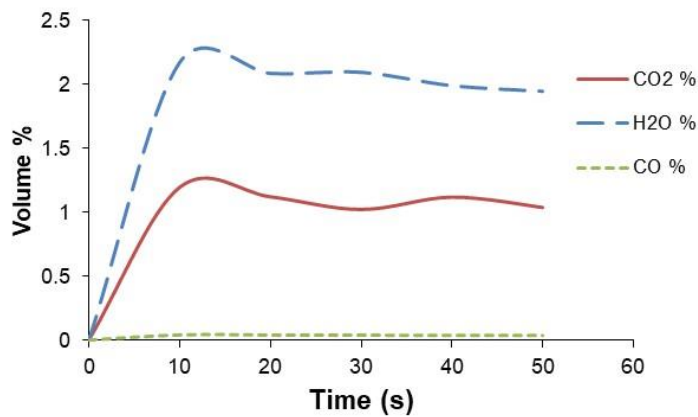


Figure 4.60 Emissions from superwool paper

It is difficult to differentiate that how much H_2O and CO_2 was emitting from kaowool and superwool paper individually. Box temperature was much less than that of actual gasification burning tests. In the actual tests, door sealant was also burning and that can also add up CO_2 inside the box. After taking into account all these factors, an adjustment was made into CO_2 , H_2O and CO emissions using the baseline obtained from blank test done upto 600 s. In the next tests

kaowool insulation underneath the biomass was heat treated and was not reused for other tests unless heat treated again.

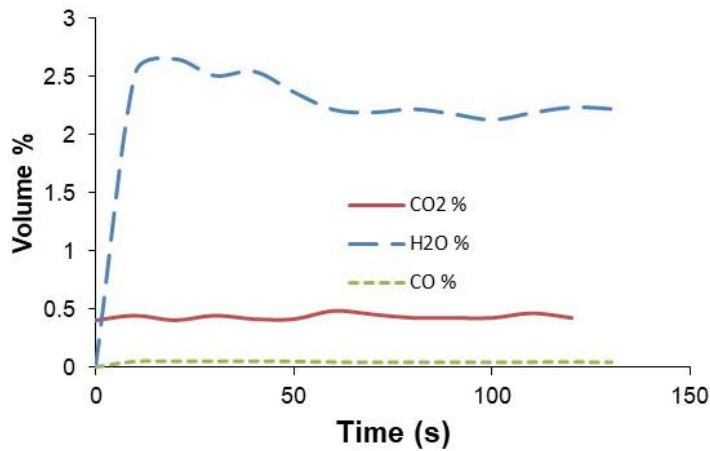


Figure 4.61 Emissions from heated box

4.9 Conclusion:

- From the TGA tests of biomass it was found that there was considerable variation in the temperature at which the biomass lost weight. This variation was due to the different proportions of hemi-cellulose, cellulose and lignin in the biomass composition. As H/C increases Stoichiometric A/F ratio decreases.
- Correlation of Sheng and Azevedo [95] did not seem to work when hemicellulose and cellulose calculated using their correlation for biomass was plotted vs stoichiometric (A/F) and showed opposite trends. It was found that calculations for the adiabatic equilibrium compositions of the products of gasification using CEA software predicted different values of equivalence ratios for different biomasses to achieve peak concentrations of CO and H₂.
- It was concluded in the initial tests that higher heat flux produced more % CO due to higher biomass temperatures.
- It was found that cone calorimeter can be used for studying gasification of biomass by making some modifications in the setup, originally deigned to study flashover fires. Insulation of the chamber (enclosure box) as well as the insulation of the sample with 20mm thick kaowool board provided better results.

- It was shown that original setup had back mixing of external air that was stopped by using a restriction (orifice grid plate) on the top of chimney to and 20 holes x-probe provided somewhat better mean sample.

Chapter 5 Results of gasification tests on cone calorimeter

Experimental results for the modified cone calorimeter with the experimental setup developed in Chapter 4 are presented here. A key feature of this work was the variation of equivalence ratio so that optimum conditions for the maximum transfer of energy from the solid biomass to the gaseous rich burning product gases are achieved. Equivalence ratio variations occurred in two ways: firstly, at a fixed air flow the mass burning rate of the biomass increased as the sample became hotter during the test; secondly, tests were carried out at different air mass flows and increases in air flow increased the mass burning rate, whilst still having a mass burning rate varying with time in the fire. There was deliberately no attempt to study lean combustion as that would be simple single stage combustion.

5.1 Influence of equivalence ratio on the product gas composition

5.1.1 Equivalence ratios at steady operation

Tests were at a radiant heat flux on the cone calorimeter of 70 kW/m^2 for different air flow rates with pine wood burning as summarised in Table 5.1. The air flow rate (litre/min) is converted to different units to make it possible to scale up the results to practical equipment size. Units of $\text{g}/(\text{m}^2 \cdot \text{s})$ are used for the discussion of the results. This can be converted to kW/m^2 by multiplying $\text{g}/(\text{m}^2 \cdot \text{s})$ by $3.05 \text{ kJ/g}_{\text{air}}$. This uses the concept of the heat release per kg of air being constant for any fuel that is burnt. The constant normally used is $3.05 \text{ MJ/kg}_{\text{air}}$ which converts to $13.1 \text{ MJ/kg}_{\text{oxygen}}$ and this assumes complete combustion, as discussed in 3.5. $13.1 \text{ MJ/kg}_{\text{oxygen}}$ is the normally used constant in oxygen consumption calorimetry that is used in the present work to determine the HRR in the primary and secondary combustion zones on the cone calorimeter.

Table 5.1 Conditions of air flow for the tests

Test no.	L/min	g/(m ² .s)	kW/(m ²)	ACH	Residence time s	Ø _m
1	3	6.10	18.6	6	600	7.8
2	4.4	9.0	27.5	8.8	409	6.0
3	5.5	11.2	34.2	10	360	4.5
4	6.3	12.8	39.0	12.6	286	4.0
5	8	16.3	49.7	16	225	3.3
6	9.4	19.2	58.6	18.8	191	2.8
7	12.5	25.6	78.1	25	144	2.0
8	15.5	31.6	96.4	31	116	1.6

It is quite common for the constant for air to be use as 3.0 MJ/kg_{air}. The measured HRR by oxygen consumption in the rich burning gasification zone can be compared with the kW/m² values in Table 5.1 and the difference is the combustion inefficiency so that the ratio of the measured oxygen consumption values to those in Table 5.1 is the combustion efficiency.

The mean equivalence ratios, Ø_m, in Table 5.1 is from the steady state burning phase of the experimental results using the stoichiometric A/F of 5.3 for the pine wood from Table 4.1. The experimental A/F is the metered air flow divided by the mass loss rate of the fuel in the steady burning phase.

ACH stands for air changes per hour and it means the number of times the air is removed from the enclosure volume per hour. It is the air flow rate in volume flow units divided by the volume of the enclosure used in the tests. ACH is not a very relevant parameter for the combustion performance, but is used in compartment fire research. If a smaller compartment was used at the same air mass flow rate, the mass flow based air flow parameters would not change but ACH would increase if the volume was smaller. A smaller volume for the chamber is desirable as this would reduce the heat losses by reducing the internal surface

area for heat losses. The ACH can also be expressed as a residence time as 3600/ACH s.

The air mass flow rate per surface area, $g/(m^2.s)$, is based on the flat surface area of the 0.1m x 0.1m test specimen surface. This area is not increased with pellets or powders so it is not the micro-surface area. It is simply a parameter that can scale up the test conditions to large scale bed areas. For example if a 1m square bed area was used in a practical equipment at say 30 $g/(m^2.s)$ then it would burn at 30 g/s and for a CV of say 16 MJ/kg would be a 0.48MW heater, with a 10m square bed it would be 48 MW combustion system. Large scale biomass fuelled systems using two stage combustion exist with this size. They normally are referred to as moving bed combustors or stoker fired combustion systems, as the continuous feed of fresh wood is accommodated by the bed moving slowly.

Figure 5.1 shows the variation of mass loss rate of pine wood with time for an air flow of 19.2 $g/(m^2.s)$, The initial peak of the mass loss rate within the first 100 seconds is partially as a result of the availability of the air in the compartment, so that essentially the initial rich combustion is in an infinite air supply and it is only later that once the initial air has been consumed in the combustion controlled by the imposed air flow. This initial fast burn period is similar to the residence time or the time to remove the initial air in the compartment, which is 191s for this air flow.

Another cause of the high initial burn rate is that there is no char layer initially and this acts as an insulation and a resistance to the release of volatiles. After this initial start up period the rich combustion settles to a steady state rate of mass loss. The period marked from 300-500s is steady state rich burning and this is used as the period of measurement for steady state. It was shown in Chapter 4 that if combustion was left to continue until all the wood had burnt, then the later burning phases would have been slower char combustion and the mass burning rate reduced. The period 300 – 500s is the steady state burning period with unburnt wood at the bottom of the pine and charred wood on top of the pine.

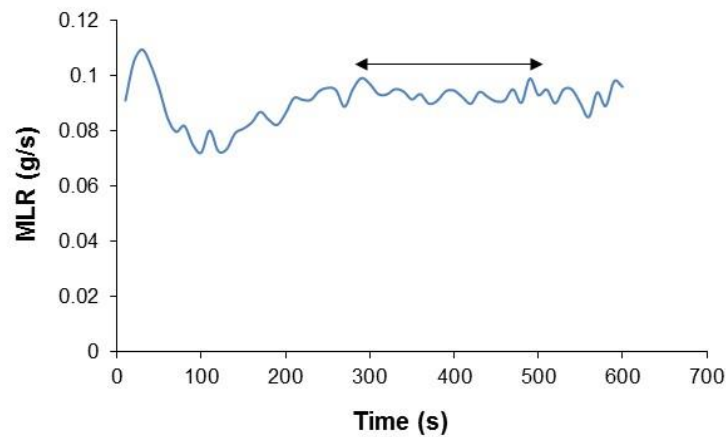


Figure 5.1 Variation of mass loss rate with time, air flow 19.2 g/(m².s)

Thermal conduction of heat is occurring through the wood and the temperature is high at the top and low at the bottom, as will be shown later. The reason the start and end of the combustion can be ignored is that in a real application of log burners you never burn the wood out completely as wood is added in batches before the previous batch has been completely burned. The start up phase might only happen once per week and the burn out phase might never happen until the heater was shut down in the summer. This is why the central region of the results between 300 and 500s are most important in this work.

In the steady state part of the rich burning there is a char layer formed on the incident radiation side of the pine and there is raw wood at the bottom of the pine layer. The porosity of char is higher than wood but the thermal insulation of char is more than wood [141]. The char layer reduces the heat transfer to the inner wood reducing the rate of pyrolysis causing a reduction in the mass loss rate to a minimum value. As time progresses the interior virgin solid receives considerable heating which can augment the pyrolysis rate and hence after 100-200 s in different tests, it attained a steady value until all the wood is completely burnt. In the test at 19.2 g/(m².s) the steady state value of mass loss rate was 0.09 g/s, as shown in Figure 5.1.

Figure 5.2 shows the mass loss rate vs time for the range of air flows in Table 5.1. Tests at high flow rate of air, 25.6 and 31.6 g/(m².s) have an initial high rate of mass loss this is due to the leaner and hotter combustion, as shown later. For the 20mm thickness this means the raw wood is consumed faster and char is produced sooner as shown in Figure 5.2.

Towards the end of the test time, due to high rate of initial burning, more combustion of biomass resulted till 600 s as compared with other tests.

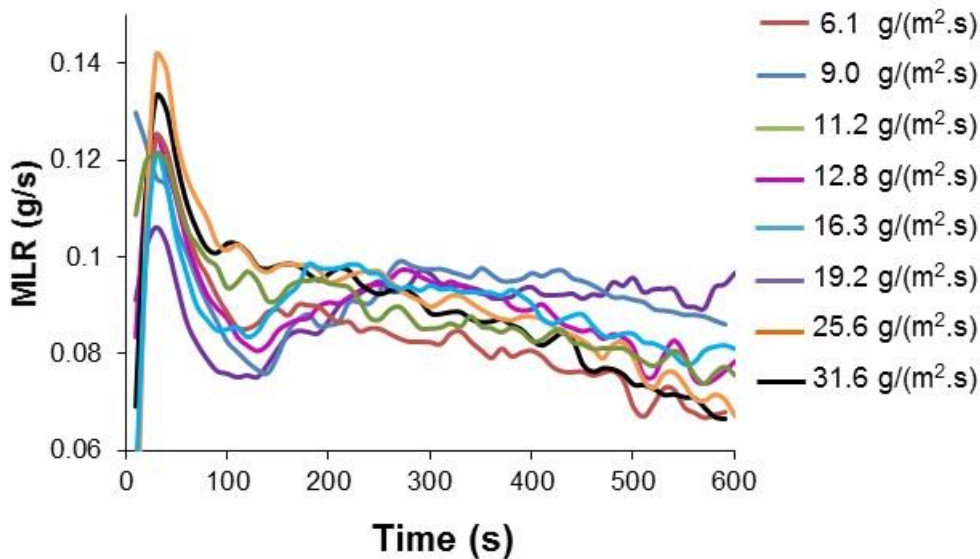


Figure 5.2 Variation of mass loss rate with time for test at different flow rates

The analysis of results was mostly focused on the steady state region of the experiment. All the parameters discussed in the following results are average over the range of 300-500 s. The same approach was employed by Plis and Wilk [70]. The aim is for these values to be representative of the operation of larger scale biomass two stage combustion systems, for boiler applications.

The ϕ_m was determined from the metered air and fuel consumption, as discussed in chapter 4, and the results for all the air flows in Table 5.1 are shown in Figure 5.3. After the initial heating period all the flow rates produced a near constant metered equivalence ratio and the range of ϕ_m was from 1.5 to 8. Average values in the range of 300 to 500s are used for the plots and are listed in the Table 5.1. The length of the test was limited to 600s due to overheating of the enclosure which caused the load cell to malfunction. Also, as discussed in the section 4.3.1, the char burn out stage represents inefficient gasification due to high CO_2 emissions and in a practical gasification burner this is not normally an operational condition, as more biomass is added to the gasification zone and complete burnout is hence not the part of this study.

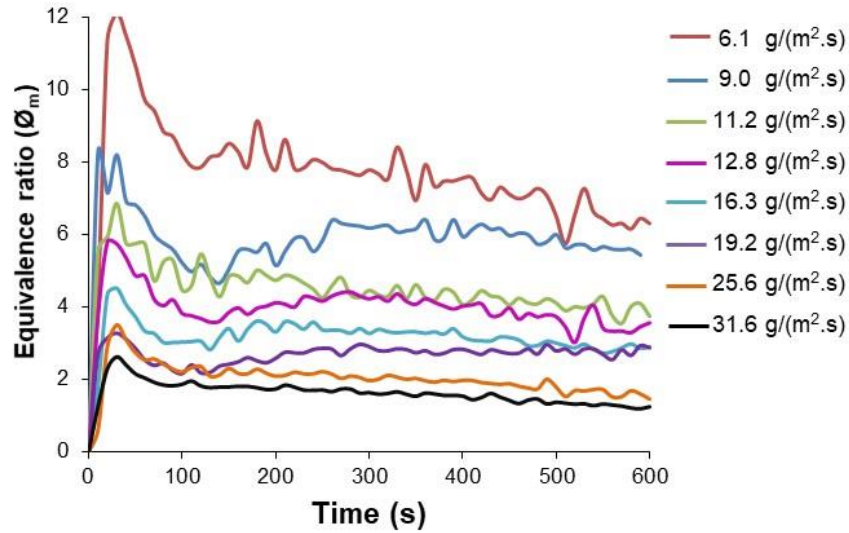


Figure 5.3 Variation of ϕ_m with the air flow rate

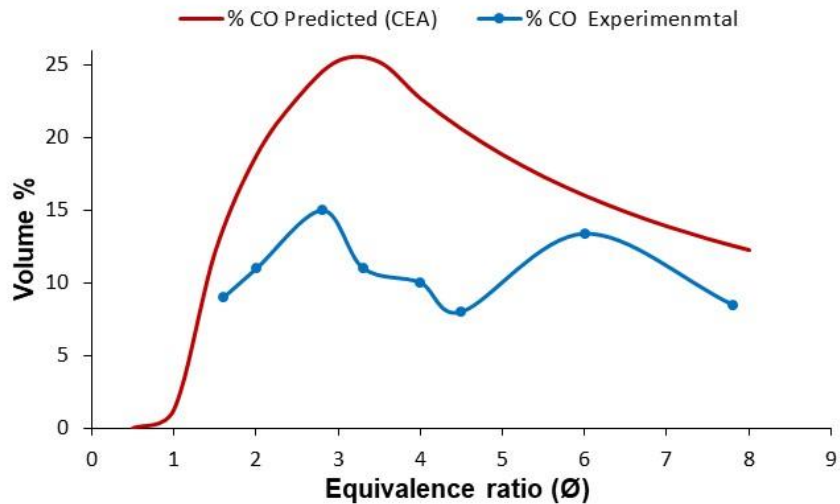


Figure 5.4 Variation of experimental and predicted (equilibrium) CO concentration with ϕ

shows the variation in the average steady state % CO with ϕ_m and comparison with the equilibrium. The maximum measured concentration of CO was 15% and was achieved with an air flow of 19.2 g/(m².s) with an equivalence ratio of 2.8. The minimum average concentration was 8.5% at $\phi_m = 7.8$. The trend of the experimental % CO follows the same shape as equilibrium % CO trend from ϕ_m 1.6 to 4.5, at $\phi_m = 6$, the peak value was not following the trend. The experiments were repeated 3 times at these conditions, but the same results were obtained each time.

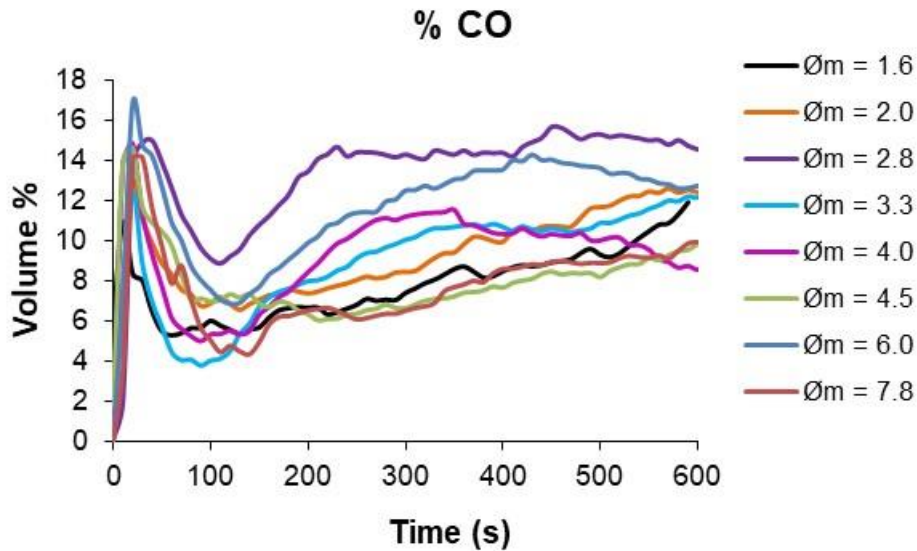


Figure 5.5 % CO variation with time in different tests listed with steady state ϕ_m

The very rich mixtures with $\phi_m = 6-8$ the CO levels were close to equilibrium and in the range $\phi_m 1.5 - 2.8$ the increased trend of CO with ϕ_m of the equilibrium predictions was followed. The difficult results to explain were the reduction in CO in the ϕ_m range of 2.8 – 6.

Figure 5.5 shows the variation in the % CO with respect to time for all the air flow rates and ϕ_m . It shows that CO concentration becomes stable for some of the tests in the time period 300-500s. in some experiments it continues to rise beyond 500s in others. Figure 5.5 shows a large difference in CO concentration between ϕ_m of 2.8 and 3.3, it will be shown later that there was a large reduction in THC concentration in the same tests. This indicates a large reduction on combustion efficiency and an associated reduction in the flame temperature. What caused this is uncertain, but it could be associated with the reduced air flow for richer mixtures and the increased char formation (equilibrium carbon increases for rich mixtures $>\phi 3.5$ as shown in

Figure 4.10.

The difference in the adiabatic equilibrium CO and experimental CO shows that equilibrium was not achieved, due to heat losses that produced gasification condition well away from equilibrium. This resulted in high hydrocarbons, when there should be no hydrocarbons at equilibrium, apart from low levels of CH_4 for $\phi > 4$ as shown in

Figure 4.10.

These hydrocarbons represent a loss in the gasification efficiency, but would burn in the second stage and do not cause a loss in energy transfer to the gas.

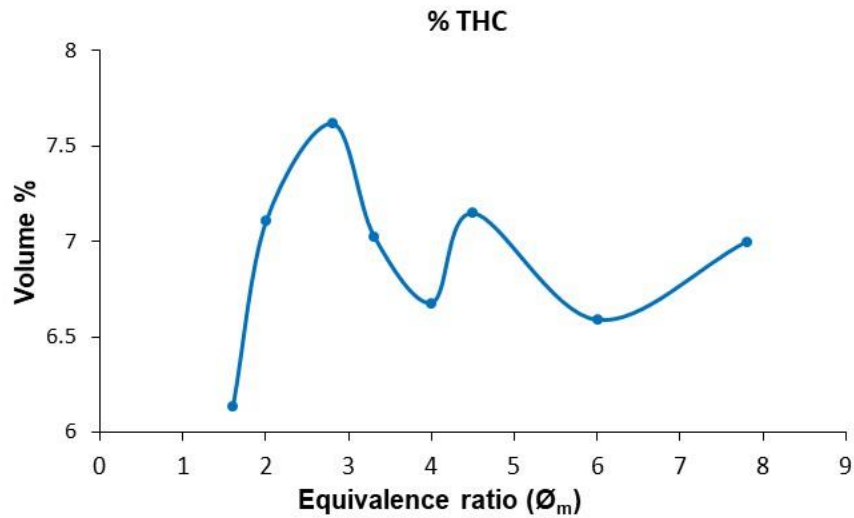


Figure 5.6 Variation of experimental % THC concentration with \varnothing_m

Figure 5.6 shows the average THC concentration as C1 equivalent, in the steady state part of the tests for different \varnothing_m . The variation in CO as a function of \varnothing_m was not very large. The trend of THC show that highest concentration was obtained at $\varnothing_m = 2.8$ and the lowest was at $\varnothing_m = 1.6$. There was a second peak in THC at $\varnothing_m = 4.5$. The shape of the trend of THC with \varnothing_m was similar to that for CO in Figure 5.4. This confirms that the regions of reduced CO and THC were regions of poor combustion efficiency, but the cause of this is not known. Average CO₂ concentration trend is shown in the Figure 5.7 as a function of \varnothing_m and the influence of \varnothing_m is very small. The \varnothing_m where CO is at a maximum concentration CO₂ is at a minimum. This is possibly due to the boudouard reaction R1, but the contribution of boudouard reaction towards CO production seems small. The higher CO₂ than equilibrium was unexpected, but is a result for rich mixtures of combustion inefficiency.

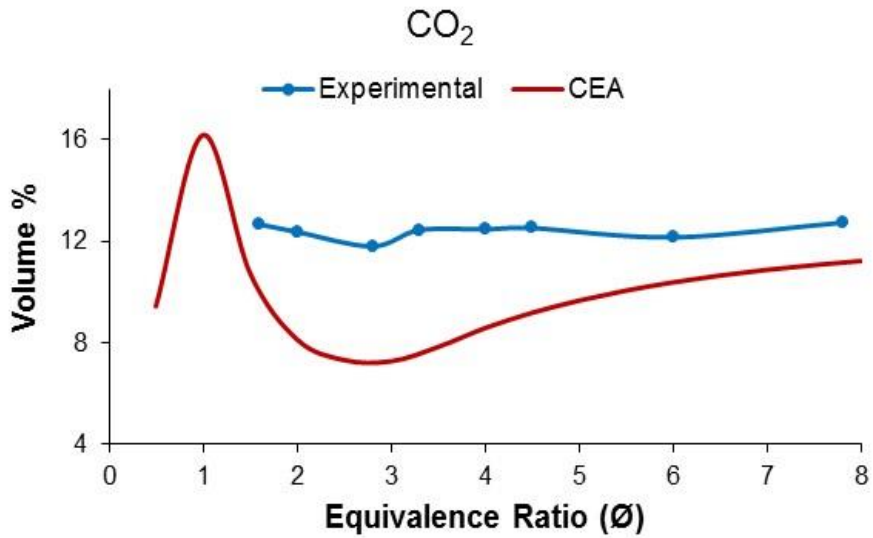


Figure 5.7 Variation of experimental and predicted (equilibrium) CO₂ concentration with \emptyset

CO and THC that is not burning effectively makes the gas composition leaner than the overall \emptyset for the wood combustion. These leaner mixtures have higher CO₂ than equilibrium.

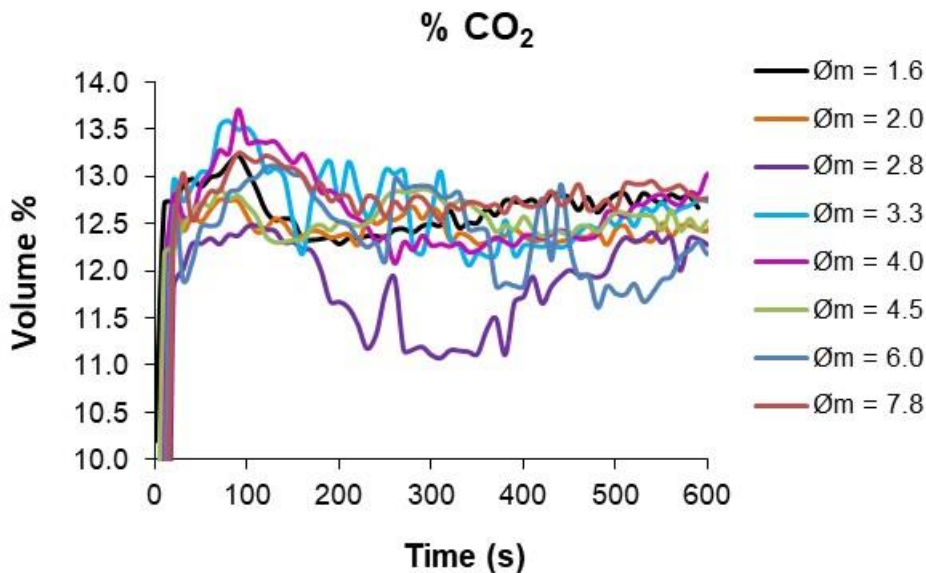


Figure 5.8 % CO₂ against time in different tests listed with steady state \emptyset_m

Figure 5.8 shows the CO₂ as a function of time for all the air flows. It shows 19.2 g_{air}/(m².s) at $\emptyset_m = 2.8$ gave the minimum CO₂, which is closer to equilibrium. The CO₂ trends were very similar for other air flows.

Figure 5.9 shows the average H₂O as a function of ϕ_m . The biomass used was not oven dried and the moisture by TGA was about 6% and the evaporation of this would contribute to the measured water vapour. However, the H₂O that was a product of rich combustion would be higher than equilibrium, as shown in Figure 5.9, for the same combustion efficiency reasons discussed for the high CO₂.

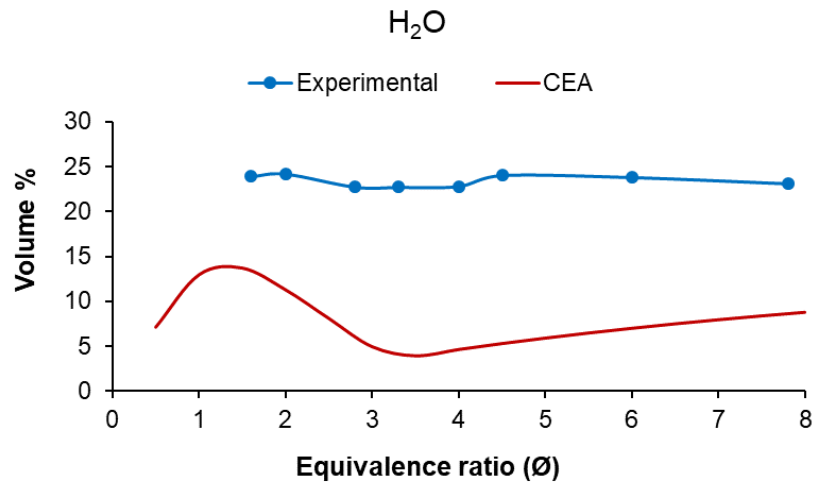


Figure 5.9 Variation of experimental and predicted (equilibrium) H₂O concentration with ϕ

Figure 5.10 shows the variation of water vapour with time for different air flows. Test at steady state value of $\phi_m = 2.8$ had the lowest water vapour emissions, for the same reason that the CO₂ was lowest. The H₂O trend in Figure 5.10 was different than the CO₂ trend in Figure 5.8. This was caused by the additional H₂O released early in the heating period from the evaporation of the water content of the wood.

As discussed in the section 4.3.4, H₂ was not measured and an equilibrium H₂ concentration was predicted from the measured CO using the water gas shift reaction R3. Comparison of the measured CO and the equilibrium CO above, shows that adiabatic equilibrium conditions were not achieved. Clearly the H₂ trends will follow those for CO and will be below equilibrium, as shown in Figure 5.11.

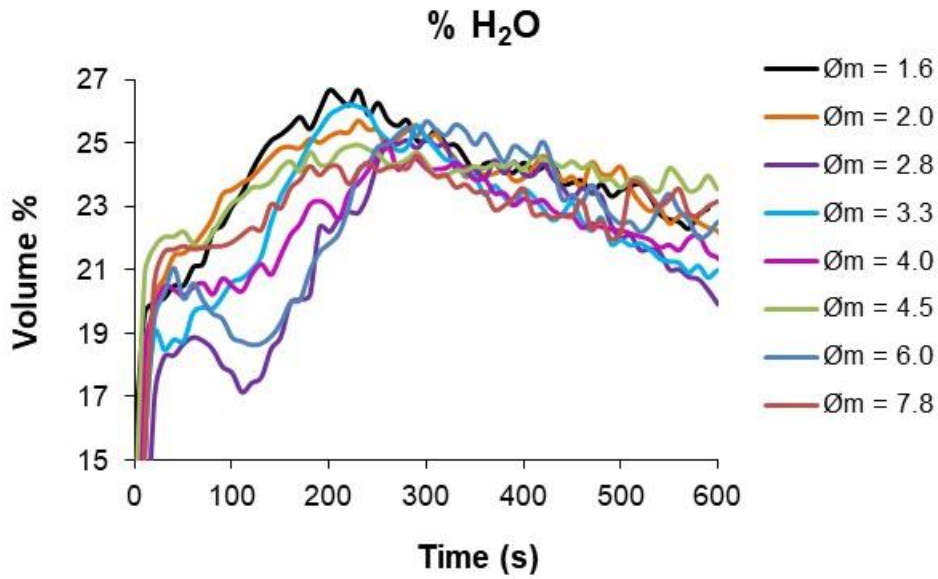


Figure 5.10 % H₂O variations with time in different tests listed with steady state \varnothing_m

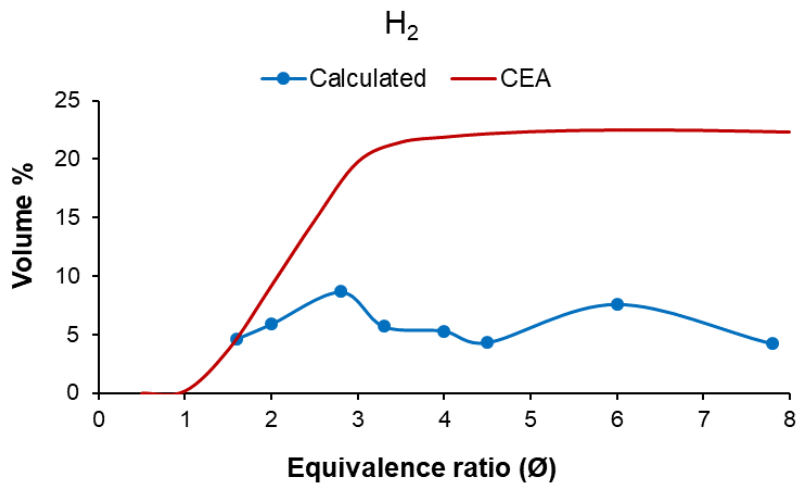


Figure 5.11 Variation of calculated and predicted (equilibrium) H₂ concentration with \varnothing

Reaction R2 (steam gasification of char) also produces CO and H₂. Reaction R5 (steam reforming of hydrocarbon) also results in the H₂ production. Without measured H₂ concentrations, the prediction of H₂ from CO may be unreliable.

shows the average CH₄ concentration over the range 0-600 s. From \varnothing_m 1.6 to 3.3 the methane concentration was higher than equilibrium, due to combustion inefficiency. The equilibrium concentration of CH₄ is very low for $\varnothing_m < 3$ as shown in

Figure 4.10. For $\phi_m > 3$ equilibrium methane was higher than the experimental results because of reactions producing CH_4 R4 (hydrogasification) and R6 (methanation) should start at these point as there is CO and H_2 and solid char C in the products to form Methane. The measured values below equilibrium were due to the poor combustion efficiency, as discussed above in relation to the measured CO being below equilibrium.

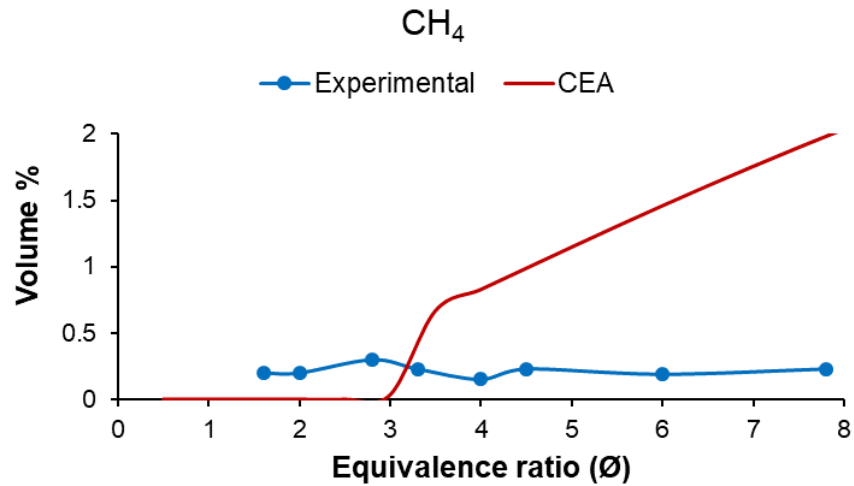


Figure 5.12 Variation of experimental and predicted (equilibrium) CH_4 concentration with ϕ

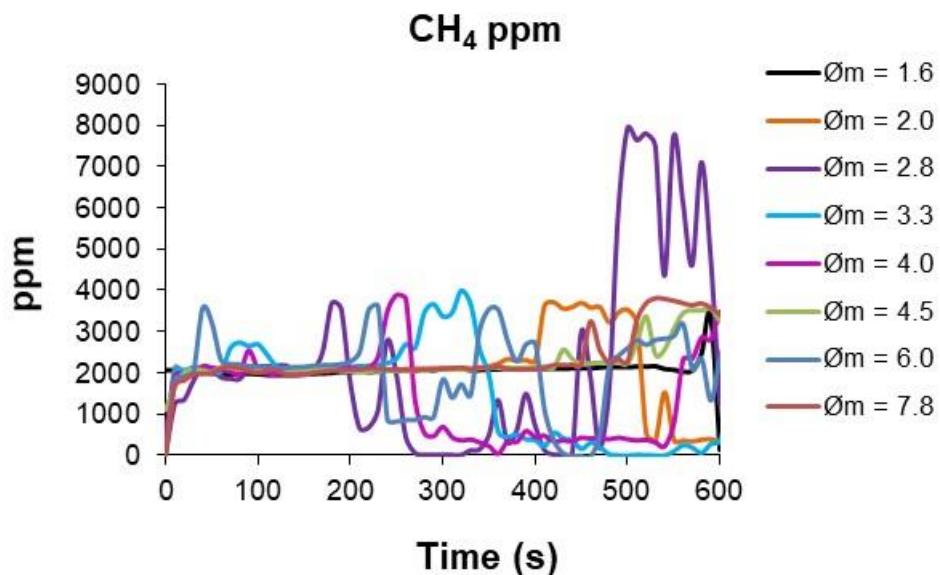


Figure 5.13 CH_4 concentration variation with time in different tests listed with steady state ϕ_m

Figure 5.13 shows the CH₄ variation with time for all the air flows. During the heating phase over the first 200s CH₄ was about 2000ppm for all air flows, with a much more complex dependence on air flow during the steady gasification period.

Figure 5.14 shows the temperature of the thermocouples inserted 3 mm from top and bottom surface of the middle wood stick in a test at the same conditions of test producing maximum % CO, at $\dot{O}_m = 2.8$, air flow 19.2 g/(m².s). With reference to the equilibrium predictions and the adiabatic flame temperature

Figure 4.10 shows that the equilibrium temperature at $\dot{O}_m = 2.8$ is 780 °C, compared with 670°C in Figure 5.14. The difference was due to the combustion inefficiency.

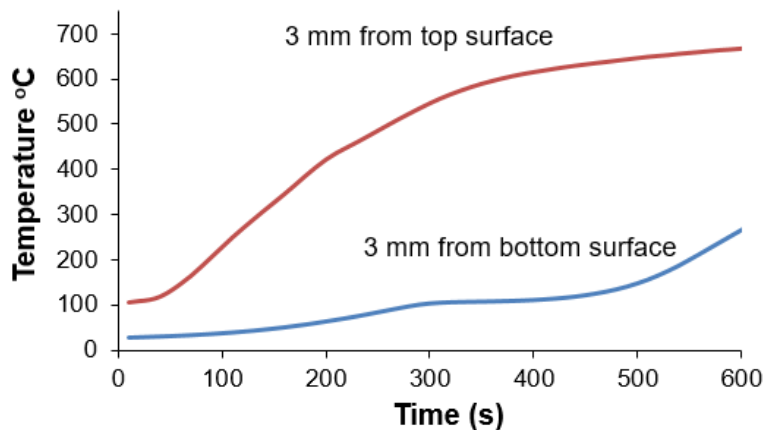


Figure 5.14 Temperature of the pine wood at two locations at air flow 19.2 g/(m².s), heat flux 70 kW/m²

Figure 5.14 shows that the fresh biomass bottom layer was at a very low temperature. For the steady state measurement period over 200 – 500s there was always unburnt and burnt wood present in the 20mm thickness, which is the reality in log boilers for most of the burn time. Gases evolved from the base of the wood as the heat conducts down to there has to pass through the upper char layer where it is heated.

Figure 5.15 shows the % O₂ on a dry basis from the O₂ analyser downstream of the FTIR. This shows that there was not much difference in the O₂ values over steady state period or the initial combustion development period, for all air flow

rates and \varnothing_m . It can be seen that control of the primary gasification zone to optimise the combustion cannot use O_2 . Yields (emission index g specie /g biomass) of the gaseous products are shown in Figure 5.16. The yields are calculated by the calculations of emission index discussed in the section 3.6.

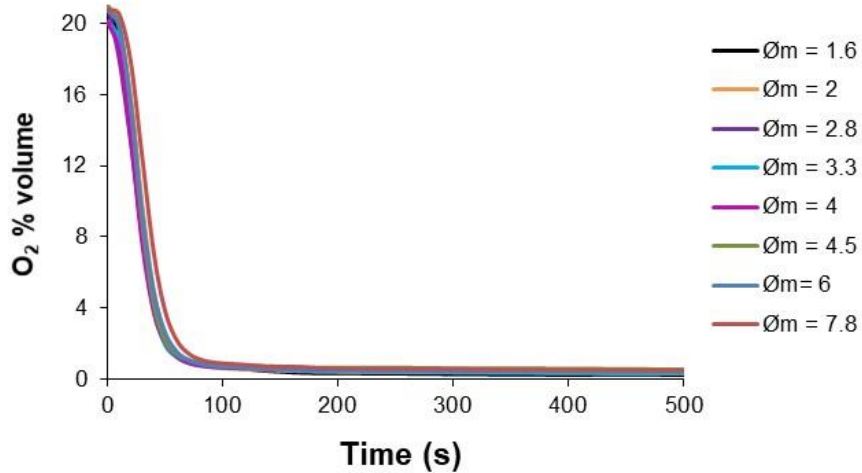


Figure 5.15 % O_2 (dry basis) from the gasification zone at different equivalence ratios for pine wood

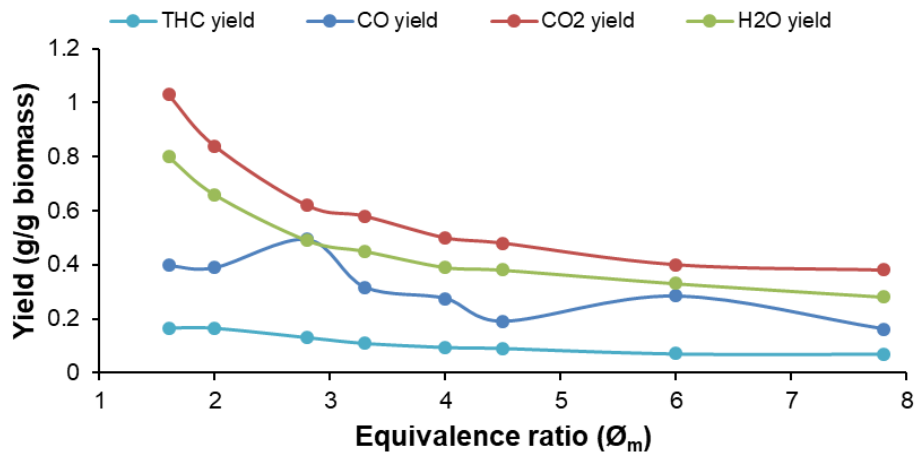


Figure 5.16 Variation in the yields (EI) of gaseous products as a function of \varnothing_m

As yields (emission index) are function of air to fuel ratio, yields of all gases appear to show a decreasing trend with increase in \varnothing_m as the air flow rate decreases. However, the yield of CO is a maximum at $\varnothing_m = 2.8$ with a value of 0.5 g/g of biomass and then decreases again with decreasing \varnothing_m , but the overall trend is an increase in CO with decreasing \varnothing_m . Figure 5.17 (a, b,& c) shows the

emissions of hydrocarbon species at $\varnothing_m = 2.8$. The acetylene and ethylene concentrations are fairly constant over the range of air flows, while trimethylbenzene (sum of 1,2,3; 1,2,4; and 1,3,5 trimethylbenzene), and xylene (sum of o, m, and p xylene), and naphthalene diminish to very low values over 200 – 450 seconds as shown in Figure 5.17 (b).

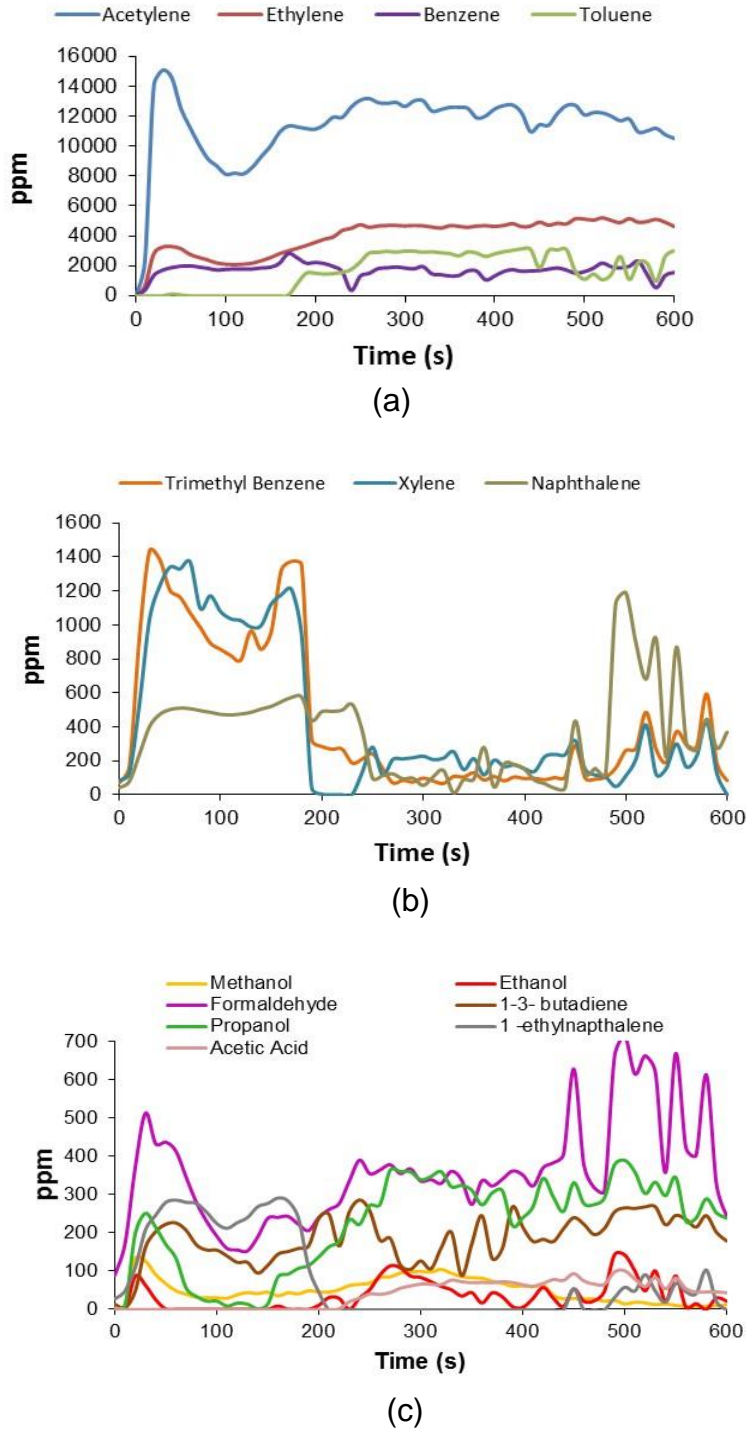


Figure 5.17 Hydrocarbon species emitted at $\varnothing_m = 2.8$

It is during the start-up phase when the boiler temperature is still low that the emissions for trimethyl benzene, xylene and naphthalene are quite high. This reinforces the need for installing an external burner i.e. natural gas burner to lower these emissions. The high proportion of these pyrolysis gases is due to the incomplete cracking. These gases reduce with increase in temperature indicating improved cracking. Toluene starts to form at 400 s showing that cracking of above gases might produce toluene. Concentrations of propanol and acetic acid also increase with increasing temperature. Benzene also reduces in concentration with rise in temperature.

5.2 Effect of equivalence ratio on HGE

As the gases and heat from the rich burning gasification zone passes to the secondary combustion zone in a two stage boiler. Air is added through a flame stabiliser to burn the gases from the primary rich burning zone. This secondary combustion will burn completely all these gases. Thus if the enthalpy of the gases is calculated from the composition and the CV of each individual gas and the sensible heat in the temperature of the gases in the chimney is added, then the efficiency of the gasification (HGE – hot gasification efficiency) can be determined as discussed in the section 3.7. This is shown in Figure 5.18 as a function of ϕ_m

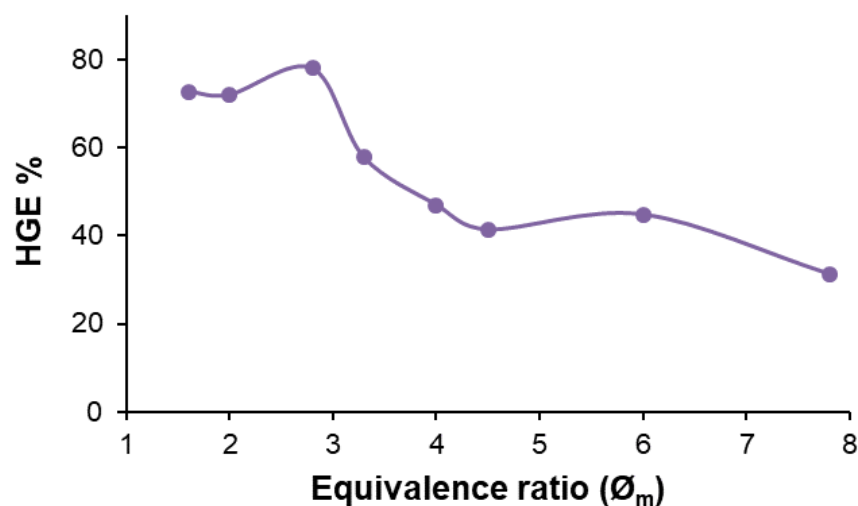


Figure 5.18 HGE as a function of ϕ_m

The average maximum high heating value was 13.12 MJ/kg at $\varnothing_m = 2.8$. However, the thermal efficiency was high for \varnothing_m 1.5 – 2.8. Figure 5.18 was based on the steady state from 300 to 500s. It can be seen that the efficiency for the gasification stage was less than that from the commercial log boilers that claim an efficiency of 90-93%. This was due to the biomass was not burnt to completion and the char burning stage of the biomass gives higher heat release due to the high CV of carbon compared with CO. The UK requirement for domestic water heating boilers is a minimum 86% thermal efficiency [142] . The 80% thermal efficiency in Figure 5.18 is close to this value and with the char combustion heat release would exceed the required thermal efficiency.

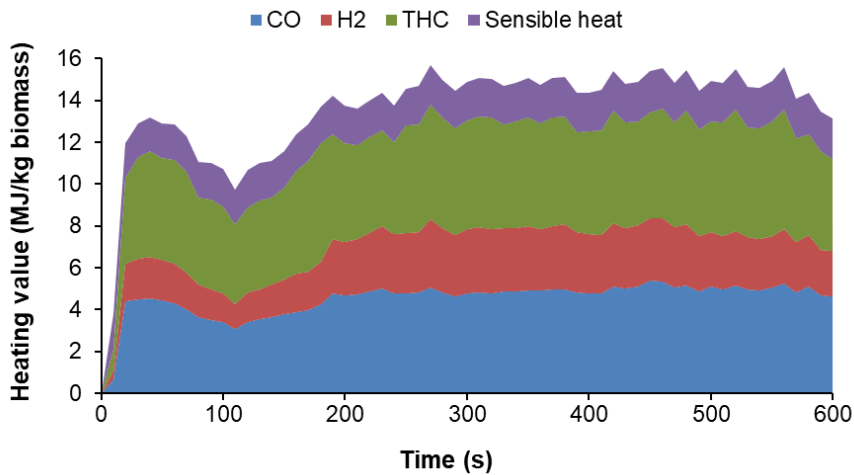


Figure 5.19 Heating value as function of time for air flow $19.2 \text{ g}/(\text{m}^2 \cdot \text{s})$, $\varnothing_m = 2.8$

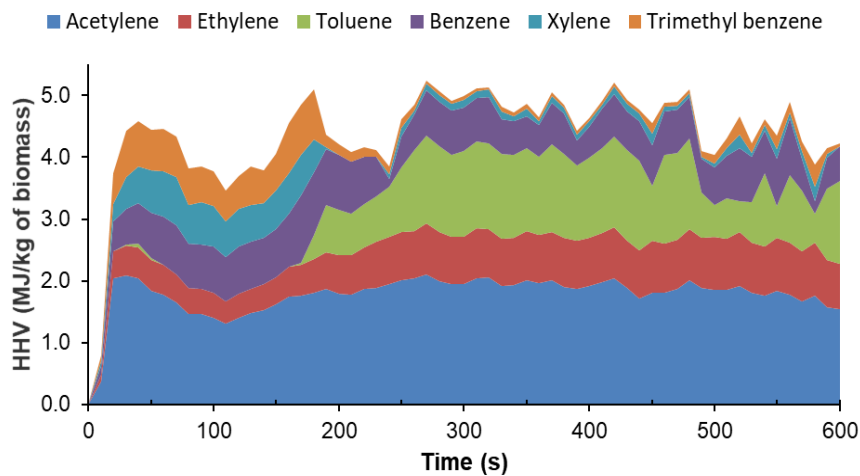


Figure 5.20 Heating value proportion of hydrocarbon gases

Figure 5.19 shows the contribution of CO, H₂, hydrocarbons and sensible heat to the higher heating value of the products of combustion. The peak energy gives a thermal efficiency of 80%. The total hydrocarbons account for over 35% of the heating value of the gas as shown in Figure 5.20.

The major components of the hydrocarbon gases from an energy content viewpoint were acetylene, ethylene, toluene, xylene, benzene, naphthalene and trimethyl benzene. These would all burn efficiently in the secondary combustion zone and so the thermal efficiency can be determined by the proportion of the energy in the gases in the chimney from the rich burn gasification stage to the energy in the raw biomass.

Table 5.2 Ultimate and proximate analysis of biomass gasification char samples

Parameter	Pine char (top layer)	Sycamore wood char	Corn cobs char
Ultimate analysis (wt.%(daf)			
Carbon	97.08	92.05	83.29
Hydrogen	2.46	1.88	2.21
Nitrogen	0.10	0.54	0.60
Sulfur	0.00	0.00	0.00
Oxygen	0.35	5.52	13.89
Proximate analysis (wt.%) (daf)			
Volatile matter	12.31	12.49	9.09
Fixed carbon	87.69	87.51	90.91
Moisture (% ar)	4.15	2.42	4.19
Ash (%ar)	6.87	6.65	12.83
Stoichiometric (A/F) dry basis	12.00	11.05	9.8
Stoichiometric (A/F) wet basis	10.68	10.04	8.2
GCV (MJ/kg) Correlation	33.97	30.57	25.9

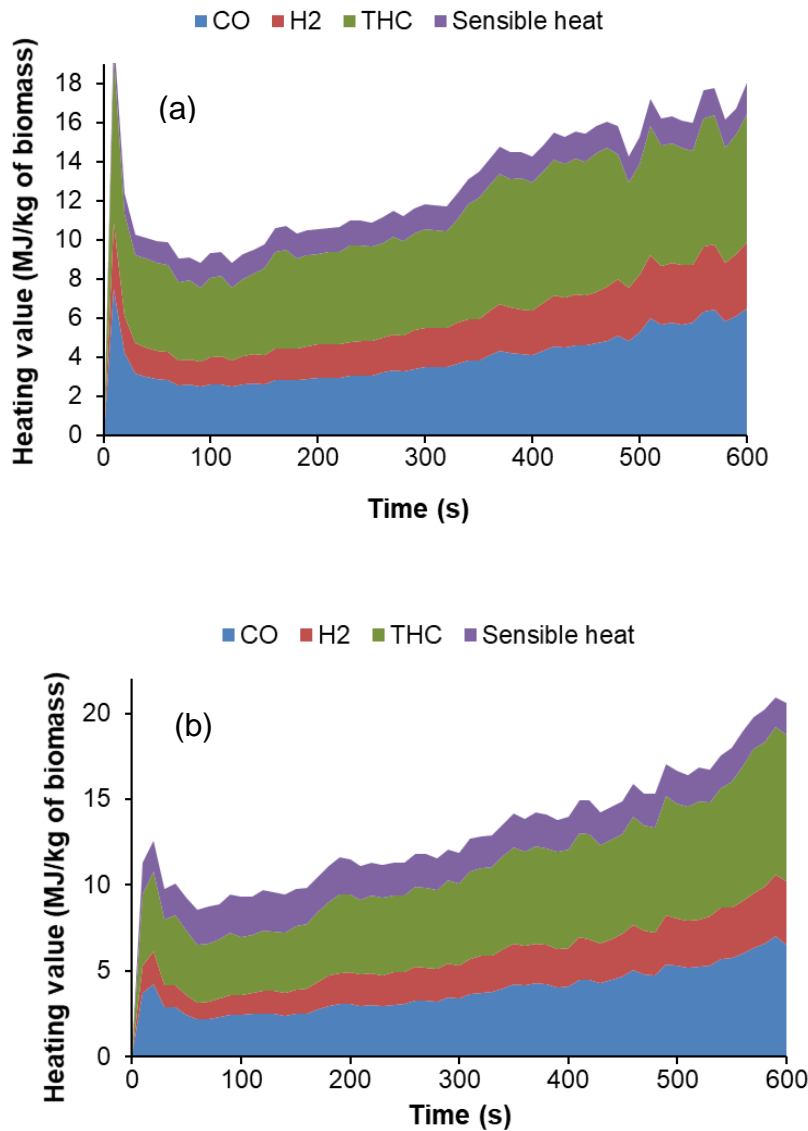


Figure 5.21 Heating value as function of time (a) air flow 25.6 g/(m².s), $\varnothing_m = 2$
(b) air flow 31.6 g/(m².s), $\varnothing_m = 1.6$

Figure 5.21 shows the heating value of the product gases as a function of time for tests at higher flow rates of air 25.6 and 31.6 g/(m².s). From 500s onward very high values of HHV were obtained as most of the biomass was burned to the char phase. The peak HGE was 95% and close to 100% and is comparable with the HGE of the best log boilers.

Figure 5.22 shows the comparison of average values of metered and carbon balance equivalence ratios in steady state phase as a function of the flow rate of air. The difference was small at high air flows, but was large at low air flows. This was due to imperfect mixing in the flue and to the gas sample not being representative of the mean – even using 20 sample holes.

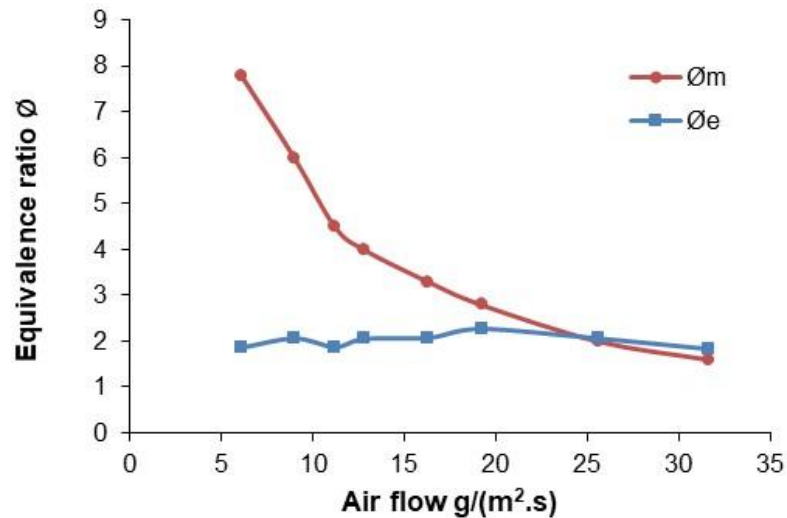


Figure 5.22 Comparison of metered equivalence ratio Φ_m with emission based equivalence ratio Φ_e for pine wood tests
For processed pellets, white wood pellets, grade B torrefied pellets and sunflower shell pellets HGE of the gasification in the first 200 s was calculated as the mass loss of the pellets occurred during this period. HGE of white wood pellets was 80%, grade B torrefied wood pellets was 81% and for sunflower shell pellets was less than 70%. If the higher emission index were obtained by having less rich combustion, this efficiency could have raised much higher.

Table 5.2 shows the TGA analysis and HHV of the top layer of pine char in a test at 19.2 $g/(m^2.s)$ and it can be seen that the top char layer has high stoichiometric (A/F) in comparison with raw pine wood. It also has a higher CV and thus its combustion in the gasification zone will improve the thermal efficiency of the process.

5.3 Effect of biomass moisture content

Biomass moisture content is one of the main causes of variability in the performance of gasifiers. According to McKendry [97], any biomass with moisture content above 30% has serious effect on the ignition and subsequently the composition and calorific value of the gas.

Two samples of ash wood were investigated, with different moisture content, at 70 kW/m² heat flux. In the previous section, optimum conditions for pine wood tests were found to be the air flow rate of 19.2 (g/m².s). Tests with different biomass were run at this air flow to make a comparison.

moisture content of the two woods is listed in the Table 4.1. Dry ash wood had 5.1 % moisture and wet wood had 9.6% moisture. A moderately low CO₂ concentration for high moisture content ash wood indicates leaner combustion, as wood with 90.9% dry content has effectively a leaner mixture. Even though the high moisture content lowers the flame temperature, a flue gas temperature of 416 °C and 390 °C was recorded for wet and dry ash wood respectively. The hotter temperature with the wet wood was due to the leaner mixture that burnt hotter.

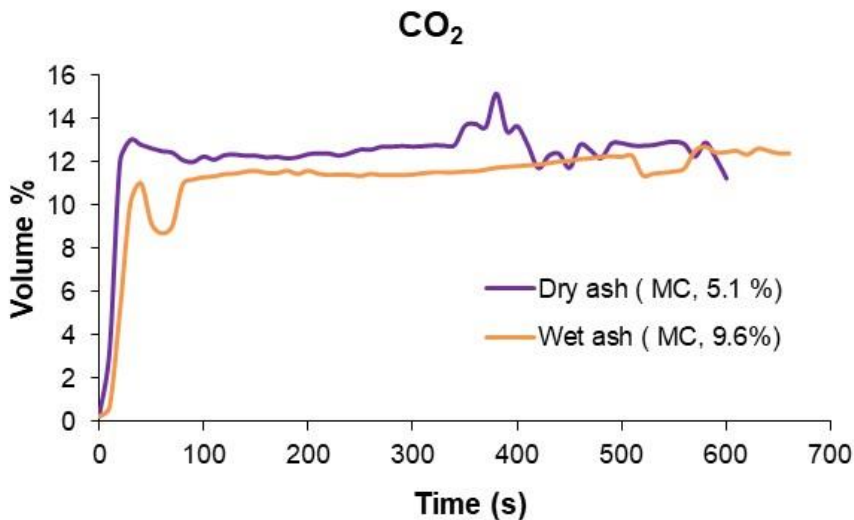


Figure 5.23 CO₂ concentration as a function of time for ash wood at different moisture content

Even though the high moisture content lowers the flame temperature, a flue gas temperature of 416 °C and 390 °C was recorded for wet and dry ash wood respectively. This is contrary to common-sense expectation but can be pegged

to high latent heat of water vapor and reduced endothermic gasification reactions rates in the case of wet biomass.

Figure 5.24 illustrates that for the dry ash wood the CO concentration generally rises to a maximum of about of 13 % between the steady state of 300-450 seconds, before gradually decreasing due to the reduced mass loss rate as the biomass approaches burnout stage. In the case of wet ash wood, the CO concentration in the flue gas was consistently low over a long time, before steeply rising from 500-600 seconds reaching a maximum value of 12%. The leaner mixture with higher temperatures would produce lower CO. The Boudouard reaction R1 which results in CO formation is favoured by high temperature due to its endothermic nature. As moisture content lowers the flame temperature Lahijani and Zainal, [143] there is a reduced rate of Boudouard reaction R1, leading to a reduced CO concentration. The peak CO observed after 500 seconds was attributed to a reduced moisture content in the biomass or completion of the drying phase.

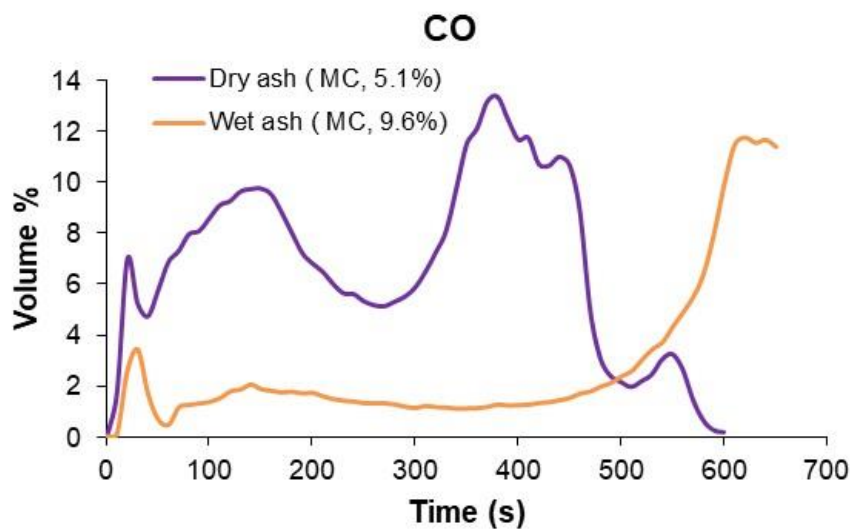


Figure 5.24 CO concentration as a function of time for ash wood at different moisture content

The trend in hydrogen production is as shown in Figure 5.25. This trend is similar to that for CO. The high moisture content reduces the temperature of the flame which has a net effect of slowing down the endothermic water gas shift reaction process. Steam gasification of carbon reaction's equilibrium constant becomes

greater than 1 at 700 °C, and only the top layer of the wood reaches this temperature, so the contribution to H₂ production might be negligible.

In the systems using steam for gasification, steam is usually injected at higher temperatures above 400 °C [74, 144] which makes it more reactive than the moisture liberated from the biomass at low temperature. The heating of the moisture content of the biomass simply vaporizes.

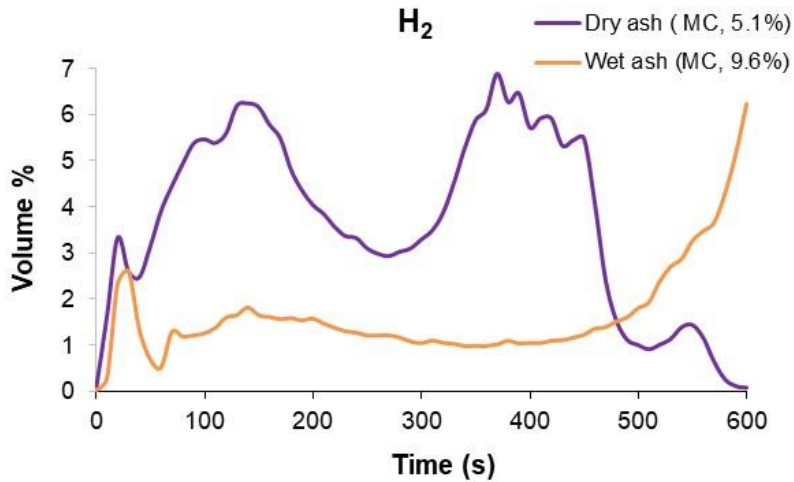


Figure 5.25 H₂ concentration (calculated) as a function of time for ash wood at different moisture content

Another path for the production of hydrogen is the thermal cracking of the hydrocarbons or tars which is only feasible at higher temperatures unlike in the gasification of wet biomass, where there is a significant reduction in temperature. The sharp increase in hydrogen concentration to 7% after 500 seconds is accompanied by the decrease in moisture content as shown in Figure 5.25.

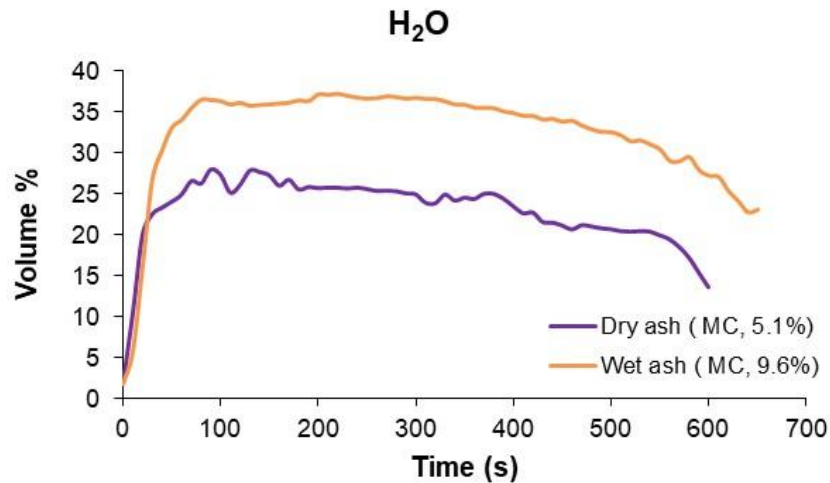


Figure 5.26 H₂O concentration as a function of time for ash wood at different moisture content

Figure 5.26 shows the water content of the gases from the rich burning gasification zone. The wetter wood has the expected higher steam production. The near constant water vapour concentration for both the dry and wet biomass samples indicates the inactivity of the water gas reaction in general in the modified cone calorimeter gasification experimental set up. With the availability of considerable water vapour and char, this inactivity could be due to low temperature and shorter residence time.

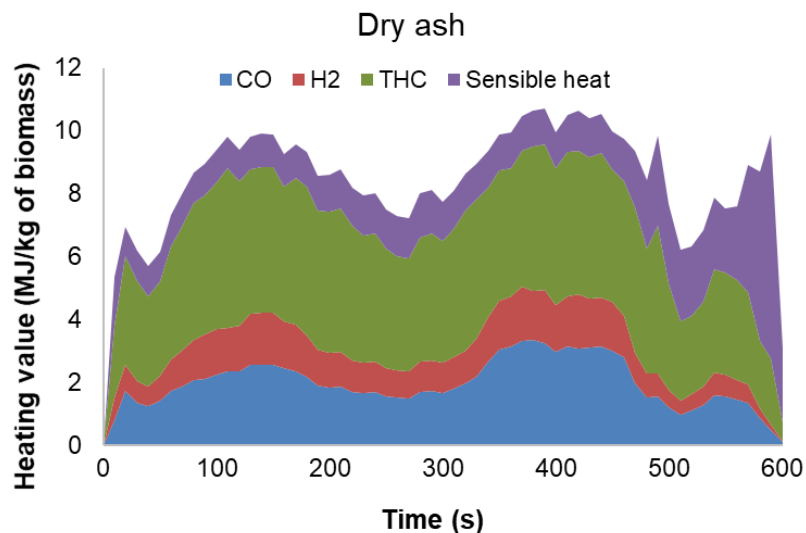


Figure 5.27 Heating value as a function of time for dry ash

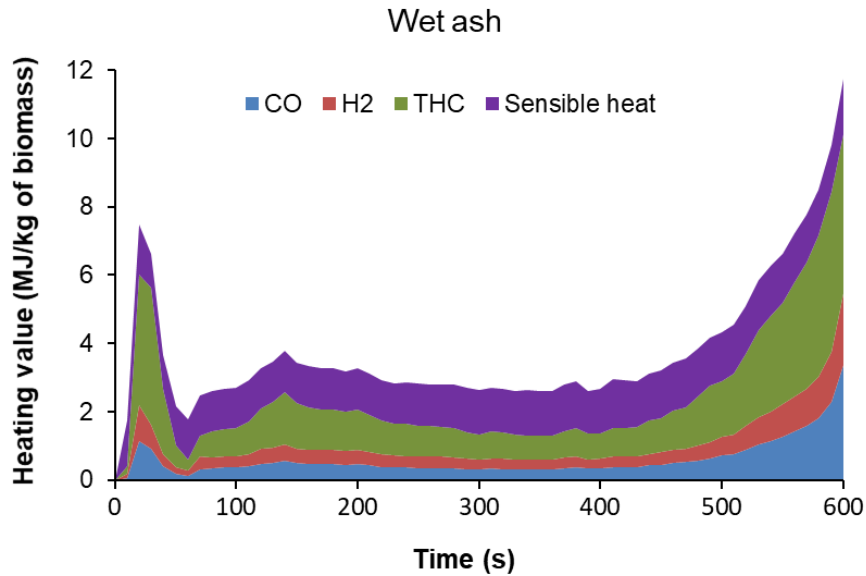


Figure 5.28 Heating value as a function of time wet ash

Figure 5.27 and Figure 5.28 shows a variation of the heating value of the gas from the gasification zone for dry and wet ash wood respectively. With the chemical characterization almost similar except for the moisture content, the HHV for wet biomass is consistently below the 4 MJ/kg. This is almost 70% less compared to the dry biomass output. The reduction in HHV is due to the low volume concentration of the combustible gases from the gasification zone as shown earlier for CO and H₂. Once moisture is evaporated, HHV rises to 11 MJ/kg towards the end of the test time.

5.4 Influence of different biomass materials on gasification

The conditions chosen for the tests of different biomass were air flow rate 19.2 (g/m².s) and heat flux 70 kW/m². The aim was to show that different biomass produce different equivalence ratio for the same air flow rate. CHNS and TGA analysis of these biomass is listed in Table 4.1. Proportions of hemicellulose, cellulose and lignin calculated using a relation from the literature, particle size, initial biomass weight in the test section and densities of biomass are reported in the Table 4.2. Some particle sizes were comparable like block wood, eucalyptus and acacia were 20x20x100 mm blocks and 20 mm insulation was placed underneath. For corn cobs 15 mm and for china's biomass 10 mm

insulation was placed underneath. Except for these three biomass, all tests were done with 20mm thick insulation underneath the biomass sample.

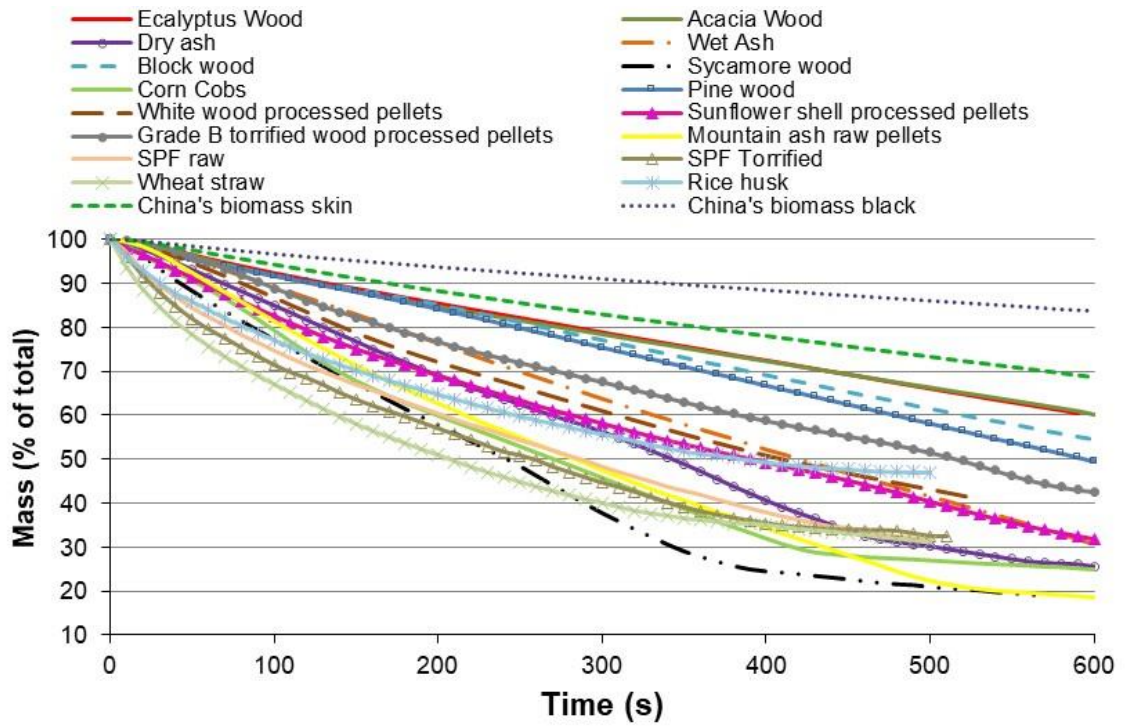


Figure 5.29 mass vs time for different biomass at air flow $19.2 \text{ g}/(\text{m}^2.\text{s})$, heat flux $70 \text{ kW}/\text{m}^2$

Figure 5.29 shows the mass (% of Total) vs time for different biomass studied burning rich inside cone calorimeter under same air flow rate.. Figure 5.29 shows the burning characteristics of different biomass are very different.

It can be seen that 30% of the original mass loss for the pine wood happened at tests time 360 s, for eucalyptus and acacia woods at 430 s. while in case of sunflower pellets same mass loss happened in 190 s, for white wood pellets, in 210s, for grade B torrefied wood pellets it happened in 270 s. Wet ash and dry ash wood 30 % of original mass loss happened in same time range as for pellets. For sycamore wood, and corn cobs it was even quick than pallets.

For biomass in very small particle size, like SPF raw, SPF torrefied, Wheat straw and rice husk burning of biomass happened in first 100 to 150 s and there was no flame after that time. It was observed for the powders like SPF raw and

torrified, that the top surface of the powder was actually fused and formed a layer that stopped volatiles to come out at higher rate, or in other words rate of heat transfer inside the biomass layer decreased and mass transfer from inside of the biomass decreased. When the char was taken out after 500 s test time for powders, and top layer was removed some unburnt material of light brown colour was seen at the bottom side of the bed.

For china's biomass pellets, it took almost 580 s to get 30% mass loss for skin colour pellets while black pellets did not lose 20% of the initial weight until 600 s. although the mass loss rate was not very low but this was due to the fact that initial mass was very high for these biomass as listed in the Table 4.2.

Figure 5.30 shows the mass loss rate (g/s) vs time for different biomass and it can be seen that all pellets and corn cobs show wide variation of mass loss rate over time, while for woods variations in mass loss over time are smaller, some wood and biomass were flamed out during the test time and these include sycamore wood, corn cobs, dry ash and mountain ash pellets all showing a rapid change in mass loss rate once flamed out. Grade B torrified wood pellets were about to be flamed out at the end of the test. Some other biomass of very small particle size including SPF raw, SPF torrified, Wheat straw and rice husk were also flamed out initially as discussed before and their mass loss rate decreases gradually over test time to about zero. It can be seen that for china's biomass skin pellets, mass loss rate was even higher than woods and for china's biomass black, mass loss rate was lower than that for woods.

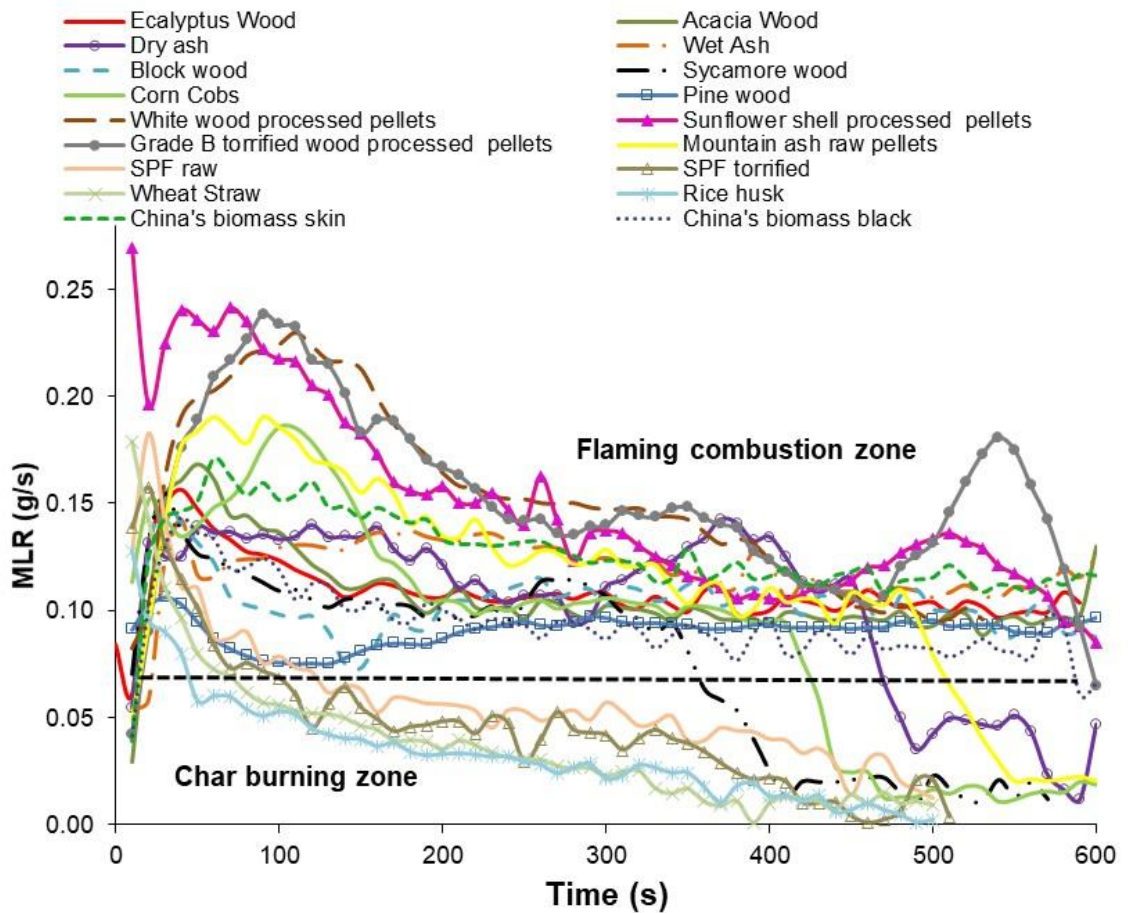


Figure 5.30 MLR (g/s) vs time for different biomass at $19.2 \text{ g}/(\text{m}^2 \cdot \text{s})$, heat flux $70 \text{ kW}/\text{m}^2$

Metered equivalence ratios (ϕ_m) produced as a result of different biomass burning is shown in the Figure 5.31. It is clear that pellets were burning fast in the first 200 s, In spite of the fact that we did not considered this time as steady state in the last section but for biomass with small particle size most of the biomass is burning in this time producing very rich conditions initially. For pine wood ϕ_m is about 2 in this time zone and for pellets ϕ_m is about 5-7. During this time fine biomass samples including SPF raw, SPF torrefied, wheat straw and rice husk were fully burnt to flameout. From 200s to 400s, ϕ_m for most of the biomass is from 2.8 to 5. Comparison after 400 s is not very good as most the pellets have lost considerable mass. This variation in the ϕ_m shows that different biomass behave differently in the log boilers depending on many factors like density, particle size etc. Although it was seen before that eucalyptus wood and sunflower shell pellets are chemical similar e.g. having same Volatile matter, O/C

ratios and H/C ratio as seen in the Figure 4.9, but burning characteristics are different inside the test section.

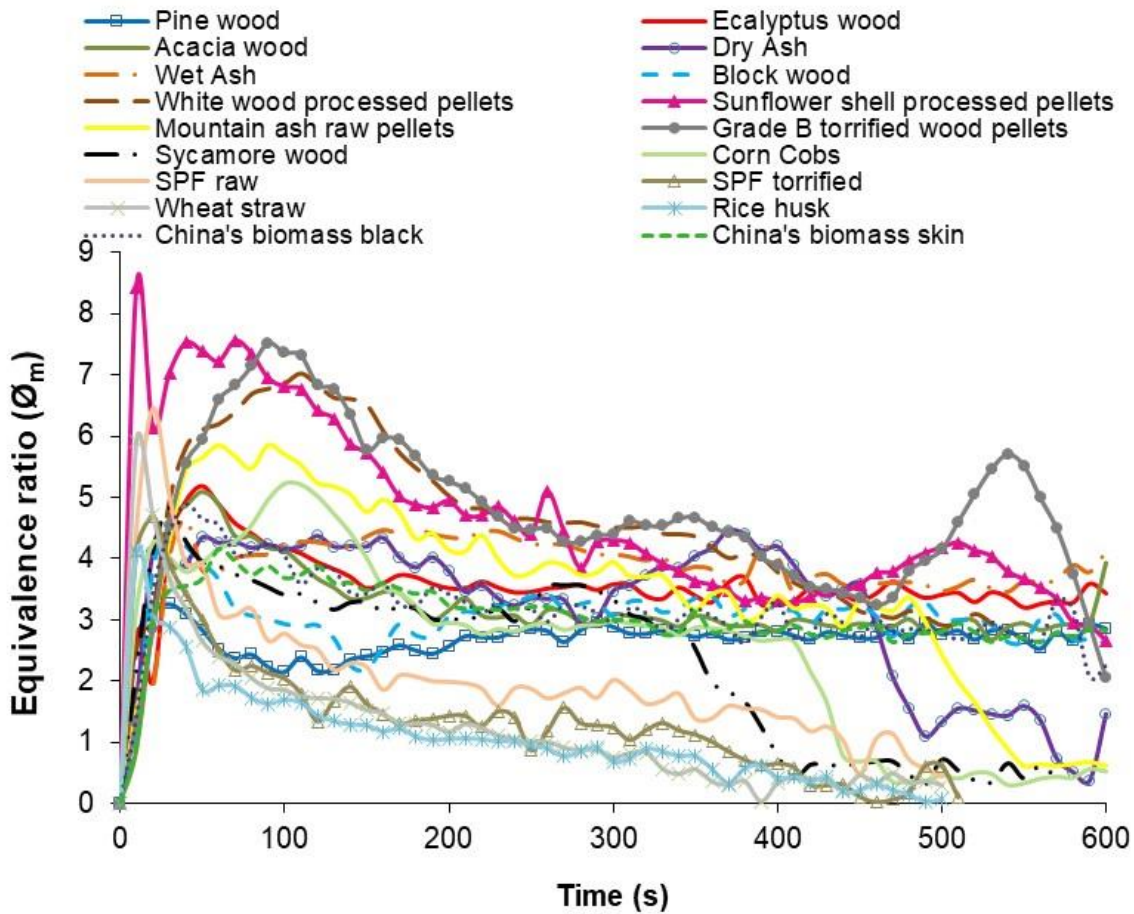


Figure 5.31 Metered equivalence ratio (\varnothing_m)

Biomass with small particle size burnt more quickly as compared with large particle size. Careful control of the primary air is required in the log boilers to achieve high efficiency as same flow rate would cause different conditions of \varnothing_m inside the gasification zone causing reduction in the efficiency if biomass is burning too rich or too lean. Even size length and thickness of logs would matter, if wood sticks are used they would cause different burning conditions compared to big logs of wood.

Figure 5.32 shows the % CO emissions for different biomass and it shows wide variations in the % CO for some biomass species. As it can be seen that pellets produce very high CO initially because the mass loss rate was very high initially causing high emissions in first 200 s. for all wood, CO rises to a peak due to initial high volatilization and then decreases after some time to a steady value

depending upon the rate of burning. Variation in % CO is due to many factors like size of the particles and the composition of the biomass in terms of cellulose, hemicellulose and lignin producing variable % CO. For very small particle samples including SPF raw, SPF torrefied, rice husk and wheat straw, CO diminished to zero during first 100 s because the density of biomass was very low and the initial mass in the same sample holder was very small and due to very small particle size it burnt to completion, also in case of SPF raw and torrefied, top burnt layer of the wood offered formed a rigid layer and acted as an insulation that reduced heat transfer inside the layer of the particles for further burning, even after 500 s burning some wood was seen unburnt when sample was removed from the cone calorimeter and cooled.

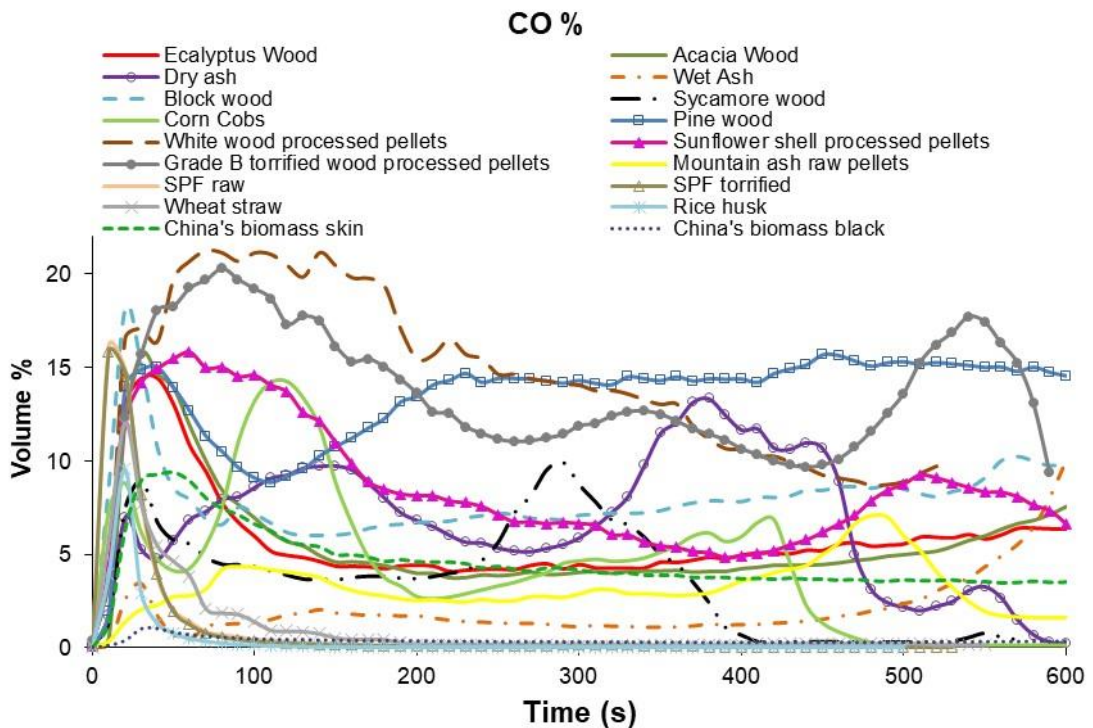


Figure 5.32 % CO for tests with different biomass at air flow 19.2 (g/m².s)

In order to understand the effect of composition on the % CO emissions, biomass % CO was plotted with subgroups having same particle size range as shown in the Figure 5.33. 5 wood sticks in Figure 5.33 (a) shows wide variation in CO

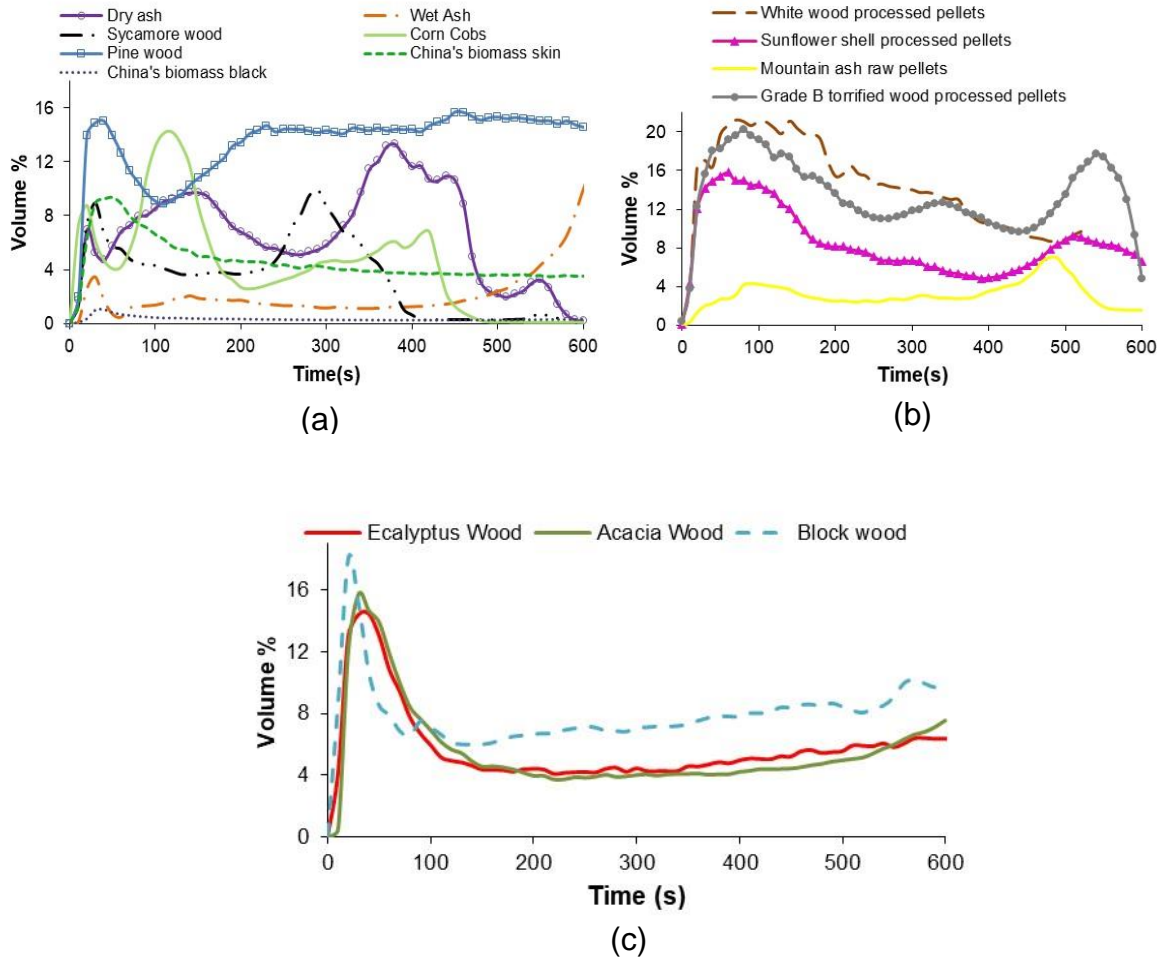


Figure 5.33 % CO for tests with different biomass (a) for 5 biomass wood sticks, corn cons and china’s biomass (B) biomass pellets (c) wood blocks

release, according to the literature [9, 74] high cellulose produces high CO during the pyrolysis of wood. Cellulose contents of sycamore wood is less than that of pine and ash wood ash shown in the Table 4.2. At the same time density is playing an important role, density of sycamore wood is very low. Density of pine wood is less as compared to ash wood, cellulose contents for these woods are comparable, but % CO shows large variations. In case of wood sticks used in the tests, outer bark was present on the sticks that possibly give less CO emissions, as in the bark hemicellulose and cellulose contents are significantly less than that in the stem wood. Wood bark is usually higher in lignin and ash contents. An important observation is the TGA analysis of pine wood that shows that it has highest yield of volatiles on as received and dry ash free basis among all biomass studied and cracking and reforming of some of the volatiles might have released more CO.

Figure 5.33 (b) shows the CO emissions from the pellets, mountain ash pellets had high moisture contents and resulted in less CO as compared with other pellets. Figure 5.33 (c) shows that block wood had higher CO emissions than other eucalyptus and acacia wood and the main difference between wood is the density. It can also be seen from the TGA analysis that block wood has higher volatiles as compared with eucalyptus and acacia wood but less than that from pine wood.

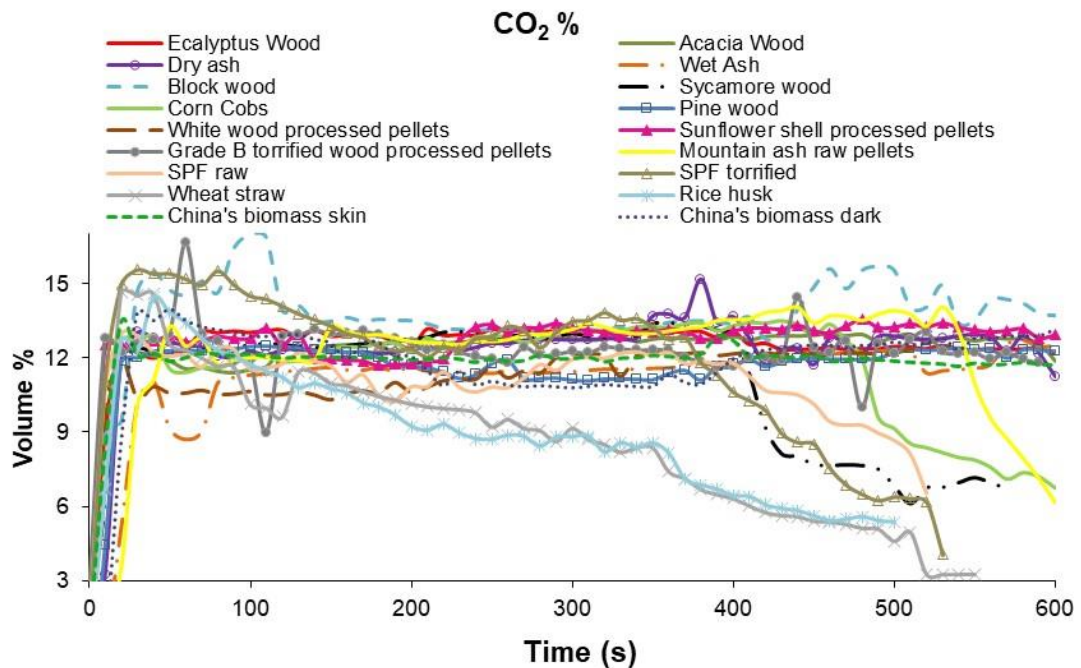


Figure 5.34 % CO₂ for tests with different biomass at air flow 19.2 (g/m².s)

Figure 5.34 shows the CO₂ emissions from the biomass species and it shows variations from 10.5 to 13% for most of the biomass species. For biomass species of small particle size including wheat straw and rice husk CO₂ started falling after 100 s due to the flame out of the biomass. In case of SPF raw and torrefied the flame out happened in 150 s but the CO₂ fell around 400 s might be due to smouldering combustion. Lowest CO₂ was observed for the white wood pellets during first 200 s showing that rich combustion was observed and there is a possibility that pellets got heated very quickly as compared with the other woods and high rates of heat transfer caused boudouard reaction to proceed towards CO formation.

Figure 5.35 show the % H₂O released from the gasification of the biomass species. Wet ash and mountain ash pellets had the highest moisture contents and show higher H₂O emissions. For mountain ash pellets H₂O decreased gradually as mass loss decreased.

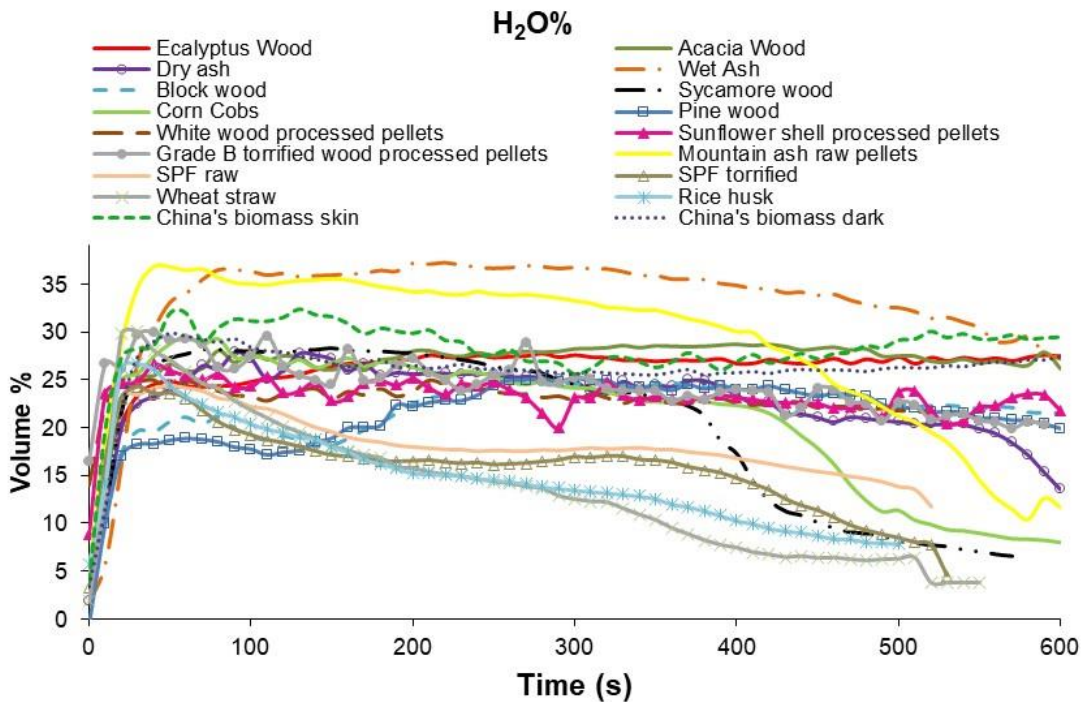


Figure 5.35 % H₂O for tests with different biomass at air flow 19.2 (g/m².s)

Eucalyptus wood, acacia wood, china's biomass skin and china's biomass black were still burning at continuous rate and H₂O contents were releasing continuously, for other pine, sunflower pellets, grade B torrifed pellets and block wood H₂O contents were decreasing slowly as biomass were gradually dried up and combustion was moving towards end. For the sycamore wood, corn cobs, mountain ash pellets and dry ash, SPF raw, SPF torrifed, wheat straw and rice husk H₂O reduced towards lower values after flame out.

H₂ calculated by water gas shift equilibrium is shown in the Figure 5.36. as H₂O contents of the biomass species is high, H₂ is expected to be low in reality than shown by the calculations of water gas shift reaction equilibrium. But for the biomass pellets high temperature might be achievable for tars cracking and more H₂ production. But source (cone heater) temperature 862 °C was a limit to a maximum achievable temperature. But it can be seen in the Figure 5.35 that H₂O

contents for the white wood pellets were lower as compared with the range of other biomass having high mass loss rate in the first 200s.

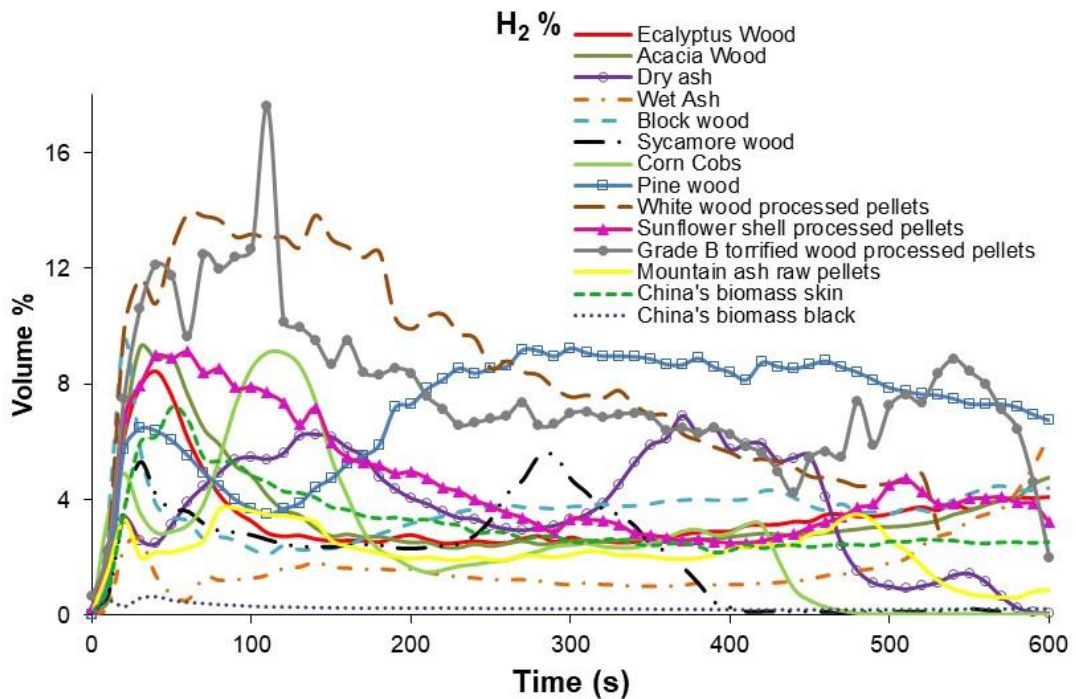


Figure 5.36 % H₂ for tests with different biomass at air flow 19.2 (g/m².s)

Figure 5.37 illustrates THC equivalent of CH₄ evolved and it can be seen that for the pellets THC emissions were even higher than the % CO released, while for the other biomasses % THC was less than or close to the % CO emissions of the biomass.

High hydrocarbons contents and tars results at low temperature gasification of the biomass, also in the updraft gasification tar contents are higher as compared to other configurations [145] Tars contents could be decreased at higher operating temperatures, but in the case of testing in cone calorimeter, load cell heating limited the testing on higher heat flux of 80-100 kW/m². It has been discussed before that in log boilers these tar contents account for higher heating value in the secondary combustion stage and it is recommended to reduce the residence time of the gases in the secondary combustion zone for the complete burning.

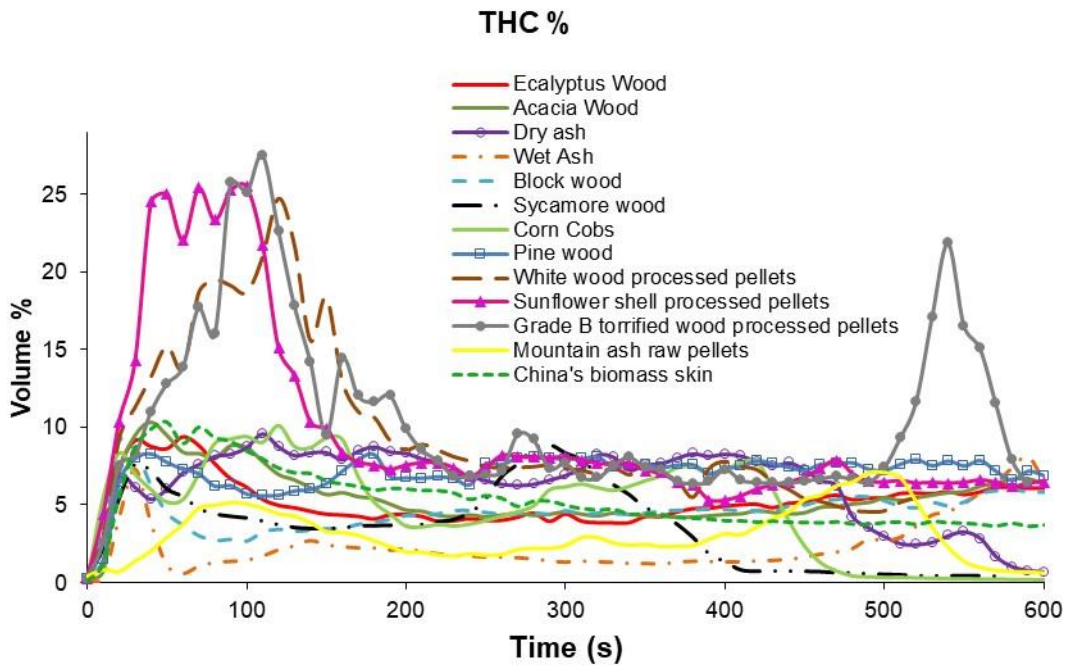


Figure 5.37 % THC for tests with different biomass at air flow 19.2 (g/m².s)

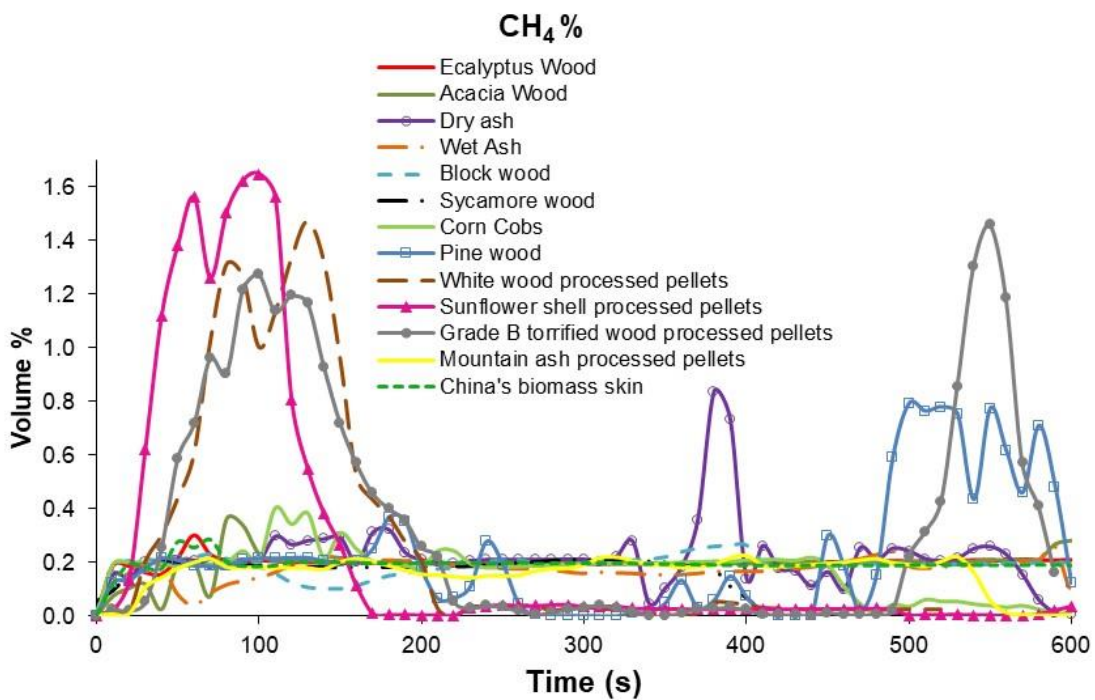


Figure 5.38 % CH₄ for tests with different biomass at air flow 19.2 (g/m².s)

Figure 5.38 illustrates the emission of CH₄ for the biomass species studied and it can be seen that for most biomass species CH₄ concentration ranged from 2000 to 2500 ppm during most of the test time. Pellets had different results for CH₄ emissions that in the start of the tests, High CH₄ emissions result during first

200 s and it could only result due to the cracking of the chemical structure of the pellets, or some binding agents might be present in the pellets causing high CH₄ initially. Some biomass show CH₄ peaks towards the end of the test time including pine wood and ash wood. The reason for these peaks could be that sufficient H₂ is present to react and form CH₄ by methanation reactions, R4, R5, R6 and R7. As these reactions are endothermic for the formation of CH₄ and sample might have attained heat required for the production of CH₄.

Emissions of acetylene C₂H₂, ethylene C₂H₄ and benzene C₆H₆ are shown in the Figure 5.39, Figure 5.40 and Figure 5.41 respectively. Sunflower pellets and white wood pellets shows highest emissions of acetylene in the first 200 s and then decrease gradually following the same trend as that of mass loss rate.

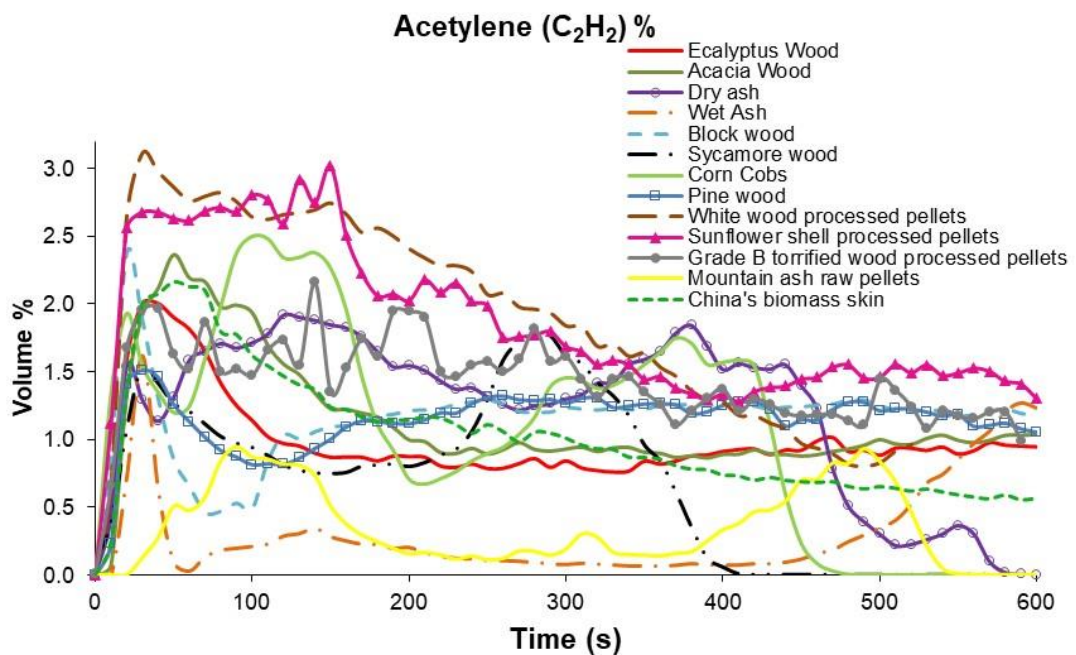


Figure 5.39 % C₂H₂ for tests with different biomass at air flow 19.2 (g/m².s)

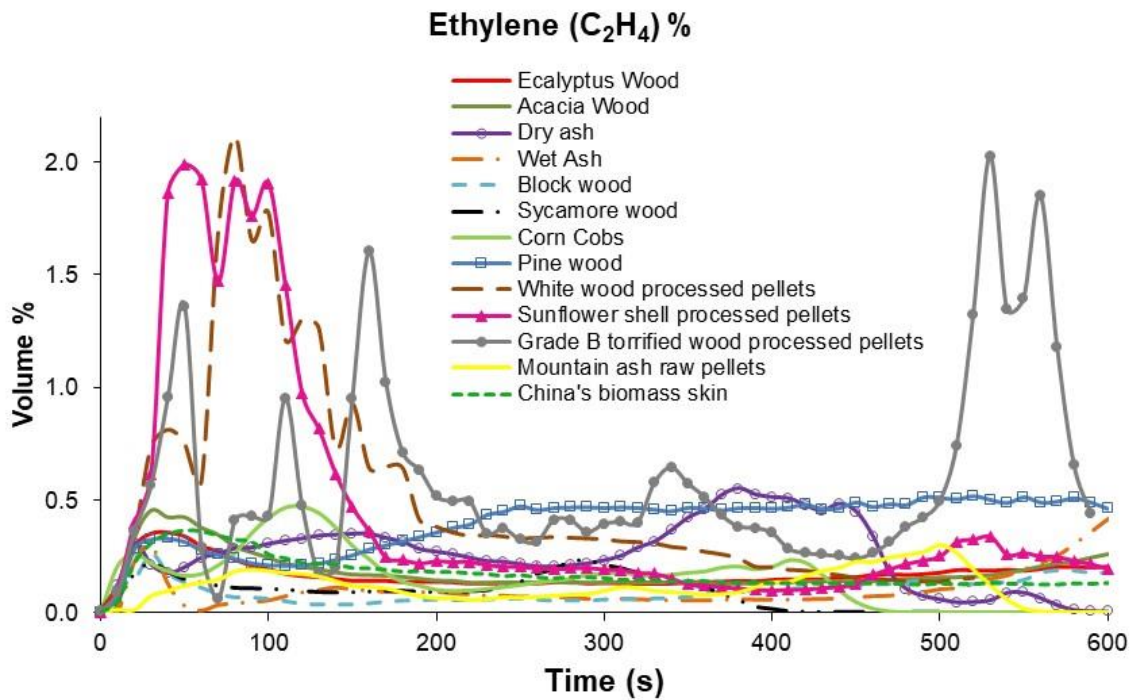


Figure 5.40 % C₂H₄ for tests with different biomass at air flow 19.2 (g/m².s)

Similarly emissions of acetylene and benzene are higher with the three pellets within initial 150-180s due to high burning rate and due to high rates of heat transfer rates within the pellets. As \dot{O}_m was very high initially for three processed densified pellets, so very rich combustion resulted in high hydrocarbon emissions during first 200s. Behaviour of mountain ash raw pellets is different from the other processed pellets as mountain ash pellets are not densified also contain the part of the wood that is bark having high lignin, another important reason for less emissions as compared to the other biomass studied is the moisture content of the moisture ash pellets that is more than 9%.

Pine wood and block wood have comparable emissions of acetylene, similarly eucalyptus wood and acacia wood have comparable emissions of acetylene, among all these wood dry ash have highest acetylene emissions. While wet ash and mountain ash raw pellets had the lowest acetylene emissions as these two biomass have comparable moisture contents i.e. more than 9%.

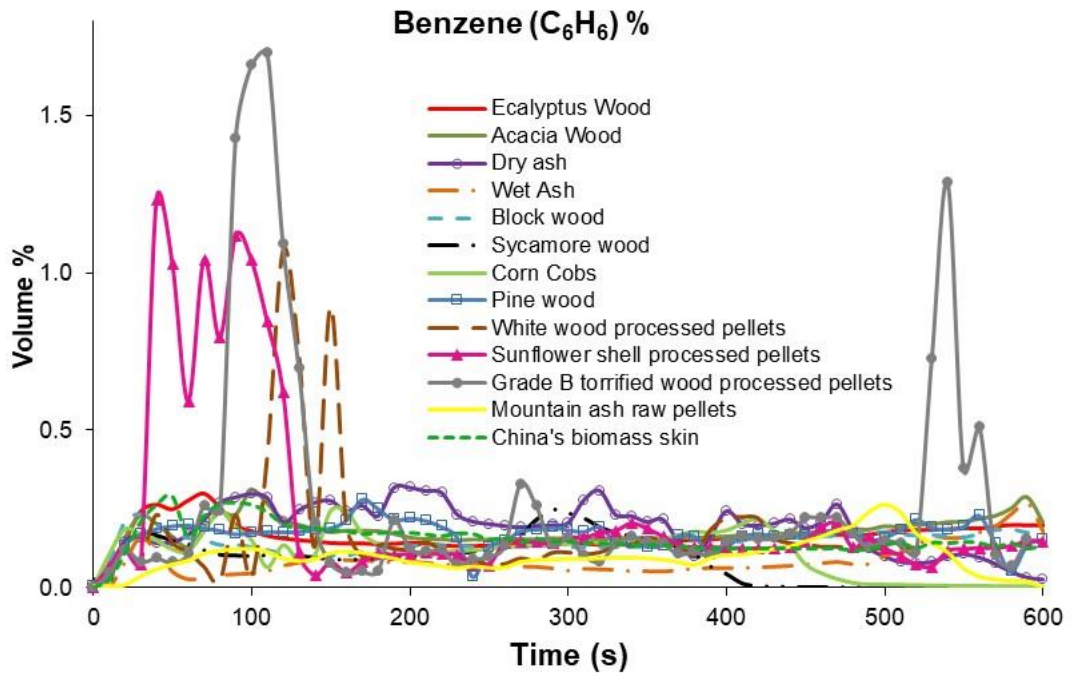


Figure 5.41 % C₆H₆ for tests with different biomass at air flow 19.2 (g/m².s)

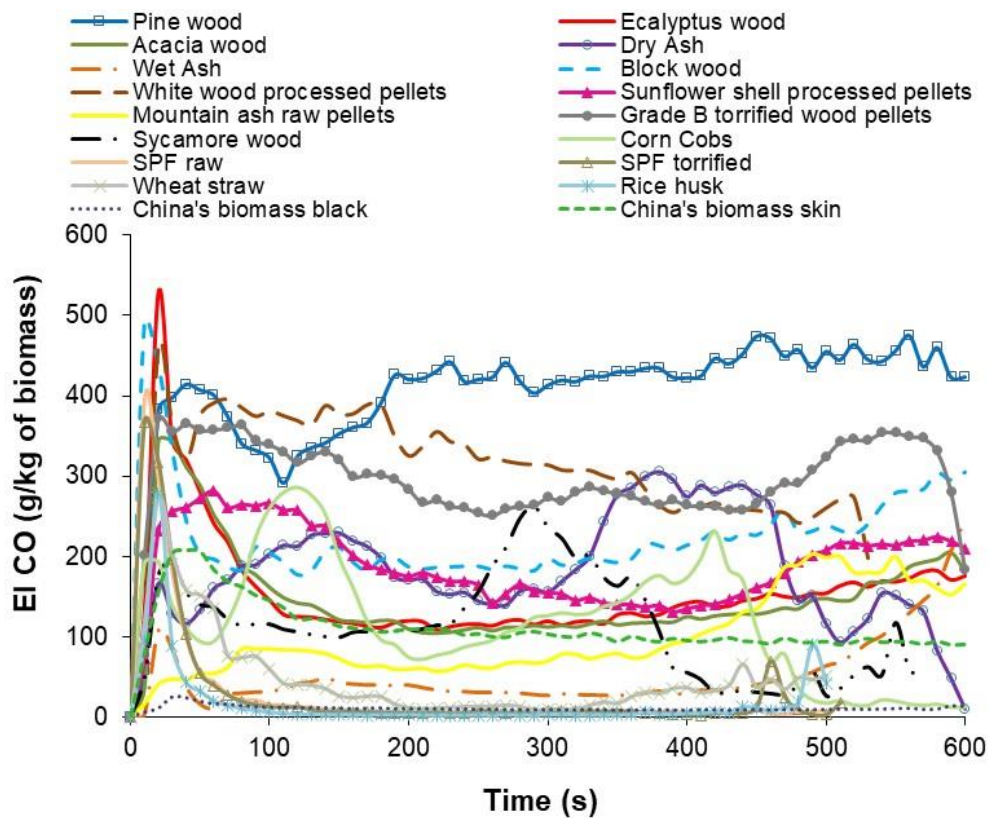


Figure 5.42 Elco (g/kg of biomass) for different biomass materials at air flow rate 19.2 (g/m².s)

Among all woods, pine wood showed the highest ethylene C_2H_4 emissions that reached a steady value of about 0.5 % after 250s. Dry ash reached the same level between 300 and 400 s. As pine has highest volatile matter these emissions of high hydrocarbons are attributed to this reason. For most of the other biomasses. Ethylene emissions were from 0.1 to 0.2% in the steady state.

Benzene is high molecular weight as compared to other hydrocarbons species discussed above and tends to be towards tars like materials, most of the biomass released benzene in the range of 0.2%, wet ash and mountain ash raw pellets released lower benzene emissions than other dry ash however released somewhat higher benzene among the other wood types during the test time.

Comparison of Elco for all biomass (Figure 5.42) shows that the yield of CO highest with pine wood and the reason is that only pine wood was optimised to produce highest CO yield. It clearly shows that all biomass did not produce high yields of CO at the same flow rate of air in the enclosure and each biomass have an optimum equivalence ratio. Equilibrium data for some biomass plotted in Chapter 4 proves this. Although in the present conditions, wood pellets have produced high concentration of carbon monoxide but it could be higher if the same exercise is repeated as done for pine wood in the previous sections to find an optimum equivalence ratio.

Figure 5.43 shows the O_2 emission from the gasification stage for different biomass materials and it shows that for most of the biomass in steady state % O_2 was less than 1%, For wet ash and mountain ash pellets, the % O_2 was slightly higher than other biomass materials. For powders and small particle sizes that were burned completely in the 100-150 seconds, O_2 started increasing, for china's biomass black it is shown that consumption of O_2 was very small and combustion was not rich.

Results in this section showed that different biomass behave differently and thus separate control of the primary air is required in the gasification zone, It can be seen in the

Figure 4.10 - Figure 4.13 that the adiabatic flame temperature changes slop sharply between equivalence ratio 3 and 4 and one of the attempt towards

possible control system should be having a temperature control system with thermocouple above and close to the throat of the primary gasification zone.

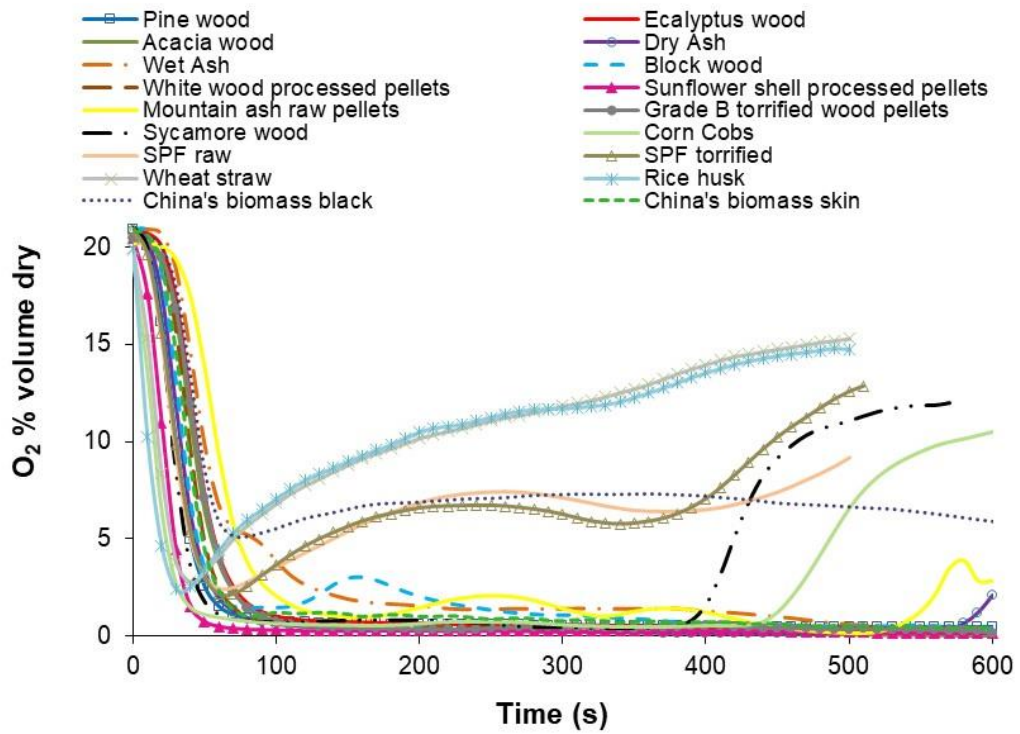


Figure 5.43 % O_2 dry for gasification of different biomasses at air flow rate $19.2 \text{ g}/(\text{m}^2 \cdot \text{s})$

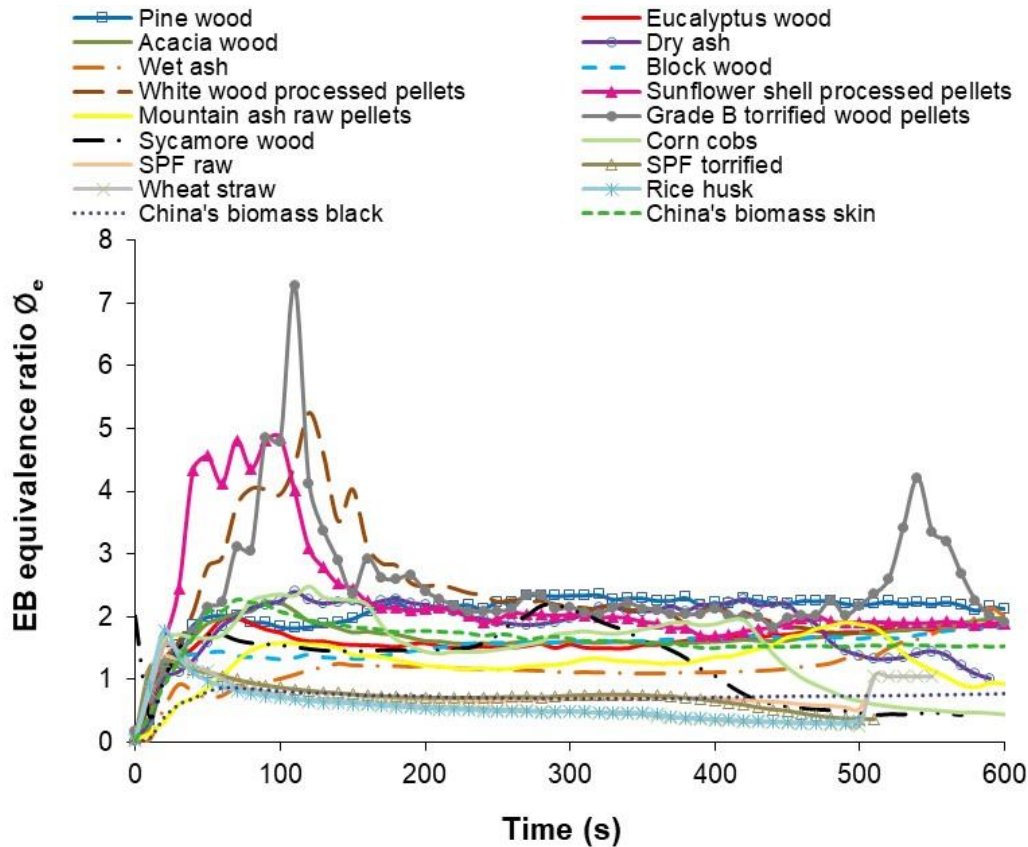


Figure 5.44 ϕ_e for different biomass at air flow $19.2 \text{ g}/(\text{m}^2.\text{s})$

and control system should change the flow rate of air between the points where rate of change of temperature with equivalence ratio shifts from low value to considerably high values, this can provide the near optimum equivalence ratios. but it is advised to have a CO sensor at this point that can optimise the % CO in the primary gasification zone, one limitation is that thig high temperature CO sensors are not developed yet but study suggest a CO sensor as well. It is shown in the Figure 5.15 and Figure 5.43 that O_2 readings cannot be used to control air flow in the rich combustion zone (gasification stage).

Emission based equivalence ratio plotted in Figure 5.44 shows that there was a difference between the ϕ_e and ϕ_m and as it was discussed in the previous section that the sampling method was not taking the real mean sample. It can be seen that in case of grade B torrefied wood pellets there were some points where two equivalence ratios were very close and it can be concluded that those were the time when measurement of the sample was somewhat representable of the actual mean value.

Composition of the gases from the FTIR were converted to masses and cumulative mass of the gases was obtained over the test time, this mass loss was in very good agreement with cumulative mass loss from load cell over test time. Figure 5.45 shows that comparison of the cumulative mass obtained from FTIR and cumulative mass loss from load cell. Difference of two masses is negative in some biomasses and positive in others. Positive difference is justified and difference can account soot, but negative difference shows that calibration error has caused it and burning was with less soot formation.

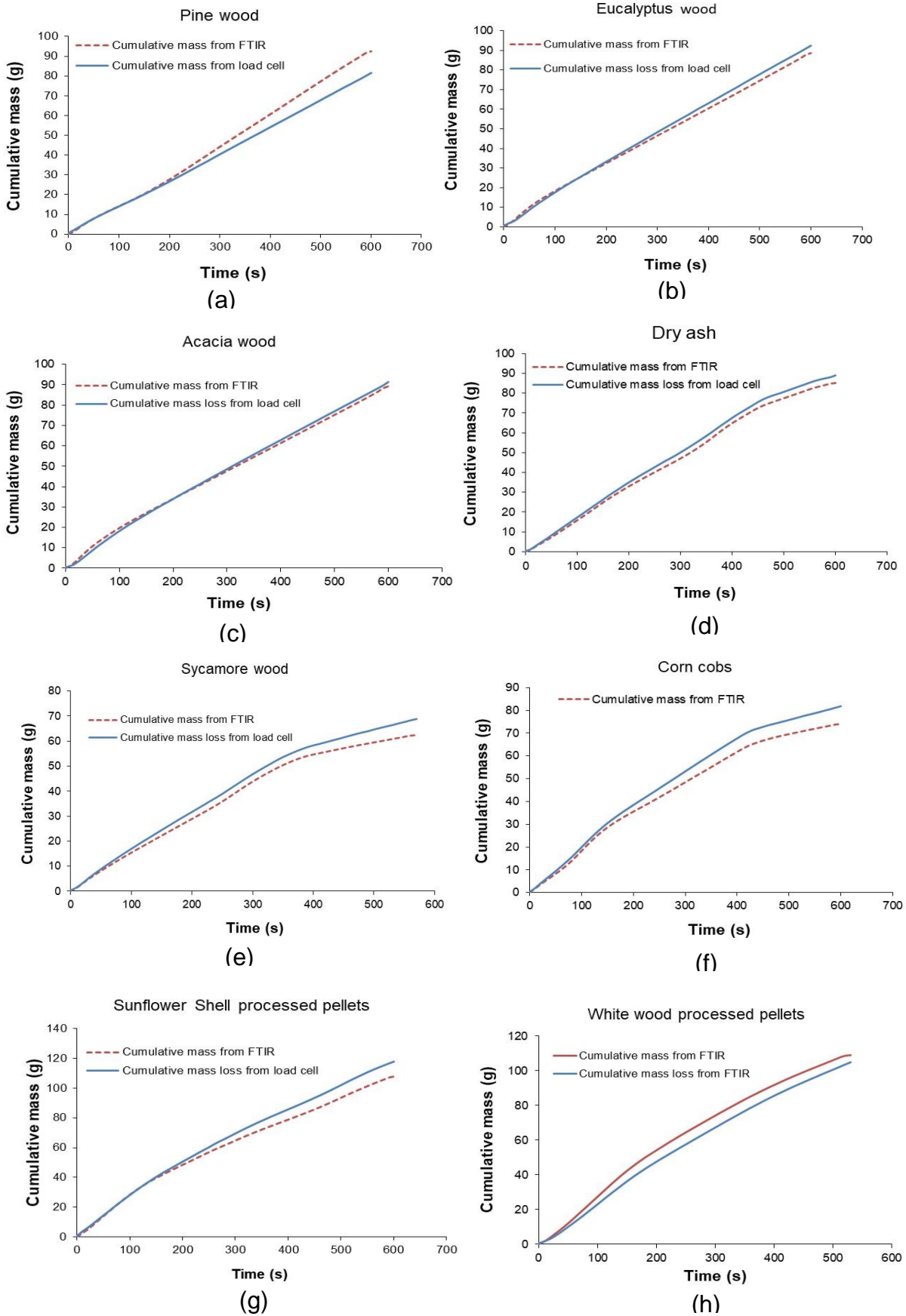


Figure 5.45 comparison of mass loss from load cell with mass obtained from FTIR for the gasification of different biomasses at air flow $19.2 \text{ g}/(\text{m}^2 \cdot \text{s})$

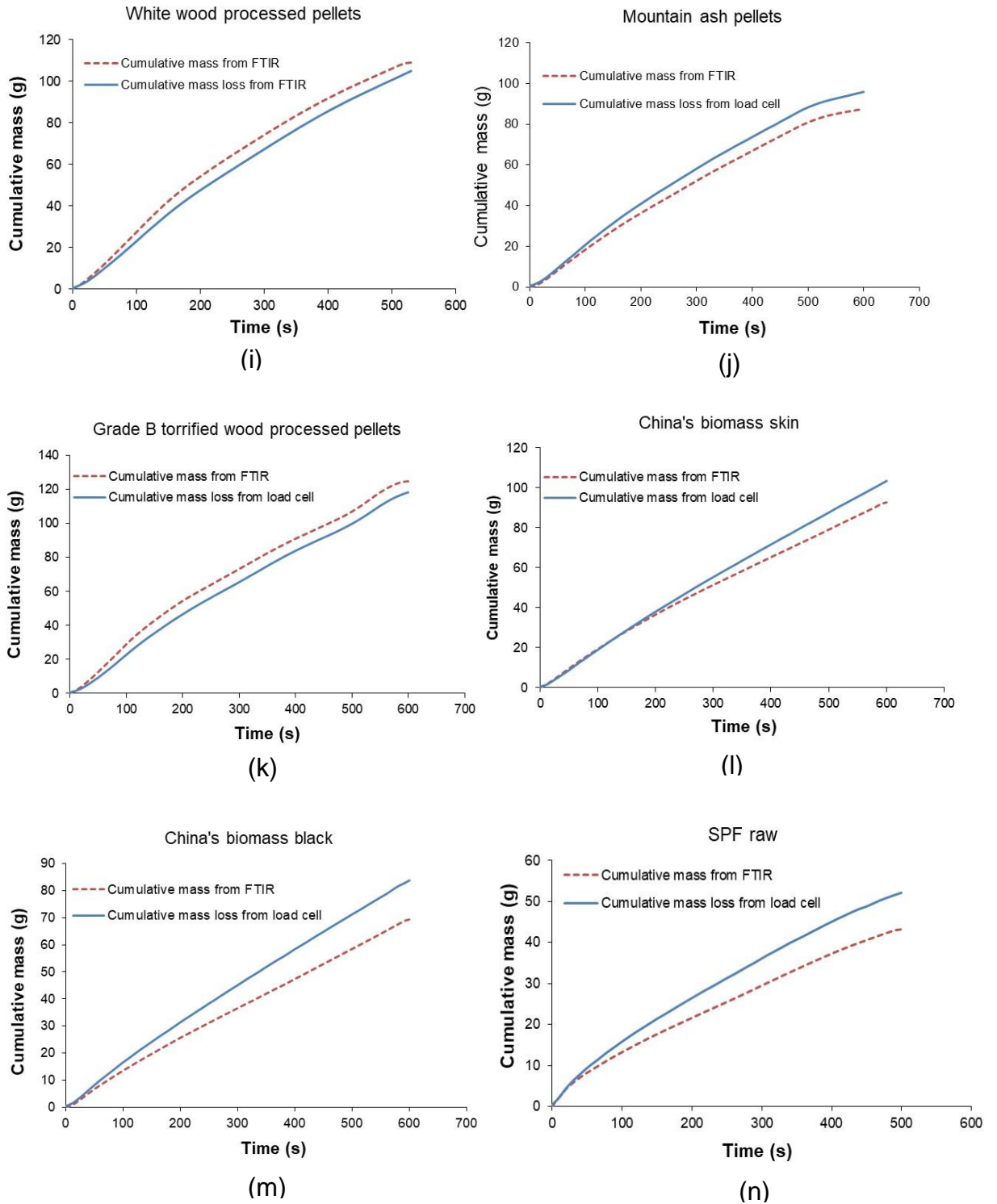


Figure 5.45 (continued)

Figure 5.46 shows the HHV and sensible heat plots in MJ/kg of gaseous products (includes condensable hydrocarbons as well). It can be seen that higher heating values depends on the emission index of the species and as the optimisation is not achieved HHV of the gases are not very high.

For processed pellets, white wood pellets, grade B torrefied pellets and sunflower shell pellets HGE of the gasification in the first 200 s was calculated as the mass loss of the pellets occurred during this period. HGE of white wood pellets was 80%, grade B torrefied wood pellets was 81% and for sunflower shell pellets was less than 70%. If the higher emission index were obtained by having less rich combustion, this efficiency could have raised much higher.

Table 5.2 shows the HHV of the chars and it can be seen for the sycamore wood and chars that most of the energy is still present in the char.

For processed pellets, white wood pellets, grade B torrefied pellets and sunflower shell pellets HGE of the gasification in the first 200 s was calculated as the mass loss of the pellets occurred during this period. HGE of white wood pellets was 80%, grade B torrefied wood pellets was 81% and for sunflower shell pellets was less than 70%. If the higher emission index were obtained by having less rich combustion, this efficiency could have raised much higher.

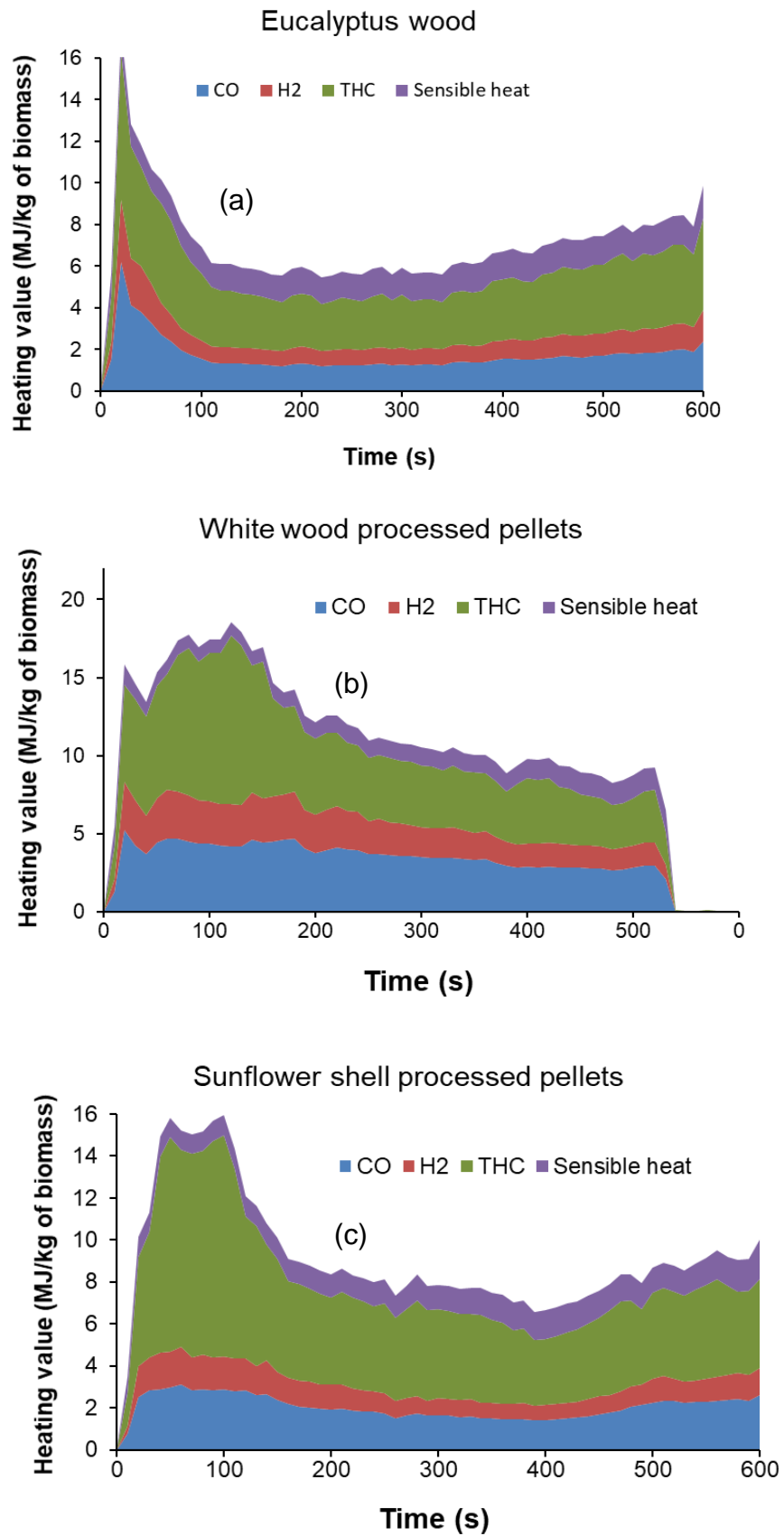


Figure 5.46 Higher heating values of gaseous products (MJ/kg of gases) for gasification of selected biomasses with time at air flow 19.2 g/(m².s)

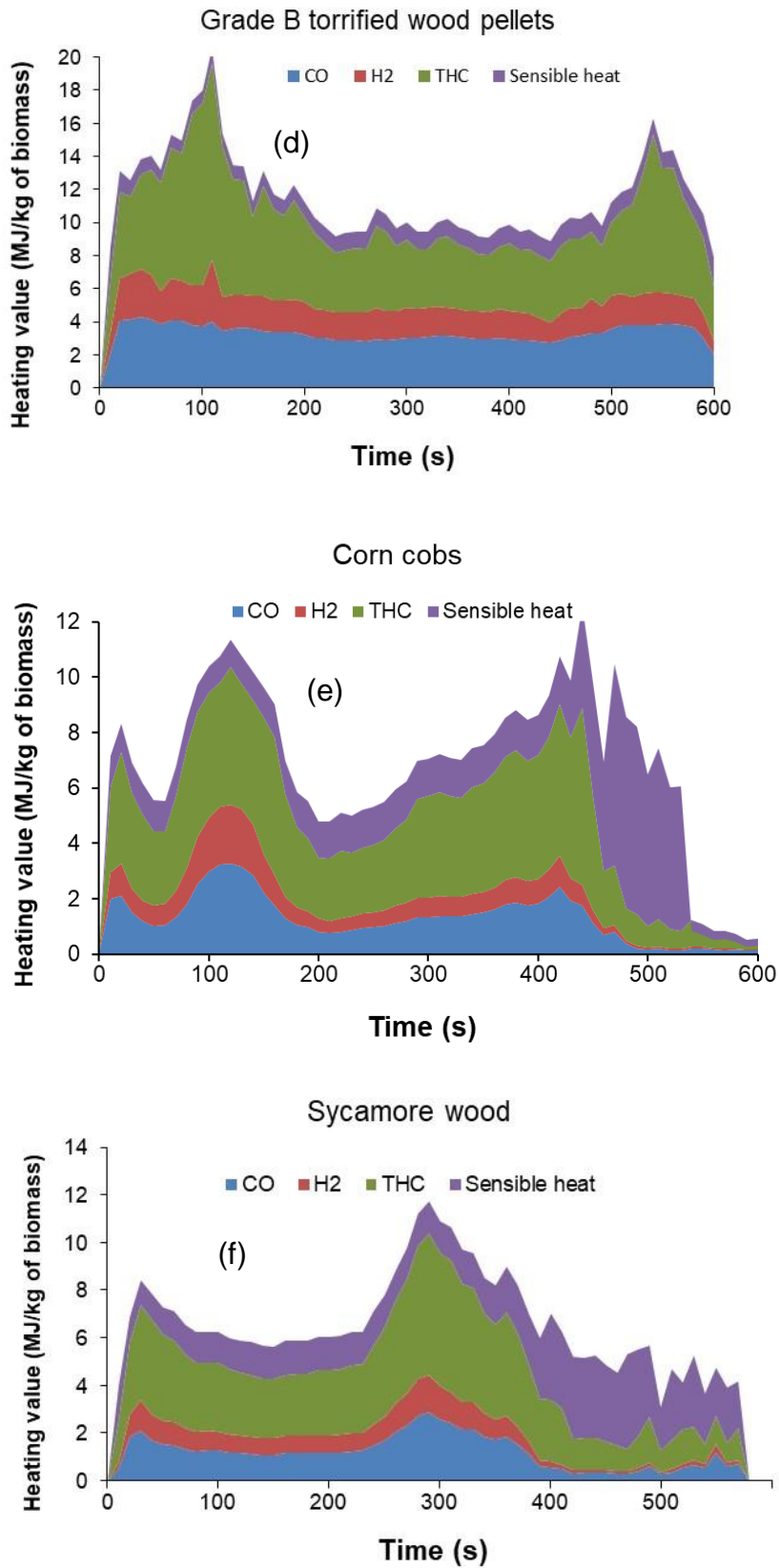


Figure 5.46 (continued)

5.5 Conclusions:

- Highest yield (0.5 g/g biomass) and % of CO (15%) for the pine wood was obtained at $\varnothing_m = 2.8$ and it was very close to the equilibrium prediction i.e. $\varnothing = 3.2$.
- It was found from the difference in the equilibrium adiabatic and experimental CO that the system never reached equilibrium, due to heat losses that produced gasification condition far from equilibrium.
- It becomes clear that the temperature of the biomass was less than that the equilibrium temperature
- It was found that high hydrocarbons were produced due to the fact that system did not reached equilibrium.
- It was found that different biomasses generated different equivalence ratios at an air flow rate that produced optimum equivalence ratio for pine wood. Pellets burned a much quicker rate and produced very rich mixture that need more flow rate of air to produce optimum mixtures and this put an emphasis on the separate control of the primary gasification zone of the log boilers.
- It was found that the particle size and the density of the biomass also play an important part for the determination of the optimum equivalence ratio other than chemistry of the biomass.
- It was found that pulverised materials could not be used for burning in the log boilers as the top surface of the biomass was fused making a crust that offered a resistance to heat and mass transfer.
- Material balance for the mass recorded from FTIR for gasification of biomass was in very good agreement with the mass loss from load cell.

Chapter 6 Results for pyrolysis tests on cone calorimeter

Pyrolysis is an important thermochemical conversion route and an unavoidable step in any biomass combustion process. Knowledge of the product gas composition from the pyrolysis of wood and its dependence on the wood composition and physical state is an essential step that would lead to more efficient and less polluting biomass boiler design.

In a log boiler, air to fuel ratio in the first stage is calculated on the basis of the elemental composition of the biomass itself rather than the products of pyrolysis. For larger fixed bed biomass combustion units, a smoother steady output is achieved by using large wood logs and therefore the pyrolysis mechanism and products from large / thick biomass particles is important.

High temperature (>600°C) pyrolysis has dominated the biomass combustion research activity in recent years as it is relevant to furnace and burner applications [103, 105, 146-148], but not as relevant to biomass boilers. In boiler combustion of solid biofuels (e.g. logs) part of the biomass pyrolysis also occurs over a much lower range of temperatures of 300-450°C. The pyrolysis products in this temperature range are therefore important for the subsequent combustion characteristics of the process, as discussed above.

Work done in this section was aimed at the investigation of the composition of these biomass pyrolysis gases over the low temperature range. Thermogravimetric analyses (TGA), from this project, for 11 different biomass samples showed that the temperature range at which 85-90% of the volatiles are driven off is from 275 to 450°C, as shown in the Figure 6.1.

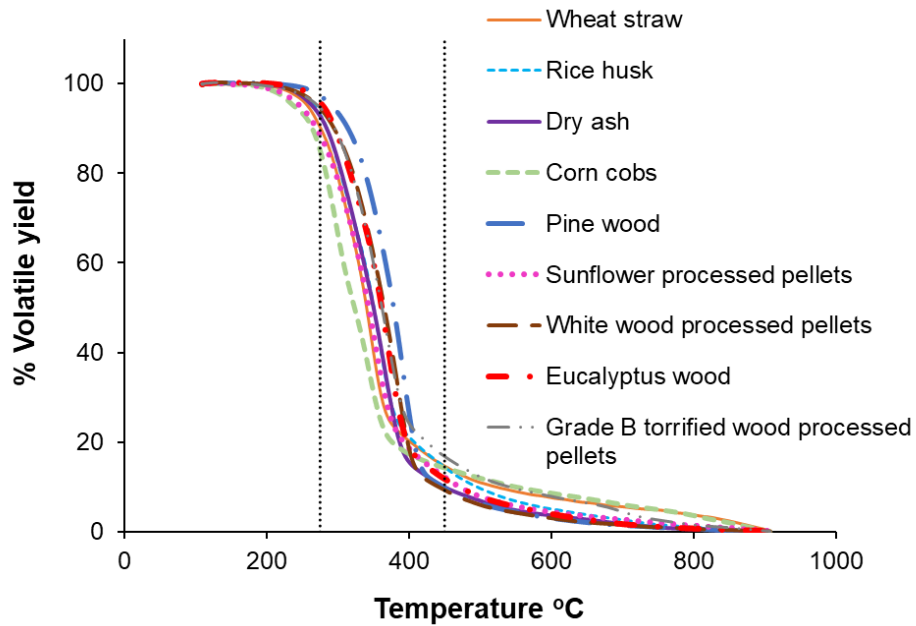


Figure 6.1 TGA % volatile yield vs temperature for biomass samples

Some of the researchers listed in Table 2.5 have used TGA in combination with an FTIR analyser to identify the volatiles and to quantify the yields. The limitation of this method is that TGA takes a tiny fraction of biomass at uniform temperature with respect to time and the flow rate is too low for many FTIR analysers including the one used in the present work. In biomass boilers the fuel is in much larger particles than samples used in TGA analysis and they are expected to behave differently. The cone calorimeter tests at larger samples and this allowed us to combine the test with available Portable FTIR unit to obtain relevant pyrolysis data for boiler applications.

Figure 6.2 shows the pine-wood volatile yield (mass loss excluding water, char and ash) vs temperature as determined by TGA analysis. It is known from the work of others [9] that pyrolysis of hemicellulose occurs from 150-350 °C, cellulose pyrolysis occurs from 275- 400 °C and lignin pyrolysis mainly occurs from 250 -900 °C but it can start from 160 °C – these ranges are also marked on

Figure 6.2 It can be seen that about 90% of the volatiles were released between 275 and 450°C (also marked on

Figure 6.2) which coincides with the cellulose decomposition temperature range but all three biomass components are involved. This demonstrates the

significance of the 275 to 450 °C range in the pyrolysis of biomass and justifies the focus of the present work.

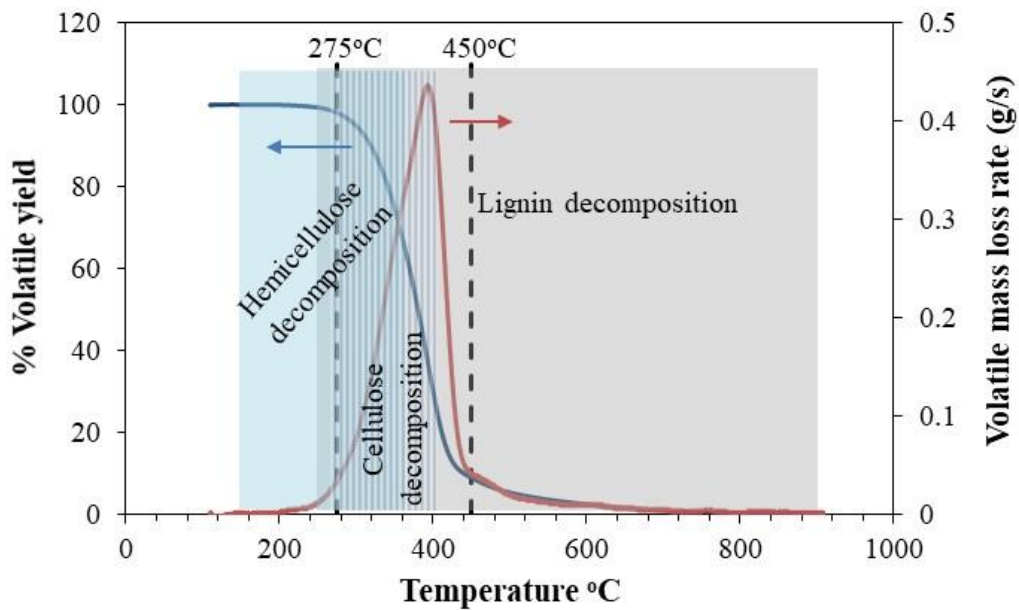


Figure 6.2 Mass loss over temperature range for pine wood from TGA analysis

Tests were performed with 5 pine wood sticks of 20 x 20 x100 mm in the same manner as done with gasification tests with 20mm kaowool insulation underneath the wood at different heat fluxes that would produce low temperatures inside the wood and hence produce data relevant to low temperature pyrolysis. Tests were done at 10, 15, 20 and 25 kW/m² heat flux to monitor the mass loss rate. Tests with thermocouples were performed separately as the insertion of thermocouples affected the operation of the load cell and the procedure actually required two identical tests one with and one without the thermocouples to get a complete data set.

6.1 Mass loss and temperature profiles of pyrolysis tests on the cone calorimeter

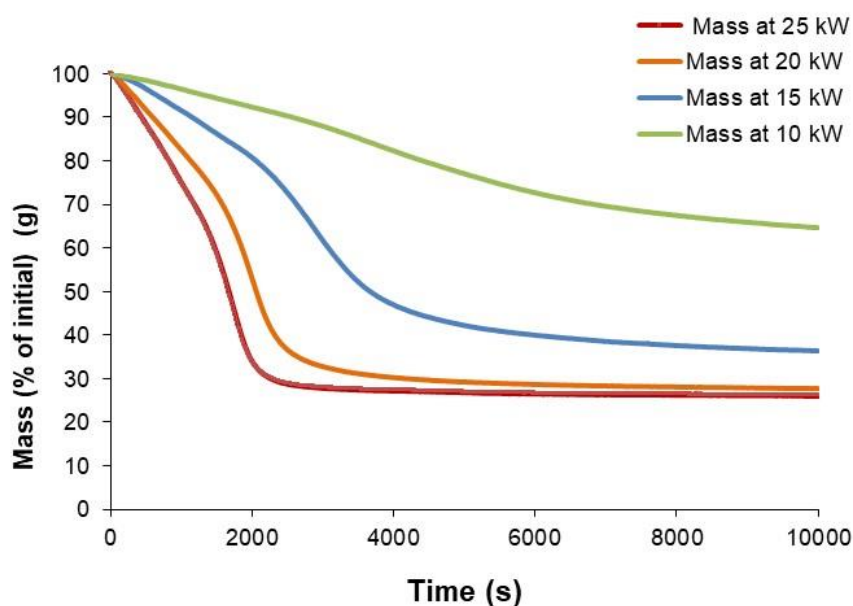


Figure 6.3 Percentage mass loss w.r.t. time for pyrolysis of pine wood

Nitrogen was used as a carrier gas at a rate of $52 \text{ g}/(\text{m}^2 \cdot \text{s})$, (25 litre/min) with a residence time of 1.2 s. The sample was placed on the load cell within the sealed box and then the box was purged with a steady flow of nitrogen until 0% O_2 was reported by the analyser. Whilst maintaining the flow of nitrogen the cone heater was switched on with a set coil temperature $^\circ\text{C}$ corresponding to desired heat flux (calibrated using a heat flux meter). During the brief heat up period (about 5 mins) the sample was prevented from heating up by keeping the shutters of conical heater closed. The distance of the top surface of pine-wood from the bottom plane of the cone heater was 25mm.

Figure 6.3 illustrates the % mass vs time over 10000 s for the pyrolysis of pine wood at four different heat flux. The faster mass loss is observed with the highest heat flux of $25 \text{ kW}/\text{m}^2$ with an abrupt levelling off at about 2000s suggesting a fairly non-responding char residue between 25 and 30%. The devolatilisation/pyrolysis process took longer at lower heat fluxes with a shallower slope and the residual mass became higher. At the lowest heating flux of $10 \text{ kW}/\text{m}^2$ the mass loss was very slow only 35% of the total mass was lost over 10000s and no sudden change in the slope of the curve during the test.

The temperature profiles of the wood, recorded near the top and near the bottom surface of the wood are shown in the Figure 6.4. The source (cone heater) temperatures corresponding to the heat fluxes of 10, 15, 20 and 25 kW/m² were 380 °C, 460 °C, 530 °C and 570 °C respectively.

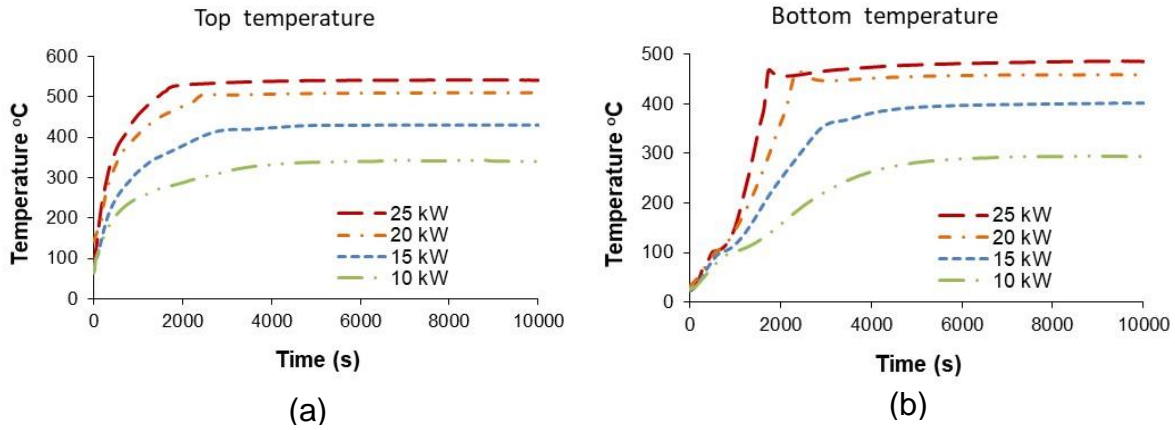


Figure 6.4 Temperature of pine wood (a) 3mm from top surface (b) 3mm from bottom surface

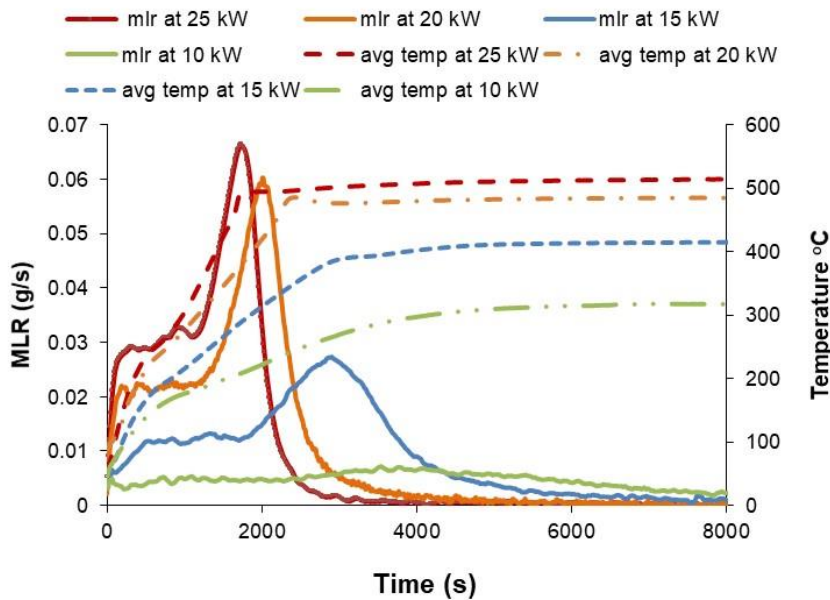


Figure 6.5 MLR (g/s) and average wood temperature w.r.t time for pine wood pyrolysis

It can be seen from the temperature profile for the test at 10 kW/m² that the variation in the top temperature continued until 5000 s and bottom temp until 6000 s, with maximum top and bottom temperatures of 340 °C and 290 °C . The mass loss rate and the average (top and bottom) temperature of the wood are also plotted in the Figure 6.5. . Mass loss rate of test with 10kW/m² was very low, upto 2000 s mass loss rate was 0.0048 g/s that raised to 0.007 upto 4000 s and decreased again, average temperature at 4000 s was about 300 °C.

The temperature profile for test at 15 kW/m² shows that variations in the top and bottom temperature continued until 2950 s and 3000 s respectively, maximum values of the top and bottom temperature was 430 °C and 395 °C. The mass loss rate of test for this tests considerably higher than the 10 kW/m² test. The mass loss rate remained nearly constant with an average value of 0.012 g/s from 500 to 1750 s, and then raised to a peak value of 0.026 g/s at 3000 s with an average temperature of wood at 385 °C at this point. The mass loss rate decreased to a low value until 5000s.

The temperature profile for test at 20 kW/m² shows that the top and bottom temperatures reached their maximum quickly as compared with the tests at lower heat fluxes. Variations in the top and bottom temperature continued until 2400 s and 2600 s respectively, maximum values of top and bottom temperature was 510 °C and 460 °C respectively. Mass loss rate remained nearly constant with an average value of 0.022 g/s upto 1300s, and then raised to a peak value of 0.06 g/s at 2000 s and average value of wood was 410 °C at this point, but temperature continued to increase after this point until 2500 s, mass loss rate decreased to a low value until 3000s. The temperature range in this test covers most of the mass loss observed in a TGA test.

The temperature profile for test at 25 kW/m² shows that the maximum value of top and bottom temperature achieved was 530 °C and 480 °C. The mass loss rate remained nearly constant with an average value of 0.03 g/s upto 1000s, and then raised to a peak value of 0.07 g/s at 1800 s with an average temperature of wood of 495 °C at this point. The mass loss rate decreased to a low value until 2500s. The temperature range in this test also cover most of the mass loss observed in a TGA test, but mass loss occurred quickly and more condensate/tars were observed in the tubes after the FTIR, and due to the

technical complications using FTIR, this condition was not chosen for comparison of the tests with various biomass species.

The heating rate of the wood based on the average temperature of the wood is shown in the Figure 6.6. The heating rate rises rapidly initially in all tests due to the fast heating rate of the top layer of the wood., After the top layer is devolatilised, the rate of heat transfer decreases in tests at 10 and 15 kW/m².

A second peak was observed in tests at 20 and 25 kW/m² and it is thought that this corresponds to the heat wave reaching the bottom of the sample. After this the heating rate reduced to zero indicating the wood temperature reached the final temperature with respect to the heat flux applied. This second heating rate peak was mirrored by a rise and peak in the mass loss rate which decayed for a significant time after the heating rate reduced to zero.

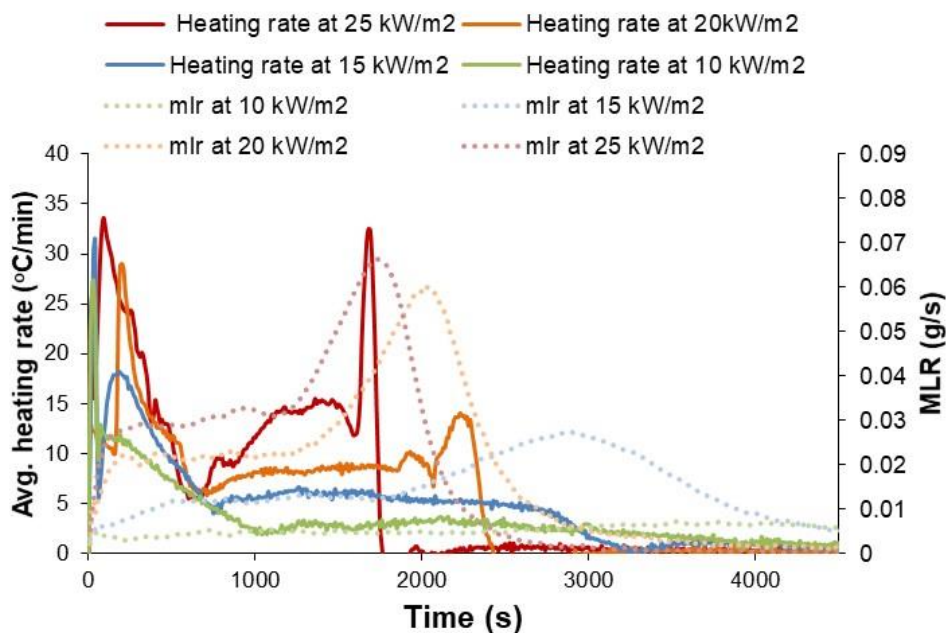


Figure 6.6 Heating rate of pine wood pyrolysis at different heat flux

As heating rate was slow, these pyrolysis tests falls in the category of conventional pyrolysis although residence time is very low.

Mass loss rates for all tests is plotted against top, bottom and average wood temperature, and compared with the mass loss rate curve for the TGA in the Figure 6.7. For test at 10 kW/m² there is no much difference in the peak mass

loss rate and a steady initial mass loss rate, however the top, bottom and average temperatures where the curve changes its shape towards peak area are 300, 250 and 200 °C respectively. TGA mass loss curve shows that mass loss curve changes shape between 250 and 300 °C. But it can be seen that wood temperature in this test does not cover the entire temperature range of TGA.

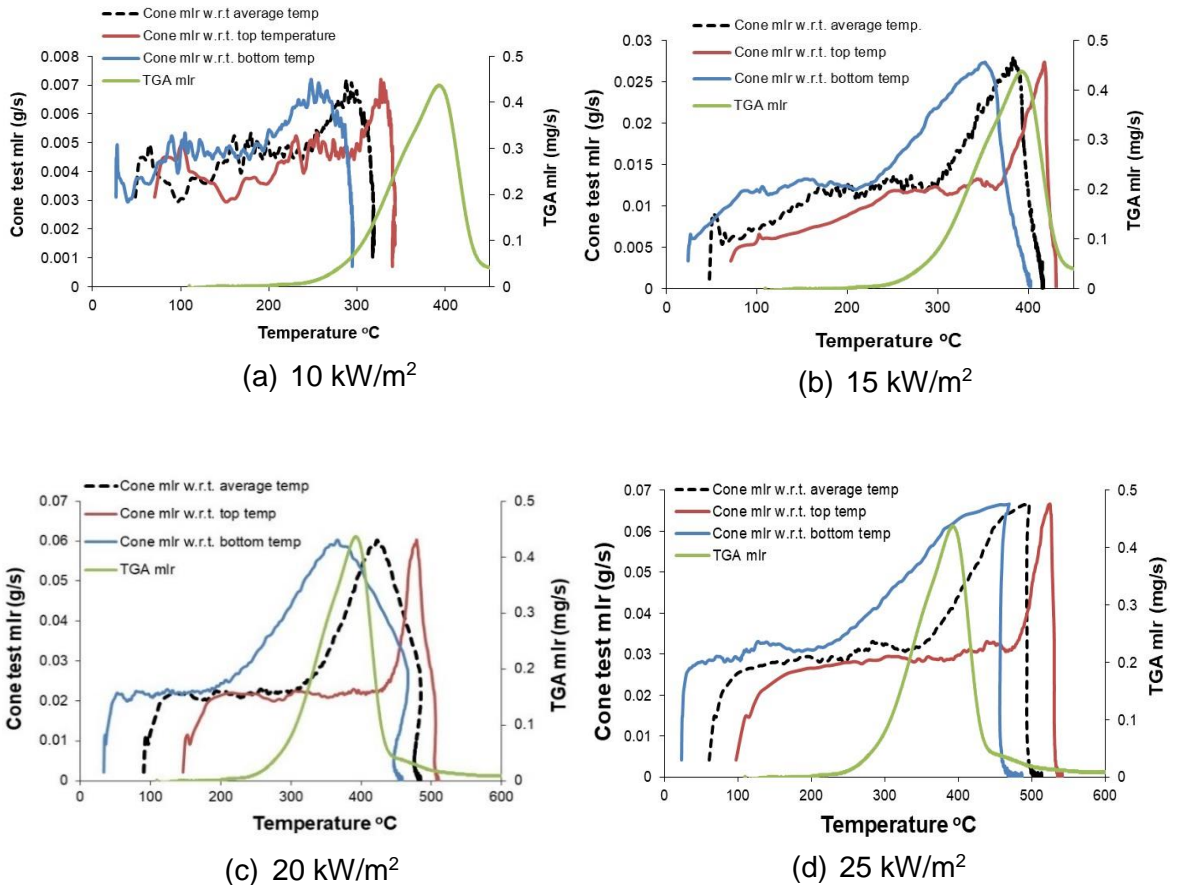


Figure 6.7 MLR vs temperature for pyrolysis tests at different heat flux

The test at 15 kW/m² (Figure 6.7 (b)) shows that the top, average and bottom temperatures where mass loss changes slope and mass loss rate increase towards the peak area 360 °C, 290 °C and 210 °C respectively. Top thermocouple temperature was 430 °C at the end of the test, however this tests covers a reasonable range of temperature change indicated by the TGA mass loss rate curve at which 80-85% of the mass loss of biomass occurs. However in this test 65% of the original mass of the wood was lost as discussed before.

The test at 20 kW/m² (Figure 6.7 (c)) shows that the top average and bottom temperatures where mass loss changes shape and move towards peak value

are 420 °C, 300 °C and 200 °C respectively. This test covered all the temperature range in which 85% of the mass loss for the TGA test occurred. Total mass loss by the end of this test was 73%.

Another test was performed at 25 kW/m² to check if the mass loss rate changes more, it was 75% of the total mass loss, a small difference as compared with the test at 20 kW/m². The top thermocouple temperature was above 500 °C.

As the aim of the current work was to compare emissions in a test at a temperature range 250-450 °C the above test and analysis demonstrated the suitability of the 20 kW/m² and this was selected for the tests with various biomass samples and for comparison to the pine wood test.

6.2 FTIR results

Fifty components were quantified by the FTIR with the Calcmeter software reporting the product gas composition with water vapour and CO₂ in volume % and CO, NO_x and other hydrocarbons in ppm.

In Figure 6.8 the pyrolysis product composition is plotted as a function of average temperature of the wood for all tests. Average temperature is chosen as the representative temperature for the emissions and this approach has also been used by Blasi in his work [107] .

At the time of start of the test, the average temperature of the wood was about 40-50 °C in different tests, water and carbon dioxide started coming off at these temperatures, as the top surface of wood became warm during heating up of the cone to the desired temperature which took about 300 s. with the sample placed inside the purged box before opening the shutter and exposing it to the heater. During this “preheating” some water vapour were released before starting measurements and FTIR read above 0% water vapours at the start.

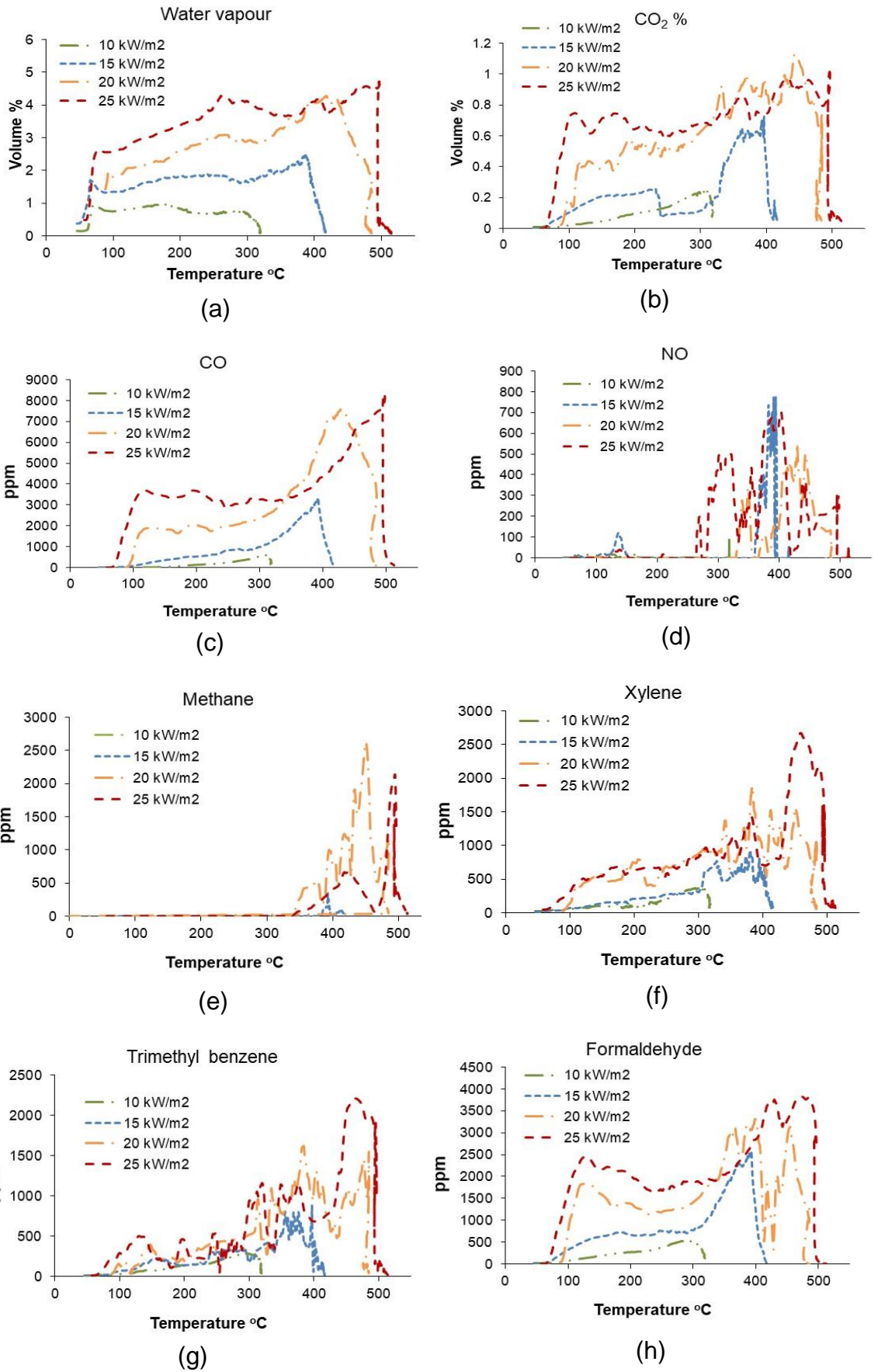


Figure 6.8 FTIR product gases concentration as a function of temperature for the of pyrolysis of pine wood at different heat flux

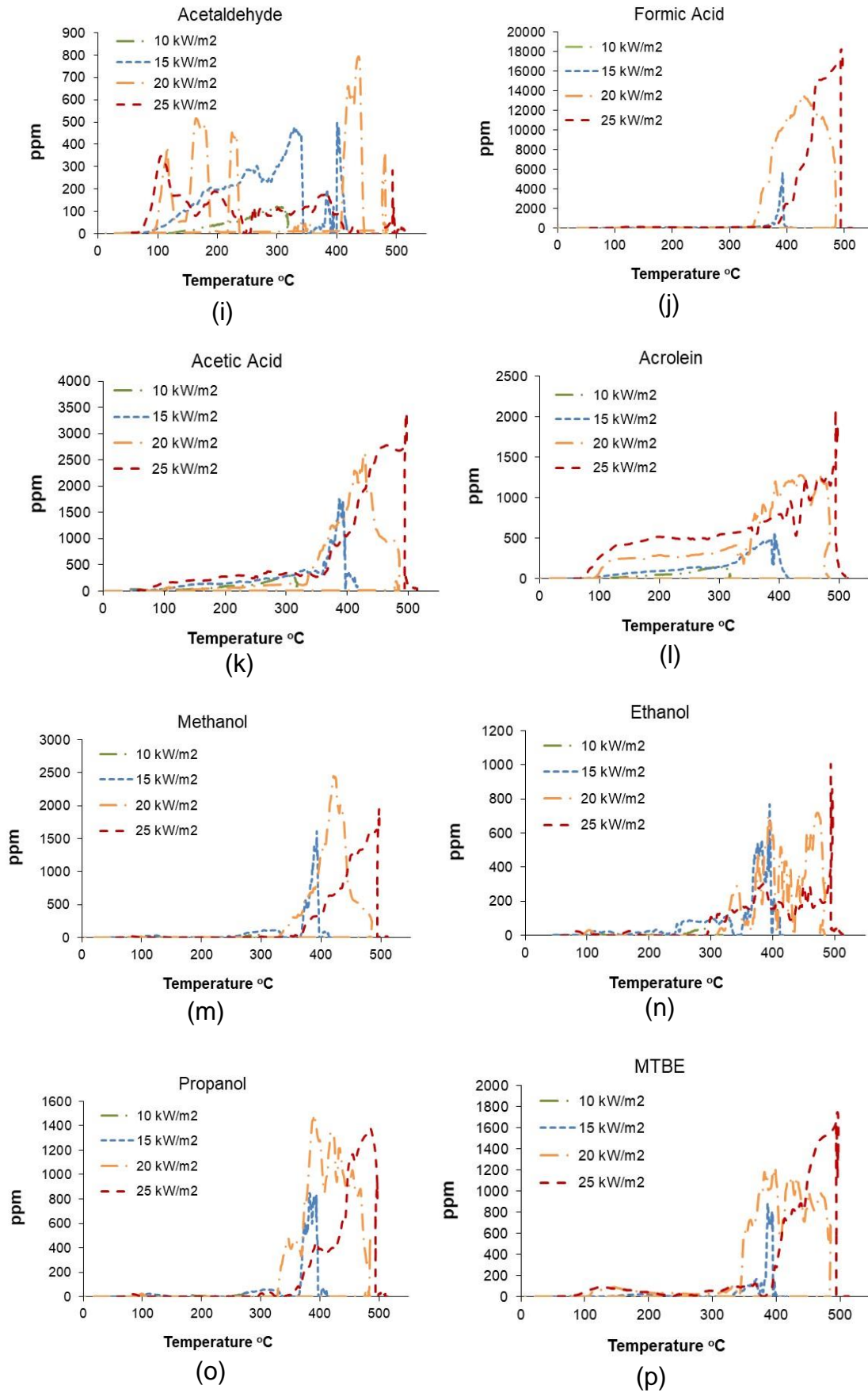


Figure 6.8 (continued)

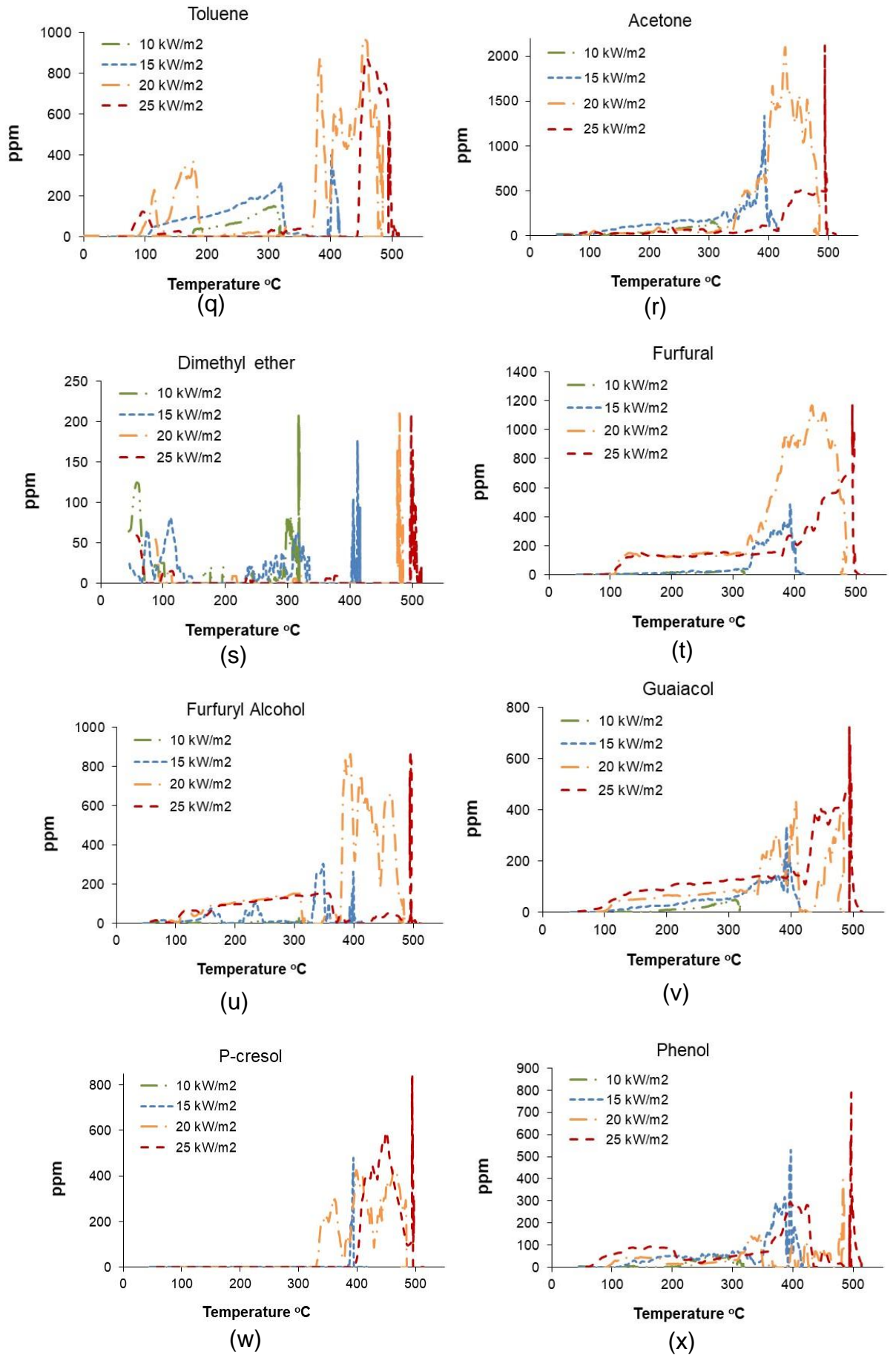


Figure 6.8 (continued)

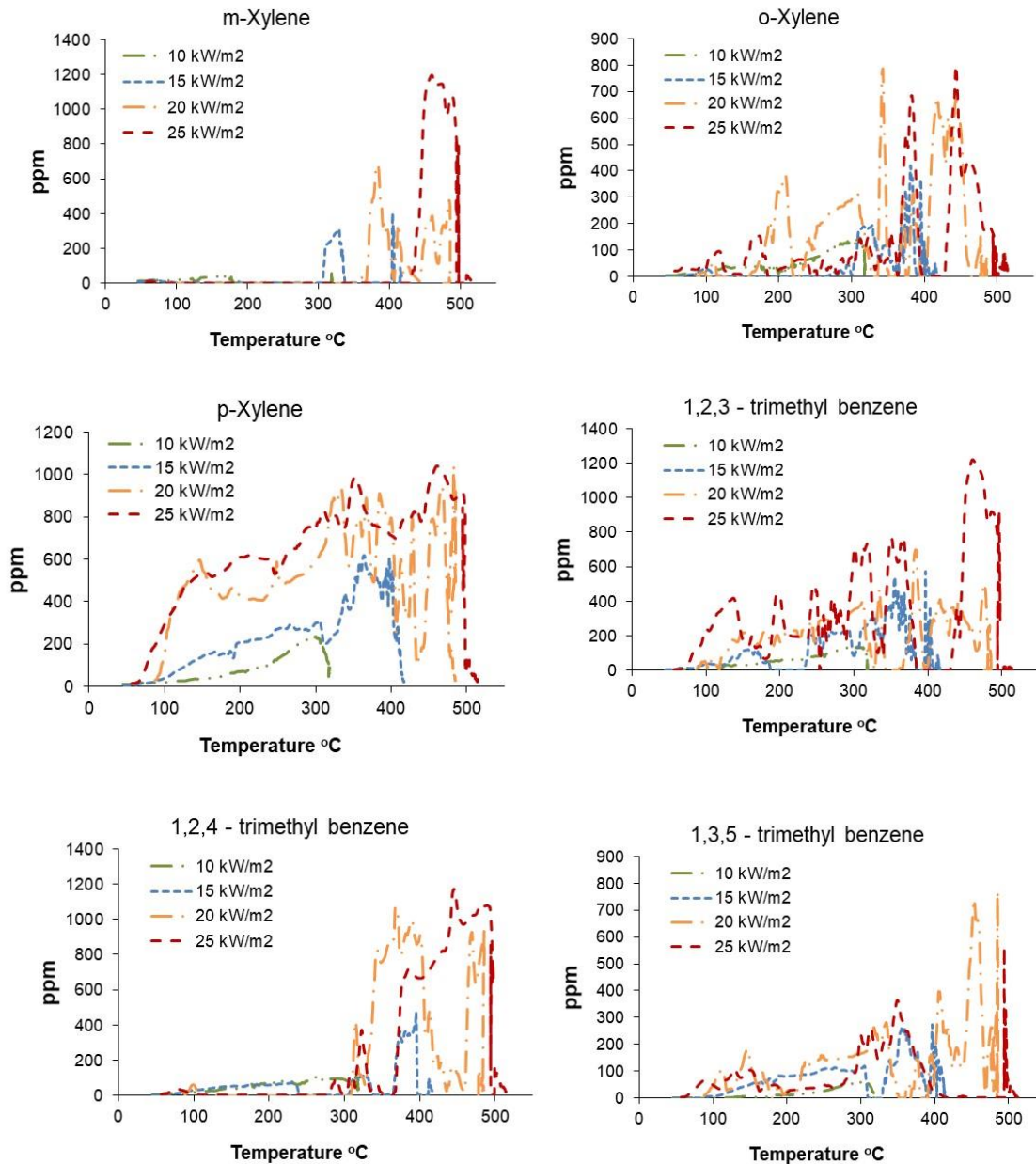


Figure 6.9 concentration vs time for o-xylene, m- xylene p-xylene, 1,2,3-trimethylbenzene, 1,2,4- trimethyl benzene, 1,3,5- trimethyl benzene.

As shown in Figure 6.8 water vapour started releasing at high rates between 50-60 °C, CO₂ between 60-80 °C, CO, xylene, trimethyl-benzene, formaldehyde, acrolein and toluene between 70-90 °C, methane at 345 °C, formic acid between 345 – 385 °C, acetic acid at 100 °C at very low concentration and at 330-360 °C at considerable concentration, acrolein from 80-100 °C, methanol from 330-370 °C, ethanol from 250-300 °C, propanol from 330-360 °C, MTBE (methyl ter-butyl ether), furfural, furfuryl alcohol, guaiacol and acetone at 100 °C, phenol between 70-100 °C and p-cresol between 330-390 °C.

Xylene plotted in Figure 6.8 are the sum of m- xylene, o- xylene and p- xylene similarly trimethyl benzene is the sum of 1,2,3-trimethylbenzene, 1,2,4-trimethyl benzene and 1,3,5-trimethyl benzene (plotted separately in Figure 6.9).

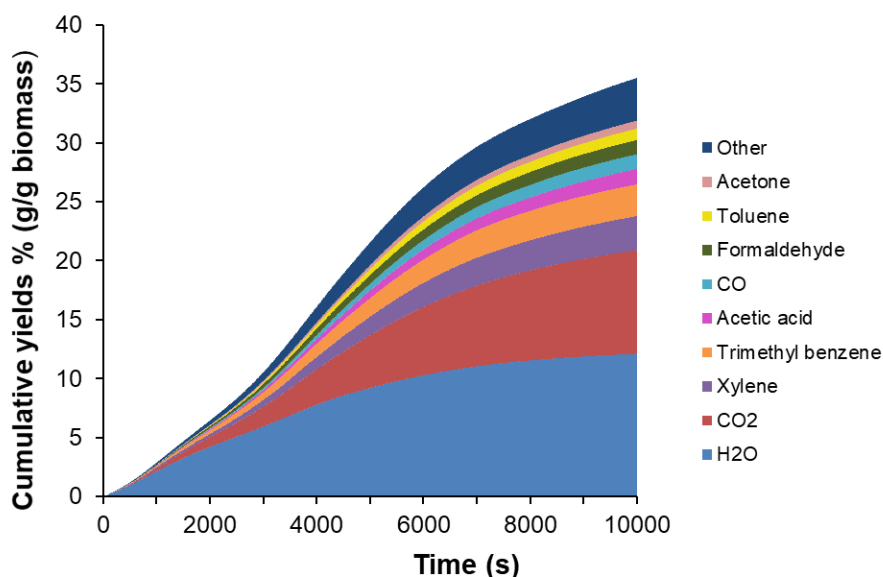


Figure 6.10 Cumulative yields (g/g biomass) for pyrolysis of pine at 10 kW/m²

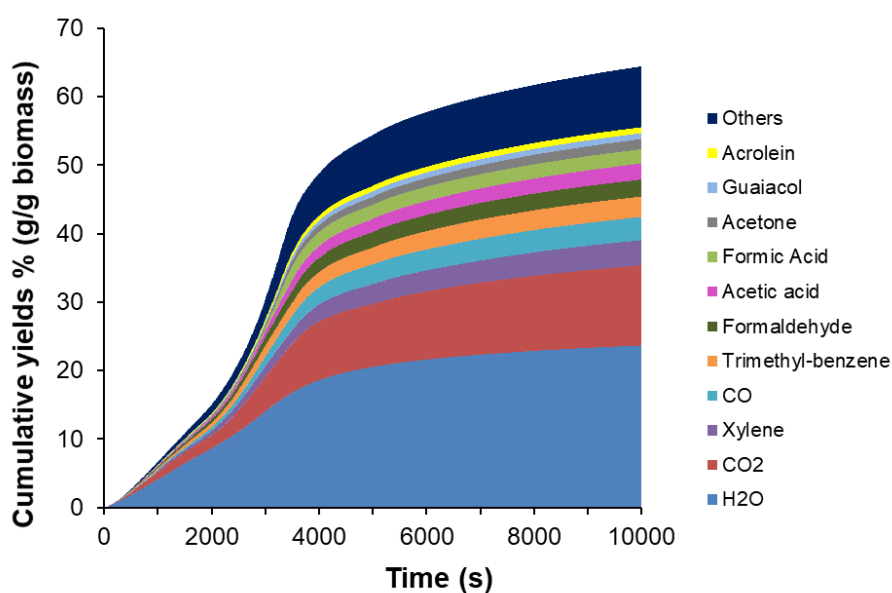


Figure 6.11 Cumulative yields (g/g biomass) for pyrolysis of pine at 15 kW/m²

Evolution of some of the hydrocarbons was not continuous, there was some discontinuity and gases released at two or more temperatures and then reached zero or to a very low concentration. For example toluene, dimethyl ether, phenol, m-xylene, o-xylene, 1,2,4,-trimethyl benzene, acetaldehyde and guaiacol has more than one peaks appearing at different temperatures. This could be due the

fact that main components of wood cellulose, hemicellulose and lignin break at different initial temperatures and produce same products with different concentration, at different temperatures as shown by the work of Yang et al [9].

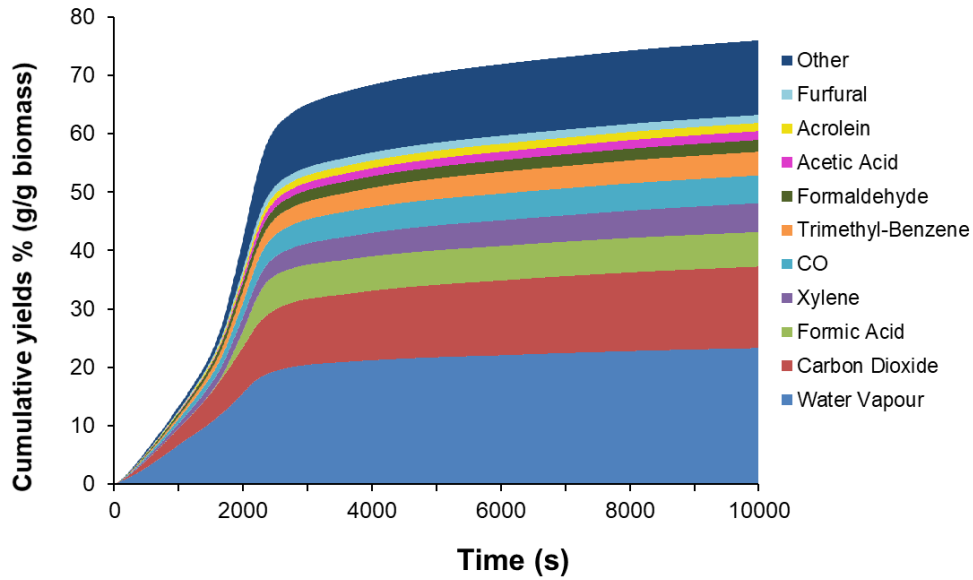


Figure 6.12 Cumulative yields (g/g biomass) for pyrolysis of pine at 20 kW/m²

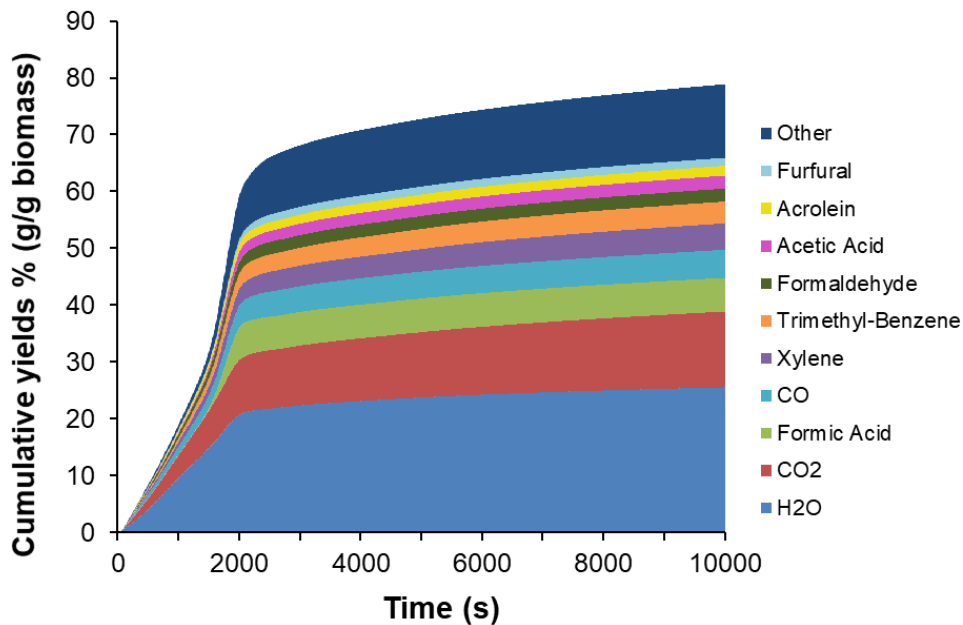


Figure 6.13 Cumulative yields (g/g biomass) for pyrolysis of pine at 25 kW/m²

In test at 10 kW/m^2 , major components detected by FTIR in order of decreasing mass proportions were H_2O , CO_2 , xylene, trimethylbenzene, acetic Acid, CO , formaldehyde, toluene and acetone (Figure 6.10).

In test at 15 kW/m^2 (Figure 6.11), formic acid was also produced as formic acid released from $345\text{-}385 \text{ }^\circ\text{C}$ and this temperature was not achieved in a test at 10 kW/m^2 .

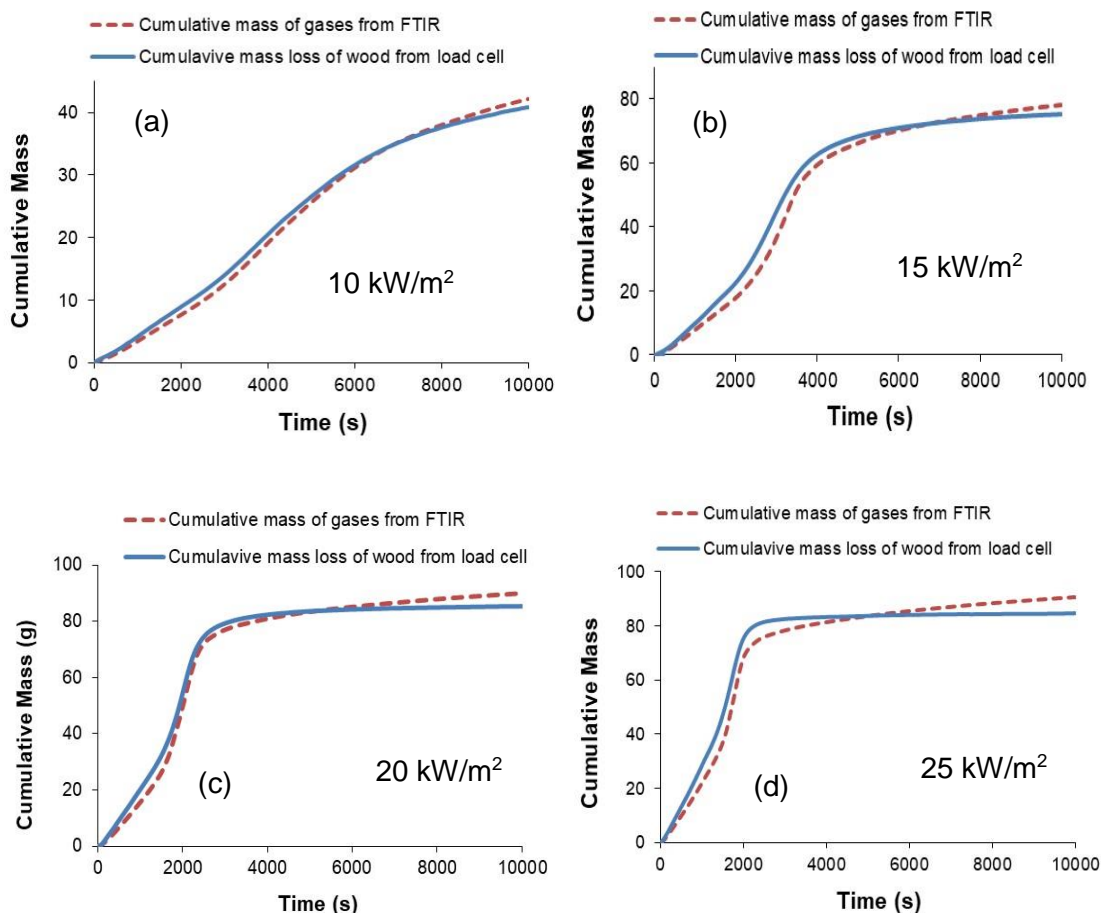


Figure 6.14 Comparison of mass obtained from FTIR with mass loss of wood from load cell for the pyrolysis of pine wood at different heat fluxes

Yields of all components seemed to increase, but order of the components in the order of decreasing mass proportions was changed slightly, More CO yield was obtained as compared with trimethyl benzene, proportion of formaldehyde increased as compared with acetic acid, guaiacol and acrolein were also among noticeable. In the test at 20 kW/m^2 (Figure 6.12), the major components detected by FTIR in order of decreasing mass proportions were H_2O , CO_2 , formic acid, xylene, CO , trimethylbenzene, formaldehyde, acetic acid, acrolein and furfural.

It can be seen that formic acid dominates the emissions, furfural is also noticeable at this condition.

Major components in test at 25 kW/m² (Figure 6.13) are same as those observed at 20 kW/m², the only difference being that CO was more dominant as compared to xylene.

H₂ is not recorded by the FTIR. Literature [9, 108] has shown that at low temperature studied in the present work, the yield of H₂ is negligible for biomass as well as individual components of biomass i.e. hemicellulose, cellulose and lignin.

FTIR gases composition was converted to mass and cumulative mass over 10000 s for all tests and it was found in very good agreement with the mass loss of wood obtained from the load cell as shown in the Figure 6.14.

Figure 6.14 shows that mass loss from load cell and mass emissions recorded by the FTIR were in very good agreement upto 7000s in tests at 10 and 15 kW/m² and upto 5000 s in tests at 20 and 25 kW/m², however, up to this time almost all volatiles have been released from the sample.

In order to check the material balance, elemental balance was also performed, C, H, O and N was calculated from all the species recorded by FTIR, TGA and elemental analysis of the left over chars was performed (

Table 6.1), for tests at heat flux 10 and 15 kW/m², top and bottom layers of the residue was analysed separately.

Table 6.2 shows the elemental balance, last two columns of the table compare the elements obtained by the difference of raw wood and char with elements obtained from FTIR. There is very good agreement of elemental balance for tests at heat flux 20 and 25 kW/m² and less agreement for tests at lower heat flux. As there is some error in the overall material balance, that is also reflected in the elemental balance.

Table 6.1 Elemental, proximate analysis and CV of char/residue left after pyrolysis of pine wood at different heat flux

Pine residue wood/char	N wt% (ar)	C wt% (ar)	H wt% (ar)	O wt% (ar)	% wt Moisture	% wt VM (ar)	% wt FC (ar)	% wt Ash	% N daf	% C daf	% H daf	% O daf	CV MJ/kg
25 kW/m ²	0.14	78.31	3.25	4.62	2.15	14.39	71.94	11.53	0.17	90.71	3.77	5.36	31.11
20 kW/m ²	0.12	76.52	3.79	14.49	3.01	18.12	76.80	2.07	0.13	80.61	4.00	15.27	30.56
Top layer 15 kW/m ²	0.10	69.36	4.03	15.17	2.91	25.79	62.88	8.42	0.11	78.23	4.55	17.11	28.03
Bottom layer 15 kW/m ²	0.04	56.57	5.34	34.09	1.77	69.88	26.16	2.19	0.05	58.90	5.56	35.50	22.87
Top layer 10 kW/m ²	0.05	66.02	4.94	24.50	1.34	44.67	50.85	3.15	0.05	69.12	5.18	25.65	26.63
Bottom layer 10 kW/m ²	0.04	56.57	5.34	30.78	3.64	77.26	15.47	3.63	0.05	61.00	5.76	33.19	23.64

Table 6.2 Elemental balance for pine wood pyrolysis (as received basis)

25 kW/m ² (ar)	Wood (114.49 g)	Char (29.84 g)	Difference (g)	Elements from FTIR (g)
C	51.61	23.37	28.25	31.98
O	48.40	1.38	47.02	50.90
H	6.50	0.97	5.53	6.85
N	0.23	0.03	0.20	0.23
20 kW/m ²	Wood (117.94 g)	Char (32.62 g)		
C	53.17	24.96	28.21	32.76
O	49.87	4.73	45.14	49.59
H	6.70	1.24	5.46	6.70
N	0.24	0.04	0.20	0.19
15 kW/m ²	Wood (118.3 g)	Char (43 g)		
C	53.33	24.32	29.01	25.84
O	50.01	14.66	35.35	44.81
H	6.72	2.30	4.42	6.11
N	0.24	0.02	0.22	0.20
10 kW/m ²	Wood (116 g)	Char (74.9 g)		
C	52.29	42.37	9.93	14.88
O	49.04	23.05	25.99	23.60
H	6.59	4.00	2.59	3.11
N	0.23	0.03	0.20	0.13

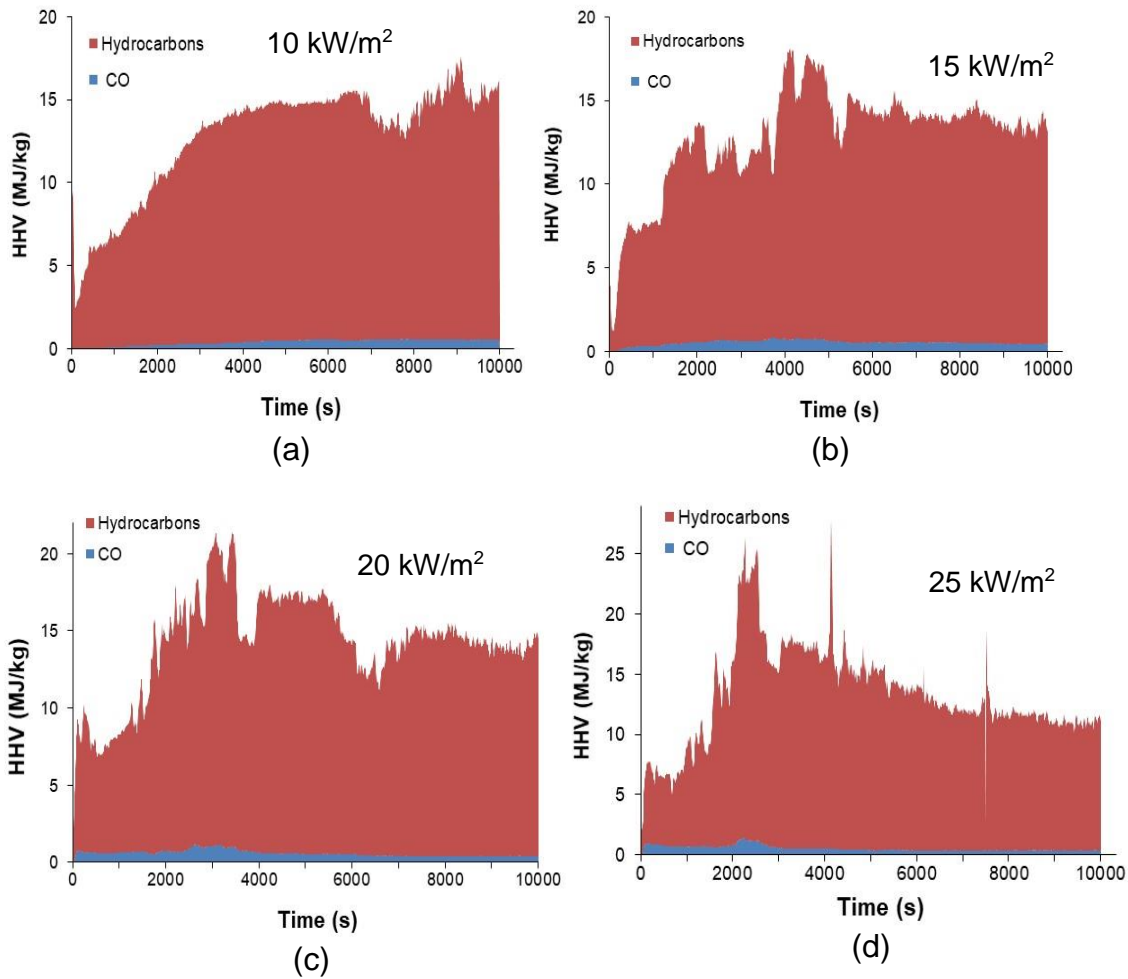


Figure 6.15 HHV of product of pyrolysis from pine wood at different heat flux

The Higher Heating Value (HHV) of the products of pyrolysis in these tests was calculated.

Figure 6.15 shows the variation of HHV (MJ/kg) of the products of pyrolysis with respect to the time of the test. Initially HHV was low due to the release of water, after 2000 it raised to higher values and average value of HHV from 2000 to 10000 s for tests at 10, 15, 20 and 25 kW/m² was 14.3, 13.9, 15.5 and 14.4 MJ/kg respectively.

Table 6.3 shows the energy balance for the pyrolysis of pine wood at different heat flux, calorific value of the char has been calculated using the correlation in [128] in equation 7 (Chapter 3). For tests at 10 and 15 kW/m², the weighted average of the CV from top and bottom char layer is used. For the gases,

average HHV over total time period is used. It can be seen that energy balance from all tests was in very good agreement from the GCV of the wood.

Table 6.4 reports the % yields of some components detected by FTIR on dry basis in tests at different heat flux. Average temperature range corresponding to these heat flux is also reported in the Table 6.4. The trends of the yields of H₂O and CO₂ is plotted in the Figure 6.16 and some hydrocarbon species and CO in Figure 6.17. There is an overall increase in the yield of H₂O and CO₂. CO₂ yield slightly decreases at heat flux 25 kW/m² as compared at 20 kW/m². Similar trend has been found by Blasi [107] with pyrolysis of big particles (cylinders) of wood where yields of CO₂ is increasing overall with some values showing an offset from the overall trend.

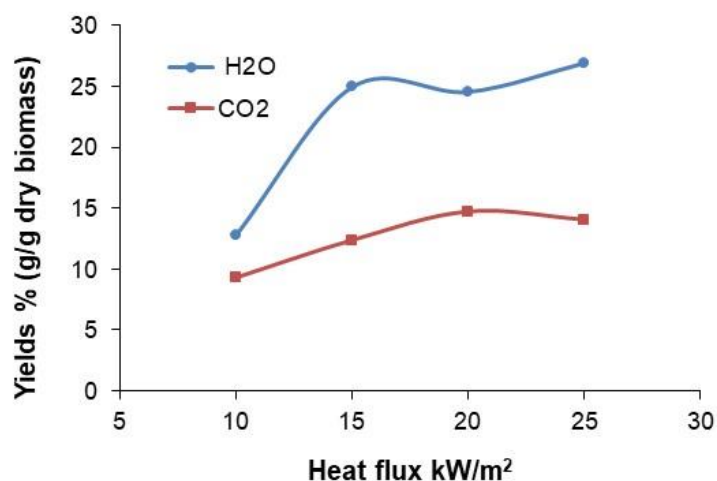


Figure 6.16 % yield of CO₂ and H₂O from pyrolysis of pine wood at different heat flux

Table 6.3 Energy balance for the pyrolysis of pine wood at different heat fluxes

25 kW/m ²	HHV MJ/kg	% Yields ratio	Energy MJ/kg biomass
Gases	13.9	72.5	10.08
Char	31.11	27.5	8.56
Total			18.63
20 kW/m ²			
Gases	14.5	71	10.30
Char	30.55	29	8.86
Total			19.15
15 kW/m ²			
Gases	13.06	62	8.04
Char	27.00	38	10.37
Total			18.41
10 kW/m ²			
Gases	13.51	32	4.32
Char	21.44	68	14.58
Total			18.90
GCV of Pine wood 18.86 MJ/kg (Table 4.1)			

Table 6.4 Yields of selected components from the pyrolysis of pine wood at different heat flux. (dry basis) (% weight)

Heat flux kW/m ²	Temp. range °C	H ₂ O	CO ₂	CO	Methane	Ethane	Propane	Formic acid	Acetic acid	Formaldehyde	Acetaldehyde	Acetylene
10	50-320	7.54	9.28	1.32	0.00	0.37	0.31	0.04	1.39	1.26	0.43	0.04
15	50-415	19.74	12.36	3.57	0.12	0.95	0.77	2.19	2.48	2.63	0.75	0.02
20	50-485	19.35	14.73	5.00	0.45	0.64	0.59	6.23	1.59	2.13	0.41	0.01
25	50-520	21.71	14.06	5.21	0.44	0.66	0.87	6.25	2.41	2.41	0.24	0.01

Heat flux kW/m ²	Temp. range °C	Benzene	Toluene	Xylene	Trimethyl- benzene	MTBE	Acrolein	Methanol	Ethanol	Propanol	Acetone	Dimethyl ether
10	50-320	0.00	1.03	3.05	2.83	0.00	0.61	0.04	0.02	0.03	0.71	0.25
15	50-415	0.05	0.94	3.88	3.15	0.70	0.92	0.56	0.50	0.67	1.57	0.13
20	50-485	0.06	1.24	5.21	4.29	1.24	1.48	0.46	0.35	0.91	1.02	0.09
25	50-520	0.02	0.65	4.90	4.05	1.14	1.83	0.41	0.34	0.56	1.03	0.10

Heat flux kW/m ²	Temp. range °C	Furfural	Furfural alcohol	Guaiacol	P-cresol	Phenol	Ethyl benzene	1-ethyl naphthalene	Naphthalene	NO	HCN
10	50-320	0.21	0.06	0.40	0.00	0.21	0.00	0.01	0.00	0.01	0.21
15	50-415	0.84	0.21	0.92	0.25	0.80	0.09	0.15	0.10	0.20	0.53
20	50-485	1.45	0.79	0.74	0.41	0.46	0.33	0.48	0.34	0.10	0.21
25	50-520	1.48	0.80	1.26	0.80	0.94	0.11	0.23	0.16	0.20	0.21

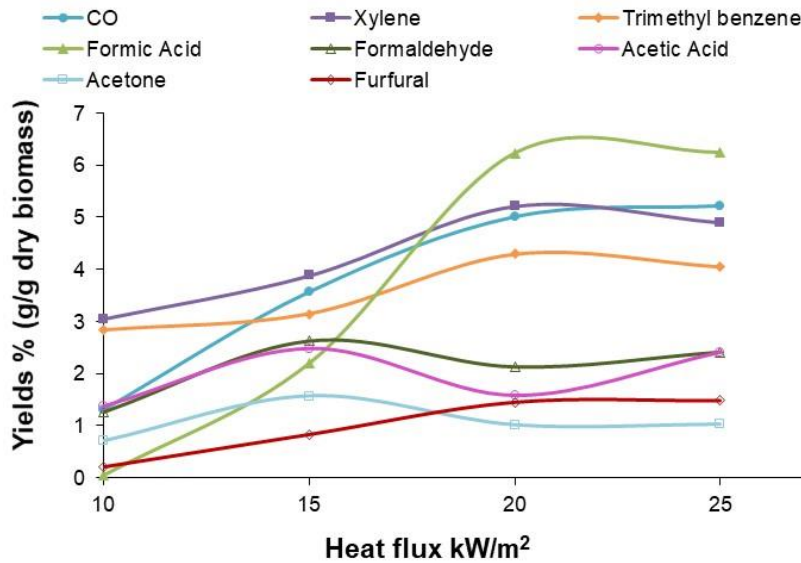


Figure 6.17 % yield of CO and some hydrocarbons from pyrolysis of pine wood at different heat flux

The yield of CO also increased with increasing heat flux. Literature shows that yield of CO is low at low temperature and lies within the range found in the present work, Scot [104] showed that yield of CO rose from 3.4 to 11 % of the mass of the wood fed as temperature increased from 500 to 600 °C, work of Yang [9] showed that high CO yield are obtained from lignin and hemicellulose above 600 °C, below 600 °C all CO produced was mainly from the decomposition of hemicellulose, cellulose contributes very little.

Yields of formaldehyde, acetic acid and acetone reached maximum at 15 kW/m² and the decreased at 20 kW/m². Formic acid showed a large increase in the yield at 20 kW/m², as formic acid was observed to be released at high temperatures as compared with other hydrocarbons. The yield of xylene and trimethyl benzene increase upto heat flux of 20 kW/m² and decreased slightly at 25 kW/m². Demirbas [92] has shown that yields of liquid products of pyrolysis decrease after reaching a maximum temperature and he found this temperature to be 800 K (527 °C) for the pyrolysis of biomass specie heating at a rate of 10 K/s however, In the work of Blasi [108], the temperature where liquid yields reach maximum was in the range from 700-750K (425-475 °C) and started decreasing after this point, yields of CO₂, CO etc. are also comparable with the present work.

In the present work methane was not found to be one of the major products of pyrolysis. However, the yield of methane increased with increasing temperature (Table 6.4), Also yield of other alkanes, e.g. ethane and propane was higher than that of methane. Yields of acetylene and benzene were very low.

The % yields of non-condensable gases, chars and liquids (components that would condense at room temperature) obtained from FTIR are shown in the Figure 6.18 for comparison with tests performed in furnace rig (results are shown in Chapter 7). In the test at 10kW/m² although the wood average temperature was slightly higher than 300 °C, but even after 10000 s most of the wood was still unconverted to char and the residue left is shown in the Appendix B Figure B.2 and the yields plotted at these points are not the actual yield of chars and liquids that should be obtained if the conversion was complete. Figure B.3 - Figure B.5 in Appendix B show the left over chars for tests at 15, 20 and 25 kW/m².

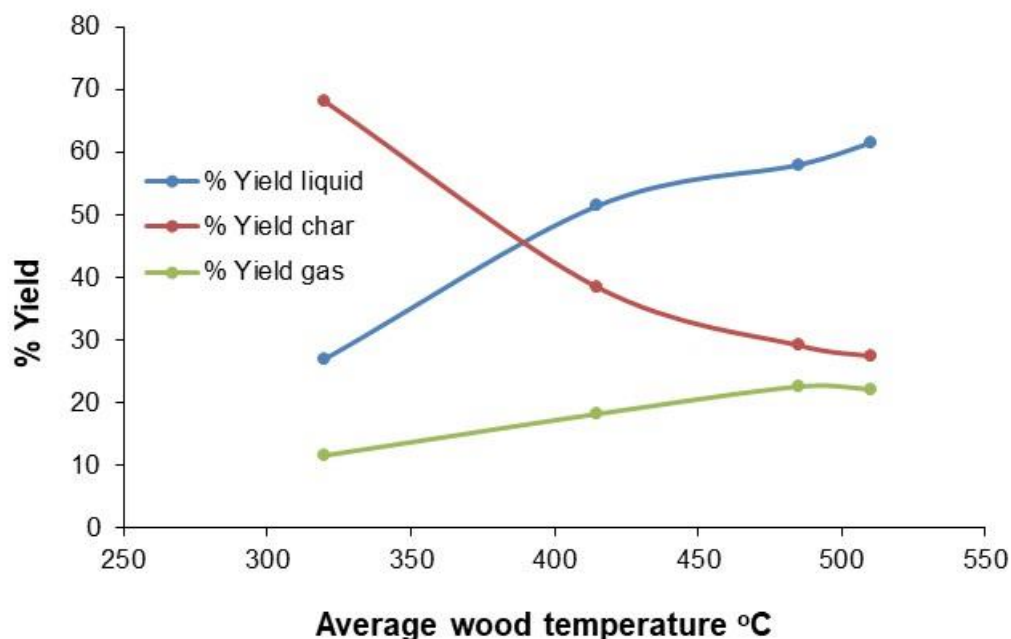


Figure 6.18 % yield for liquids (at room temperature) , gases and chars for the pyrolysis of pine wood at different temperatures

6.3 Effect of biomass types on pyrolysis

For the comparison of pyrolysis behaviour of different biomass species all tests were performed at heat flux of 20 kW/m² as in the test with pine wood it was seen

that temperature of the wood covered the TGA temperature range for the release of maximum volatiles. Test time was chosen to be 5000 s because in rests with pine wood at this heat flux almost all the volatiles were released upto 5000 s.

Mass loss vs time for the samples is shown in the Figure 6.19. Release of volatiles from some biomass was slow while from others it was rapid. devolatilization of eucalyptus and acacia was very different from each other. Mass loss from eucalyptus was gradual and the sharp change in the slop of the curve appeared at 2300 s where rate of release of volatiles speeds up while in case of acacia wood, slope of curve changes at 1400 s and slope of the curve was very steep showing rapid release of the volatiles. More char was obtained from the eucalyptus wood as compared with acacia wood at the end of the test.

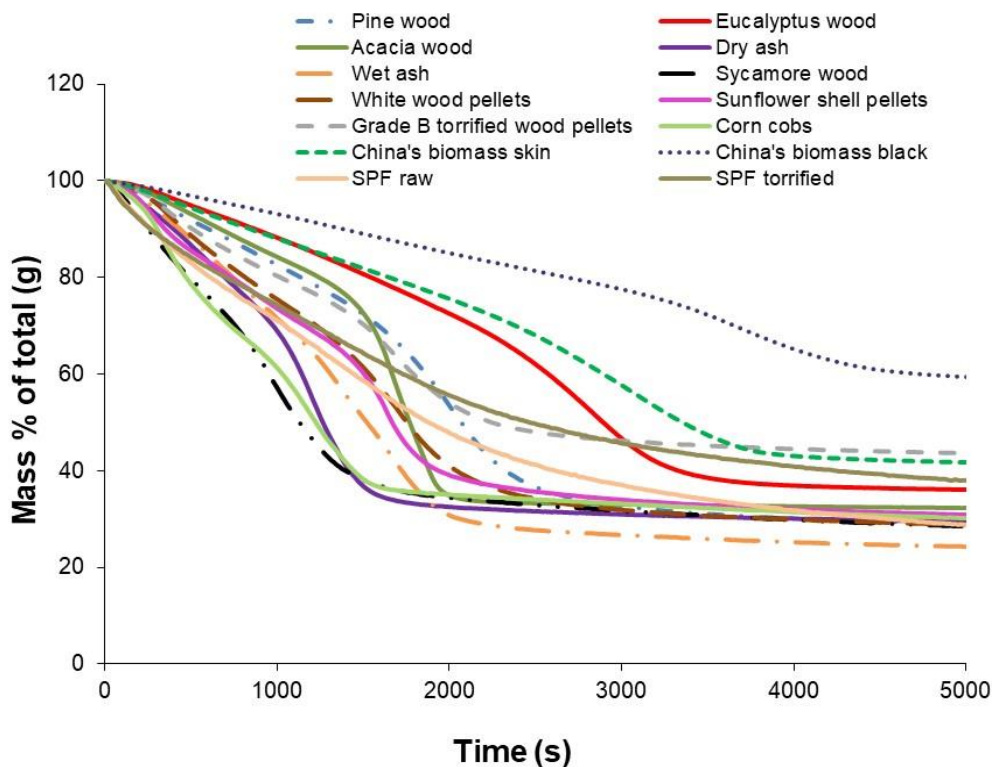


Figure 6.19 Mass vs time for pyrolysis of biomass at heat flux 20 kW/m²

More char was obtained from the eucalyptus wood as compared with acacia wood at the end of the test. It can be seen from the Table 4.2 that the density of acacia wood was 5% higher than that from eucalyptus wood, but the size of the wood was same, i.e. a block of 20x20x100 mm, it can also be seen from the Table 4.1 that the volatile matter of acacia wood was higher than that from

eucalyptus and the ash contents of eucalyptus wood were much higher than that from ash wood.

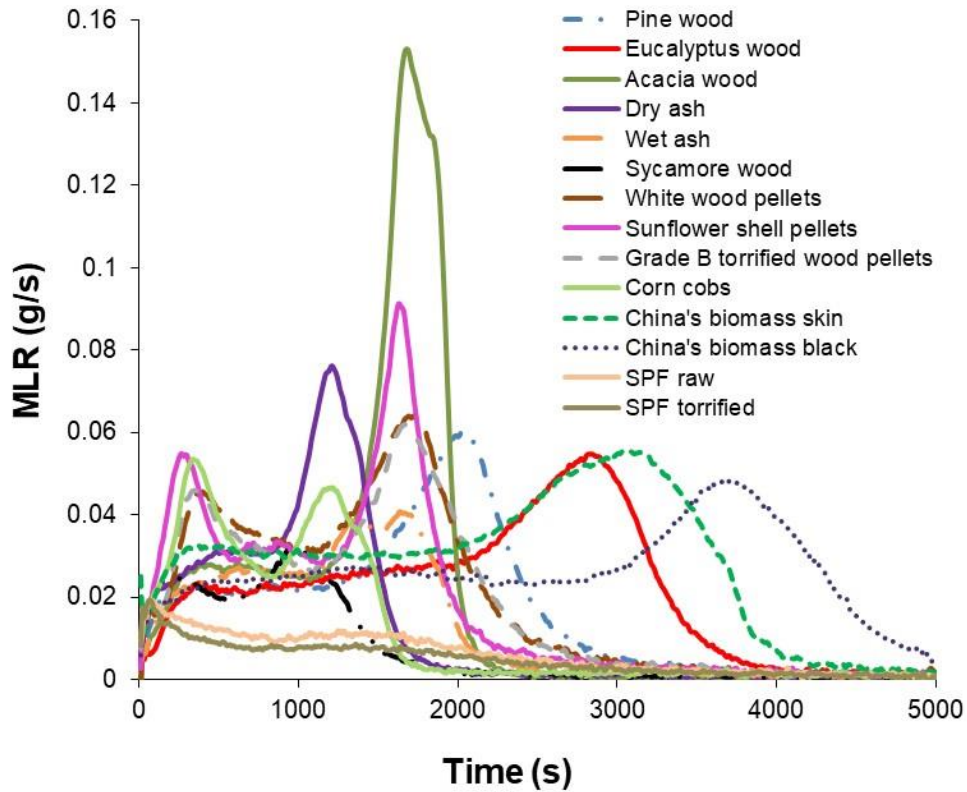


Figure 6.20 Mass loss rate (g/s) vs time for pyrolysis of biomass at heat flux 20 kW/m²

Density of china's biomass black is highest of all biomass species and it released volatiles gradually and slowly and over the larger span of time as compared with other biomasses. 40.7 % of total mass was lost during 5000 s. TGA also shows that 43% volatiles were released on as received basis for this biomass.

Density of china's biomass skin is comparable with the eucalyptus wood, but initial weight and size of the sample were different. Release of volatiles was comparably fast from dry ash and sycamore wood almost all volatiles were released upto 2000 s. Mass loss rate (Figure 6.20) for all woods was initially constant and then raised to a peak value by changing in the slope of mass loss curve and then fell to a very low value. For pellets (white wood pellets, sunflower shell pellets, grade B torrefied wood pellets), sycamore wood and corn cobs there were two peaks of the mass loss rate, initial peak was low while second

peak was large. Mass loss from grade B torrefied wood pellets was 60% while from other pellets was 70% of the total mass loss. It can be seen from Table 4.1 that ash contents of grade B torrefied wood pellets are very as compared with other pellets resulting in less mass loss as compared with other pellets.

Mass loss from SPF raw and torrefied was very slow and gradual over 2000 s.

6.4 FTIR results for the pyrolysis of different biomass species

The release of some of the major products of pyrolysis with respect to time is shown in Figure 6.21. It can be seen that during 5000 s most of the volatiles and water has been released. Biomass was not dried before the test and the water vapour concentration is the sum of initial moisture contents of the biomass as well as the water produced due to the breakup of the structure of the wood and biomass.

Peak concentration of CO₂ was obtained with acacia wood and the reason was the sudden releases of volatiles in short span of time caused the concentrations to reach peak values and the calculated yield would show the actual contribution due to CO₂ in acacia wood.

It was seen previously that formic acid was released from the pine wood between average temperature of 350 – 400 °C. It can be seen that eucalyptus wood started releasing formic acid at about 2500 s (Figure 6.21), from china's biomass skin and black it started releasing at 2300 s and 3700 s respectively. It can be concluded that these woods reach at average temperature of 350 – 400 °C at time these times.

White wood pellets showed the maximum concentration of formaldehyde. Most researchers explain as different peaks of mass loss rate and species concentration due to the different decomposition temperatures for hemicellulose, cellulose and lignin, initial peaks are at low temperatures and are attributed towards the decomposition of hemicellulose. e.g initial peaks of all emissions shown below are due to the hemicellulose decomposition in the biomass.

Xylene is plotted as sum of o-xylene, m-xylene and p-xylene and Trimethyl benzene (TMB) as sum of 1,2,3- TMB, 1,2,4- TMB and 1,3,5 TMB.

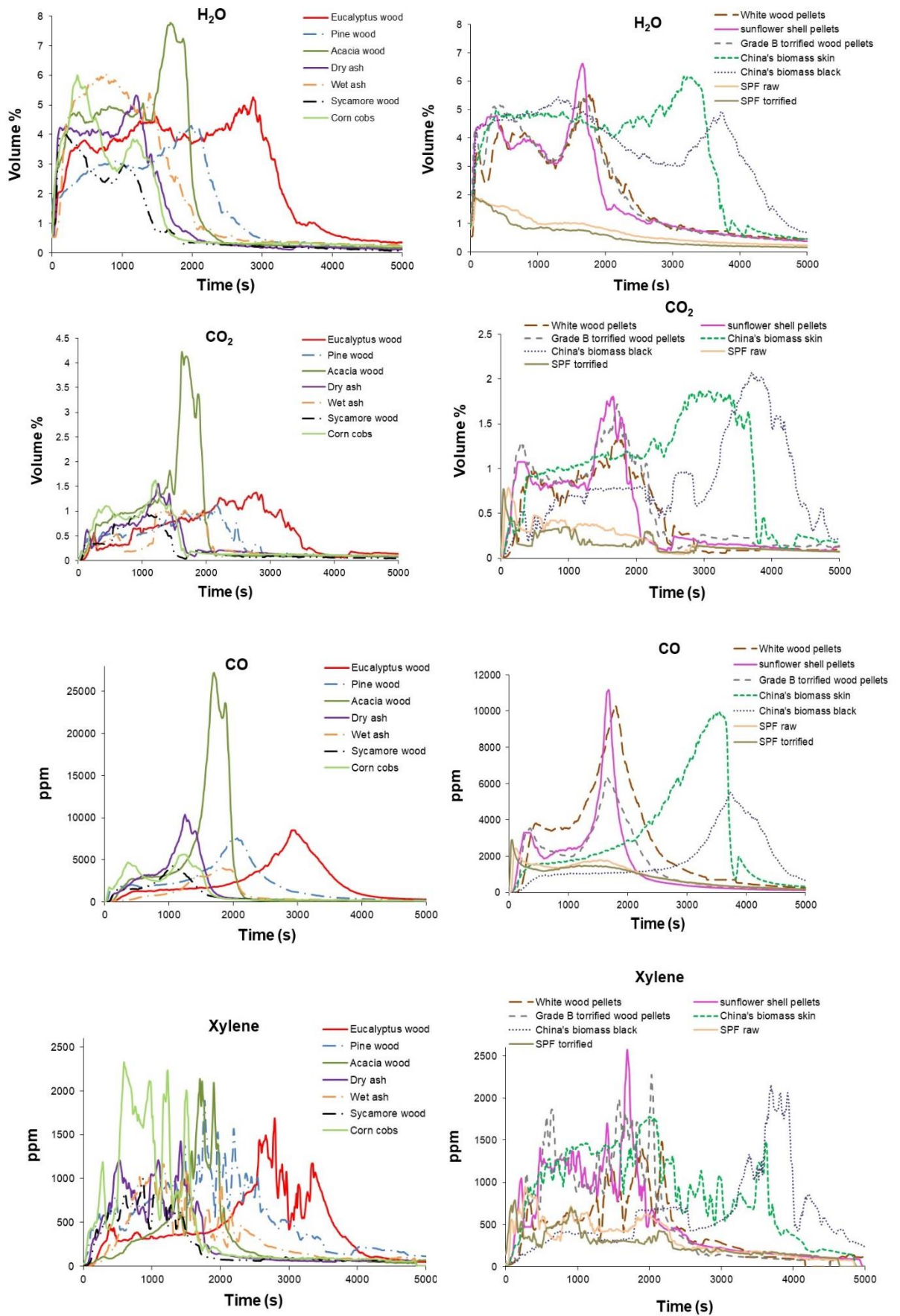


Figure 6.21 Product gases concentration recorded from FTIR as a function of time for the of pyrolysis of different biomass at heat flux 20 kW/m²

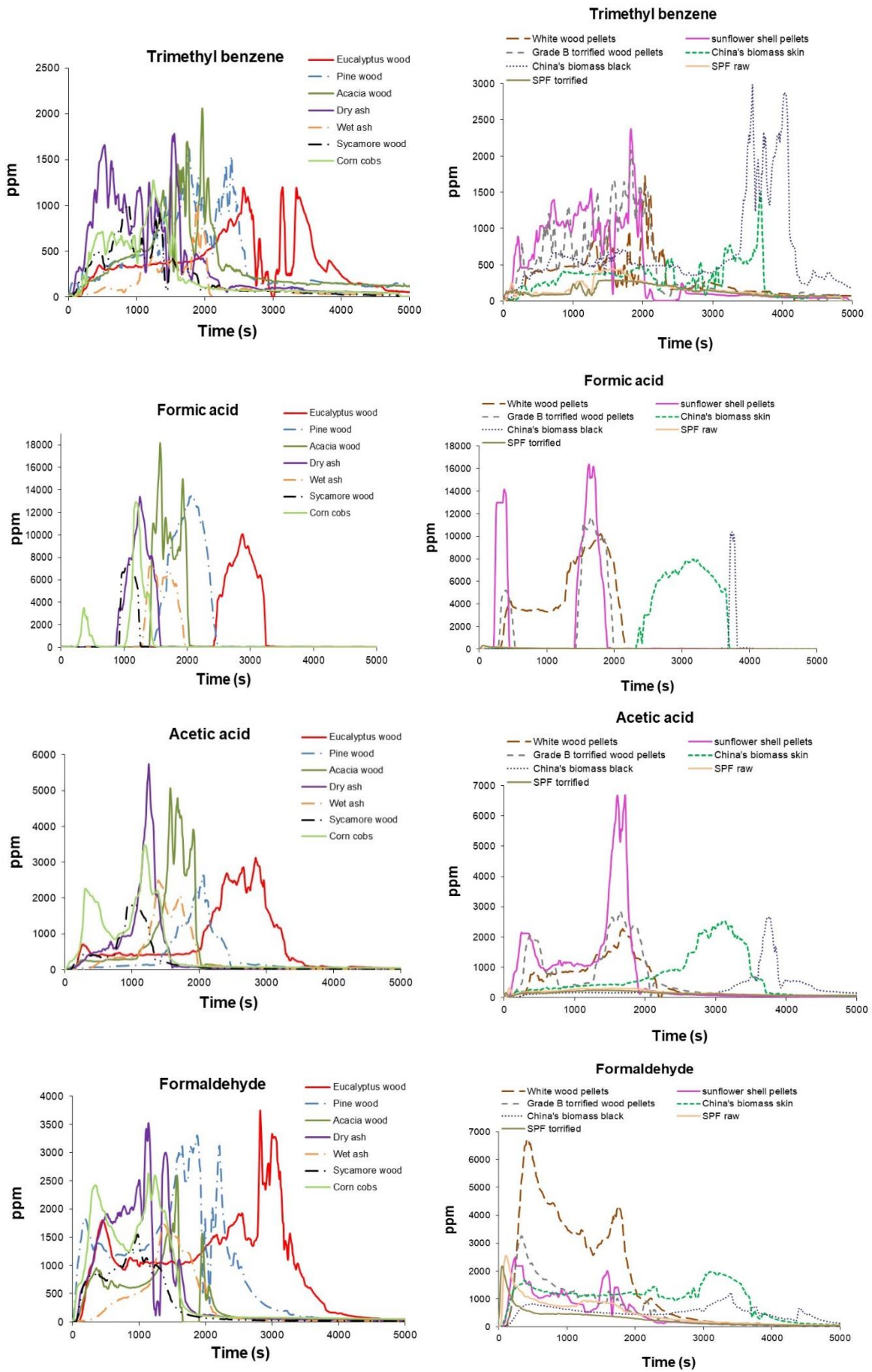


Figure 6.21 (continued)

6.4.1 Product yields

The contribution of individual gases towards the total mass loss from a biomass can be seen in the cumulative mass yields plots in

Figure 6.22 (wet basis). Water is the major product of pyrolysis. The released water contains the water contribution from the moisture contents of the biomass as well. CO₂ is the second major product of pyrolysis. Order of other components is different for different biomasses. Unlike pine wood, CO is the third main components in the pyrolysis of acacia wood, eucalyptus wood and china's biomass skin.

Formic acid is the third major component in the pyrolysis of pine wood (Figure 6.12), dry ash, white wood pellets and sunflower shell pellets while xylene was the third major product for the pyrolysis of corn cobs, Grade B torrefied pellets, SPF raw and SPF torrefied. Corn cobs and sunflower shell pellets produced more acetic acid as compared with other biomasses. Highest yield of formaldehyde was obtained with white wood pellets.

Formaldehyde was the sixth dominant product by mass in the pyrolysis of SPF raw and SPF torrefied. Yield of guaiacol was found to be higher in the pyrolysis of biomass samples having small particle size, e.g. SPF raw and SPF torrefied. Similarly acetaldehyde was also present in SPF raw and torrefied and reason could only be the particle size of the sample. It can be concluded that particle size is important and effects the yields of the products of pyrolysis.

Dry basis yields of selected components are reported in the Table 6.5. Different relative yields of some gaseous or condensable components can only be explained by the ratio of hemicellulose, cellulose and lignin in the biomass.

Highest yield of CO₂ was obtained with acacia wood, experiment was repeated twice to check the CO₂ yield and results were showing similar yields, cellulose contents of acacia wood were higher than other wood except dry ash and china's biomass skin. Another thing noted was that char yield of the acacia wood was less than that from eucalyptus wood but lignin contents were higher than that from eucalyptus wood. TGA showed (Table 4.1) that acacia wood had slightly

higher volatile matter as compared with eucalyptus wood and ash contents of eucalyptus wood were much higher than that of acacia wood.

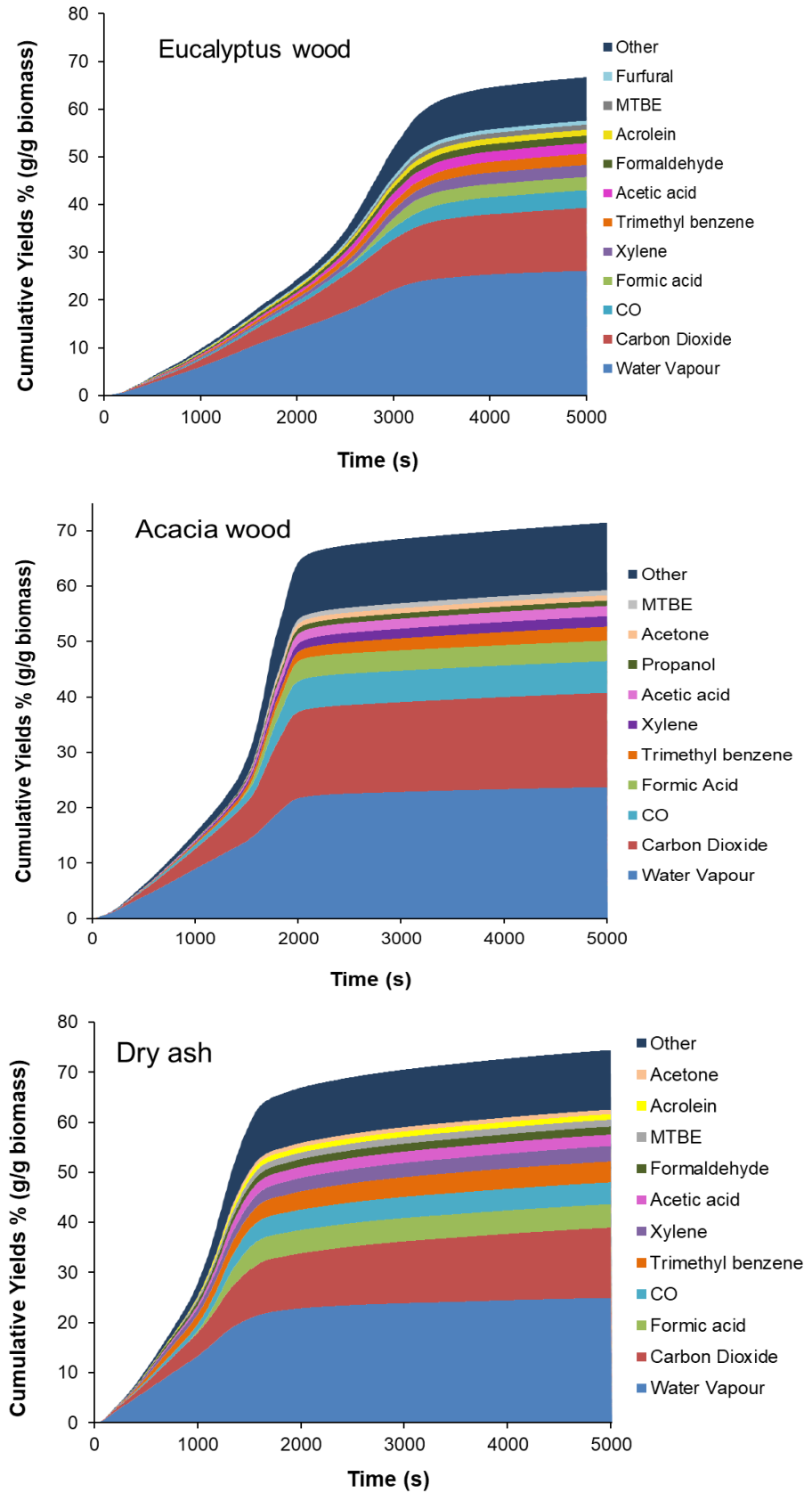


Figure 6.22 comparison of cumulative yields of products of pyrolysis from different biomass at heat flux 20kW/m^2

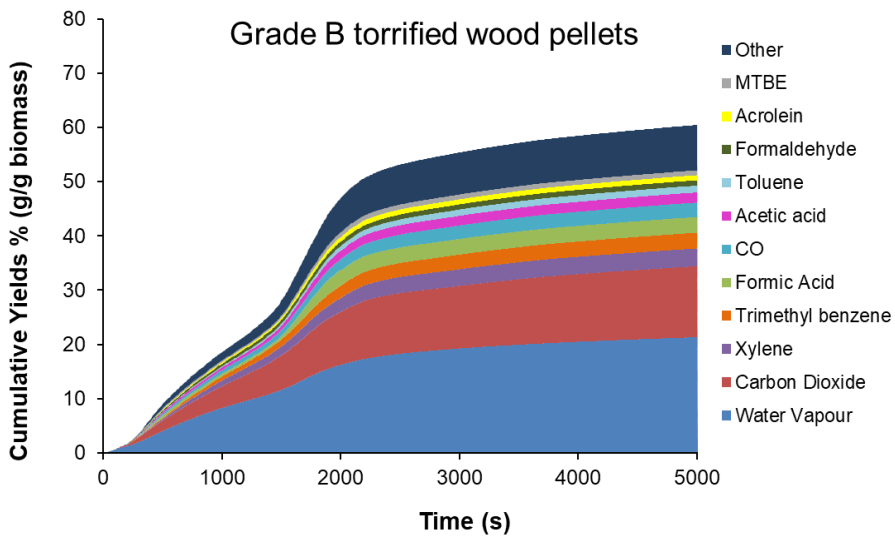
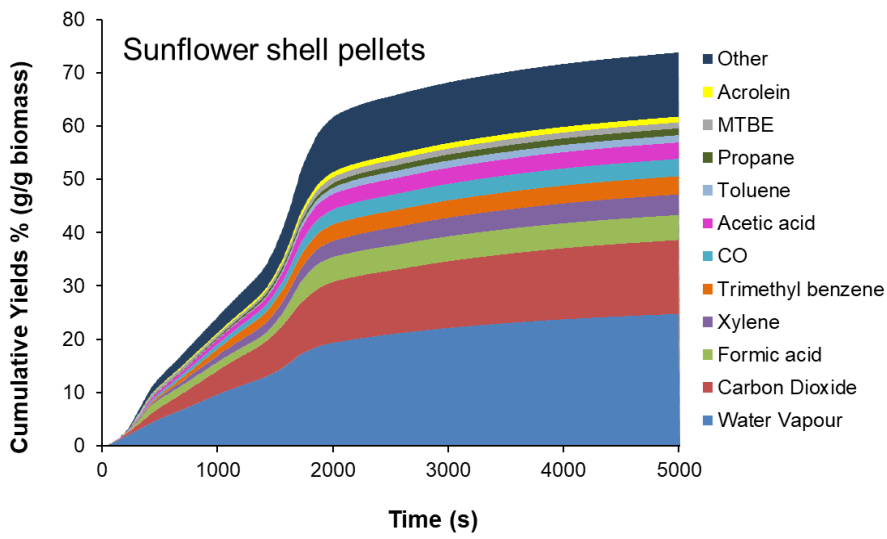
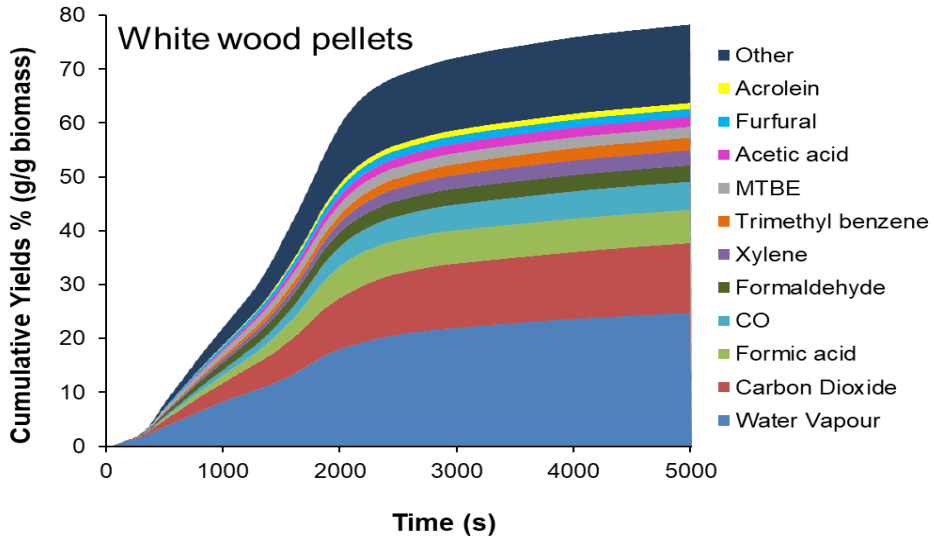


Figure: 6.22 (continued)

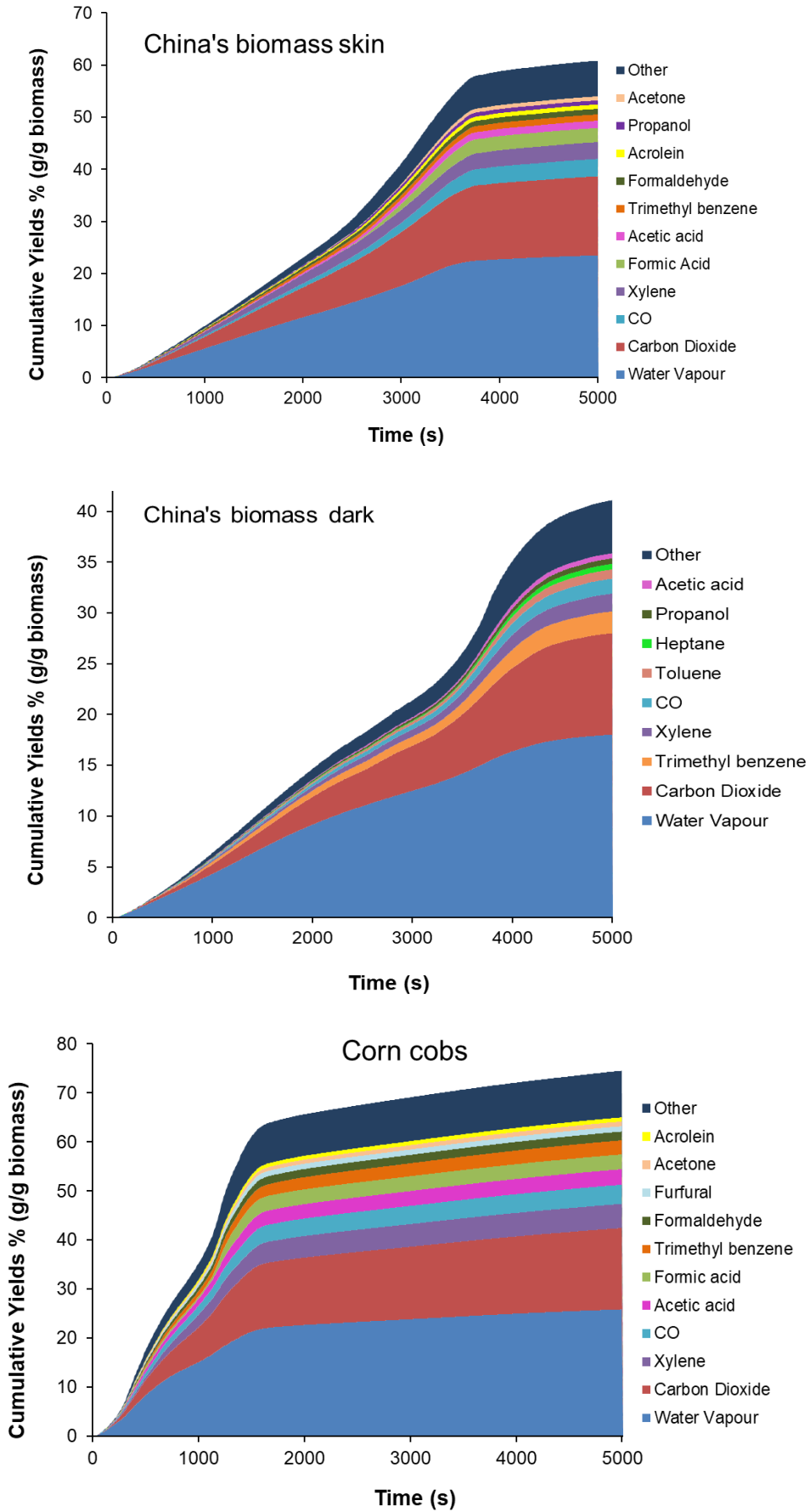


Figure: 6.22 (continued)

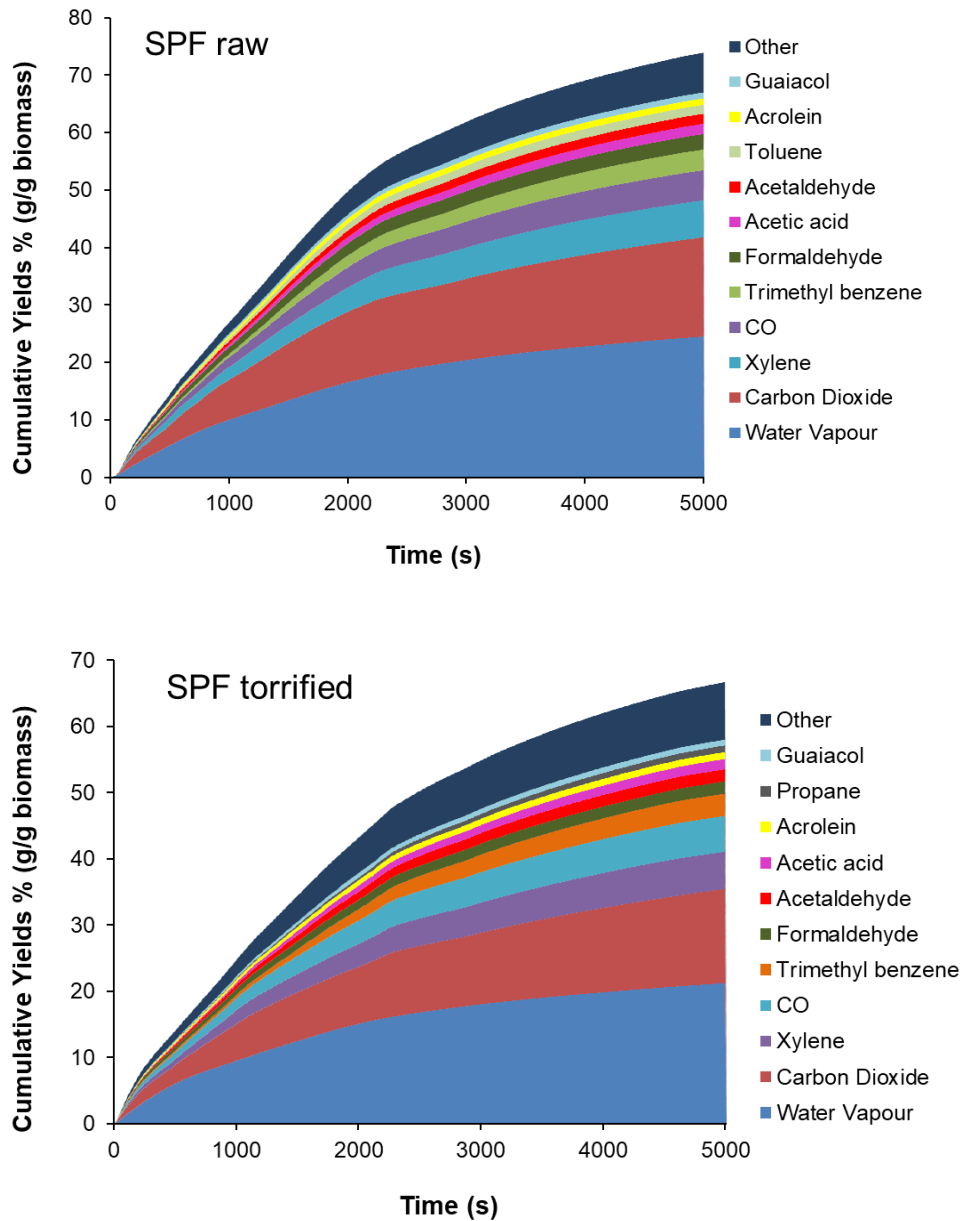


Figure: 6.22 (continued)

High yield of CO₂ was obtained with SPR raw, corn cobs and sycamore wood as well. Table 4.2 shows that all these biomass have more hemicellulose contents as compared with other biomasses studied for the pyrolysis. And literature [9] shows that hemicellulose produce highest CO₂ at low temperature. Also some researchers [149] have shown that hemicellulose produced more acid as compared to lignin and cellulose, while from Figure 6.23, it was seen that white wood pellets, sunflower shell pellets and pine wood have highest yields of acids and by looking back at Table 4.2, it can be seen that these biomass do not have highest levels of hemicellulose among the studied samples.

Table 6.5 (a) Yields (% weight dry biomass) of the some products of pyrolysis of different biomass at heat flux 20 kW/m²

Biomass	Temp. °C	H ₂ O	CO ₂	CO	Methane	Ethane	Propane	Formic acid	Acetic acid	Formaldehyde	Acetaldehyde	Acetylene
Pine wood	50-485	19.35	14.73	5.00	0.45	0.64	0.59	6.23	1.59	2.13	0.41	0.01
Eucalyptus wood		21.52	13.18	3.70	0.48	0.59	0.44	2.96	2.36	1.68	0.13	0.01
Acacia wood		19.37	18.07	6.08	0.29	0.59	0.68	3.90	1.98	0.61	0.95	0.00
Dry ash		21.14	14.79	4.61	0.35	0.41	0.52	4.93	2.42	1.69	0.58	0.01
Wet ash		32.97	15.55	3.15	0.23	0.63	0.62	3.91	2.32	1.07	0.26	0.00
Sycamore wood		21.79	17.49	4.32	0.30	0.48	0.78	3.22	2.45	1.50	0.86	0.02
Sunflower shell pellets		20.22	14.78	3.48	0.35	0.51	1.37	5.00	3.27	1.10	0.39	0.03
White wood pellets		21.54	13.54	5.45	0.39	0.39	0.77	6.48	1.94	3.14	0.14	0.01
Grade B torrefied wood Pellets		16.84	13.89	2.83	0.24	0.30	0.55	3.07	1.98	1.04	0.20	0.01
Corn cobs		20.83	17.83	4.20	0.15	0.88	0.48	3.23	3.40	1.92	0.11	0.02
China's biomass skin		18.35	16.34	3.59	0.16	0.30	0.32	2.93	1.51	2.10	0.11	0.01
China's biomass black		12.11	10.78	1.59	0.09	0.27	0.30	0.30	0.54	0.46	0.44	0.00
SPF raw		20.02	18.39	5.57	0.11	0.94	0.82	0.31	1.92	2.86	1.85	0.00
SPF torrefied		17.05	15.02	5.74	0.18	0.86	1.07	0.37	1.65	1.97	1.93	0.00

Table 6.6 (b) Yields (% weight dry biomass) of the some products of pyrolysis of different biomass at heat flux 20 kW/m²

Biomass	Temp. °C	Benzene	Toluene	Xylene	Trimethyl- benzene	MTBE	Acrolein	Methanol	Ethanol	Propanol	Acetone	Dimethyl ether
Pine wood	50-485	0.06	1.24	5.21	4.29	1.24	1.48	0.46	0.35	0.91	1.02	0.09
Eucalyptus wood		0.03	0.42	2.68	2.53	1.16	1.31	0.72	0.47	0.82	0.52	0.18
Acacia wood		0.33	0.66	2.01	2.69	0.97	0.91	0.80	0.29	1.03	1.01	0.20
Dry ash		0.06	0.86	3.24	4.39	1.44	1.17	0.65	0.55	0.66	0.97	0.27
Wet ash		0.02	1.03	4.04	1.77	1.02	1.19	0.72	0.30	0.99	1.16	0.18
Sycamore wood		0.01	1.07	4.06	3.99	0.82	1.07	0.50	0.32	0.79	1.30	0.19
Sunflower shell pellets		0.05	1.44	4.11	3.63	1.20	1.14	0.89	0.60	0.98	0.97	0.24
White wood pellets		0.03	0.55	2.95	2.43	2.14	1.16	0.60	0.75	1.02	1.06	0.12
Grade B torrefied wood Pellets		0.00	1.34	3.47	3.08	0.96	0.99	0.47	0.64	0.83	0.58	0.15
Corn cobs		0.00	0.48	5.28	3.09	0.77	0.90	0.63	0.16	0.84	1.04	0.28
China's biomass skin		0.01	0.80	3.46	1.30	0.35	0.90	0.29	0.48	0.85	0.83	0.34
China's biomass black		0.01	0.98	1.89	2.32	0.15	0.47	0.33	0.39	0.58	0.32	0.06
SPF raw		0.01	1.65	6.84	3.83	0.06	1.20	0.25	0.49	0.44	0.76	0.15
SPF torrefied		0.00	1.28	5.94	3.54	0.08	1.11	0.34	0.59	0.57	0.90	0.16

Table 6.7 (c) Yields (% weight dry biomass) of the some products of pyrolysis of different biomass at heat flux 20 kW/m²

Biomass	Temp. °C	Furfural	Furfural alcohol	Guaiacol	P-cresol	Phenol	Ethyl benzene	1-ethyl naphthalene	Naphthalene	NO	HCN	Char
Pine wood	50-485	1.45	0.79	0.74	0.41	0.46	0.33	0.48	0.34	0.10	0.21	29.12
Eucalyptus wood		0.90	0.43	0.52	0.41	0.47	0.18	0.33	0.32	0.09	0.21	37.82
Acacia wood		0.49	0.56	0.45	0.45	0.47	0.32	0.84	0.51	0.01	0.18	34.08
Dry ash		0.74	0.76	0.57	0.51	0.42	0.42	0.45	0.36	0.23	0.35	31.10
Wet ash		1.19	0.84	0.82	0.73	0.40	0.12	0.11	0.25	0.20	0.21	26.44
Sycamore wood		0.94	0.34	0.81	0.65	0.57	0.05	0.19	0.31	0.12	0.58	30.77
Sunflower shell pellets		0.83	0.51	0.83	0.57	1.08	0.45	0.50	0.36	0.28	0.40	32.50
White wood pellets		1.53	0.63	0.93	0.76	0.48	0.16	0.40	0.33	0.23	0.35	29.77
Grade B torrefied wood Pellets		0.38	0.39	0.56	0.32	0.44	0.09	0.35	0.30	0.17	0.32	46.39
Corn cobs		1.17	0.34	0.80	0.49	0.57	0.02	0.20	0.11	0.16	0.42	32.24
China's biomass skin		0.61	0.45	0.36	0.23	0.32	0.29	0.34	0.22	0.38	0.27	44.78
China's biomass black		0.28	0.16	0.30	0.10	0.24	0.03	0.17	0.13	0.03	0.17	62.26
SPF raw		0.15	0.28	1.11	0.00	0.58	0.04	0.25	0.17	0.00	0.47	30.21
SPF torrefied		0.10	0.49	0.91	0.00	0.68	0.07	0.50	0.36	0.00	0.45	40.16

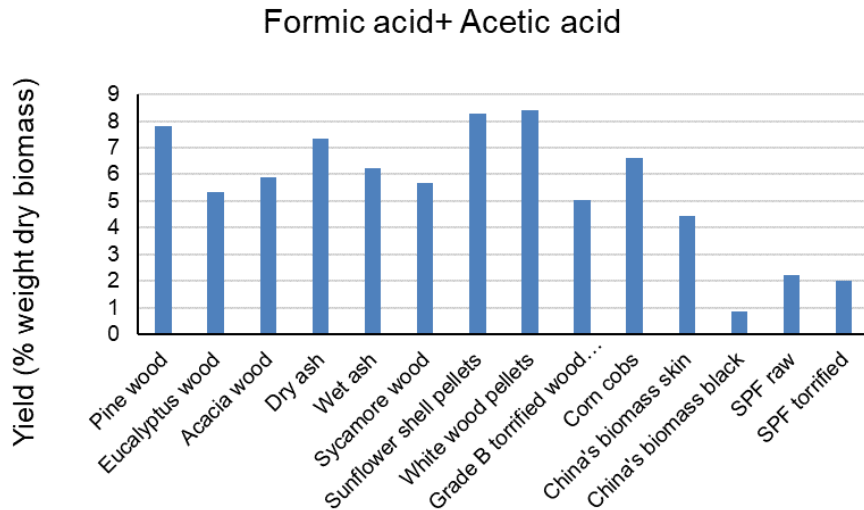


Figure 6.23 Yield (% weight) of acids with pyrolysis of different biomass

Highest yield of alcohols (methanol, ethanol and propanol) Figure 6.24 was observed with sunflower shell pellets and white wood pellets, SPF raw showed lowest yield of alcohols. SPF raw has low cellulose contents and high hemicellulose contents as compared with these two pellets. But it was also seen in the Figure 4.3-4.4 that eucalyptus wood and sunflower shell pellets were very close chemically, similarly acacia wood and white wood pellets were close chemically, but it can be seen that yields of the products are variable.

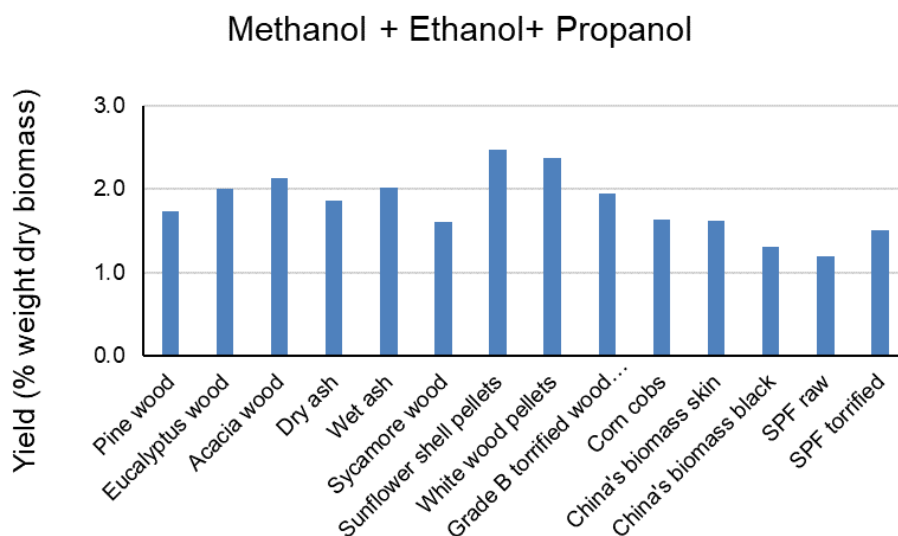


Figure 6.24 Yield (% weight) of alcohols with pyrolysis of different biomass

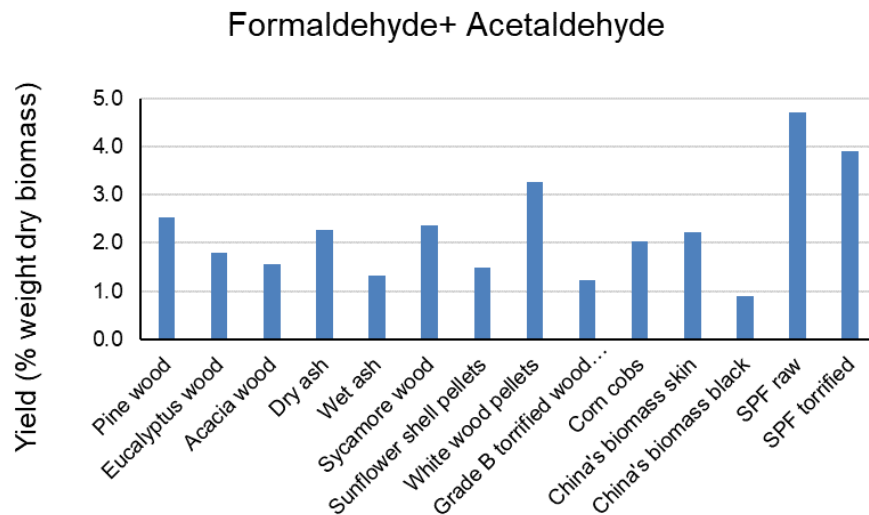


Figure 6.25 Yield (% weight) of aldehydes with pyrolysis of different biomass

Highest yield of aldehydes Figure 6.25 were obtained with SPF raw and torrefied and the only factor that might have caused this is the particle size of the sample that was very small as compares with others.

It is found in the literature that lignin of biomass has high contribution towards phenols, guaiacols and cresols etc. Highest yield of these components was obtained with sunflower shell pellets. Although the calculated % of lignin in the sunflower shell is same as most of the others but it is a known fact that shell usually have high lignin contents to give strength to the shell body.

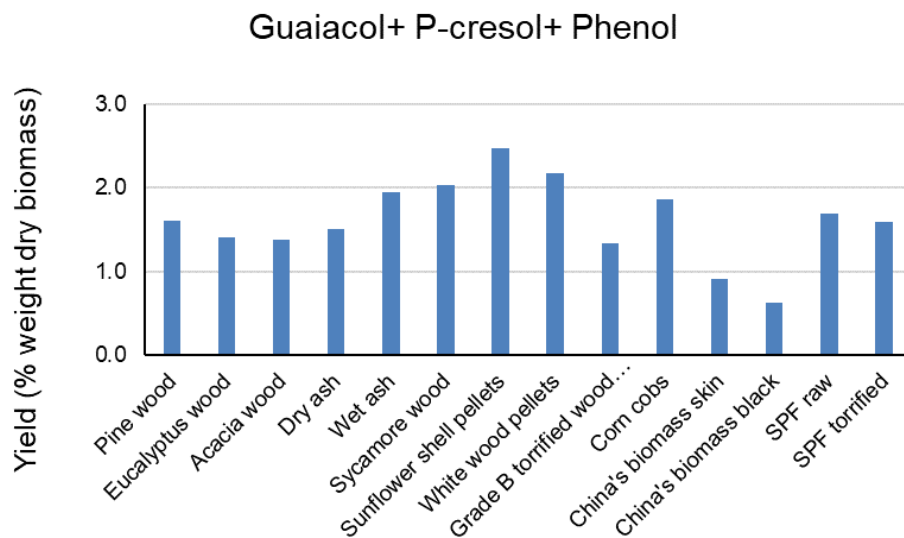


Figure 6.26 Yield (% weight) of phenols and cresols of different biomass

6.5 Temperature distribution inside different woods

Tests were performed with thermocouples inserted 3mm from top edge and 3mm from bottom edge in different wood type to observe the temperature distribution and to relate temperature with mass loss rate and emission of different gaseous species. Acacia wood, dry ash and sycamore wood were selected for the tests, pine was done before. Table 4.2 shows that these wood vary in density to large extend from each other.

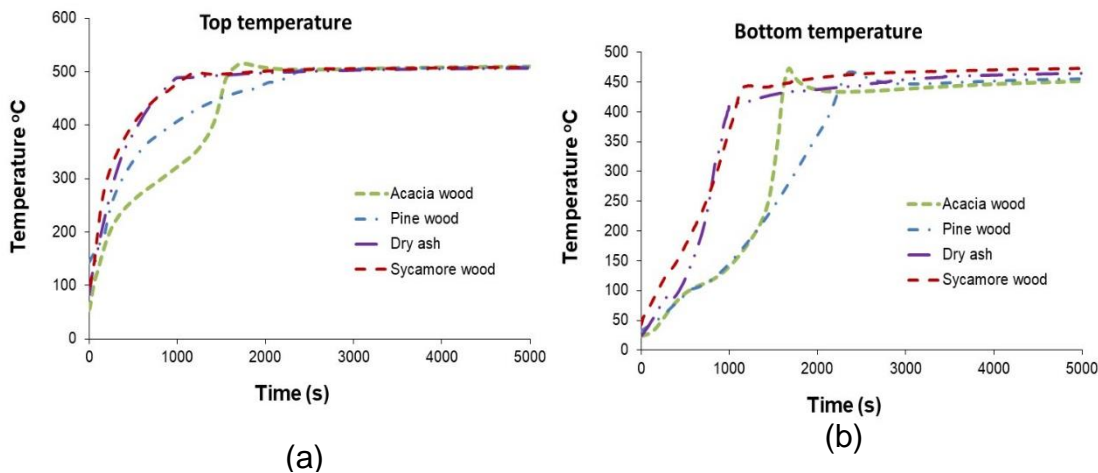


Figure 6.27 Temperature of woods (a) 3mm from top surface (b) 3mm from bottom surface

Comparison of the variation of top temperature (3mm from top surface) and bottom temperature (3mm from bottom) can be seen in Figure 6.27. It can be seen that final top temperature for all woods was same as that was depending upon the source (heater) temperature while the bottom final temperature for all the woods was slightly different depending upon the density of the wood. Dry ash and sycamore wood were round shape and reached the final temperatures quickly as compared with pine and acacia wood. Pine wood's top and bottom temperature raised gradually. Temperature profiles for acacia wood were different from the others and these types of profiles were seen in literature [107] for beech wood and redwood. Acacia wood's top and bottom temperature reached the peak in about 1700 s and it happened quickly as compared with pine wood.

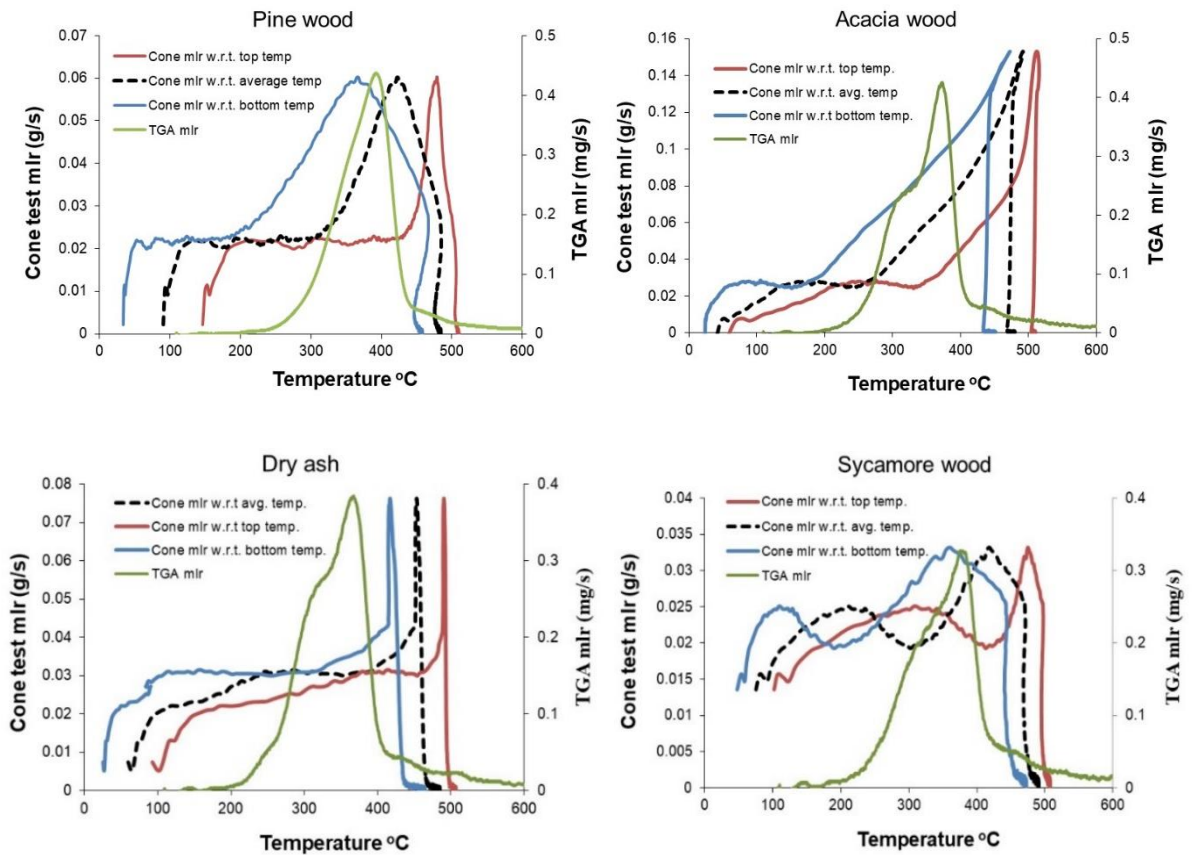


Figure 6.28 Cone test mlr and TGA mass loss rate vs time for different wood types.

Mass loss rate of each wood from cone tests was plotted vs, top bottom and average temperature and TGA mass loss rate curve was also plotted vs temp. for pine (Figure 6.28) , acacia and dry as there was one period of almost constant mass loss rate, and in case of sycamore wood there was an initial peak instead if constant mass loss rate. There was an increase in the mass loss rate towards the peak mass loss rate shape of this mass loss vs temp is different for all woods for pine wood its very wide area showing gradual increase and gradual decrease of mass loss rate, while in case of acacia wood there was a gradual increase but then ass loss increased suddenly and suddenly fell down. In case of dry ash the increase in the mass loss rate towards peak and falling down was over very narrow temperature range and in case of sycamore it was over wider span of temperature. Comparison of TGA peaks with cone test mass loss peaks show that in case of pine and sycamore wood the temperatures of peak TGA mass loss lies between the cone mass loss vs. average and bottom temperatures while for acacia and dry ash the peak TGA mlr temperature lies before the peaks of

the mass loss rate of cone tests. Average temperature of the wood was chosen to plot the emissions of the components.

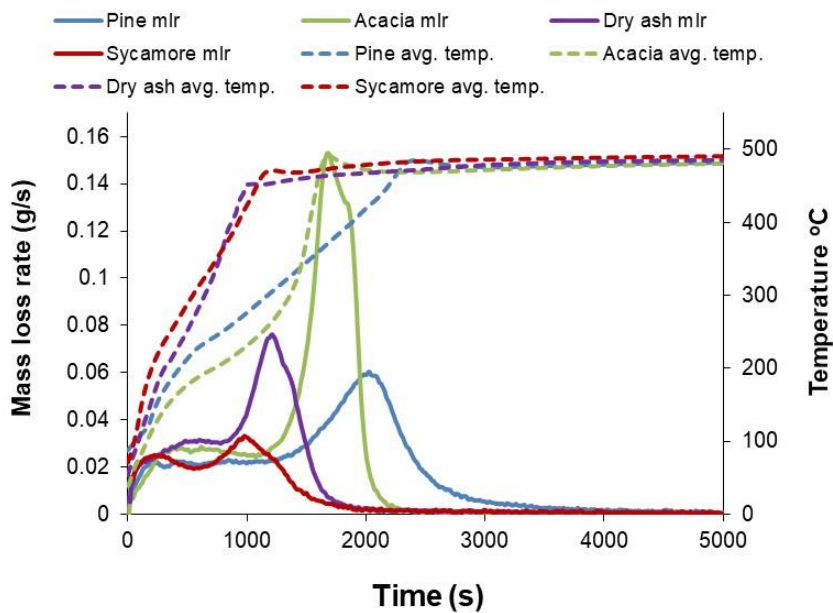


Figure 6.29 variation of mass loss rate and average temperature as a function of time.

Variations of mass loss rate and average temperatures with time (Figure 6.29) show that peak mass loss and peak average temperatures for some woods occurred at same time, for sycamore and pine there was a time lag between peak mass loss rate and peak average temperatures. Temperature profile of the acacia wood shows the reason for the sudden release of volatiles over very narrow time span and very high peaks of concentration obtained though.

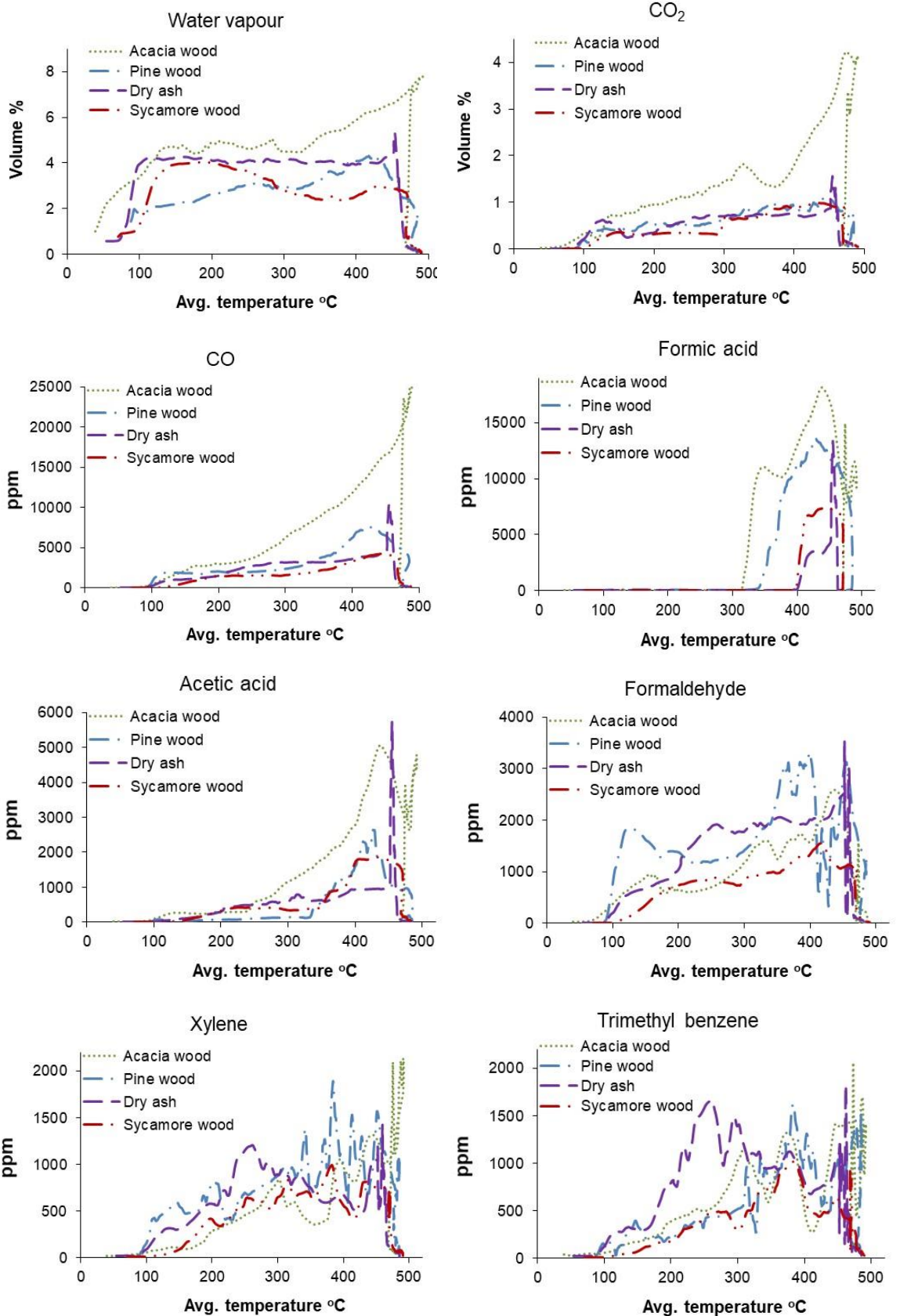


Figure 6.30 Concentration vs avg. wood temp. for some gaseous products from the pyrolysis of different wood types at heat flux 20 kW/m².

Table 6.8 Top and avg. temp. corresponding to the release of products of pyrolysis and comparison with literature.

Components	Present work						Basilakis et al. [101]	Meng et al. [102]	Chen et al. [150]	Wang et al. [151]
	Sycamore, ash wood		Pine wood		Acacia wood					
	Top temp. °C	Avg. wood temp. °C	Top temp. °C	Avg. wood temp. °C	Top temp. °C	Avg. wood temp. °C	Wheat straw	Corn cobs, tree roots, Bagasse	Populus deltoids	Pyrolytic lignin
							Temp. °C	Temp. °C	Temp. °C	Temp. °C
H ₂ O	60	60	60	60	60	60	50		50	
CO ₂	150	100	150	100	150	100	200	200	200	100
CO	160	100	160	100	160	100	200	220-250	200	200
Methane	450	400	450	340	270	180	220	330	240	200
Ethane	130	100	130	100	160	100				
Ethylene	450	450	450	370	400	320				
Formic acid	450	400	450	330	400	320	200			160
Acetic acid	330	100	440	100	330	100	150	200-220		160
Formaldehyde	140	100	150	100	100	80	200			100
m-xylene	170	100	450	100	250	100				
o-xylene	160	100	250	100	250	180				
p-xylene	160	100	150	100	160	100				
1,2,3 - TMB	170-200	100	170	100	170	100				
1,2,4 – TMB	150	100	440	100	160	100				
1,3,5 - TMB	160	100	160	100	450	100				
Toluene	170	100	170	100	270	180				
Acetone	450	300	440	300	370	300				
Methanol	200	100	440	330	200	100	180			150
Ethanol	160	100	440	300	270	200				
Propanol	170	100	440	330	200	180				
Phenol	260	100	150	320	180	120				200
Ammonia	450	150-450	220	400	400	330	100	200-280		

Concentration of some components were plotted vs avg. wood temperature (Figure 6.30) to observe that if all wood shows the release of different species at same temperature or not. In the plotted concentration shown most of the components were released at same temperature by all the wood except formic acid.

In order to make a comparison with the literature regarding TG-FTIR tests regarding the temperature at which different product species are released, average and top thermocouple temperature corresponding to the release of products of pyrolysis are listed for the present work in the Table 6.8.

It was seen that for most of the components, sycamore wood, dry ash and pine wood had same corresponding temperatures except alcohols, acetic acid, m-xylene and 1,2,4-TMB. While the corresponding release temperatures of acacia wood was very different for many components as compared with other wood types.

TG FTIR tests (in Table 6.8) show the release of CO and CO₂ at 200 °C while in present work if emissions are plotted vs avg. wood temperature, then its 100 oC, and if plotted vs top thermocouple temperature then corresponding temperature is 160 °C.

TGA tests shows the release of acetic acid, formic acid and acetaldehyde at temperatures close to 200 °C, while in the present work corresponding avg. and top temperatures are much higher than this.

It can be concluded that similar compounds can be released due to decomposition of hemicellulose, cellulose or lignin and there release temperatures can be different from one biomass to another as shown by TGA data in Table 6.8 as well.

6.6 Mass balance

Cumulative mass loss of the biomass from the load cell was plotted against the cumulative mass of gases obtained from the FTIR and the plots show very good agreement upto 2000 s for most of the biomass studied Figure 6.31. Difference in the two curves appear when the concentrations of the species reach maximum

values and it could be due to the calibration extrapolation at high concentrations but this difference is within than 10%.

Overall material balance of biomass species balances 100% upto 2000 -3000 s but at the end of the test the only difference in material balance is the extra grams that came from the cumulative summation of FTIR gases.

Table 6.9 Overall mass balance for the pyrolysis tests on cone calorimeter

Biomass	Initial weight (g)	Final char (g)	Mass loss from load cell (g)	Mass from FTIR (g)	Difference (g)
Pine wood	117.94	32.62	85.32	89.95	-4.63
Eucalyptus wood	165.305	58.63	106.675	110.72	-4.045
Acacia wood	150.39	48.37	102.02	108.1	-6.08
Dry ash	91.13	26.89	64.24	68.37	-4.13
Wet ash	99	23.96	75.04	82.17	-7.13
Sycamore wood	54	15.31	38.69	40.91	-2.22
Sunflower shell pellets	131.168	40.09	91.078	97.7	-6.622
White wood pellets	133.48	38.09	95.39	102.51	-7.12
Grade B torrefied wood Pellets	161.38	70.55	90.83	98.61	-7.78
Corn cobs	84.38	25.34	59.04	63.33	-4.29
China's biomass skin	245.22	102.43	142.79	150.63	-7.84
China's biomass black	321.38	185.55	135.83	132.91	2.92
SPF raw	44.17	12.55	31.62	32.97	-1.35
SPF torrified	40.2	15.31	24.89	26.95	-2.06

Yields of the components obtained from the liquid phase are reported in the Table 2.6. Literature [92, 109, 111, 152, 153] has shown that major liquid compounds are acetic acid, hydroxy acetone, hydroxy acetaldehyde and levoglucosan. Most of the literature analyses the GC detectable phase of the condensate and separates total pyrolysis liquid in two phase, aqueous phase

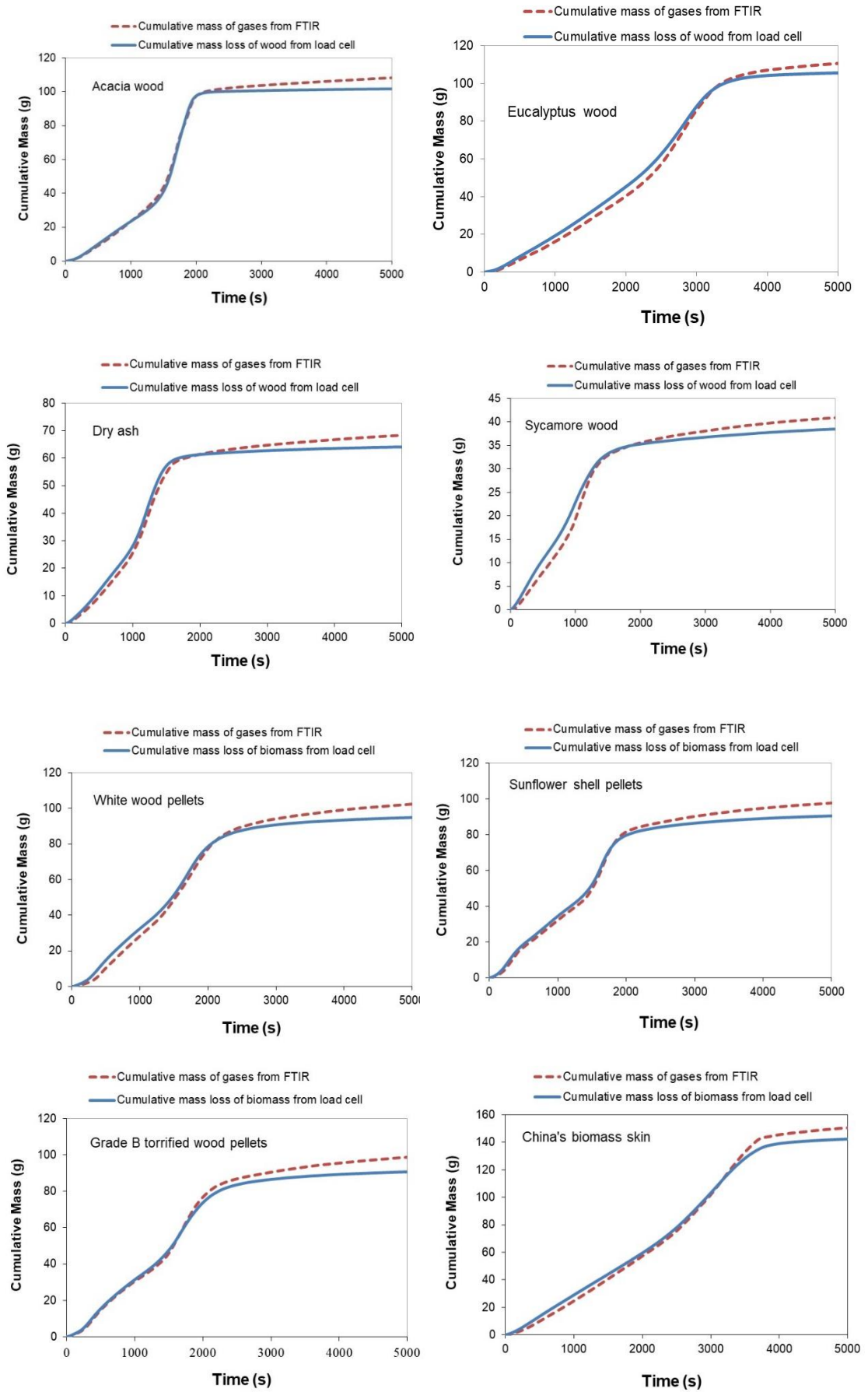


Figure 6.31 Comparison of mass obtained from FTIR with mass loss of biomass from load cell for the pyrolysis of different biomass at heat flux 20 kW/m^2

and oil phase [92, 153]. While others researchers [109, 111] do not separate the phase and still getting same compounds.

In the present work major compounds found are formic acid, xylene and trimethylbenzene and acetic acid. Present work uses Hot sampling system and analyse the components with FTIR. Boiling points of xylene and trimethylbenzene is below 180 °C, but levoglucosan have a boiling point higher than 300 °C and could not be detected by FTIR. The difference results can be due to different analysis techniques.

There are different parameter that can effect results e.g. residence time, heating rate, particle size, type of reactor, condensation etc. In the present work, some components were missing by the FTIR library e.g. some syringols, some guaiacols (eugenols etc.), some types of phenols (dimethyl phenols, dimethoxy phenol etc.) but the literature [92, 111] have reported very low yields of these compounds.

6.7 Energy contents of the products of pyrolysis

Figure 6.32 reports the HHV of the gases produced in units MJ/kg of gas. Peak values in the graphs corresponds the time at which gas yield was maximum. It can be seen that major contribution towards HHV was from hydrocarbons, while contribution from CO was negligible. In the Figure 6.32 hydrocarbons are classified as oxygenated hydrocarbons and other hydrocarbons without oxygen are termed as CH hydrocarbons. CH hydrocarbons included benzene toluene, xylene trimethylbenzene, alkanes and olefins making a major contribution to the energy of gaseous vapours. These energy graphs can also give an idea about the behaviour of a biomass during gasification. e.g. Eucalyptus wood released volatile after 2000s, HHV of the volatiles from eucalyptus wood was very low in the initial 2000s, it was seen in the gasification tests that hard wood were not giving high % of CO as compared with pine wood during the test time and it is due to the high density of this wood as compared with pine wood.

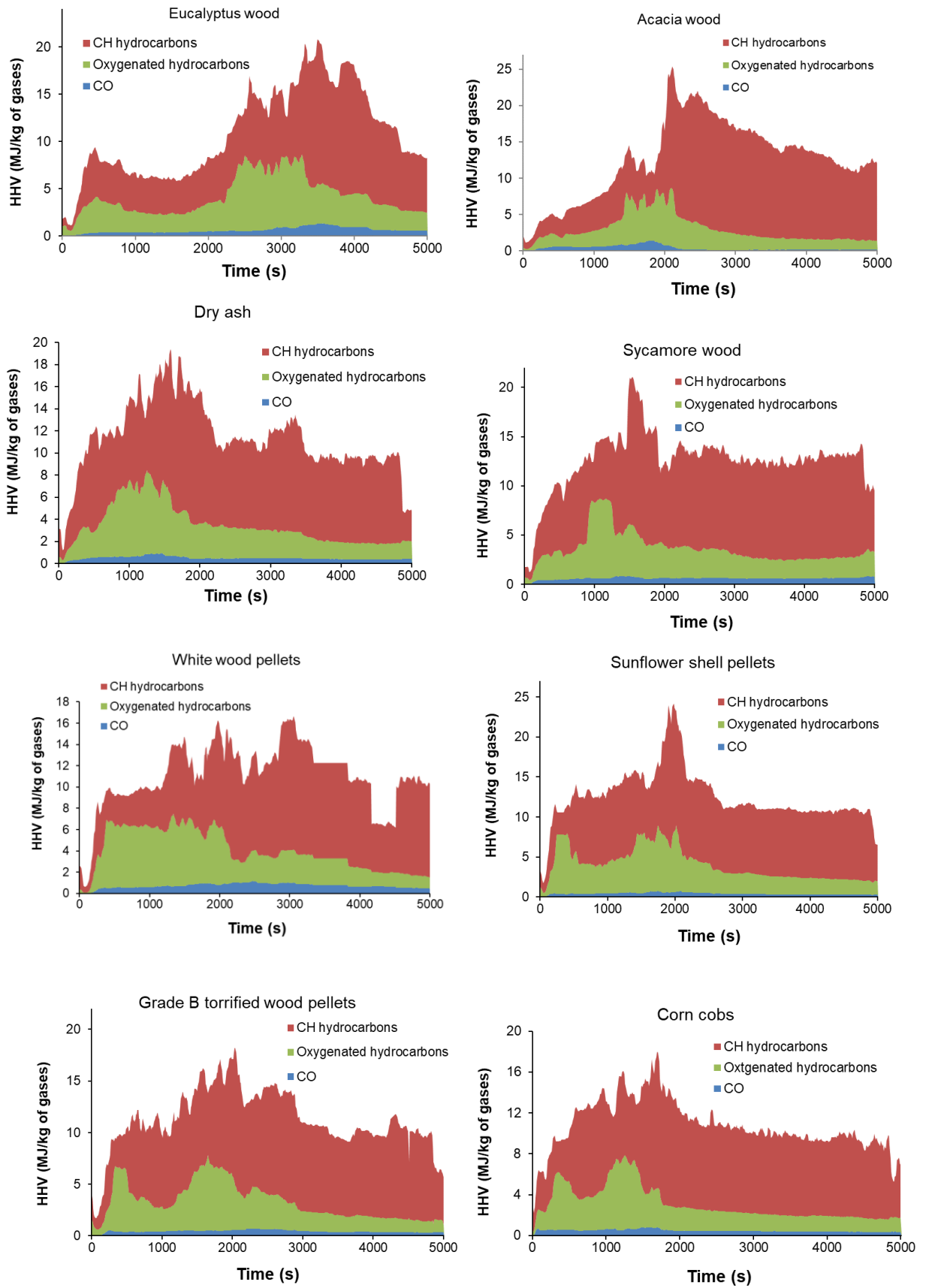


Figure 6.32 HHV MJ/kg of the products of pyrolysis of different biomass at heat flux 20 kW/m²

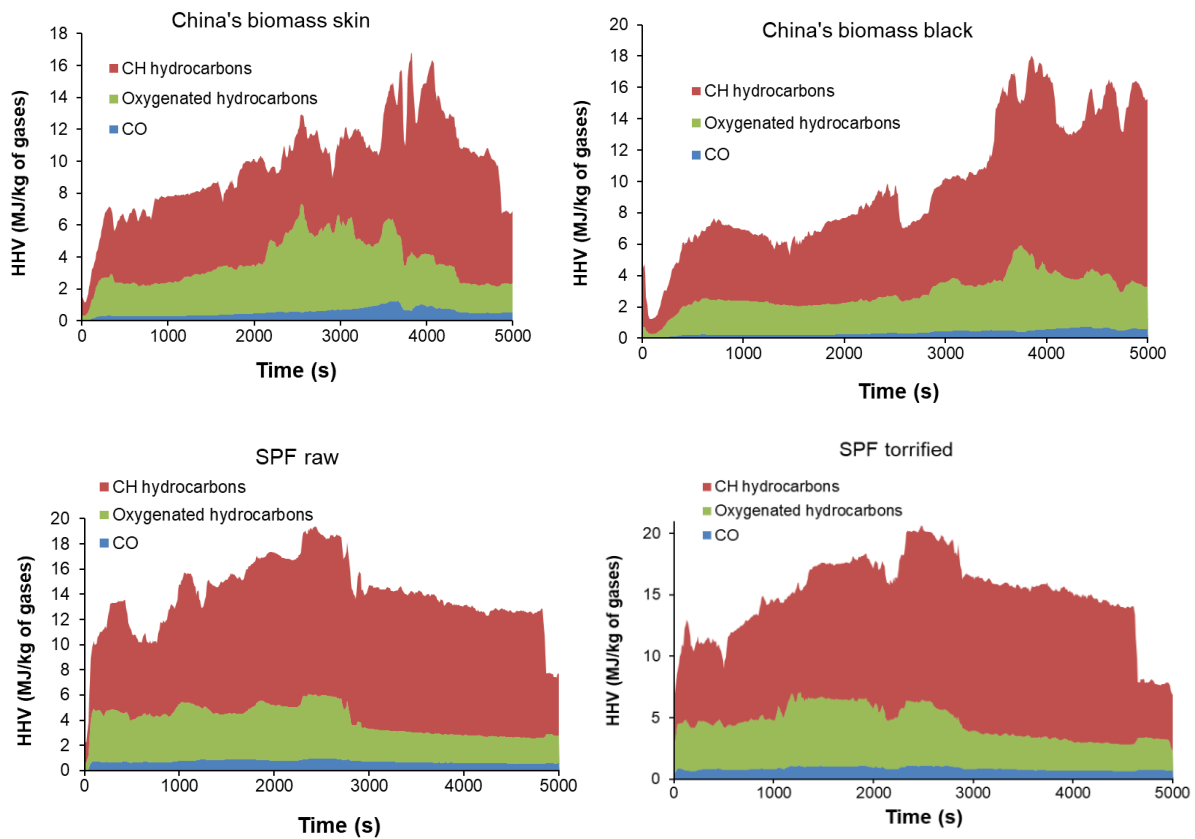


Figure: 6.32 (continued)

6.8 Conclusions

- Products of pyrolysis from large biomass particles were studied using FTIR under low temperature (275 -500 °C) conditions on the cone calorimeter. The average wood temperature at which biomass started releasing volatiles in appreciable quantities was higher than that predicted from the TGA of biomass because of the resistance to the heat and mass transfer inside the big wood particles.
- Tests at different temperatures on the pine wood pyrolysis showed that at low temperature (average wood temperature 320 °C, heat flux at 10 kW/m²) formic acid was not formed that was a major pyrolysis product at high heat flux of 20 and 25 kW/m².
- Thermocouples tests allowed the release temperature of the individual components to be recorded for the large particle sizes.

- Major compounds found using FTIR by weight in no order were H₂O, CO₂, xylene, trimethylbenzene, CO, Formic acid, Acetic acid, acrolein, acetone and furfural, propanol and MTBE.
- Different woods behaved differently towards the devolatilisation of the biomass, some woods released volatiles much quicker than the others and possible reason was the variability of hemicellulose, cellulose and lignin contents of the biomass.
- Material balance from FTIR quantitative emissions was in very good agreement with the mass loss from the load cell.
- The cumulative energy content of the different pyrolysis products and of the remaining char gave comparable energy content to the GCV of the fuel determined by experiments (bomb calorimetry).
- Overall this part of the study identified the most significant pyrolysis products of biomasses in the lower temperature range and showed that the yields change significantly with temperature and type of biomass indicating that finetuning the performance of biomass boilers would have to take into account and control these variables

Chapter 7 RESULTS FOR PYROLYSIS TESTS ON FURNACE REACTOR

As discussed in Chapter 3 most of the previous work on the pyrolysis of biomass was performed in test rigs where gases from the reactor were condensed to separate water and pyrolysis oils [92, 107, 111]. In this work (Chapter 6) we used the Cone Calorimeter combined with a heated (180 °C) sampling and FTIR system to quantify the pyrolysis products - which were effectively kept in gaseous form. In order to validate the tests done with low temperature pyrolysis on the cone calorimeter, pyrolysis tests were performed inside a vertical furnace described in Section 3.10.

One of the purpose of using this vertical furnace rig was to record emissions as a function of fixed temperature in a preheated furnace. However this was not achieved as the biomass was placed inside the reactor first and reactor was purged before furnace was heated. The temperature was controlled via feedback from a thermocouple placed in the centre of the walls of the furnace. Another thermocouple was inserted inside the middle of the sample pine blocks stock in a basket to record the actual biomass bed temperature. Only the output of the biomass thermocouple was recorded. The other thermocouple (controller) was not connected to a data logger.

The FTIR analyser was also used in these tests sampling after the condenser and impingers in order to identify and quantify any remaining gaseous pyrolysis components in the exhaust gas stream.

This furnace is used to produce char by slow pyrolysis at high temperature. The heating time of the furnace is from 30 to 45 minutes for the temperature range studied in the present work. In this study the flow rate of nitrogen was high (2.5 litres/min) so that the residence time of the gases inside the reactor was less than a minute. There was no load cell to record the mass of the biomass as was

done in cone calorimeter tests, so the weight of the biomass was done before and the remaining char was weighed after the test.

Four temperatures were chosen 300, 350 400 and 450 °C. The Initial mass of the biomass was about 323 g. Length of the test was 15000 s.

The heating rates of the biomass based on the thermocouple temperature are shown in the Figure 7.1.

The actual heating rate and the temperature experience by individual wood blocks cannot be calculated. The wood blocks closer to the tube walls could have higher temperature than that showed by the thermocouple that was in the middle of the sample. The average heating rates (°C/min) for tests at 350 °C and 400 °C are very close. It took about 3100 s for these two tests to attain the desired temperature (Figure 7.2).

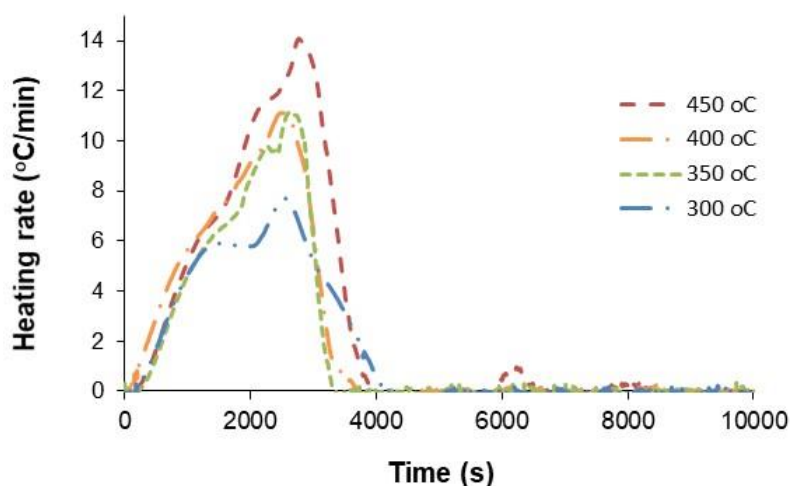


Figure 7.1 Heating rate of pine wood pyrolysis inside the furnace reactor

It took about 3700 s in others tests (300 °C and 450 °C) to attain the desired temperature.

In these tests residence time of the vapours in the system was not sufficiently high to collect all the condensable products in the catch pot and impingers, some tars were collected in the filter box of the FTIR. The FTIR also recorded most of the components present in the library including aldehydes, acids, xylene, trimethylbenzenes, acrolein, phenol, cresol, furans, along with alkanes and gases.

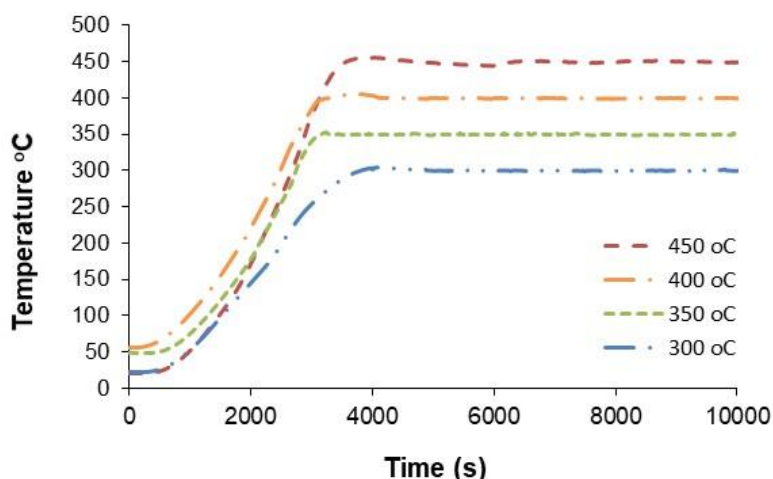


Figure 7.2 Temperature profiles for the pyrolysis at selected temperatures

7.1 FTIR emissions

The devolatilisation time of some of the components is shown in the Figure 7.3. For test at 300 °C, devolatilisation of CO₂ and CO continued upto 10000 s, while at other temperatures it took 5000 to 6000 s. Devolatilisation becomes fast in test at highest temperatures with narrow temperature range. Less release of volatiles in 300 °C shows more char production. As temperature increases, char yield decreases as a result of competition between primary reactions of char and volatile formation with the latter becoming more favoured.

Concentration of the components is plotted vs thermocouple temperature (Figure 7.4) to observe the initial temperature at which a component is released as done in the cone tests. The release temperature for CO and CO₂ was about 200 °C. The same temperature has been observed in the literature compared in Table 6.8, but it can be seen that at about 170 -180 °C small quantities of these gases start to release. The release temperature of methane and formic acid was different at different target test temperatures.

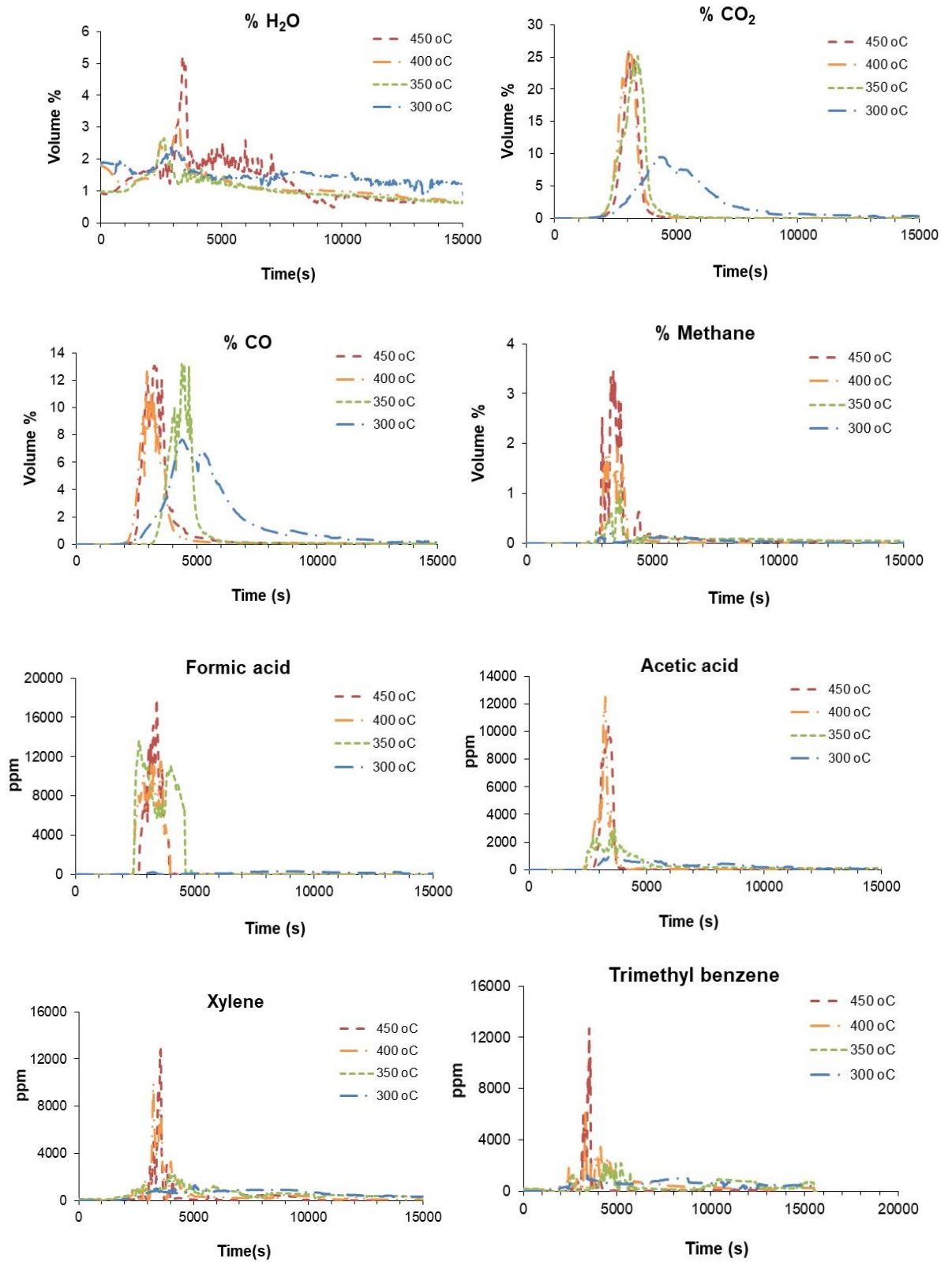


Figure 7.3 Selected specie concentration as a function of time

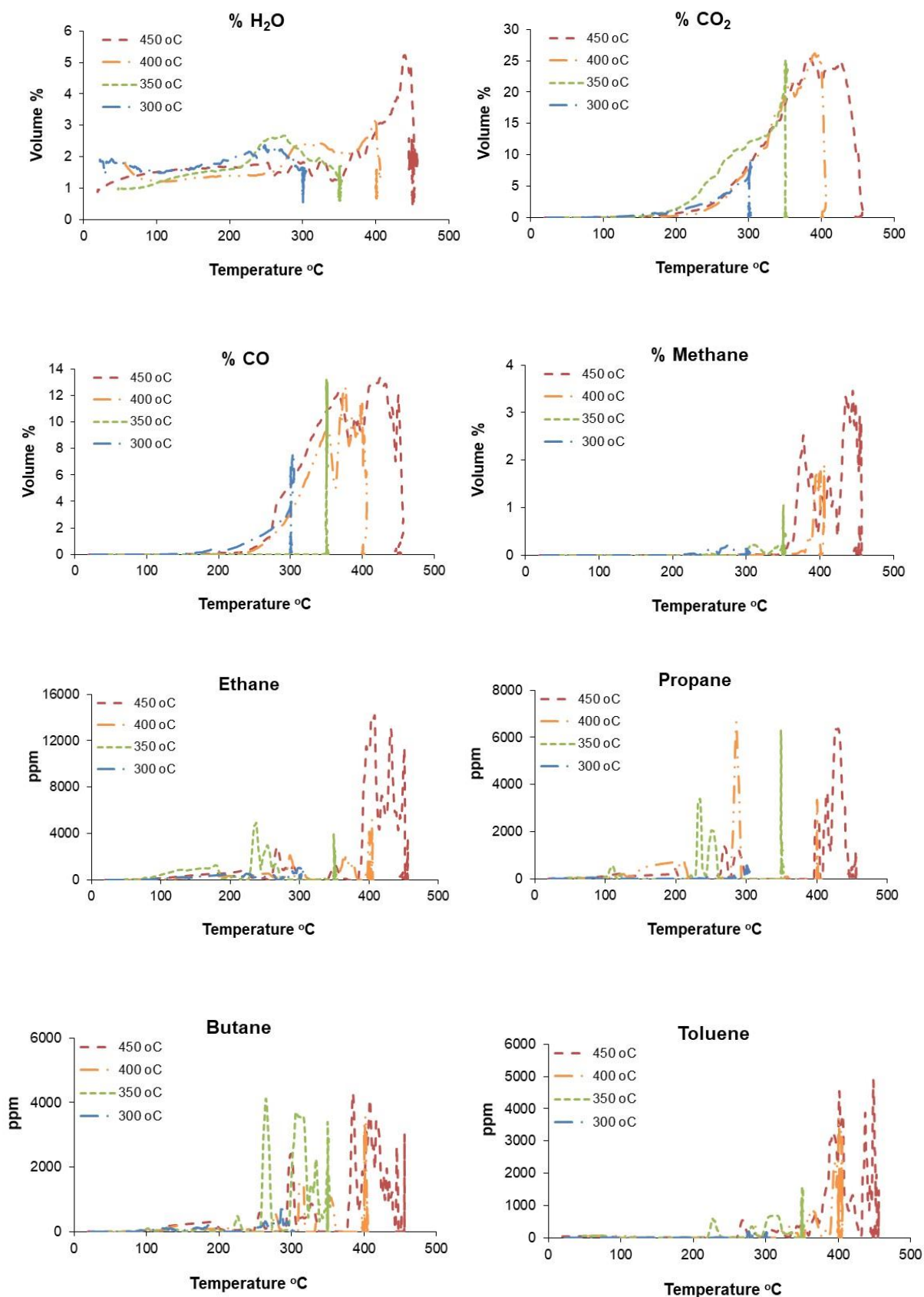


Figure 7.4 Specie concentration vs time for the pyrolysis of pine wood at different temperatures in furnace reactor

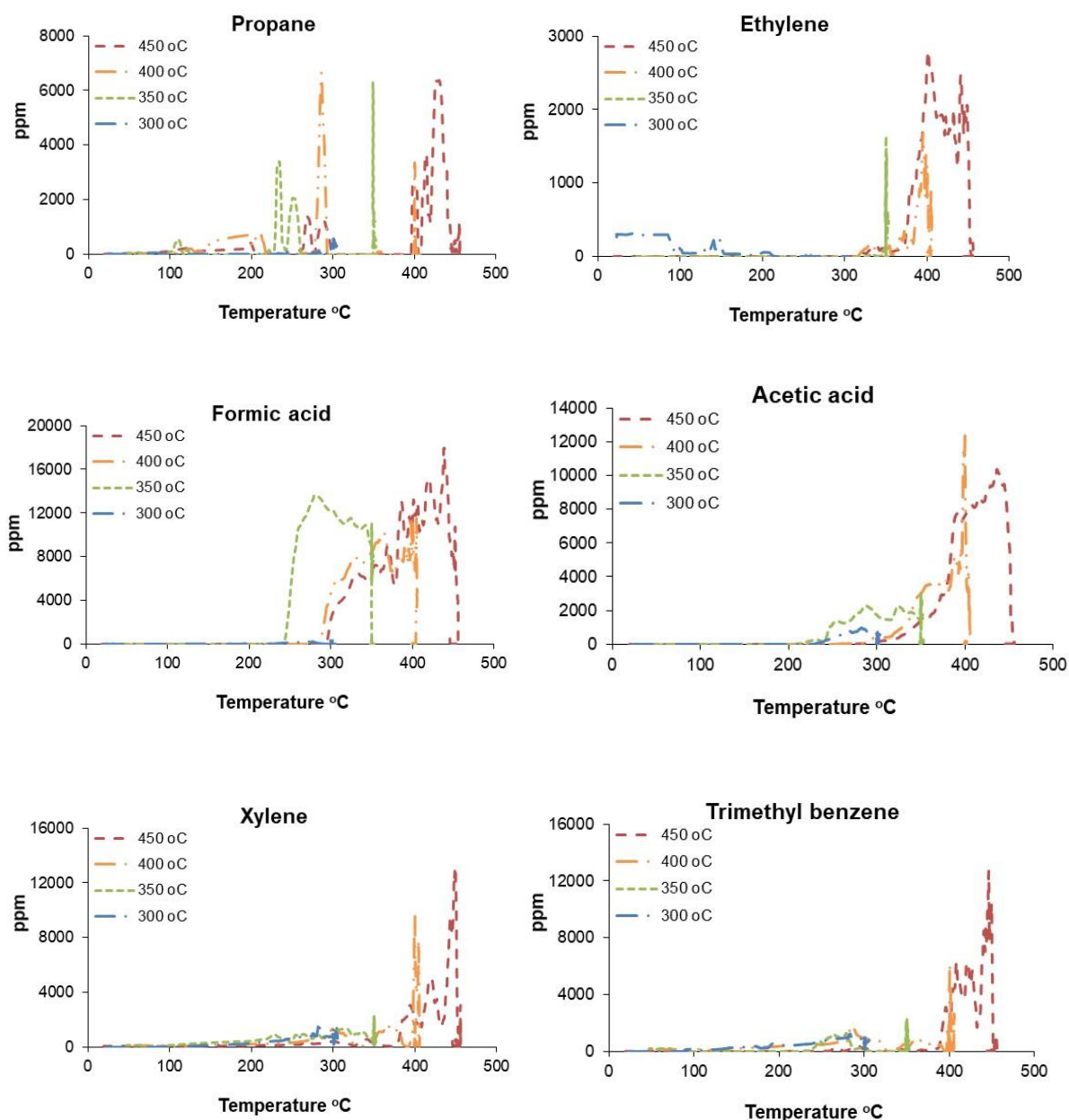


Figure 7.4 (continued)

7.2 Yields of liquids gases and chars

Yields of liquid (including water), char and gases (on dry basis) obtained in each test is plotted in Figure 7.5 (a), (b) and (c) respectively. Gases are taken as the components that are gases at room temperature and condensable components (acids, aldehydes, alcohols, hydrocarbons etc.) measured by the FTIR were considered to the liquids. The trend is same as found in the literature [62, 111, 118, 154]. As temperature increases, char yield decreases as a result of competition between primary reactions of char and volatile formation with the

latter becoming more favoured [62]. The yield of liquid products increase due to primary formation of tar vapours, if temperatures increased further after 450 °C a maxima could be obtained and liquid yield would decrease after the maxima due to the decomposition of tars, this trend has been shown by many researchers [62, 92, 111] as discussed in section 2.10. Yield of gases increases with increase in temperature.

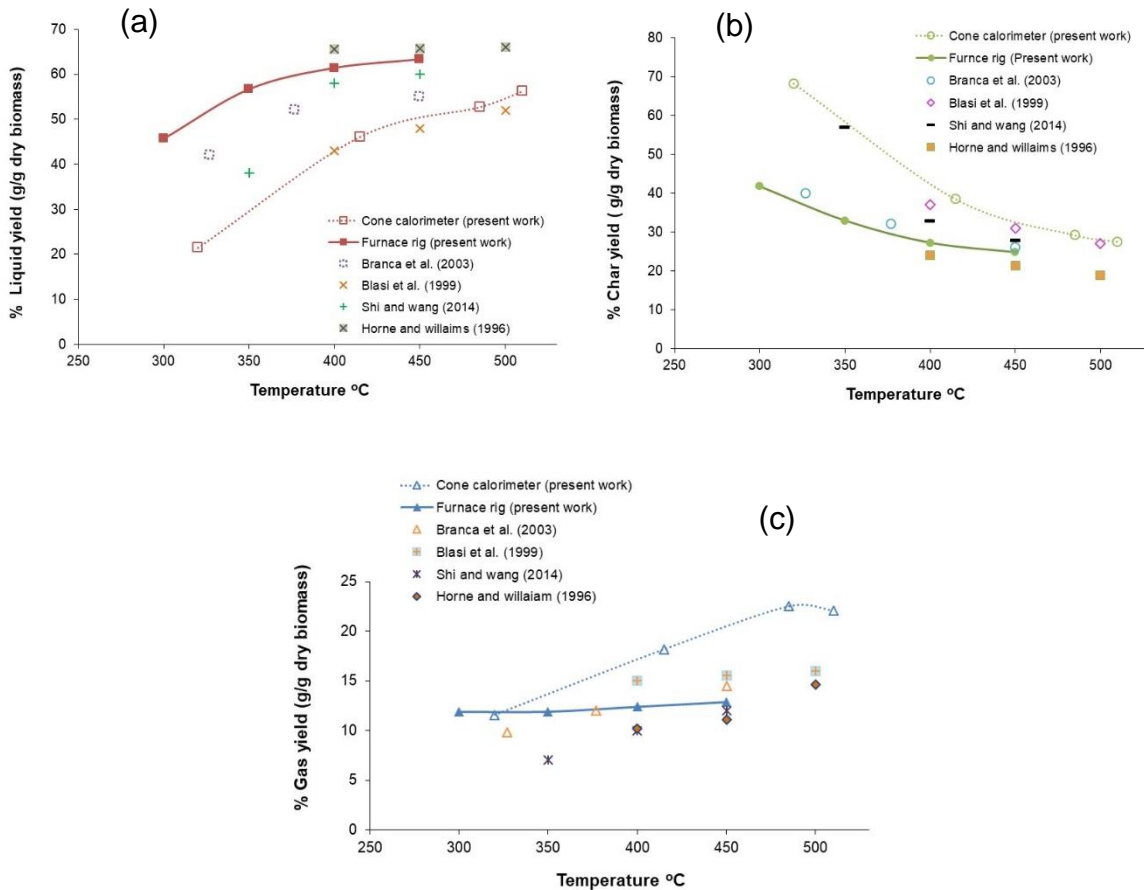


Figure 7.5 % yields of (a) liquid (b) char (c) gas on dry basis for the pyrolysis of pine wood cubes and comparison cone tests and literature [108, 111, 118, 154]

Char yield decreased from 41% to 25% as temperature was increased from 300 °C to 450 °C. Liquid yield increased from 45 % to 63% while gas yield increased from 11.8 to 12.8% upon increasing temperature from 300 °C to 450 °C. The yields of gases and char are very close to the work of Branca et al. [111]. They have plotted liquid yields but the sum of liquid char and gas yield for their work is not 100% and they have plotted water separately. % liquid yield is very close to the work of Horne and Williams [154] with flash pyrolysis, and Shi and Wang

[118]. As in the present work the vapour quenching time was more than a minute (1.6 minute) still getting high liquid yields, although the heating rate of biomass was slow.

Comparison of the yields of liquid, char and gas in the furnace rig with the yields obtained from cone calorimeter after 400 °C shows that yields of liquids are higher in the furnace rig than that of the cone calorimeter. Residence times of the gases in the furnace rig was high as compared in the cone calorimeter, the average heating rates in the rigs are also different but comparison cannot be made as actual heating rates of the particles are unknown. Pyrolysis chars from the tests in furnace rig are shown in Appendix C Figure C.1-Figure C.4. It can be seen that even at 300 °C, most of the wood is converted to char unlike in the cone calorimeter test at 10 kW/m², where most of the wood was not converted to char (Appendix B), this shows the importance of particle size as well.

The yields of CO₂ and CO in the present work are in very good agreement with work of [111] for the pyrolysis of beech wood and [107] for pyrolysis of different wood species. The trend of CO₂ changes after 400 °C, but literature [108] also shows some data points offset the overall trend. CO₂ yields obtained in the furnace rig are different (less) from that obtained in the cone calorimeter. The difference in CO₂ yield in different studies in literature has also been noted. Another work of Blasi [108] shows high CO₂ yields for wood and agriculture residues upto 17.5-18.7% and is comparable with the CO₂ obtained in the cone calorimeter tests.

It has been found in the literature that distribution among gases, organic condensable products, water and char from lignocellulosic fuel pyrolysis is highly affected by size and physiochemical properties of the particles, external heating rate and reactor configuration. [62]

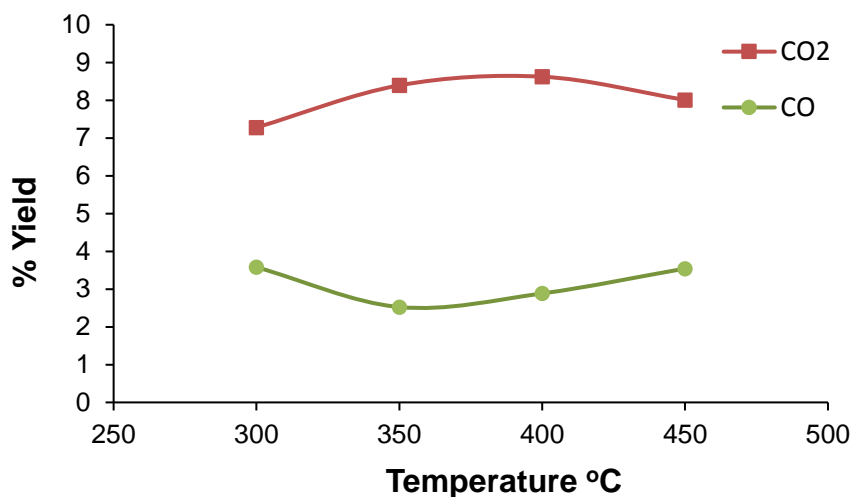


Figure 7.6 % yields of CO₂ and CO on dry basis

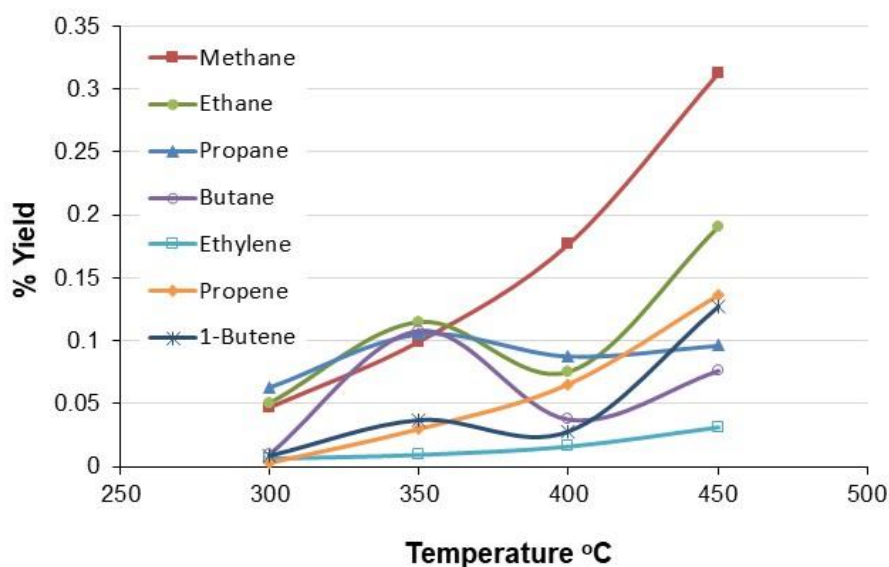


Figure 7.7 % yields of gaseous products from the pyrolysis of pine wood

Yields of alkanes and alkene hydrocarbon gases upto C₄ have been shown in the Figure 7.7. Yields of methane, ethane and ethylene are comparable with the literature [104, 108].

7.3 Pyrolysis liquids

Pyrolysis liquids obtained from these tests were unfortunately not stored properly (were stored in plastic bottles at room temperature) and was not possible to analyse on GC-MS due to decomposition of the components and formation of

very tarry compounds with particles. One sample(pyrolysis condensate at 300 °C) was analysed and the procedure was as follows: 100 ml of the liquid was mixed with 100 ml of dichloromethane (DCM). This was mixed and poured into the separating funnel and no separation of aqueous and oil phase was achieved probably due to decomposition of the mixture. After two hours the sample was taken from the bottom side of the separating funnel and 100 ml of water was added and placed in another separating funnel to observe any separation between the aqueous and oil phases. No separation was observed in any of the tests. A sample was then taken from the bottom side of the funnel and 5 µL of the sample was injected in 1 ml of DCM in a vial. The vial was placed in a refrigerator overnight and was analysed next day in the GC-MS with a total ion chromatograph.

The component peaks identified with the above technique are shown in Appendix D Figure D.1. The temperature programme and other parameters for the GC-MS are also given in the Appendix D. The accompanying Table D.1 lists all the possible compounds identified by the NIST library search. Some components e.g. furfural, 2(5H)-furanone, and some phenols that match other research reports [54] are highlighted as the most likely components.

7.4 Conclusions

- As discussed before, one of the purpose of the work on this reactor was to study the emissions from biomass pyrolysis at fixed temperatures, but this task was not achieved as biomass was placed into the reactor before starting the heater, and it took about 3000-4000 s to reach desired temperature and most of the gases has already been driven off during heating process. The average sample temperature showed that it took long to heat up biomass in this reactor compared with the tests on the cone calorimeter. Tests at 10kW/m² on the cone calorimeter showed little conversion as compared with test at 300 °C in the furnace reactor
- The second purpose of the work was to check that if FTIR was reading the same gases as on Cone calorimeter. The FTIR also showed xylenes and trimethylbenzene as residence time of vapours was very low to get all liquids as condensates in the present work on furnace rig.

- Comparison of the yields of liquid, gases, chars, and individual gases e.g CO₂, CO from furnace reactor with yields obtained from cone calorimeter showed that yields of the pyrolysis products depend on the number of parameters including particle size, heating rate, type of reactor, residence time of the gases inside the reactor.

Chapter 8 Conclusions and future work

8.1 Applications of biomass two stage combustion

Pakistan is facing an energy crisis and it was shown that the energy potential from the forests and agricultural wastes of Pakistan can fulfil 20.2% of the annual consumption of electricity. Forest waste wood and sustainably harvested wood could contribute 9.5% of electricity with oil seed residues contributing 8.2% of electricity and banana tree wastes contributing 2.5%.

Most biomass combustion systems for heat or steam power generation use two stage combustion with the first stage operating fuel rich and producing a gas that is passed to the second stage where air is added to complete combustion and raise the temperature of the gas. This high temperature gas can be used to generation hot water for heating purposes and equipment for this is available in the 10kW – 1 MW size range. Alternatively the heat can be used to generate steam, which is then used for electric power generation. This systems tend to be available in a larger size range of 10 MW electric or higher. For both thermal heat and electricity applications the rich burning first stage combustion essentially gasifies the biomass fuel and produces a gas of composition CO, H₂ and hydrocarbons plus the inerts CO₂ and H₂O.

This research was concerned with the optimisation of the energy transfer from solid biomass energy to gaseous fuel energy and conversion efficiencies of up to 80% were demonstrated. The application of the energy in the gases was not of concern in the thesis and hot water, steam and electricity production use the same principles of rich burning primary combustion.

Most previous applications of gasification of biomass or coal have been to produce a gas for application in gas turbines, this was not the objective of this work, but the principles developed in the research could be applied to gas turbines. This would require the rich combustion to be carried out in the high

pressure air downstream of the compressor with a downstream lean burning low NO_x combustor. The high temperature high pressure gases would then be passed to the turbine which would generate electrical power with the waste heat from this used to generate steam and more electricity. However, thermodynamic models of combined cycle gas turbine cycles using the gasification of coal or biomass show that it is difficult to achieve an overall thermal efficiency better than 47%, which is achievable by simple steam cycle systems. This is why there are hardly any applications of biomass gasification in CCGT operation today and most applications of biomass for electricity generation use the steam cycle route. However, in terms of number of applications, the use of two stage combustion for thermal heat in the 10kW – 1 MW thermal range is dominant. The large scale generation of electricity from biomass uses pulverised biomass burning in single stage turbulent flames. This was not the application of the present work, which is directed at biomass log combustion and biomass pellet combustion.

8.2 The principles of two stage combustion

Two stage biomass burning splits the combustion air into a primary rich burning gasification zone and a secondary lean burning combustion zone. In the primary gasification zone biomass is burnt rich which results in the formation of CO, H₂ and hydrocarbons. Complete rich combustion occurs and the hot gases are passed to a burner where secondary air is added around the central hot gas feed to mix the primary gases with the secondary air and complete the oxidation of the gases and raise the temperature prior to the heat extraction in the water heater or steam generator. This type of boiler can be fed with chips, pellets or logs, but logs are most commonly used as they are the lowest fuel cost option. Continuously feed biomass chip or pellet boilers work in a similar way with the biomass first gasified and then the gases are burnt in a secondary zone.

The research showed that for each biomass there exists an optimum equivalence ratio for rich biomass burning at which the energy content of the gases generated is maximised. For pine wood this was an equivalence ratio of about 3, but for other biomass varied between 2.5 and 6. This means that to optimise two stage combustion the air split ratio needs to be controlled, but the

optimum split would be biomass composition dependent. It was suggested that a means to control this would be on the basis of the temperature of gases exiting the gasification zone, which equilibrium combustion calculations indicate could be used to locate the point at which the temperature started to increase as the air supply was increased to the primary gasification zone. This was shown to be close to the optimum energy conversion equivalence ratio. Currently most biomass two stage gasification boilers operate with a fixed air split, which is controlled with a single air fan and two orifices that control the flow split. For optimisation of any biomass two air fans are required with the air flow ratio controlled by the fan speed.

8.3 Elemental and TGA results

From the elemental and proximate analysis of biomass it was found that the variation of H/C and O/C lead to variations in the stoichiometric air to fuel ratio of the biomass on dry ash free basis from 4.7 to 7.5 for the range of biomass studied in the present work.

From the TGA tests of biomass it was found that there was considerable variation in the temperature at which the biomass lost weight. This variation was due to the different proportions of hemi-cellulose, cellulose and lignin in the biomass composition.

For the biomass range studied, hemicellulose, cellulose and lignin was calculated from the correlation of Sheng and Azevedo [95]. However, this correlation produced unexpected results in that lignin has a high stoichiometric A/F of about 9, hemicellulose about 3 and cellulose about 6. Thus, a high lignin content should have a high A/F and a high hemicellulose content should have a low stoichiometric A/F. However, plots of the predicted lignin and hemicellulose content as a function of the stoichiometric A/F showed the opposite trend to that expected.

8.4 Equilibrium calculations

Calculations for the adiabatic equilibrium compositions of the products of rich combustion gasification of biomass were performed using CEA software. It was

shown that different biomasses have different values of the optimum equivalence ratios at which CO and H₂ % in the product gas were highest. This means that to optimise a two stage combustion biomass heater, the equivalence ratio of the primary zone should be controlled. A method to do this was proposed based on measuring the temperature of the outlet gases from the rich burning zone.

8.5 Development of the experimental methodology

This work showed that the cone calorimeter that is commonly used in Fire research could be adapted for use in studying two stage combustion of biomass in a fixed bed gasifier format. This uses a 100mm square test sample of solid biomass which sits on a load cell that measures the rate of mass loss. A calibrated conical radiant heat gives a uniform heating across the surface of the test biomass. A thermal gasification zone moves down through the wood so that fresh gasified gases are being produced until only char is left. In this work there was an air box around the test specimen and this was used to control the air supply to the combustion zone and to control the rate of burning.

In the initial set of tests it was shown that rich metered equivalence ratios ϕ_m were achieved, but the resulting % of CO was very low. It was concluded that heat losses from the test wood combustion to the enclosure walls and the load cell support, caused the combustion conditions to be far from the adiabatic equilibrium combustion that was calculated using the CEA software. The solution was to reduce the heat losses.

Insulation of the compartment (enclosure box) was carried out and the heat losses from the sample holder to the supporting metal were reduced by placing a 20 mm thick insulation under the sample holder. This improved the results but there were problems in measuring the mean composition of the gases exiting the chimney placed at the cone heater exit. Two problems were identified: a single hole sample probe did not produce a mean sample and a multihole probe was required; oxygen was found in the sample and this could only occur if there was air back flowing down the chimney. The back mixing problem was solved by placing a grid plate restrictor at the outlet of the chimney. A better mean gas sample was achieved using a 20 hole sample probe with the holes on centres of

equal area. However, the mean gas sample was still not in good agreement with the metered A/F.

8.6 Gasification of biomass in the cone calorimeter

For the pine wood gasification, the variation in the CO as a function of the equivalence ratio was compared with the predicted equilibrium concentration of CO obtained from Chemical Equilibrium and Applications (CEA) software. The trend was found to be the similar with some exceptions. The highest yield (0.5 g_{CO}/g biomass) and % of CO (15%) for the pine wood was obtained at $\phi_m = 2.8$ and it was very close to the equilibrium prediction i.e. $\phi = 3.2$. The gas analysis showed that there were high levels of hydrocarbons present that should not be there if adiabatic equilibrium had been achieved. This was the main reason for the measured CO being lower than the predicted CO.

It was concluded from the difference in the equilibrium adiabatic and experimental CO that the system never reached equilibrium, due to heat losses and lower temperature of the pine wood bed. Only the top layer of the biomass was at high temperature and the other layers were at low temperatures that produced gasification conditions well away from equilibrium.

High yields of hydrocarbons was obtained due to the fact that system did not reach equilibrium. However, in the log boilers these hydrocarbons are burned in the secondary combustion zone and do not contribute towards combustion inefficiency in the gasification zone. This high proportion of hydrocarbons in the product gas is not a disadvantage but an advantage as it increases the CV of the gas and all the energy is released in the secondary combustion zone. Only if the objective is produce hydrogen and capture CO₂ by oxidising CO and hydrocarbons, is the presence of high hydrocarbons a problem. As the objective was to maximise the conversion of solid biomass energy into gaseous energy, then the proportion of hydrocarbons is not a problem, provided none are lost by condensation in transfer to the secondary combustion stage.

It was found that the different biomasses generated different equivalence ratios at an air flow rate that produced optimum equivalence ratio for pine wood.

Equilibrium calculations also showed that all biomass do not have same value of optimum equivalence ratio.

Biomass pellets burned at a much higher rate and produced very rich mixtures that need increased flow rate of air inside the primary gasification zone to produce the optimum mixture. It was found that the particle size and bulk density of the biomass also play an important part in the determination of the optimum equivalence ratio.

It was found that the high moisture content of the biomass feed at low gasification zone temperatures caused a reduced gasification efficiency. High moisture content biomass cannot be used to start up the gasification inside the log boilers, at higher temperatures, adding up some biomass with high moisture content could produce high H_2 and it needs more study.

FTIR recorded most of the products of combustion and the mass obtained from FTIR was in very good agreement with that lost from the load cell.

It was found that pulverised materials could not be used for burning in the log boilers as the top surface of the biomass was fused making a crust that offered a resistance to heat and mass transfer.

It was suggested to control the primary air in the log boilers using a temperature control attached to a thermocouple near the throat of the primary gasification zone, As adiabatic flame temperature shows a sharp change near the optimum equivalence ratio for gasification of the most of the biomass as shown by the results of the equilibrium concentrations of product gases using CEA model, the point where change start should be the suggested point to obtain near optimum equivalence ratio. However better control can be obtained by using a CO sensor as well.

8.7 Energy conversion efficiency for gasification rich combustion

HGE of pine wood at optimum condition was 80%. Maximum contribution to energy was from CO, then from H_2 , however, a large quantity of energy was shown to be released from hydrocarbons in decreasing order as acetylene,

ethylene, toluene and benzene. For the other biomass gasification efficiency was less than 80% and reason was no one of them was optimised. Emissions of CO from biomass pellets were far high as compared to solid wood but as the emission index (EI) was low due to very rich combustion causing combustion inefficiency. HGE for white wood pellets and grade B torrefied wood pellets in biomass combustion period was about 80%.

8.8 Pyrolysis tests on the cone calorimeter

Products of pyrolysis from large biomass particles were studied using the heated Gasmeter FTIR using nitrogen instead of air, on the cone calorimeter with the insulated enclosure around the radiantly heated test specimen. The average wood temperature at which biomass started releasing volatiles in appreciable quantities was higher than that predicted from the TGA of biomass because of the resistance to the heat and mass transfer inside the wood thickness. There was a better agreement with the average wood temperature.

Tests on different temperatures on the pine wood pyrolysis showed that at low temperature (average wood temperature 320 °C, heat flux at 10 kW/m²) formic acid was not formed that was a major pyrolysis product at high heat flux of 20 and 25 kW/m².

Thermocouples tests allowed the release temperature of the individual components of the gas to be determined.

8.9 Heated FTIR performance for gas composition analysis.

The present work relied extensively on the Gasmeter heated FTIR and its calibration. This enabled the composition of gases evolved from heating wood in nitrogen to be determined as a function of the wood temperature. It also enabled a full composition analysis of the rich zone gasification combustion, which is the first time that this has been done. Major compounds found using FTIR were H₂O, CO₂, xylene, trimethylbenzene, CO, formic acid, acetic acid, acrolein, acetone and furfural, propanol and MTBE.

The energy and mass balance between the FTIR and the measured mass loss was in very good agreement. This could only be achieved if the calibration of the FTIR by the manufacturers was reliable.

8.10 The cone calorimeter as a biomass characterisation method

This work has shown that the modified cone calorimeter is a useful technique to investigate two stage combustion of biomass and to optimise the operating conditions of rich burn gasification zones. It uses larger test specimens that in other evaluation techniques such as TGA, elemental analysis, drop tube combustion and hence is closer to practical biomass combustion.

8.11 Future work

- An improved gas sample probe is required to achieve a better mean gas sample with better agreement between the metered A/F and the A/F by carbon balance from the mean exhaust gas composition.
- To find a better cooling mechanism of load cell in order to increase test time.
- Future work should investigate higher gasification zone temperatures using co-combustion with natural gas. The aim would be to achieve gasification closer to equilibrium, as well as being able to start the process automatically by gas firing. Aljumaiah et al. [140] have shown that this process can work for log gasification with around 70% of the energy in natural gas replaced by biomass energy, which is a 70% reduction in CO₂ emissions.
- A proper second stage flame stabiliser with controlled air flow should be included in the current set up in order to study and understand the overall operation of the combustion zone and the correlation with emissions.
- To study the variation of CO and energy contents as a function of equivalence ratio for other biomasses as to check the optimum equivalence ratios, In this study only pine wood was tested for this exercise due to the time constraints.
- To attach a hydrogen analyser downstream of FTIR to record the actual H₂ contents.

- To establish the viability of improving the hydrogen gas yield for gasification of high moisture content biomass. This can be achieved by modification to preheat the combustion air to temperatures above 400°C using an electrical heater to simulate heat recovery from the exhaust waste heat.
- Use of an insulation of the compartment that does not results in the emission of CO₂ and H₂O or absorbs moisture and release it during burning e.g. refractory bricks. In the present work the rig had to be operated hot for some time to reduce this background contamination of the process to low levels. Similarly the gap between the chimney and the box should be filled with non-combustible material and chimney should be bolted to the box instead of just resting on its own.
- A new log/gasification boiler should be designed uses the principles found in this research, with no heat extraction from the rich burning zone and control of the total air flow and of the air split. This should be able to demonstrate a biomass energy to thermal energy conversion that is higher than currently on the market. Also it would enable the study of the combined char burn out and the gasification of the char that would occur at the bottom of the deeper combustion bed. The new design should be capable of co-firing with natural gas for start-up, as well as for achieving higher gasification zone temperatures and potentially better thermal conversion efficiencies. This new design should be capable of being scaled up to MW+ size.

REFERENCES

1. IEA, *World Energy Outlook, 2016*, International Energy Agency, : Paris, France, 2016.
2. IPCC, *Climate Change 2014, synthesis Report*. Geneva, Switzerland, 2015.
3. IEA, *World Energy Outlook 2013*, International Energy Agency: Paris France, 2013.
4. UNFCCC. *Kyoto Protocol*. 2017 [Last accessed 4th April 2017]; Available from: http://unfccc.int/kyoto_protocol/items/2830.php.
5. UNFCCC. *Paris Agreement*. 2017 [Last accessed 4th April 2017]; Available from: http://unfccc.int/paris_agreement/items/9485.php.
6. BP. *BP Statistical Review of World Energy*
2016 [Last accessed 30th March 2016]; Available from: <https://www.bp.com/content/dam/bp/pdf/energy-economics/statistical-review-2016/bp-statistical-review-of-world-energy-2016-full-report.pdf>.
7. World-Energy-Council. *World Energy Resources; Bioenergy 2016*. 2016 [Last accessed 4th April 2017]; Available from: https://www.worldenergy.org/wp-content/uploads/2017/03/WEResources_Bioenergy_2016.pdf.
8. Demirbaş, A., *Biomass resource facilities and biomass conversion processing for fuels and chemicals*. Energy Conversion and Management, 2001. **42**(11): p. 1357-1378.
9. Yang, H., et al., *Characteristics of hemicellulose, cellulose and lignin pyrolysis*. Fuel, 2007. **86**(12–13): p. 1781-1788.
10. Jenkins, B.M., Baxter, L.L., Miles Jr, T.R., and Miles, T.R., *Combustion properties of biomass*. Fuel Processing Technology, 1998. **54**(1–3): p. 17-46.
11. Department for Business Energy and Industrial strategy, U.-G. *Digest of United Kingdom Energy Statistics*. 2016 [Last accessed 22.03.2017]; Available from: <https://www.gov.uk/government/collections/digest-of-uk-energy-statistics-dukes>.
12. Department for Business Energy and Industrial strategy, U.-G. *UK Energy in Brief 2016*. 2016 [Last accessed 4th April 2017]; Available from: <https://www.gov.uk/government/statistics/uk-energy-in-brief-2016>.

13. Committee on Climate Change, C. *Carbon budgets: how we monitor emissions targets*. 2008 [Last accessed 31st March 2017]; Available from: <https://www.theccc.org.uk/tackling-climate-change/reducing-carbon-emissions/carbon-budgets-and-targets/>.
14. McKendry, P., *Energy production from biomass (part 2): conversion technologies*. Bioresource Technology, 2002. **83**(1): p. 47-54.
15. Formica, M., Frigo, S., and Gabbrielli, R., *Development of a new steady state zero-dimensional simulation model for woody biomass gasification in a full scale plant*. Energy Conversion and Management, 2016. **120**: p. 358-369.
16. Bridgeman, T.G., Jones, J.M., Shield, I., and Williams, P.T., *Torrefaction of reed canary grass, wheat straw and willow to enhance solid fuel qualities and combustion properties*. Fuel, 2008. **87**(6): p. 844-856.
17. Prins, M.J., Ptasinski, K.J., and Janssen, F.J.J.G., *More efficient biomass gasification via torrefaction*. Energy, 2006. **31**(15): p. 3458-3470.
18. Batidzirai, B., et al., *Biomass torrefaction technology: Techno-economic status and future prospects*. Energy, 2013. **62**(0): p. 196-214.
19. NEPRA. *State of Industry Report 2015*. 2015 [Last accessed 4th April 2017]; Available from: <http://www.nepa.org.pk/Publications/State%20of%20Industry%20Reports/State%20of%20Industry%20Report%202015.pdf>.
20. Indexmundi. *Factbook*. 2014 [Last accessed 5th April 2017]; Available from: <http://www.indexmundi.com/pakistan/>.
21. Ministry-of-Petroleum-and-Natural-Resources-Pakistan, *Pakistan Energy Yearbook*, 2012.
22. Ministry-of-Finance-Pakistan. *Energy*. 2016 [Last accessed 5th April 2017]; Available from: http://finance.gov.pk/survey/chapters_16/14_Energy.pdf.
23. Azad, A.R. *over 40 percent of textile industry has shifted to Bangladesh?* 2012 [Last accessed 5th April 2017]; Available from: <https://defence.pk/pdf/threads/over-40-percent-of-pakistans-textile-industry-has-shifted-to-bangladesh.207565/>.
24. Saeed, M.A., et al., *Agricultural Waste Biomass Energy Potential In Pakistan*, in *International Bioenergy (Shanghai) Exhibition and Asian Bioenergy Conference* ETA-Florence Renewable Energies: Shanghai, China, 2015.
25. Asif, M., *Sustainable energy options for Pakistan*. Renewable and Sustainable Energy Reviews, 2009. **13**(4): p. 903-909.
26. Alternative Energy Development Board, M.o.W.a.P.G.o.P. *Final Report on Biomass Atlas of Pakistan*. 2017 [Last accessed 6th April 2017];

- Available from:
<http://www.aedb.org/index.php/component/jdownload/15-bioenergy-reports/87-biomass-atlas-of-pakistan?Itemid=101>.
27. FAO. *Pakistan Forestry Outlook Study*. 2009 [Last accessed 9th September 2015]; Available from:
<http://www.fao.org/docrep/014/am623e/am623e00.pdf>.
 28. Rahim, S.M.A. and Hasnain, S., *Agroforestry trends in Punjab, Pakistan*. African Journal of Environmental Science and Technology, 2010. 4(10): p. 639-650.
 29. Tanvir, M.A., Khan, R.A., Siddiqui, M.T., and Ch., A.k. *Growth Behaviour and Price Variations of Farm Grown Bombax ceiba (Simal) in Punjab 2003* [Last accessed 29th January 2014]; Available from:
http://www.fspublishers.org/published_papers/36731..pdf.
 30. FAO. *WOODFUEL PRODUCTION AND MARKETING IN PAKISTAN NATIONAL WORKSHOP*. 2000 [Last accessed 6th April 2017]; Available from:
<http://www.fao.org/docrep/006/AD565E/ad565e00.pdf>.
 31. FAO. *Global Forest Resources Assessment 2010, Country Report Pakistan* 2010 [Last accessed 29th January 2014]; Available from:
<http://www.fao.org/forestry/20410-070585b62fd17653faf962214591cef02.pdf>.
 32. Pakistan-Forest-Institute-Peshawar. *FOREST ECONOMICS*. 2012 [Last accessed 6th April 2017]; Available from:
<http://pfi.gov.pk/Forest%20Economics.html>.
 33. Khan, M.M. and Khan, M.H. *Die Back of Sissoo*. no date [Last accessed 29th November 2013]; Available from:
<http://www.fao.org/docrep/008/ae910e/ae910e08.htm>.
 34. Christersson, L. and Verma, K. *Short-rotation forestry – a complement to “conventional” forestry*. 2006 [Last accessed 28th November 2013]; Available from:
<ftp://ftp.fao.org/docrep/fao/008/a0532e/A0532e07.pdf>.
 35. IEA. *Biomass for Power Generation and CHP*. 2007 [Last accessed 4th September 2015]; Available from:
<https://www.iea.org/publications/freepublications/publication/essentials3.pdf>.
 36. Eurelectric. *Efficiency in Electricity Generation*. 2003 [Last accessed 28th May 2013]; Available from:
<http://www.eurelectric.org/Download/Download.aspx?DocumentID=13549>.
 37. Ministry-of-Finance-Pakistan. *Agriculture*. 2014 [Last accessed 4th September 2015]; Available from:
http://www.finance.gov.pk/survey/chapters_14/02_Agriculture.pdf.

38. Ahmad, M. and Salim, M. *Oil seeds: problems and potential* 2011 [Last accessed 9th september 2015]; Available from: <http://www.pakissan.com/english/allabout/seeds/oil/problems.and.potential.shtml>.
39. FAO. *Definition and classification of Commodities*. 1994 [Last accessed 9th september 2015]; Available from: <http://www.fao.org/waicent/faoinfo/economic/faodef/fdef14e.htm>.
40. Pütün, E., Uzun, B.B., and Pütün, A.E., *Fixed-bed catalytic pyrolysis of cotton-seed cake: Effects of pyrolysis temperature, natural zeolite content and sweeping gas flow rate*. *Bioresource Technology*, 2006. **97**(5): p. 701-710.
41. Nhuchhen, D.R. and Abdul Salam, P., *Estimation of higher heating value of biomass from proximate analysis: A new approach*. *Fuel*, 2012. **99**(0): p. 55-63.
42. Volli, V. and Singh, R.K., *Production of bio-oil from de-oiled cakes by thermal pyrolysis*. *Fuel*, 2012. **96**(0): p. 579-585.
43. Gerçel, H.F., *The production and evaluation of bio-oils from the pyrolysis of sunflower-oil cake*. *Biomass and Bioenergy*, 2002. **23**(4): p. 307-314.
44. Ateş, F., Miskolczi, N., and Saricaoğlu, B., *Pressurized pyrolysis of dried distillers grains with solubles and canola seed press cake in a fixed-bed reactor*. *Bioresource Technology*, 2015. **177**: p. 149-158.
45. Pandey, S.N. and Gurjar, R.M., *Production of particle boards from cottonseed hulls*. *Agricultural Wastes*, 1985. **13**(4): p. 287-293.
46. Raclavska, H., Juchelkova, D., Roubicek, V., and Matysek, D., *Energy utilisation of biowaste — Sunflower-seed hulls for co-firing with coal*. *Fuel Processing Technology*, 2011. **92**(1): p. 13-20.
47. Khsushk, D.A.M. and Cheema, I. *Banana cultivation and marketing* 2008 [Last accessed 4th september 2015]; Available from: <http://www.pakissan.com/english/news/newsDetail.php?newsid=17293>.
48. Mahar, R.B. *Converting Waste Agricultural Biomass into Energy Source*. 2010. 26,27.
49. Pakistan-Bureau-of-Statics. *Agriculture Statistics*. 2017 [Last accessed 4th April 2017]; Available from: <http://www.pbs.gov.pk/content/agriculture-statistics>.
50. Rosal, A., Rodríguez, A., González, Z., and Jiménez, L., *Use of banana tree residues as pulp for paper and combustible*. *International Journal of Physical Sciences*, 2012. **7**(15): p. 2406 - 2413.
51. Basu, P., *Combustion and Gasification in Fluidized Beds*. 2006: CRC Press

52. Basu, P., *Biomass gasification and pyrolysis: practical design and theory*. 2010: Academic Press
53. Debdoubi, A., et al., *The effect of heating rate on yields and compositions of oil products from esparto pyrolysis*. International Journal of Energy Research, 2006. **30**(15): p. 1243-1250.
54. Biagini, E., Barontini, F., and Tognotti, L., *Devolatilization of Biomass Fuels and Biomass Components Studied by TG/FTIR Technique*. Industrial & Engineering Chemistry Research, 2006. **45**(13): p. 4486-4493.
55. Mohan, D., Pittman, C.U., and Steele, P.H., *Pyrolysis of Wood/Biomass for Bio-oil: A Critical Review*. Energy & Fuels, 2006. **20**(3): p. 848-889.
56. Encinar, J.M., González, J.F., Rodríguez, J.J., and Ramiro, M.a.J., *Catalysed and uncatalysed steam gasification of eucalyptus char: influence of variables and kinetic study*. Fuel, 2001. **80**(14): p. 2025-2036.
57. Wang, L., Weller, C.L., Jones, D.D., and Hanna, M.A., *Contemporary issues in thermal gasification of biomass and its application to electricity and fuel production*. Biomass and Bioenergy, 2008. **32**(7): p. 573-581.
58. Rapagnà, S., Jand, N., Kiennemann, A., and Foscolo, P.U., *Steam-gasification of biomass in a fluidised-bed of olivine particles*. Biomass and Bioenergy, 2000. **19**(3): p. 187-197.
59. Gil, J., Corella, J., Aznar, M.a.P., and Caballero, M.A., *Biomass gasification in atmospheric and bubbling fluidized bed: Effect of the type of gasifying agent on the product distribution*. Biomass and Bioenergy, 1999. **17**(5): p. 389-403.
60. Gabra, M., Pettersson, E., Backman, R., and Kjellström, B., *Evaluation of cyclone gasifier performance for gasification of sugar cane residue—Part 1: gasification of bagasse*. Biomass and Bioenergy, 2001. **21**(5): p. 351-369.
61. Smooth, L.D. and Smith, P.J., *Coal Combustion and Gasification*. 1985: The Springer Chemical Engineering Series. p. 88-89
62. Di Blasi, C., *Combustion and gasification rates of lignocellulosic chars*. Progress in Energy and Combustion Science, 2009. **35**(2): p. 121-140.
63. Solar Energy Research Institute, U.D.o.E., *A Survey of Biomass Gasification*. Vol. II, Principles of gasification. 1979
64. Miles, T. *The Boudouard Equation*. 2017 [Last accessed 14th April 2017]; Available from: <http://gasifiers.bioenergylists.org/reedboudouard>.
65. Barrio, M., Gøbel, B., Rimes, H., Henriksen, U., Hustad, J.E. and Sørensen, L.H., *Steam Gasification of Wood Char and the Effect of Hydrogen Inhibition on the Chemical Kinetics*. Progress in

- Thermochemical Biomass Conversion (ed A. V. Bridgwater). 2001, Oxford, UK: Blackwell Science Ltd
66. Gottuk, D.T. and Lattimer, B.Y., *Effect of Combustion Conditions on Species Production*, in *SFPE Handbook of Fire Protection Engineering*, M.J. Hurley, et al., Editors. 2016, Springer New York: New York, NY. p. 486-528.
 67. Abdulaziz, A.S.A., *Compartment Fire Toxicity: Measurements and Aspects of Modelling*, in *School of Chemical and Process Engineering* University of Leeds, 2016.
 68. Chan., S.H., *An exhaust emissions based air-fuel ratio calculation for internal combustion engines*. Proc. Instn Mech Engrs, Part D: Journal of automobile engineering, 1996. **210**: p. 273-280.
 69. Puig-Arnavat, M., Bruno, J.C., and Coronas, A., *Modified Thermodynamic Equilibrium Model for Biomass Gasification: A Study of the Influence of Operating Conditions*. Energy & Fuels, 2012. **26**(2): p. 1385-1394.
 70. Plis, P. and Wilk, R.K., *Theoretical and experimental investigation of biomass gasification process in a fixed bed gasifier*. Energy, 2011. **36**(6): p. 3838-3845.
 71. Zainal, Z.A., Rifau, A., Quadir, G.A., and Seetharamu, K.N., *Experimental investigation of a downdraft biomass gasifier*. Biomass and Bioenergy, 2002. **23**(4): p. 283-289.
 72. Qin, K., Lin, W., Jensen, P.A., and Jensen, A.D., *High-temperature entrained flow gasification of biomass*. Fuel, 2012. **93**(0): p. 589-600.
 73. Narváez, I., Orío, A., Aznar, M.P., and Corella, J., *Biomass Gasification with Air in an Atmospheric Bubbling Fluidized Bed. Effect of Six Operational Variables on the Quality of the Produced Raw Gas*. Industrial & Engineering Chemistry Research, 1996. **35**(7): p. 2110-2120.
 74. Lv, P.M., et al., *An experimental study on biomass air–steam gasification in a fluidized bed*. Bioresource Technology, 2004. **95**(1): p. 95-101.
 75. Aljbour, S.H. and Kawamoto, K., *Bench-scale gasification of cedar wood – Part I: Effect of operational conditions on product gas characteristics*. Chemosphere, 2013. **90**(4): p. 1495-1500.
 76. Wu, C., et al., *Nickel-catalysed pyrolysis/gasification of biomass components*. Journal of Analytical and Applied Pyrolysis, 2013. **99**(0): p. 143-148.
 77. Hernández, J.J., Aranda-Almansa, G., and Bula, A., *Gasification of biomass wastes in an entrained flow gasifier: Effect of the particle size and the residence time*. Fuel Processing Technology, 2010. **91**(6): p. 681-692.

78. Luo, S., et al., *Hydrogen-rich gas from catalytic steam gasification of biomass in a fixed bed reactor: Influence of particle size on gasification performance*. International Journal of Hydrogen Energy, 2009. **34**(3): p. 1260-1264.
79. Di Blasi, C., Signorelli, G., and Portoricco, G., *Countercurrent Fixed-Bed Gasification of Biomass at Laboratory Scale*. Industrial & Engineering Chemistry Research, 1999. **38**(7): p. 2571-2581.
80. Lucas, C., Szewczyk, D., Blasiak, W., and Mochida, S., *High-temperature air and steam gasification of densified biofuels*. Biomass and Bioenergy, 2004. **27**(6): p. 563-575.
81. Gordillo, G. and Annamalai, K., *Air-Steam Gasification of Dairy Biomass Using Small Scale Fixed Bed Gasifier*. 2009(48821): p. 357-366.
82. Wang, Y., Yoshikawa, K., Namioka, T., and Hashimoto, Y., *Performance optimization of two-staged gasification system for woody biomass*. Fuel Processing Technology, 2007. **88**(3): p. 243-250.
83. Czernik, S., et al., *Gasification of Residual Biomass via the Biosyn Fluidized Bed Technology*, in *Advances in Thermochemical Biomass Conversion*, A.V. Bridgwater, Editor. 1993, Springer Netherlands: Dordrecht. p. 423-437.
84. Collard, F.-X. and Blin, J., *A review on pyrolysis of biomass constituents: Mechanisms and composition of the products obtained from the conversion of cellulose, hemicelluloses and lignin*. Renewable and Sustainable Energy Reviews, 2014. **38**: p. 594-608.
85. Sebayang, A.H., et al., *A perspective on bioethanol production from biomass as alternative fuel for spark ignition engine*. RSC Advances, 2016. **6**(18): p. 14964-14992.
86. Hosoya, T., Kawamoto, H., and Saka, S., *Pyrolysis gasification reactivities of primary tar and char fractions from cellulose and lignin as studied with a closed ampoule reactor*. Journal of Analytical and Applied Pyrolysis, 2008. **83**(1): p. 71-77.
87. Font Palma, C., *Modelling of tar formation and evolution for biomass gasification: A review*. Applied Energy, 2013. **111**: p. 129-141.
88. Asmadi, M., Kawamoto, H., and Saka, S., *Gas- and solid/liquid-phase reactions during pyrolysis of softwood and hardwood lignins*. Journal of Analytical and Applied Pyrolysis, 2011. **92**(2): p. 417-425.
89. Maniatis, K. and Beenackers, A.A.C.M., *Tar Protocols. IEA Bioenergy Gasification Task*. Biomass and Bioenergy, 2000. **18**(1): p. 1-4.
90. Demirbaş, A., *Mechanisms of liquefaction and pyrolysis reactions of biomass*. Energy Conversion and Management, 2000. **41**(6): p. 633-646.

91. Shen, D.K., Gu, S., and Bridgwater, A.V., *Study on the pyrolytic behaviour of xylan-based hemicellulose using TG-FTIR and Py-GC-FTIR*. Journal of Analytical and Applied Pyrolysis, 2010. **87**(2): p. 199-206.
92. Demirbas, A., *The influence of temperature on the yields of compounds existing in bio-oils obtained from biomass samples via pyrolysis*. Fuel Processing Technology, 2007. **88**(6): p. 591-597.
93. Werther, J., et al., *Combustion of agricultural residues*. Progress in Energy and Combustion Science, 2000. **26**(1): p. 1-27.
94. Antal, M.J., Jr. and Varhegyi, G., *Cellulose Pyrolysis Kinetics: The Current State of Knowledge*. Industrial & Engineering Chemistry Research, 1995. **34**(3): p. 703-717.
95. Sheng, C. and Azevedo, J.L.T., *Modeling biomass devolatilization using the chemical percolation devolatilization model for the main components*. Proceedings of the Combustion Institute, 2002. **29**(1): p. 407-414.
96. Olivier, A., Benjamin, C., Arnaud, D., and Guillain, M., *Product Yields and Kinetics of Biomass Fast Devolatilization: Experiments and Modeling*. CHEMICAL ENGINEERING TRANSACTIONS, 2014. **37**.
97. McKendry, P., *Energy production from biomass (part 1): overview of biomass*. Bioresource Technology, 2002. **83**(1): p. 37-46.
98. Lv, D., et al., *Effect of cellulose, lignin, alkali and alkaline earth metallic species on biomass pyrolysis and gasification*. Fuel Processing Technology, 2010. **91**(8): p. 903-909.
99. Merci, B. and Beji, T., *Fluid Mechanics Aspects of Fire and Smoke Dynamics in Enclosures*. 2016, London, UK: CRC press, Taylor & Francis Group
100. Saeed, M.A., Andrews, G.E., Phylaktou, H.N., and Gibbs, B.M., *Global kinetics of the rate of volatile release from biomasses in comparison to coal*. Fuel, 2016. **181**: p. 347-357.
101. Bassilakis, R., Carangelo, R.M., and Wójtowicz, M.A., *TG-FTIR analysis of biomass pyrolysis*. Fuel, 2001. **80**(12): p. 1765-1786.
102. Meng, A., et al., *Quantitative and kinetic TG-FTIR investigation on three kinds of biomass pyrolysis*. Journal of Analytical and Applied Pyrolysis, 2013. **104**: p. 28-37.
103. Pielsticker, S., et al., *Simultaneous investigation into the yields of 22 pyrolysis gases from coal and biomass in a small-scale fluidized bed reactor*. Fuel, 2017. **190**: p. 420-434.
104. Scott, D.S. and Piskorz, J., *The flash pyrolysis of aspen-poplar wood*. The Canadian Journal of Chemical Engineering, 1982. **60**(5): p. 666-674.

105. Commandré, J.M., Lahmidi, H., Salvador, S., and Dupassieux, N., *Pyrolysis of wood at high temperature: The influence of experimental parameters on gaseous products*. Fuel Processing Technology, 2011. **92**(5): p. 837-844.
106. Liu, Q., et al., *Mechanism study of wood lignin pyrolysis by using TG-FTIR analysis*. Journal of Analytical and Applied Pyrolysis, 2008. **82**(1): p. 170-177.
107. Di Blasi, C., Branca, C., Santoro, A., and Gonzalez Hernandez, E., *Pyrolytic behavior and products of some wood varieties*. Combustion and Flame, 2001. **124**(1-2): p. 165-177.
108. Di Blasi, C., Signorelli, G., Di Russo, C., and Rea, G., *Product Distribution from Pyrolysis of Wood and Agricultural Residues*. Industrial & Engineering Chemistry Research, 1999. **38**(6): p. 2216-2224.
109. Torri, C., et al., *Comparative analysis of pyrolysate from herbaceous and woody energy crops by Py-GC with atomic emission and mass spectrometric detection*. Journal of Analytical and Applied Pyrolysis, 2010. **88**(2): p. 175-180.
110. Li, K., Zhang, L., Zhu, L., and Zhu, X., *Comparative study on pyrolysis of lignocellulosic and algal biomass using pyrolysis-gas chromatography/mass spectrometry*. Bioresource Technology, 2017. **234**: p. 48-52.
111. Branca, C., Giudicianni, P., and Di Blasi, C., *GC/MS Characterization of Liquids Generated from Low-Temperature Pyrolysis of Wood*. Industrial & Engineering Chemistry Research, 2003. **42**(14): p. 3190-3202.
112. Monteiro Nunes, S., Paterson, N., Dugwell, D.R., and Kandiyoti, R., *Tar Formation and Destruction in a Simulated Downdraft, Fixed-Bed Gasifier: Reactor Design and Initial Results*. Energy & Fuels, 2007. **21**(5): p. 3028-3035.
113. Spellman, F.R., *Forest-based biomass energy: concepts and applications*. Energy and the Environment, ed. A. Ghassemi. 2012, New York: Taylor & Francis Group, CRC Press. p. 232
114. Septien, S., et al., *Effect of particle size and temperature on woody biomass fast pyrolysis at high temperature (1000–1400°C)*. Fuel, 2012. **97**: p. 202-210.
115. Yan, R., et al., *Influence of temperature on the distribution of gaseous products from pyrolyzing palm oil wastes*. Combustion and Flame, 2005. **142**(1-2): p. 24-32.
116. Williams, P.T. and Nugranad, N., *Comparison of products from the pyrolysis and catalytic pyrolysis of rice husks*. Energy, 2000. **25**(6): p. 493-513.

117. Williams, P.T. and Besler, S., *The influence of temperature and heating rate on the slow pyrolysis of biomass*. Renewable Energy, 1996. **7**(3): p. 233-250.
118. Shi, X. and Wang, J., *A comparative investigation into the formation behaviors of char, liquids and gases during pyrolysis of pinewood and lignocellulosic components*. Bioresource Technology, 2014. **170**: p. 262-269.
119. Font, R., Marcilla, A., Verdu, E., and Devesa, J., *Kinetics of the pyrolysis of almond shells and almond shells impregnated with cobalt dichloride in a fluidized bed reactor and in a pyroprobe 100*. Industrial & Engineering Chemistry Research, 1990. **29**(9): p. 1846-1855.
120. Andrews, G.E., *Small Scale Biomass Burners – Gasification Boilers*, ERRI, SPEME, University of Leeds, UK 2013.
121. Puig-Arnavat, M., Bruno, J.C., and Coronas, A., *Review and analysis of biomass gasification models*. Renewable and Sustainable Energy Reviews, 2010. **14**(9): p. 2841-2851.
122. Koppejan, J. and Loo, S.v., *The Handbook of Biomass Combustion and Co-firing*. 2008, UK: Earthscan
123. Glas, I.a.s. *Log wood boilers*. 2017 [Last accessed 17th september 2017]; Available from: <http://www.glas.ie/wp-content/uploads/2011/01/GLAS-Brochure-log-boilers.pdf>.
124. Guntamatic. *Guntamatic biomass boilers heating range*. [Last accessed 22nd September 2017]; Available from: http://www.treco.co.uk/assets/technical/New_Guntamatic_Brochure2.pdf.
125. Fröling, G. *Froling S3 Turbo Firewood Boiler*. 2017 [Last accessed 17th September 2017]; Available from: <https://www.froeling.com/ww/products/scheitholz/s3-turbo.html>.
126. Viessman. *VITOLIGNO 250-S: Heating with wood*. 2017 [Last accessed 20th January 2017]; Available from: <https://www.viessmann.co.uk/en/residential-buildings/biomass-boilers/log-boilers/vitoligno-250-s.html>.
127. Zainal, Z.A., Ali, R., Lean, C.H., and Seetharamu, K.N., *Prediction of performance of a downdraft gasifier using equilibrium modeling for different biomass materials*. Energy Conversion and Management, 2001. **42**(12): p. 1499-1515.
128. Channiwala, S.A. and Parikh, P.P., *A unified correlation for estimating HHV of solid, liquid and gaseous fuels*. Fuel, 2002. **81**(8): p. 1051-1063.
129. Babrauskas, v., *Development of the cone calorimeter, a bench scale heat release rate apparatus based on oxygen consumption*, in NBSIR 82-2611 National Bureau of Standards, 1982.

130. Babrauskas, V., *Hazard Calculations*, in *SFPE Handbook of Fire Protection Engineering*. 2002, National Fire Protection Association: Quincy, Massachusetts. p. 3-49.
131. Gasmeter Technologies Oy, *Gasmeter Calcmet for windows - User's guide and reference manual*: Helsinki, FINLAND, 2010.
132. Li, H., et al., *Evaluation of a FTIR Emission Measurement System for Legislated Emissions Using a SI Car*, SAE International, 2006.
133. Daham, B., et al. *Application of a portable FTIR for measuring on-road emissions*. SAE Technical paper series, 2005. DOI: 10.4271/2005-01-0676.
134. Fitzpatrick, E.M., et al., *Emission of Oxygenated Species from the Combustion of Pine Wood and its Relation to Soot Formation*. Process Safety and Environmental Protection, 2007. **85**(5): p. 430-440.
135. Alarifi, A., *Compartment Fire Toxicity: Measurements and Aspects of Modelling*, in *School of Chemical and Process Engineering* The University of Leeds: Leeds, 2016.
136. SYSTECH-illinois. *Paramagnetic Cells*. 2017 [Last accessed 24th May 2017]; Available from: <https://www.systechillinois.com/ru/support/technologies/paramagnetic-cells>.
137. Environmental-Pollution. *Short Notes on Non-Dispersive Infra-Red (NDIR) Analyzer*. 2017 [Last accessed 24th May 2017]; Available from: <http://www.environmentalpollution.in/pollution/regulation-and-monitoring/4-short-notes-on-non-dispersive-infra-red-ndir-analyzer/1886>.
138. Huggett, C., *Estimation of rate of heat release by means of oxygen consumption measurements*. Fire and Materials, 1980. **4**(2): p. 61-65.
139. Sara McAllister, J.-Y.C., A. Carlos Fernandez-Pello, *Fundamentals of Combustion Processes*. Mechanical engineering series. 2011, New York, London: Springer
140. Aljumaiah, O., et al. *Wood Crib Fires under High Temperature Low Oxygen Conditions*. in *Sixth International Seminar on Fire and Explosion Hazards*. 2010. University of Leeds, UK. Proceedings
141. Kung, H.-C., *A mathematical model of wood pyrolysis*. Combustion and Flame, 1972. **18**(2): p. 185-195.
142. Andrews, G. and Kim, M. *The Optimum Position of Water Heat Transfer Coils Downstream of a Radial Swirler in a 20kW Heater*. in *13th International Conference on Heat Transfer, Fluid Mechanics and Thermodynamics (HEFAT2017)*. 2017. Portoroz, Slovenia: 13th International Conference on Heat Transfer, Fluid Mechanics and Thermodynamics (HEFAT2017).

143. Lahijani, P. and Zainal, Z.A., *Gasification of palm empty fruit bunch in a bubbling fluidized bed: A performance and agglomeration study*. Bioresource Technology, 2011. **102**(2): p. 2068-2076.
144. Wei, L., et al., *Steam gasification of biomass for hydrogen-rich gas in a free-fall reactor*. International Journal of Hydrogen Energy, 2007. **32**(1): p. 24-31.
145. Bridgwater, A.V., *The technical and economic feasibility of biomass gasification for power generation*. Fuel, 1995. **74**(5): p. 631-653.
146. Guerrero, M., et al., *Pyrolysis of eucalyptus at different heating rates: studies of char characterization and oxidative reactivity*. Journal of Analytical and Applied Pyrolysis, 2005. **74**(1–2): p. 307-314.
147. Dupont, C., et al., *Biomass pyrolysis experiments in an analytical entrained flow reactor between 1073 K and 1273 K*. Fuel, 2008. **87**(7): p. 1155-1164.
148. Zanzi, R., Sjöström, K., and Björnbom, E., *Rapid high-temperature pyrolysis of biomass in a free-fall reactor*. Fuel, 1996. **75**(5): p. 545-550.
149. Zhao, C., Jiang, E., and Chen, A., *Volatile production from pyrolysis of cellulose, hemicellulose and lignin*. Journal of the Energy Institute, 2016.
150. Chen, Y., et al., *Modeling of biomass pyrolysis kinetics*. Symposium (International) on Combustion, 1998. **27**(1): p. 1327-1334.
151. Wang, S., et al., *Comparison of the pyrolysis behavior of pyrolytic lignin and milled wood lignin by using TG–FTIR analysis*. Journal of Analytical and Applied Pyrolysis, 2014. **108**: p. 78-85.
152. Butler, E., Devlin, G., Meier, D., and McDonnell, K., *Fluidised bed pyrolysis of lignocellulosic biomasses and comparison of bio-oil and micropyrolyser pyrolysate by GC/MS-FID*. Journal of Analytical and Applied Pyrolysis, 2013. **103**(Supplement C): p. 96-101.
153. Azeez, A.M., Meier, D., Odermatt, J., and Willner, T., *Fast Pyrolysis of African and European Lignocellulosic Biomasses Using Py-GC/MS and Fluidized Bed Reactor*. Energy & Fuels, 2010. **24**(3): p. 2078-2085.
154. Horne, P.A. and Williams, P.T., *Influence of temperature on the products from the flash pyrolysis of biomass*. Fuel, 1996. **75**(9): p. 1051-1059.

Appendix A

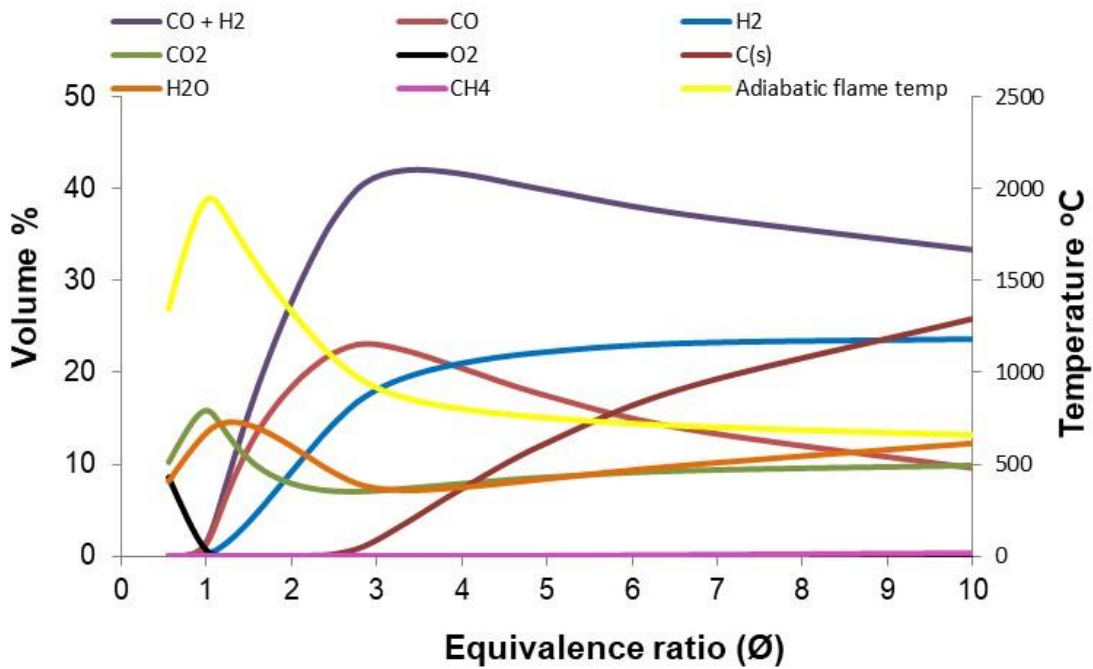


Figure A.1 Equilibrium concentrations and adiabatic flame temperature of gaseous products as a function of \emptyset for pine wood gasification using FLAME software.

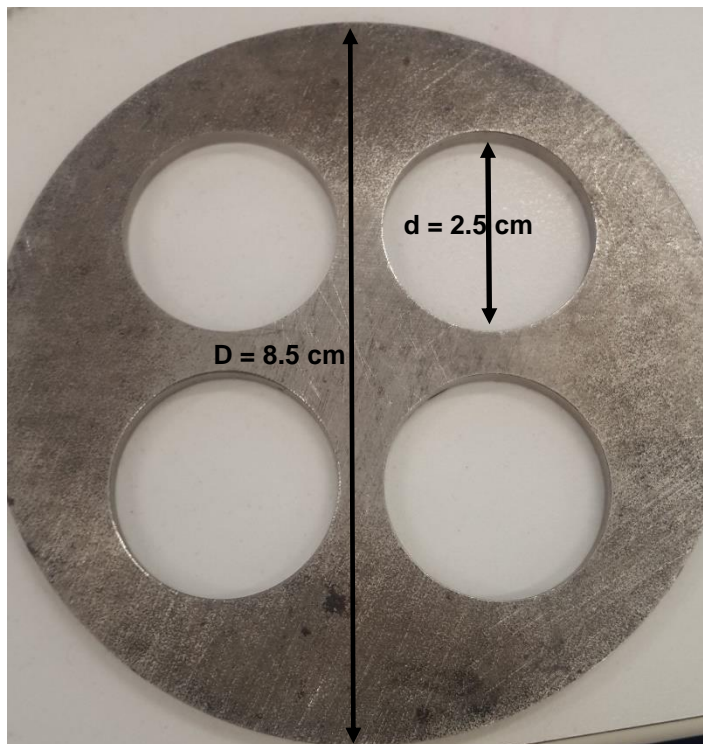


Figure A.2 Grid plate mixer place under chimney



Figure A.3 X -probe (holes blocked after tests when facing downward during sampling)



Figure A.4 X -probe (holes condition after tests when facing upward during sampling)



Figure A.5 Chimney exit grid plate cover for chimney

Appendix B



Figure B.1 Tars left after pine wood pyrolysis test at 25 kW/m² on cone calorimeter



Figure B.2 Wood-char left after pine wood pyrolysis test at 10 kW/m² on cone calorimeter



Figure B.3 Char left after pine wood pyrolysis at 15 kW/m² on cone calorimeter



Figure B.4 Char left after pine wood pyrolysis at 20 kW/m² on cone calorimeter



Figure B.5 Char left after pine wood pyrolysis at 25 kW/m² on cone calorimeter

Appendix C



Figure C.1 Pyrolysis char at 300 °C from furnace reactor



Figure C.2 Pyrolysis char at 350 °C from furnace reactor

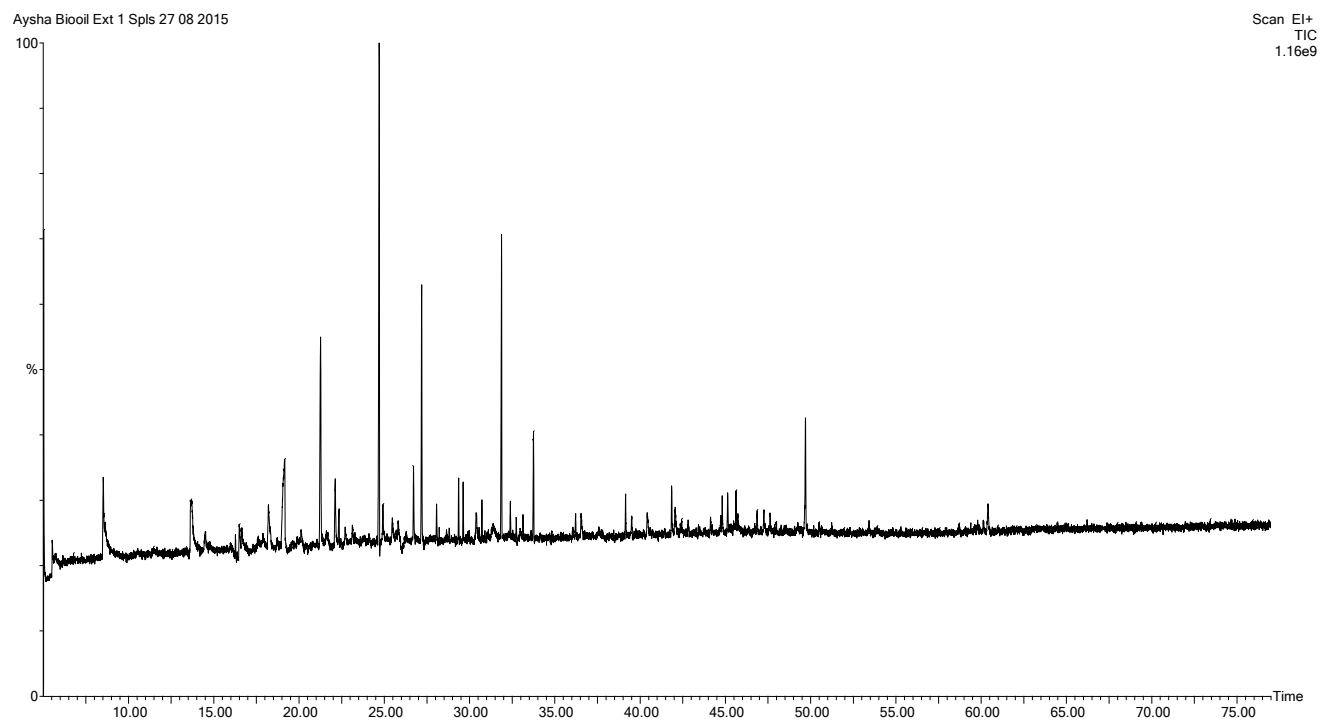


Figure C.3 Pyrolysis char at 400 °C from furnace reactor



Figure C.4 Pyrolysis char at 450 °C from furnace reactor

Appendix D



PERKIN ELMER CLARUS 560S GC/MS ACQUISITION PARAMETERS

Oven: Initial temp 40°C for 10 min, ramp 5°C/min to 300°C, hold 15 min, Inj auto=300°C, Volume=0 µL, Split=10:1, Carrier Gas=He, Solvent Delay=5.00 min, Transfer Temp=250°C,
Source Temp=180°C, Scan: 50 to 500Da, Column 30.0m x 250µm

Figure D.1 GC/MS total ion chromatograph plot for pyrolysis liquids from pine wood pyrolysis on furnace rig at 300 °C

Table D.1 Components detected by GC/MS from pyrolysis liquids (Pyrolysis at 300 °C on furnace rig)

Laboratory Name	ERRI Analytical Laboratory, University of Leeds											
Report	GC/MS Qualitative Library Search Report											
Data File Name	C:\TurboMass\2015.PRO\Data\Aysha Biooil Ext 1 Spls 27 08 2015.raw											
Acquired	08/28/2015 10:49:55 AM											
Sample ID												
Description	DCM extract											
Tune File	C:\TurboMass\2015.PRO\ACQUDB\Tune 350V.IPR											
Instrument	Perkin Elmer Clarus 560S											
Processing Method	Qualitative Processing.qlm											
GC Method	C:\TurboMass\2015.PRO\ACQUDB\Qualitative Splitless GC.mth											
MS Method	C:\TurboMass\2015.PRO\ACQUDB\Qualitative Full Scan.EXP											
Vial Number	81											
Reported	#####											
#	RT	Hit No	Name	Match	R Match	Area	Area %	CAS no.				
1	5.023	1	Spiro[9,9]difluorene-2,2'-dicarboxylic acid, 7,7'-dinitro-	623	676	42600000	1.272					
1	5.023	2	1,4:5,8-Dimethanonaphthalene-2,3-diol, 5,6,7,8,9,9-hexachloro-1,2,3,4,4a,5,8,8a-octahydro-, diacetate, (1a,2a,3a,4a,4aa,5a,8a,8aa)-	573	609	42600000	1.272	34408-22-5				
1	5.023	3	1,16-Cyclocorynan-16-carboxylic acid, 17-(acetyloxy)-19,20-didehydro-10-methoxy-, methyl ester, (16.xi.,19E)-	533	728	42600000	1.272	55724-49-7				
2	5.534	1	1',1'-Dicarboethoxy-1a,2a-dihydro-17a-propionoxy(3'H)cycloprop[1,2]androsta-1,4,6-trien-3-one	514	545	2.06E+08	6.141					
2	5.534	2	1'-Carboethoxy-1'-cyano-1a,2a-dihydro-17a-propionoxy-3'H-cycloprop[1,2]androsta-1,4,6-trien-3-one	472	541	2.06E+08	6.141	75857-77-1				

2	5.534	3	Delsoline	468	500	2.06E+08	6.141	509-18-2
3	8.515	1	Furfural	629	898	8.04E+08	24	98-01-1
3	8.515	2	3-Furaldehyde	623	913	8.04E+08	24	498-60-2
3	8.515	3	Furan, 2,5-dimethyl-	541	754	8.04E+08	24	625-86-5
4	13.67	1	2(5H)-Furanone	478	920	7.22E+08	21.56	497-23-4
4	13.67	2	2(3H)-Furanone	409	849	7.22E+08	21.56	20825-71-2
4	13.67	3	2-Hexene, (E)-	392	755	7.22E+08	21.56	4050-45-7
5	14.52	1	Molybdenum, hexacarbonylbis(ü(5)-2,4-cyclopentadien-1-yl)di-,	414	436	2.73E+08	8.144	12091-64-4
5	14.52	2	Tungsten(0), ü-2-acrylic acid, methyl ester-ü-2-E-cyclooctene-tetracarbonyl-	411	521	2.73E+08	8.144	
5	14.52	3	Tungsten, dicarbonylbis(ü-4-2-methylenecycloheptanone)	410	451	2.73E+08	8.144	
6	16.5	1	4,25-Secoobscurinervan-4-ol, 25-ethyl-15,16-dimethoxy-, 25-acetate, (4á,22à)-	432	460	18790000	0.561	72101-38-3
6	16.5	2	2,3-Pentanedione	420	925	18790000	0.561	600-14-6
6	16.5	3	cis-1-Ethoxy-1-butene	409	807	18790000	0.561	
7	16.65	1	2á,4a-Epoxymethylphenanthrene-7-methanol, 1,1-dimethyl-2-methoxy-8-(1,3-dithiin-2-ylidene)methyl-1,2,3,4,4a,4b,5,6,7,8,8a,9-dodecahydro-, acetate	487	519	51420000	1.535	
7	16.65	2	Molybdenum, tricarbonyl-[N-butyl-bis[2-(butylphosphino)ethyl]amine]	445	500	51420000	1.535	
7	16.65	3	Difuro[2',3':5,6:3'',2'':7,8]perlylo[1,12-def][1,3]dioxepin-8,15-dione, 10,11,12,13-tetrahydro-1,7-dihydroxy-10,13-dimethyl-	440	486	51420000	1.535	39657-83-5

8	17.61	1	17-(1,5-Dimethylhexyl)-10,13-dimethyl-4-(2-nitrophenyl)hexadecahydrocyclopenta[a]phenanthrene	450	489	74740000	2.231	
8	17.61	2	2,2'-Bithienyl, 5,5'-bis(trimethylstannyl)-	426	436	74740000	2.231	143367-56-0
8	17.61	3	Tetramethyl 1,1'-(1,8-naphthylene)bis(1,2,3-triazole-4,5-dicarboxylate)	419	439	74740000	2.231	91165-61-6
9	17.89	1	Acetic acid, 4,4,6a,8a,11,11,14b-heptamethyl-7,13-dioxo-1,2,3,4,4a,5,6,6a,7,8,8a,9,10,11,12,12a,13,14,14a,14b-eicosahydropicen-3-yl ester	453	499	46060000	1.375	
9	17.89	2	Acetic acid, 4,4,6a,8a,11,12,14b-heptamethyl-7,13-dioxo-1,2,3,4,4a,5,6,6a,7,8,8a,9,10,11,12,12a,13,14,14a,14b-eicosahydropicen-3-yl	434	476	46060000	1.375	
9	17.89	3	3'H-Cycloprop(1,2)-5-cholest-1-en-3-one, 1'-carboethoxy-1'-cyano-1,2-dihydro-	430	436	46060000	1.375	75857-80-6
10	18.21	1	17-(1,5-Dimethylhexyl)-10,13-dimethyl-3-styrylhexadecahydrocyclopenta[a]phenanthren-2-one	434	494	56410000	1.684	
10	18.21	2	Picolinyl 7,10,13,16-docosatetraenoate	407	520	56410000	1.684	
10	18.21	3	3-Carene	390	861	56410000	1.684	13466-78-9
11	19.16	1	2-Cyclopenten-1-one, 2-hydroxy-3-methyl-	623	896	68070000	2.032	80-71-7
11	19.16	2	1,2-Cyclopentanedione, 3-methyl-	615	873	68070000	2.032	765-70-8
11	19.16	3	1,2-Cyclohexanedione	553	798	68070000	2.032	765-87-7
12	19.63	1	Molybdenum, hexacarbonylbis(ü(5)-2,4-cyclopentadien-1-yl)di-,	446	480	31040000	0.9267	12091-64-4
12	19.63	2	Delsoline	406	443	31040000	0.9267	509-18-2
12	19.63	3	8-[2-(2-Amino-phenyl)-2-oxo-ethyl]-3-(1-hydroxy-1-methyl-ethyl)-6a,7,10b-trimethyl-dodecahydro-benzo[f]chromene-7-carboxylic acid	405	428	31040000	0.9267	

13	19.9	1	Cycloheximide tritms	429	466	22630000	0.6755	
13	19.9	2	1,3,5-Triazine, 2-[(3,4-dichlorophenyl)thio]-4,6-bis(trichloromethyl)-	422	472	22630000	0.6755	24478-10-2
13	19.9	3	7-Chloro-N-[[4'-chloro-5-[[diethylamino]methyl]-6-ethoxy]-1,1'-biphenyl-3-]-quinoline-4-amine	408	543	22630000	0.6755	
14	20.11	1	Acetic acid, 4,4,6a,8a,11,11,14b-heptamethyl-7,13-dioxo-1,2,3,4,4a,5,6,6a,7,8,8a,9,10,11,12,12a,13,14,14a,14b-eicosahydropicen-3-yl ester	448	482	26490000	0.7908	
14	20.11	2	3,19-Epoxyandrost-5-en-7-ol-17-one, 4,4-dimethyl-3-methoxy-16,16-propylenedithio-	446	476	26490000	0.7908	
14	20.11	3	2,5-Dichloro-3-ethoxycarbonyl-4,6-di(4-methylphenylthio)pyridine	445	511	26490000	0.7908	
15	21.26	1	Phenol, 2-methoxy-	887	907	37130000	1.108	90-05-1
15	21.26	2	Mequinol	845	865	37130000	1.108	150-76-5
15	21.26	3	2-Cyclopenten-1-one, 3,4,4-trimethyl-	781	797	37130000	1.108	30434-65-2
16	21.6	1	Spiro[9,9]difluorene-2,2'-dicarboxylic acid, 7,7'-dinitro-	468	506	27040000	0.8074	
16	21.6	2	Aconitane-1,7,8,14-tetrol, 20-ethyl-6,16-dimethoxy-4-(methoxymethyl)-, 14-acetate, (1à,6á,14à,16á)-	445	495	27040000	0.8074	50676-21-6
16	21.6	3	2,2'-Bithienyl, 5,5'-bis(trimethylstannyl)-	437	449	27040000	0.8074	143367-56-0
17	22.12	1	Maltol	505	838	22040000	0.658	118-71-8
17	22.12	2	Pyrimidine-4,6-diol, 5-methyl-	457	770	22040000	0.658	18337-63-8
17	22.12	3	Pyrazole-5-carboxamide, 4-amino-	437	681	22040000	0.658	
18	24.7	1	2-Methoxy-5-methylphenol	886	890	43070000	1.286	1195-09-1

18	24.7	2	Phenol, 2-methoxy-4-methyl-	884	884	43070000	1.286	93-51-6
18	24.7	3	Phenol, 4-methoxy-3-methyl-	859	869	43070000	1.286	14786-82-4
19	27.19	1	Phenol, 4-ethyl-2-methoxy-	878	884	20100000	0.6001	2785-89-9
19	27.19	2	Benzene, 1,4-dimethoxy-2-methyl-,	808	814	20100000	0.6001	24599-58-4
19	27.19	3	5-Isopropyl-3,3-dimethyl-2-methylene-2,3-dihydrofuran	802	809	20100000	0.6001	81250-44-4
20	31.87	1	Phenol, 2-methoxy-4-(1-propenyl)-	932	944	22630000	0.6755	97-54-1
20	31.87	2	Phenol, 2-methoxy-4-(1-propenyl)-, (Z)-	921	921	22630000	0.6755	5912-86-7
20	31.87	3	Phenol, 2-methoxy-4-(1-propenyl)-, (E)-	921	921	22630000	0.6755	5932-68-3